SUB-SURFACE PETROCHEMISTRY, STRATIGRAPHY AND HYDROTHERMAL ALTERATION OF THE DOMES AREA, OLKARIA GEOTHERMAL FIELD, KENYA.

XAVIER SHIOYA MUSONYE

Faculty of Earth Science
University of Iceland
2015

SUB-SURFACE PETROCHEMISTRY, STRATIGRAPHY AND HYDROTHERMAL ALTERATION OF THE DOMES AREA, OLKARIA GEOTHERMAL FIELD, KENYA.

Xavier Shioya Musonye

60 ECTS thesis submitted in partial fulfilment of a
Magister Scientiarum degree in Geology

Advisor(s)
Anette K. Mortensen
Björn S. Harðarson

Faculty Representative
Guðmundur H. Guðfinnsson

Faculty of Earth Science
School of Engineering and Natural Sciences
University of Iceland
Reykjavik, May 2015

Sub-surface petrochemistry, stratigraphy and hydrothermal alteration of the Domes area, Olkaria geothermal field, Kenya.
60 ECTS thesis submitted in partial fulfilment of a *Magister Scientiarum* degree in Geology

Faculty of Earth Science
School of Engineering and Natural Sciences
University of Iceland
Sturlugata 7
101 Reykjavík
Iceland

Telephone: 525 4000

Bibliographic information:
Xavier Shioya Musonye, 2015, Sub-surface petrochemistry, stratigraphy and hydrothermal alteration of the Domes area, Olkaria geothermal field, Kenya.
Master's thesis, Faculty of Earth Sciences, University of Iceland, pp. 154.

Printing: Háskólaprent, Fálkagata 2, 107 Reykjavík, Iceland, May 2015.

Abstract

Wells OW-905A, OW-910 and OW-917 have been drilled in the Domes area of the Olkaria geothermal field. Wells OW-905A and OW-910 have been drilled inside the caldera while OW-917 has been drilled on the eastern margins of the caldera rim. The caldera rim is characterised by a ring of rhyolitic domes to the east, south and southwest margins. Plans are underway to expand production drilling to the east of the Domes field. This study presents an in-depth look at the variation in reservoir characteristics across the Domes field and to the east of the ring structure. The study also delineates magma differentiation processes involved in the evolution of the GOVC. Wells OW-905A and OW-910 cut across seven stratigraphic units namely basalt, trachybasalt, basaltic trachyandesite, trachyandesite, trachyte, rhyolite and tuff. Well OW-917 only cuts across trachyte and rhyolite. Intrusives cut by the wells include micro-granite, syenitic, trachytic and basaltic dykes. Well OW-910 has a high abundance of high-temperature alteration minerals, OW-905A has moderate abundance while OW-917 has low abundance of these minerals. Higher temperatures are observed at shallower depth in OW-910, at relatively greater depth in OW-905 and at greater depth in OW-917. High permeability is observed in wells OW-905A and OW-910. Well OW-917 shows poor permeability. Well OW-905A is located in a recharge zone, OW-910 in the up-flow zone close to the heat source and OW-917 in a down-flow zone. The main magma differentiation processes involved in generation of the basalt-trachyte suite are fractional crystallisation and magma mixing. Rhyolites have been generated through fractionation of trachytes and anatexis of syenites. The GOVC has had different episodes of eruptions. Its plumbing system consists of independent discrete magma chambers and conduits in which magma underwent modification before eruption.

Útdráttur

Jarðhitaholur OW-905A, OW-910 og OW-917 voru boraðar á Domes-svæði Olkaria-jarðhitasvæðisins. OW-905A og OW-910 eru staðsettar innan ætlaðrar öskju, en OW-917 á austurjaðri hringbrotsins. Áætlanir eru um að bora fleiri vinnsluholur austan Domes-svæðisins. Í þessari rannsókn eru breytingar í eiginleikum jarðhitakerfisins þvert yfir Domes-svæðið allt austur fyrir hringmyndunina skoðaðar nákvæmlega. Í rannsókninni er líka fjallað um kvikuþróun sem átti sér stað við upphleðslu Olkaria-megineldstöðvarinnar. Holur OW-905A og OW-910 liggja gegnum sjö mismunandi gerðir jarðlaga, þ.e. basalt, trakýbasalt, basaltískt trakýandesít, trakýandesít, trakýt, rhýólít og túff. Í OW-917 er einungis trakýt og rhýólít. Þær gerðir innskota sem holurnar voru boraðar gegnum eru míkrógranít, sýenít-, trakýt- og basaltgangar. Hola OW-910 er mjög rík af háhitasíðsteindum, OW-905A hefur minna magn, en OW-917 er snauð af slíkum steindum. Hátt hitastig kemur fram á tiltölulega litlu dýpi í OW-910, á meira dýpt í OW-905 og á mestu dýpi í OW-917. Mjög góð lekt er í borholum OW-905A og OW-910, en OW-917 hefur lága lekt. Hola OW-905A er staðsett í aðfærslustreymi, OW-910 í uppstreymissvæði nærri varmagjafa og OW-917 í niðurstreymissvæði. Helstu kvikuferli sem áttu sér stað við þróun basalt-trachýtsyrpunnar voru hlutkristöllun og kvikublöndun. Rhýólítkvika hefur myndast við hlutkristöllun á trakýtkviku og uppbræðslu á sýeníti. Olkaria-eldstöðin hefur gengið gegnum eldgosahrinur. Kvikufærslukerfi hennar samanstendur af sjálfstæðum kvikuhólfum og kvikuæðum þar sem kvika þróaðist áður en gos urðu.

Dedication

This work is dedicated to my parents Mr. and Mrs. Musonye.

Table of Contents

List of Figures

List of Tables

Abbreviations

UNU-GTP	United Nations University Geothermal Training Programme
KenGen	Kenya Electricity Generating Company
EARS	East African Rift System
ISOR	Iceland GeoSurvey
XRD	X-ray diffractometry
ICP-OES	Inductively Coupled Plasma-Optical Emission Spectroscopy
ppm	parts per million
GOVC	Greater Olkaria Volcanic Complex
TAS	Total alkali versus silica
OW	Olkaria Well
Ma	Million years
Ka	Thousand years
Bp	Before present
m a.s.l	meters above sea level

Acknowledgements

I thank the UNU-GTP for having given me this chance to pursue my studies under their sponsorship. I am indebted to the director UNU-GTP, Mr. Ludvik and the rest of the UNU-GTP staff for their continued support. I thank the University of Iceland and Iceland GeoSurvey (ISOR) for providing me with the necessary research facilities that made it possible for me to conduct my research. I express my sincere gratitude to Kenya Electricity Generating Company (KenGen) for having granted me permission to come and pursue my studies.

Special thanks goes to my supervisors, Anette K. Mortensen, Björn S. Harðarson and Guðmundur H. Guðfinnsson for your critical comments, close and continous guidance, during my research work. I am indebted to Hjalti Franzson for his advice and helpful suggestions on various aspects of my research work. Special thanks goes to Sæmundur Ari Halldórsson for your guidance and assistance during ICP-OES sample preparation, analysis and data cleaning, your advice and helpful suggestions on various aspects of my findings. I am indebted to Júlíana Signý Gunnarsdóttir for her assitance during my borehole analysis lab work.

My sincere thanks goes to my colleagues, Victor Otieno and Samuel Munyiri for their support during data collection. To all the UNU-GTP masters and PhD students, I acknowledge you for making me feel home away from home, you are great people! Lastly, I express my gratitude to friends and family members who gave me the moral support and encouragement throughout my study period.

1 Introduction

The Olkaria geothermal area is located within the Greater Olkaria Volcanic Complex (GOVC), which is 125 km northwest of Nairobi city. The precise location is in the south central Kenyan Rift Valley to the immediate southwest of Lake Naivasha (0° 53'S; 36° 18'E) (Figure 1). The GOVC is bound to the north, east and south by Eburru, Longonot and Suswa volcanic centres, respectively. It is flanked to the west by the western rift margins. All these neighbouring volcanic centers have distinct calderas as opposed to the GOVC. Some scientific studies have proposed a caldera to have existed within the GOVC, as seen by a ring of rhyolitic domes, mainly found on the eastern and southern margins of the GOVC (Simiyu et al., 1998, Clarke et al., 1990). Other studies have not found evidence for the existence of a caldera (Onacha, 1993). The GOVC is a multi-centered volcanic field covering 240 km^2 (Clarke et al., 1990). It is located in the south central Kenyan Rift Valley which coincides with an area associated with high volcanism during rift development (Simiyu et al., 1995; Simiyu and Keller, 1997). The estimated crustal thickness in this region is 35 km (Simiyu et al., 1995; Simiyu and Keller, 1997). Clarke et al. (1990) observed 80 different volcanic centres, mainly composed of comenditic rhyolite. They occur as steep-sided domes of lava and/or pyroclastic rocks or thick lava flows with restricted lateral extent.

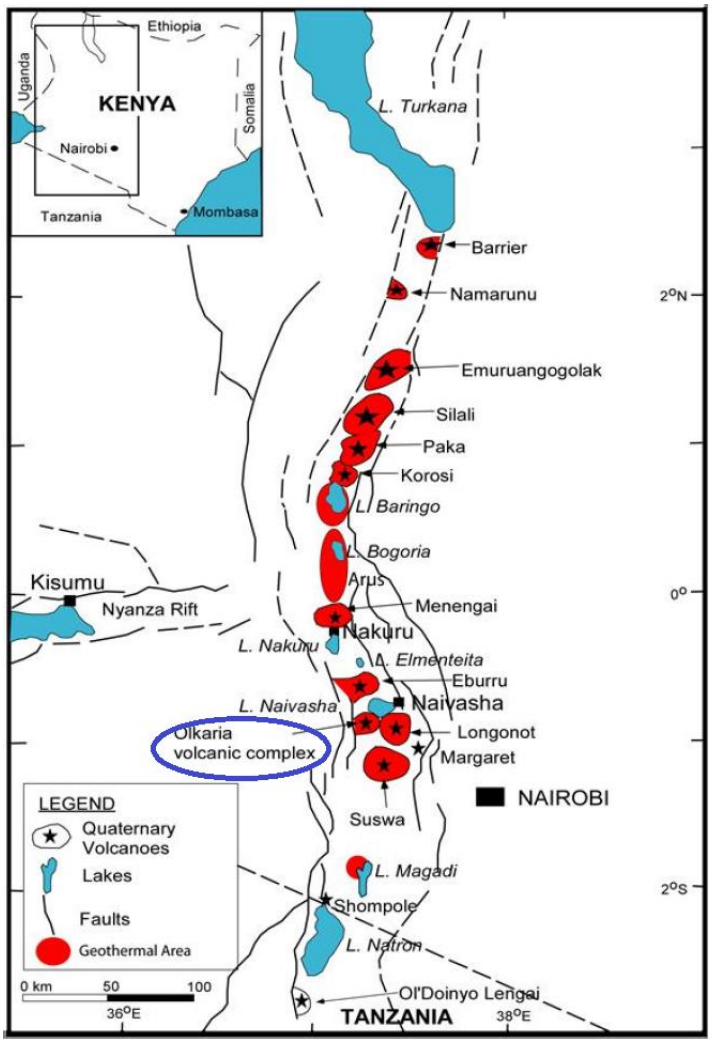

Figure 1: Location of Olkaria Volcanic Complex and other volcanic centres within the Kenyan Rift (from Ofwona et al., 2006).

The GOVC is associated with a region of late Quaternary volcanism. Similar late Quaternary volcanic centres occur in the axial region of the Kenyan Rift Valley. They include from north to south: Emuruangogolak, Silali, Paka, Korosi, Menengai, Longonot, Eburru and Suswa (Figure 1). These volcanic centers are

characterised by shallow intrusions, which have resulted in the high thermal gradient measured at these volcanic centres. Unlike Olkaria and Eburru, which are in their geothermal power production stage, the other volcanic centres are yet to be developed to this level. Production drilling is ongoing in Menengai in order to gather enough steam before installing turbines for power generation. The rest of the volcanic centres are still in various exploration stages. However, there is a potential for geothermal production at these centres according to the surface exploration studies already done in these regions (Omenda, 1993; Riaroh and Okoth, 1994).

Olkaria geothermal field is a high-temperature geothermal field with an approximate resource area of 204 km^2. It has been divided into seven sections for the purpose of easy development (Figure 2). These include the Olkaria East, Olkaria Southwest, Olkaria Southeast, Olkaria Northeast, Olkaria Northwest, Olkaria Central and the Domes fields, the Domes field being the focus of this study. These sections exhibit different reservoir characteristics in regard to reservoir enthalpy, formation temperature, fluid chemistry and alteration mineralogy. Variation in reservoir characteristics has also been noted within some of the sections, including the Domes field. Olkaria geothermal field provides a good case study for fluid-rock interaction behaviour within a high-temperature geothermal system. Plans have been underway to extend the production drilling to the east of the Domes field. Two step-out wells (OW-917 and OW-922) have been drilled on the eastern side of the Domes area outside the ring structure in order to investigate the resource potential in this region (Figure 3).

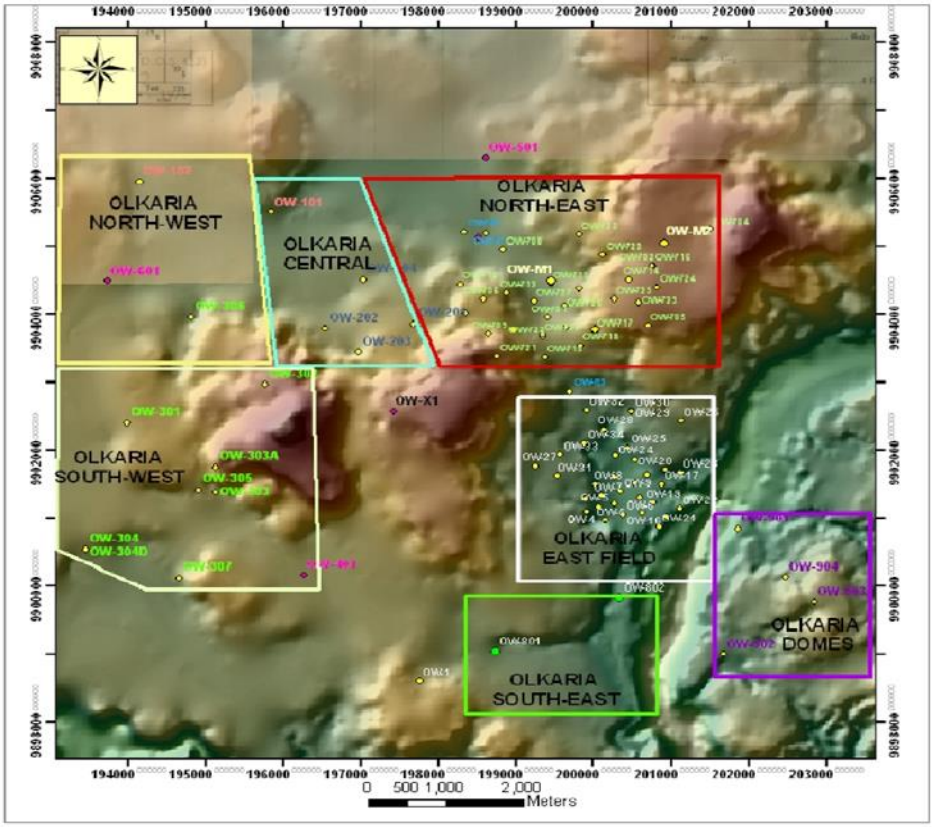

Figure 2: The seven sections (fields) of the Greater Olkaria geothermal area (from KenGen, 2012).

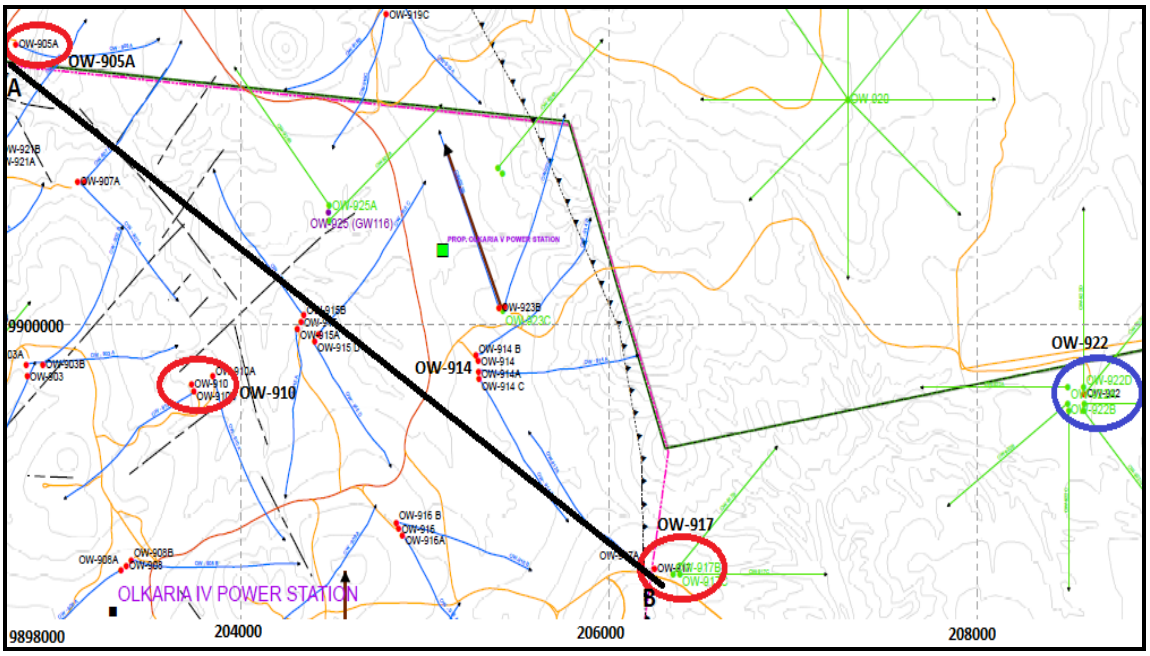

Figure 3: Map showing the location of study wells (circled in red) and one of the step-out wells OW-922 (circled blue) within the Domes area.

The main objective of this study is to understand the reservoir characteristics of the area to the east of the Domes (mainly the area outside the ring structure) in comparison with the Domes area (mainly the area inside the ring structure), and to identify marker horizons for the purposes of stratigraphic correlation and inferring buried faults within the Domes area. Three boreholes, OW-905A, OW-910 and OW-917, were chosen for this study. The stratigraphic study was aimed at investigating the variation in lithostratigraphy, alteration mineralogy, temperature and permeability within the Domes field along a NW-SE traverse. This traverse runs from the northwest end at OW-905A, passing through the central part (OW-910) of the field to the east of the Domes ring structure at OW-917. The drill cuttings give information about fluid-rock interaction at depth and how this has affected the well production along this NW-SE traverse (A-B in Figure 3). The study provides important information that will help in deciding whether to expand production drilling to the east of the Domes ring structure. The drill cuttings from the three wells were used in this study.

A number of researchers have carried out petrological and geochemical studies to determine the evolution of the rhyolites and basalts of the GOVC (Davies and Macdonald, 1987; Macdonald et al., 1987; Black et al., 1997; Scaillet and Macdonald, 2001; Heumann and Davies, 2002; Macdonald et al., 2008 and Marshall et al., 2009). These studies were mainly carried out on surface samples. Furthermore, Omenda (1997) conducted petrochemical analysis of some drill cuttings obtained from drill holes from the Olkaria geothermal area in his doctoral dissertation on the geochemical evolution of Quaternary volcanism in the south-central portion of the Kenyan rift. He analysed six drill cutting samples of basaltic rock (from Olkaria East field, North East and West), two trachytic drill cuttings (from Olkaria North East and Olkaria East field) and two comendites (from Olkaria Northeast field). These analyses have not been able to delineate the stratigraphic chemical rock composition range beneath the GOVC.

The main objectives of the petrochemical study presented in this thesis are to outline the petrogenesis and differentiation of magma groups from the surface down to 3000 m depth; to find out if the chemical composition of igneous rocks within the Olkaria geothermal field show a bimodal or linear distribution on a TAS diagram for the purpose of proper rock type classification of drill cuttings; to map the geochemical relationship between samples from the three wells in order to determine if any displacement has occurred along the proposed ring structure; to find out the effect the degree of alteration has on the chemical composition of the rocks and to investigate whether there are any petrochemical differences between surface rocks and rocks at depth. Petrochemical study will provide an important input for further water-rock interaction research.

1.1 Geothermal Development

Exploration for the exploitation of the Olkaria geothermal field began in the 1960's, culminating with the drilling of two geothermal wells (Simiyu, 2010). This work continued in the early 1970's. In 1973, drilling of deep exploration wells began, funded by the United Nations Development Program (UNDP). This continued until 1977 and in 1978 production drilling commenced after a feasibility report had been published in 1977. Production drilling continued until 1981, when sufficient resource was confirmed for the installation of the first power plant, Olkaria I (Ouma, 2009). The three units that constitute the Olkaria I power plant were commissioned in 1981, 1983 and 1985, respectively, with each generating 15 MWe. The Olkaria I power plant is located within the Olkaria East field and the steam fed to the turbines is tapped from wells drilled in this field. In all, 26 wells supply steam to the plant (Ouma, 2011). Excess steam obtained through drilling of more production wells in this field and parts of the Northeast field enabled the installation of additional two units at the Olkaria I power station, units IV and V. The construction began in July 2012. Each unit generates 70 MWe. They were commissioned by the end of 2014.

The first appraisal well in the Olkaria Northeast field was drilled in 1985. This was after a scientific review of the exploration wells that had been drilled in areas around Olkaria East to verify the location of faults and fractures that were believed to enhance the flow of geothermal fluids in the area. By 1988, five additional appraisal wells had been drilled in the Olkaria Northeast field, which proved the availability of a resource (Ouma, 2011). By 1993, 33 wells had been drilled in the Olkaria Northeast field. These wells were to be used for production, re-injection and monitoring (Ouma, 2011). The estimated production capacity from these wells was about 105 MWe. The construction of Olkaria II unit 1 and 2 power plant, which is located in the Olkaria Northeast field, began in September 2000 and was completed at the end of November 2003. Each unit produces 35 MWe. With continued drilling, unit 3, which produces 35 MWe, was commissioned in 2010. The Olkaria II power plant produces a total of 105 MWe.

The Olkaria Southwest field, also known as Olkaria West, has been developed by an independent power producer (OrPower Inc.). Appraisal and production drilling was carried out in this field by the OrPower company between February 2000 and March 2003. Nine wells were drilled, which proved the availability of adequate steam to produce 48 MWe for the Olkaria III power plant. A 12 MWe binary pilot power plant was installed in September and December 2000 in units of 8 MWe and 4 MWe, respectively. The remaining 36 MWe

were commissioned by the end of 2008. Continued production drilling saw the installation of another unit, thereby increasing the power production to 110 MWe by February 2014.

The first exploration wells drilled in Olkaria Central had inverted temperature profiles and low-enthalpy fluid. Three more wells were drilled between 1994 and 1997. All of them had inverted temperature profiles with only one well being able to discharge. Oserian Development Company Ltd utilizes 2 MWe from Olkaria Central in the form of steam from one well leased from Kenya Electricity Generating Company (KenGen). It has a single unit binary plant. The plant, which was commissioned in 2004, provides electricity for farm operations.

Exploration wells drilled in Olkaria Northwest showed poor results. Oserian Development Company utilizes steam from one well leased from KenGen to fumigate green houses, enrich soils with CO_2, and to heat fresh water with the use of heat exchangers.

The first well drilled in the Olkaria Southeast field showed poor results. More geophysical work was carried out and more wells sited. Currently appraisal drilling is on-going in this field to explore the size and availability of a resource in this part of the area.

Geo-scientific studies in the Domes area were carried out between 1992 and 1997. Exploration drilling took place in 1998 and 1999. Three wells (OW-901, OW-902, and OW-903) were drilled (Ouma, 2011). All the three wells were successful and able to discharge. Further geophysical work coupled with a review of data from the three wells resulted in the siting of six appraisal wells in 2007. These were deviated wells and were drilled to a depth of between 2800 m to 3000 m. All of the six wells showed good results with some of them encountering temperatures as high as over 300 °C. The data from these wells aided in the siting of production wells. At the end of 2011, about 30 wells had been drilled in the Domes field. Data from these wells proved the presence of enough steam to support a 180 MWe power plant. Construction of a 140 MWe power plant, known as Olkaria IV, began in July 2012. The power plant was commissioned in October 2014 and is currently connected to the power grid.

The time from the drilling of geothermal wells until a geothermal power plant can be connected to the grid is considerably long. To make better use of this time, KenGen decided to employ geothermal wellhead generator technology to utilize steam from drilled production wells even before the geothermal power plants are constructed. Wellhead generators are small power producing units with generation capacity of between 5 MWe and 10 MWe. As of March 2015, 49.6 MWe from wellhead generation had been installed with 32.8 MWe being generated in the Domes field, while 17.8 MWe were generated in Olkaria East. KenGen plans to put in place wellhead generating units producing a total of 128 MWe by December 2015. Five of these units are currently being installed in the Domes field.

2 Geological setting

2.1 Regional geology

The East Africa Rift System (EARS) is divided into two branches, the eastern branch and the western branch. The western branch runs through Uganda, Rwanda, Democratic Republic of Congo and Tanzania, where it joins the eastern branch. The eastern branch runs from the Red Sea in the Afar region, through Djibouti, Ethiopia, Kenya, Tanzania and then fading off in Beira in Mozambique. The Kenyan Rift forms part of the eastern branch of EARS (Figure 4). The evolution of EARS dates back 30-45 Ma. The evolution of the Red Sea-Ethiopian rift is connected to the long-term kinematics of three major plates; the Nubian, Somalia and Arabia plates (Corti, 2011), beginning 45 Ma ago. Corti (2011) states that this rifting process was enhanced by the start of the Afar plume. Moreover, the extension of the rift from Northern Kenya all the way to Beira in Mozambique is proposed to have been enhanced by the start of the Kenyan plume, which dates back to 30 Ma. This plume exploited the weak collision zones at the contact between the Archean Tanzanian craton and the Proterozoic orogenic belts (Smith and Mosley 1993). Magmatism began at the Turkana rift in the north, migrating southwards through central to southern Kenya, to the eastern margins of the Tanzanian craton, finally reaching Beira in Mozambique 5-8 Ma ago. Magmatism also propagated north of Baringo in the Kenyan rift valley (Macdonald et al., 2001).

Magmatism related to the Kenyan Rift started during the Miocene about 30 Ma at the Turkana Rift. This was initiated by a north to south elongated crustal up warping, known as the Kenyan Dome (Baker et al., 1972; Bechtel et al., 1987). Baker and Wollenberg (1971), Williams (1972) and Hay and Wendlandt (1995) observed that phonolitic fissure flows occurred on the crest of this up warp. These are considered to be the most extensive and chemically homogeneous lava flows in the rift. The estimated volume of the phonolites in the Kenyan Rift is about 25,000 km^3 (Baker et al., 1972). Volcanism off the rift axis is believed to have taken place concurrently with the rifting process during the Quaternary period. This off-rift volcanism resulted in the formation of Mount Kenya, Chyulu Hills and Huri Hills found on the eastern flanks of the rift.

After the Miocene eruptions, the resulting lavas were affected by faulting events. This was followed by massive and extensive Pliocene eruptions and successive faulting episodes. These faulting episodes produced high-angle normal faults within the rift floor. These massive and extensive eruptions and the subsequent faulting episodes have been divided into four main phases (Baker et al., 1988). The first phase was the eruption of the Mau-Kinangop tuffs and ash flows that are mainly characterised by trachytic ignimbrites. These

eruptions are estimated at about 22,000 km^3 in volume (Baker et al., 1972). The faulting episode that occurred after the ignimbritic eruptions converted an earlier half graben to a full graben.

The developing graben was associated with fissure flow eruptions of trachytes, basalts, mugearites and benmoreite. The second phase was initiated by faulting of the eruptives that filled the developing graben, coupled with progressive inward migration of the fault zones. This resulted in the formation of step-faulted platforms (Mau escarpments) accompanied by fissure eruptions of the Limuru flood trachytes (Baker et al., 1988). The third and fourth phases occurred during the Quaternary. These two phases were triggered by block faulting which created high-angle normal faults within the rift floor. These fractures served as conduits for the Quaternary volcanic eruptions of mafic to felsic composition. The third phase is mainly characterised by basalts (estimated at about 11,000 km^3), and the fourth by basaltic trachyandesites and trachyandesites (estimated at about 3,000 km^3). The spreading rate of the EARS is estimated at 2.6 cm/year in the Red Sea, about 1 cm/year in Afar, 0.7 cm/year in the Ethiopian Rift, and 0.5 mm/year in the Western and Eastern Rifts (Jestin et al., 1994).

Crustal thickness overlying the Kenyan Dome is 30-35 km (Mechie et al., 1997). Geophysical studies, for example by Keller et al. (1994) and Simiyu and Keller (1997), indicate that a mantle material of low density and low seismic velocity lies below the rift. This mantle comes close to the base of the crust at 35 km. Other studies have indicated this to be the asthenospheric mantle (Latin et al., 1993).

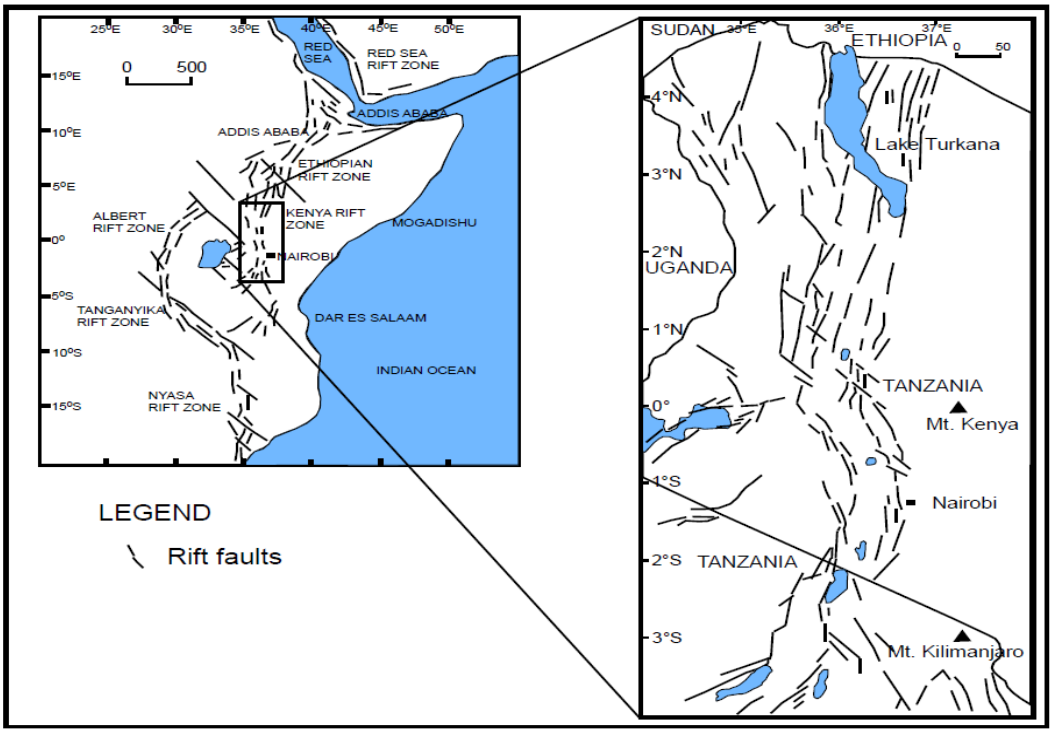

Figure 4: The Kenyan Rift Valley within the East Africa Rift system (from Dunkley et al., 1993).

It has been proposed that the convecting asthenospheric mantle was the driving force of the EARS rifting initiation (Baker and Wollenberg, 1971). The basis of this model is the fact that volcanism preceded the major rift faulting episodes. Marshall et al. (2009) also argued for the convecting asthenospheric mantle as the driving force based on geochemical analysis of rocks from the EARS.

Seismic studies indicate that the most intense volcanism took place within the central sector of the rift (Henry et al., 1990; Simiyu et al., 1995; Simiyu and Keller, 1997). The estimated thickness for the volcanic succession in this region is on the order of 5 km. Stratigraphic correlation determined by Baker at al. (1972) and data from geothermal wells (up to 3 km deep) also point to this thickness.

Various researchers have put forth different hypotheses to explain the origin of the intermediate to felsic lavas from the Miocene to the present. Weaver et al. (1972), Ferrara and Treuil (1974), Baker et al. (1977), Latin et al. (1993) and Class et al. (1994) propose that the lavas evolved from partial melting of the upper mantle, followed by fractional crystallisation. They carried out trace element and isotopic studies to support their arguments. Latin et al. (1993) argued that such large volumes cannot be produced by crustal anatexis. They associated the large volume of eruptives to partial melting of the mantle within the asthenospheric plume. The volume of eruptives associated with EARS rifting process is approximately 220,000 km^3 (Williams, 1972).

On the other hand, Hay et al. (1995a) and Hay and Wendlandt (1995) argue that the petrogenesis of the plateau phonolites is by partial melting of alkaline basalt in the lowermost part of the crust. Strontium isotope ratios ($^{87}Sr/^{86}Sr$) of the plateau phonolites are characteristic of either an enriched mantle or crustal contamination of mantle derived magmas. This model may not be feasible because it requires the existence of basaltic "underplating" prior to petrogenesis of the phonolites, while the volcanic activity that preceded the phonolite flows was minimal (Baker et al., 1972; Latin et al., 1993) and unlikely to be sufficient to have developed the required basaltic "underplating". Therefore, the presence of this sequence remains questionable. Nash et al. (1969), and Goles (1976) proposed that the generation of phonolite was by fractional crystallisation of basalts associated within the Kenyan rift.

Controversy has equally been raised concerning the petrogenesis of the felsic rocks within the rift. Two hypotheses regarding their origin have been put forth; on the one hand, generation by crustal anatexis and, on the other, by fractional crystallisation. Davies and Macdonald (1987) using the results of Sr and Nd isotope studies proposed that the Olkaria comendites have been derived from crustal melts at 6 km depth. Macdonald et al. (1987) interpreted major and trace elements data to show that closed system fractional crystallisation alone could not account for compositional variations in the rhyolites. They favoured a model of partial melting of heterogeneous crustal source rocks, followed by crystal fractionation with volatiles promoting peralkalinity and affecting trace element distribution patterns. Black et al. (1997) also favoured anatexis of Precambrian crust for the generation of the comendites. In contrast, Black et al. (1997) considered the felsic magmas to be products of protracted crystal fractionation of basaltic parents. They used $^{230}Th/^{232}Th$ ratios and showed that the initial Olkaria peralkaline rhyolites have initial $^{230}Th/^{232}Th$

ratios (~0.73-0.77) lower than the Olkaria basalts (0.88-~1.2). This confirmed that the basalts and rhyolites were not part of a cogenetic suite.

2.2 Geology of GOVC

The geology of the Olkaria Volcanic Complex and its surrounding area has been well documented by Clarke et al. (1990). GOVC is a young (≤20 ka) multi-centered complex dominated by peralkaline rhyolite domes and lavas on the surface (Marshall et al., 2009). The GOVC is located in the south-central Kenyan rift, where the orientation of the rift changes from a NNW-SSE orientation in the north to a N-S in the south. The width of the rift here is estimated at 60-70 km. Approximately 80 small volcanic centres have formed within this complex. These volcanic centers are structurally controlled and formed by eruptions through fault zones. The centres occur either as steep-sided domes, formed of lavas and/or pyroclasts, or they occurs as thick lava flows of restricted lateral extent. The Olkaria Complex is Quaternary in age and is bounded by three other volcanic complexes within approximately 40 km distance. Eburru is located to the north, Longonot to the east and Suswa to the south. To the west, the Olkaria Complex is bound by the western rift margin. Whereas the surrounding complexes have clearly defined calderas, Olkaria volcanic complex does not have an obvious caldera. However, Clarke et al. (1990) observed the existence of a ring of rhyolitic domes to the east, south and southwest of the Olkaria complex to indicate a possible caldera. These rhyolitic domes form along a ring fracture, which is part of the proposed caldera rim. Seismic studies indicate anomalies that coincide with this proposed caldera rim (Simiyu et al., 1998). However, this hypothesis has drawn a fair amount of criticism. Studies of subsurface geology indicate the absence of ignimbrites, which tend to be associated with caldera collapse (Omenda, 1998). Resistivity studies conducted by Onacha (1993) have equally failed to record any anomalies at the proposed caldera rim.

2.2.1 Surface geology and the evolution stages of GOVC

Clarke et al., (1990) described the surface geology of GOVC. The surface geology comprises pumice lapilli, ash deposits, pyroclasts and comenditic lava flows (Figure 5). The pumice lapilli is mainly found in the western and south-western parts of the Olkaria geothermal field. The ash deposits and pyroclasts are unconsolidated and vary from weakly to highly weathered. They are also oxidised as a result of interaction with cold groundwater flow making them brown in colour. They cover most of the Olkaria geothermal field with a relatively thick deposit in the Domes field as observed from data from geothermal wells. A large fraction of pumice (LP^1 to LP^8 in Figure 6) and pyroclastic deposits in Olkaria field are said to have originated from Longonot volcano (Clarke et al., 1990). Longonot volcano is located about 20 km east of Olkaria. Analysed data from the old pyroclastic deposits in Olkaria show that they originated from Olkaria, Longonot and perhaps Suswa, which is located 40 km south of Olkaria. Suswa volcano has been active during the same period as Longonot and Olkaria (Clarke et al., 1990). However, the contribution of each of these volcanic centers to the pyroclastic deposits has not been quantified. The Olkaria

geothermal complex is the only area within Kenyan rift with comendites on the surface (Macdonald et al., 2008). The comendites are mostly exposed in the Olkaria East area.

On the basis of their geological work, Clarke et al. (1990) outlined the evolution of GOVC together with the surface geology of the surrounding areas. On the basis of the age of the highstands of the local lakes, they placed the initiation of evolution for GOVC at 22-20 ka BP. They then divided the evolution of GOVC into six stages.

Formation of the Olkaria Trachyte Formation (Ot) and the Maiella Pumice Formation (Mp) characterised the first stage (Figure 6). The pumice formation, which is believed to have erupted from vents within the complex, is mainly found to the west of the complex, while the Olkaria Trachyte Formation is found to the southwest of the complex, where it is mainly exposed in gullies and ridges.

Stage 2 was characterised by caldera collapse according to Clarke et al. (1990). This was based on the field evidence of a well-developed ring structure, the presence of a ring of rhyolite domes, intra-ring volcaniclastic sediment, apparent resurgent activity within the ring structure, and the distribution of fumaroles. This left a depression of 11 km by 7.5 km. The caldera collapse was accompanied by the eruption of welded pyroclastic rocks of Ol Njorowa Pantellerite Formation (O^1). This formation is only exposed in the deepest parts of the Ol Njorowa Gorge.

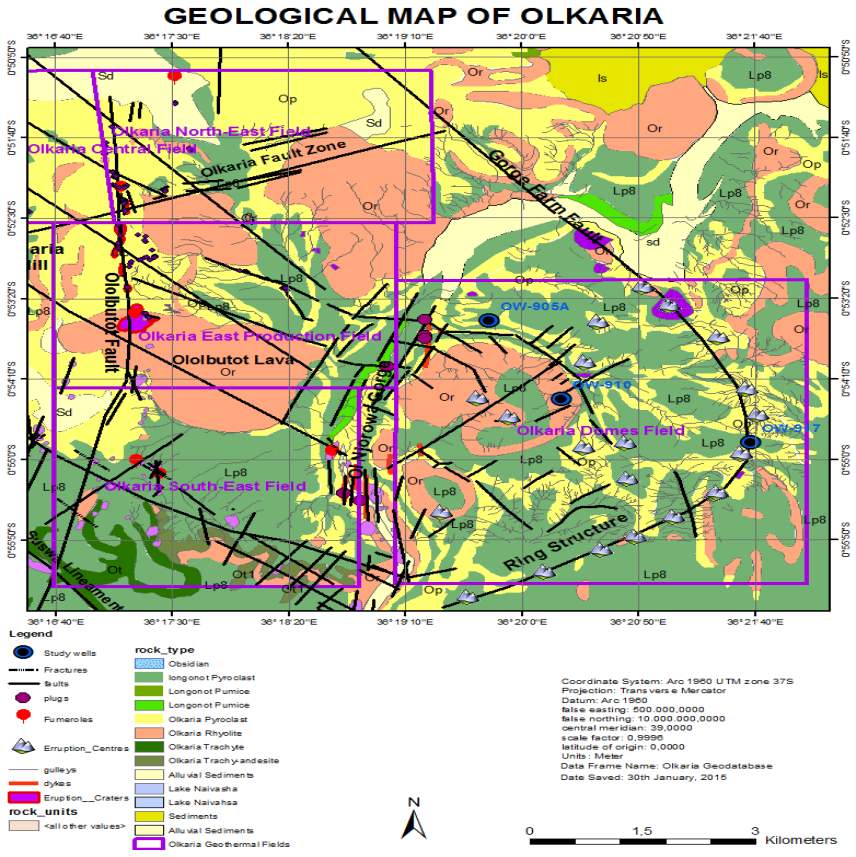

Figure 5: Surface geology and structures of Olkaria geothermal area (Modified from Clarke et al., 1990).

Stage 3 was characterised by post-caldera magmatism. The magmatism deposited the Lower Comendite Member of the Olkaria Formation. This comprises rhyolite lavas (O^2) and pyroclastics (Op^2). The Formation has been dated at >9150±110 BP.

Stage 4 was a period of ring dome formation (O^3) and eruption of thick surge deposits (Op^3). This stage is associated with the deposition of the Middle Comendite Member. The age dates for this member are between 9150±110 and 3280±120 BP (Clarke et al., 1990) based on ^{14}C dates.

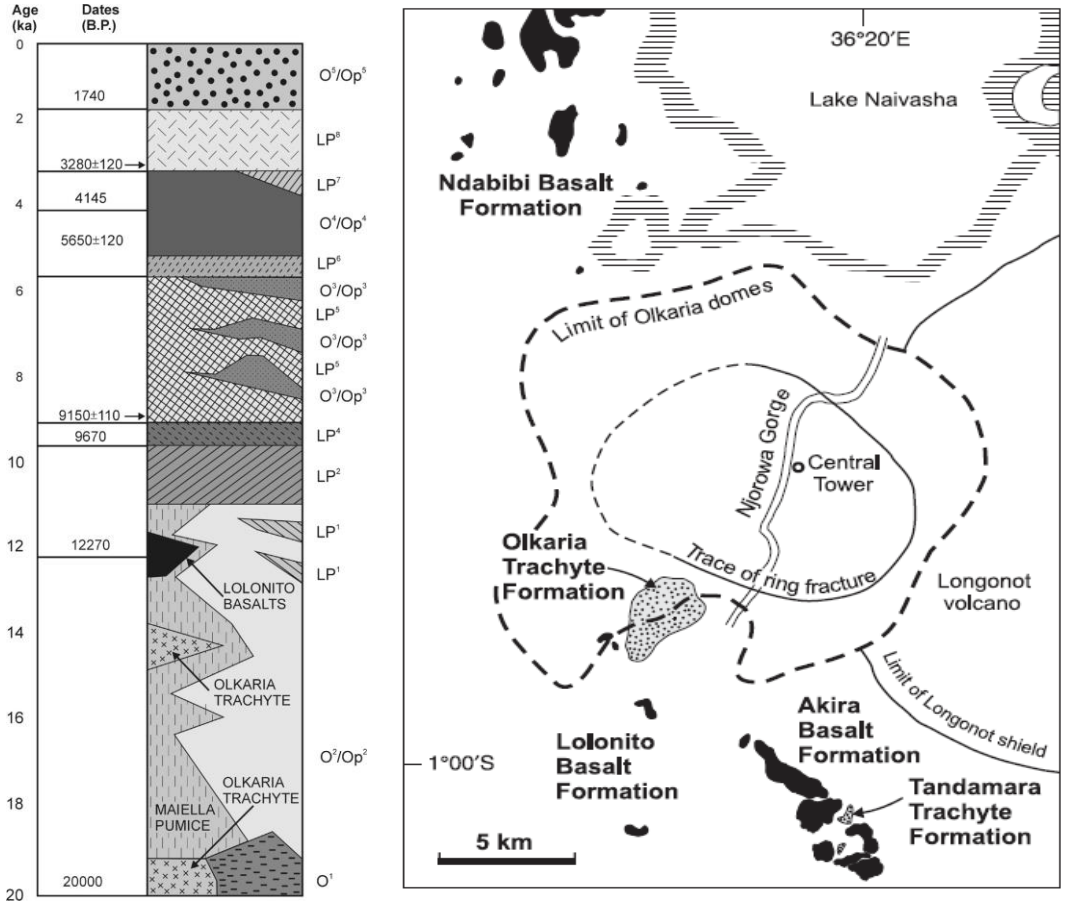

Figure 6: Stratigraphic column (from Marshall et al., 2009) for the GOVC and its surface formations (from Clarke et al., 1990) (together with the surrounding areas).

Stage 5 involved the resurgence of the caldera floor, accompanied by the formation of short and thick comenditic lava flows that constitute the Upper Comendite Member (O^4) (Figure 6).

Stage 6 involved the eruptions of comendite lavas from a north-south fissure system (O^5). The eruptions were characterised by very thick flows. The youngest of the comendite flows (Ololbutot lava) has been ^{14}C dated 180±50 BP.

To the south of the Domes field, lava flows and pyroclastic cones occur, forming the Lolonito Basalt Formation (Ba^1) (Figure 6). Eruption age for this formation has been placed at <0.45 Ma (Clarke et al., 1990). This Formation is believed to represent an earlier

phase of the younger Akira Basalt Formation (Ba). The Akira Basalt Formation mainly consists of lavas, scoria and spatter cones.

The Tandamara Trachyte Formation (Tt) is composed of welded scoriaceous lapilli and blocks of rheomorphic ignimbrite. The formation is geographically associated with and has the same general age as the Akira Basalt Formation (Clarke et al., 1990).

To the north of the Domes field, an 11 km wide low-lying area between the Olkaria and the Eburru Volcanic Complexes forms the Ndabibi plains. Mafic volcanism accompanied rhyolite emplacement on these plains. The Ndabibi Basalt Formation (Bn) is comprised of older faulted lavas and pyroclastic cone units of pre-caldera age and younger units of Surtseyan tuff cones (kBt) with equivalent fall tuffs (kBtm) and transitional Surtseyan-strombolian ash cones (Bt). These younger units are largely contemporary with the post-caldera rhyolites dated <20 ka BP.

2.2.2 Petrochemistry of the surface rocks of GOVC

Macdonald et al. (2008) carried out geochemical analysis on surface rocks from Olkaria Volcanic Complex and its surroundings. Their aim was to determine the chemical composition of these rocks, re-examine the petrogenesis of peralkaline rhyolitic magmas and to determine the role of fractional crystallisation, magma mixing and re-mobilisation of pre-existing material in the evolution of the basalt-trachyte suite. In their study, they collected samples from the Olkaria and Tandamara Trachyte Formations (9 and 3 samples respectively), the Lolonito, Akira and Ndabibi Basalt Formations (6, 4 and 16 samples respectively), the Olkaria Comendite Formation (6 samples) and magmatic inclusions (34 samples) in the post-caldera comendites. The magmatic inclusions are mainly basaltic and trachytic magmas, which together with benmoreites and mugearites forms an extensive suite of inclusions in the rhyolites in the GOVC.

From this analysis, they divided the rocks into three groups (Figure 7). In the TAS classification scheme (Figure 7), Group 1 rock type range from basalt-hawaiite-mugearite-benmoreite-trachyte to rhyolite (Macdonald et al. 2008). The basalts are close to silica-saturation while the trachytes are mainly metaluminous. However, five trachyte samples were found to be mildly peralkaline. No compositional variation was discerned from the mafic rocks of the Akira, Lolonito and Ndabibi Formations. MgO plots for this group indicate that with decreasing MgO abundance, there is increase in SiO_2, Na_2O, K_2O, Ga, Rb, Nb, Ta, Light Rare Earth Elements (LREE), Mo, Sn, Zr, Hf , Th and decrease in CaO, Ni, Cr, Co, V and Sc (Figure 8). FeO, TiO_2, P_2O_5, Li and Sb abundances peak at ~3-4% MgO (Figure 8). A comparison of incompatible trace element ratios shows their tendency of remaining constant (for example Zr/Nb, Zr/Y, Ce/Y, Ce/Zr, Rb/Zr and Th/U) in the range of basalt-benmoreite, while showing greater ranges in the trachytes. Rocks in Group 1 showed a significant range of many elements at any given MgO value (Figure 8). Macdonald et al. (2008) stated that there were several lines of descent during magma evolution. This variability was enhanced by basalt-basalt (or hawaiite) mixing and mixing between various combinations of benmoreite, trachyte, mugearite and rhyolite in the more evolved rocks. The mixing caused variation similar to those from crystal-melt process. This makes it difficult to quantify the mixing.

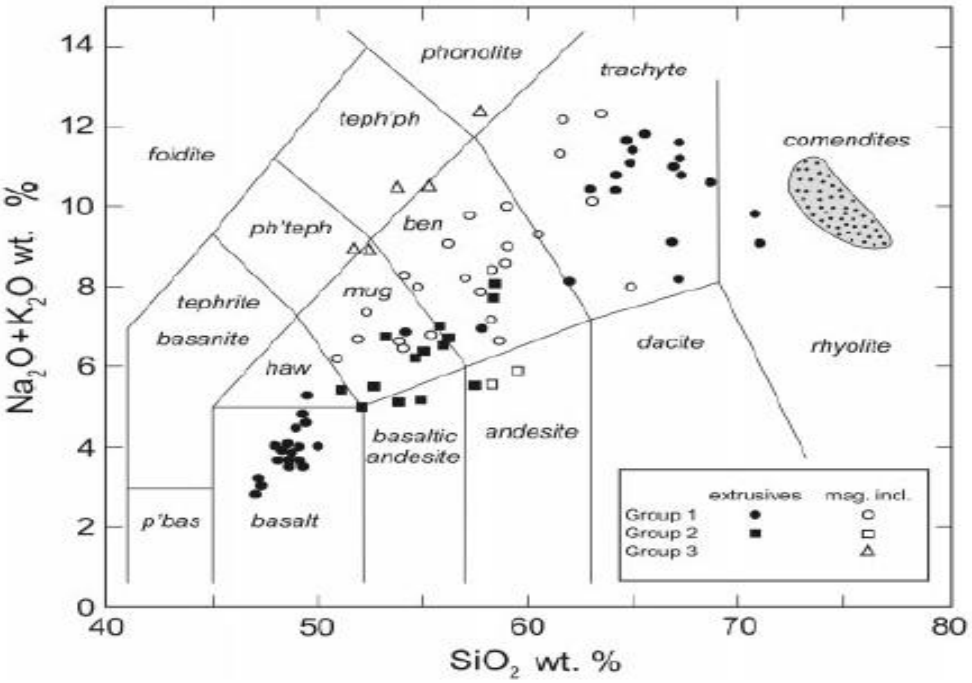

Figure 7: TAS classification scheme for GOVC surface rocks. Extrusives include high-level dykes and plugs, bombs and blocks in pyroclastic deposits (from Macdonald et al., 2008).

Macdonald et al. (2008) also used Thornton-Tuttle Differentiation index (DI) to further establish reason for the scatter. The DI was used to infer about the differentiation processes of the trachytes and rhyolites. The MgO plot fail to show what processes are taking place of the more evolved compositions. Hence the use of DI to infer these processes. He found out that with increasing DI, there was an overall increase in SiO_2, Al_2O_3, K_2O, Zr, Nb and the LREE while there was a decrease in TiO_2, FeO, MgO, CaO, P_2O_5, Ba, Sr, Y and Na_2O/K_2O (Figure 9). No systematic compositional differences were noted between the Olkaria trachytes, Tandamara trachytes and the trachytic melt inclusions. However, the trachytic melt inclusions are slightly less evolved than the Olkaria and Tandamara trachytes. The trachyte trends included metaluminous to peralkaline types indicating trachytic magma evolution along several lineages close to alumina under saturation (Macdonald et al., 2008). The relationship between trachytes and the least evolved post-caldera comendites is shown in Figure 9. The Differentiation Index (DI) plots show that comendites generally lie on an extension of the trachyte field. This is typical of a crystal fractionation relationship. Major element variations in this group are consistent with the fractionation of an olivine-clinopyroxene-plagioclase assemblage in the range 8-3.5 wt% MgO, clinopyroxene-plagioclase-FeTi-oxides-apatite from 3.5 to 1.5 wt% MgO and sanidine-clinopyroxene-FeTi-oxides-apatite±olivine in the trachytes.

Group 2 has a bulk composition ranging from hawaiite-benmoreite. However, it is compositionally different from Group 1, formed by the mixing of basaltic and trachytic or rhyolitic magmas. It is stated that mingling was more common than complete hybridization in this group. This may have been as a result of insufficient time for complete mixing or density and viscosity barriers. Group 3 samples are mainly magmatic inclusions and are silica-undersaturated. The compositional trends of group 2 and 3 samples in the TAS

classification scheme (Figure 7 and 10), together with their compositional features, correlate with mafic and trachyte/rhyolitic magma mixing (Macdonald et al., 2008). However, in many cases, the presence of feldspar xenocrysts makes it a three-component calculation. When compared to Group 1 rocks of similar MgO values, *ne*-normative rocks of Group 3 had higher Na_2O, Rb, Th and REE. They also show a modest LREE ($[La/Yb]_{CN}$~9) enrichment. These rocks provide evidence of extensive interaction with the host comendites.

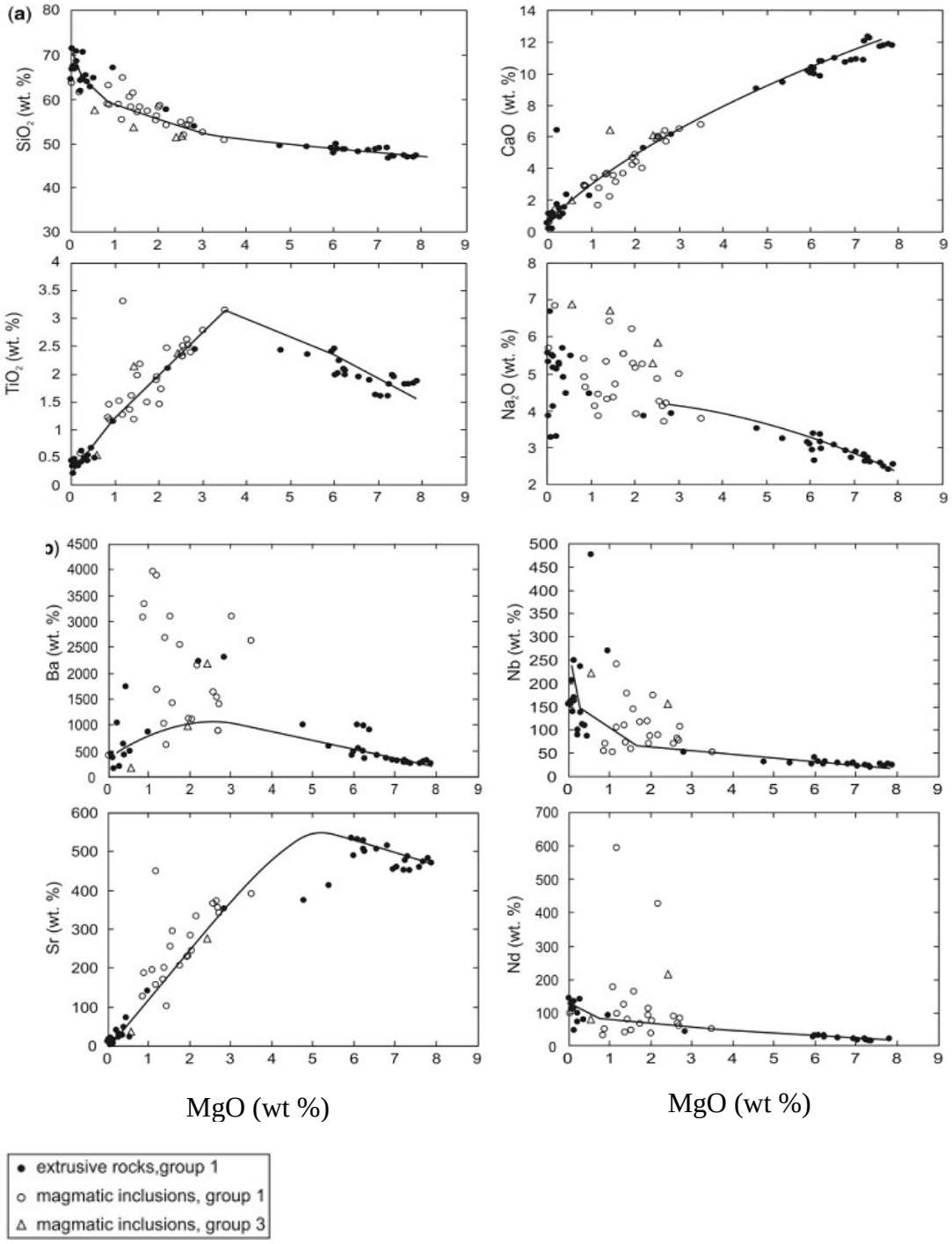

Figure 8: MgO plots against major and trace elements (from Macdonald et al., 2008).

Macdonald et al. (2008) suggested that there has been selective diffusion into the magmatic inclusions of a Na-F-rich fluid. This imparted, *inter alia*, a *ne*-normative, and in other cases peralkaline character to these rocks. Rocks in this group range from close to peralkaline (Peralkalinity Index of 0.94-0.95) to clearly peralkaline (Peralkalinity Index of up to 1.39). From this analysis, Macdonald et al. (2008) concluded that crystal fractionation of basaltic magmas generated mugearitic magmas. Mixing between basaltic magmas was common. Post-caldera comendites, benmoreitic and trachytic magmas of group 1 and 3 were produced by further crystal fractionation along several lines of descent. Mingled and hybridized magmas were produced by two to three component mixing between mugearites, benmoreites and less commonly trachytes, while Group 2 rocks were generated by basalt-trachyte/rhyolite magma mixing.

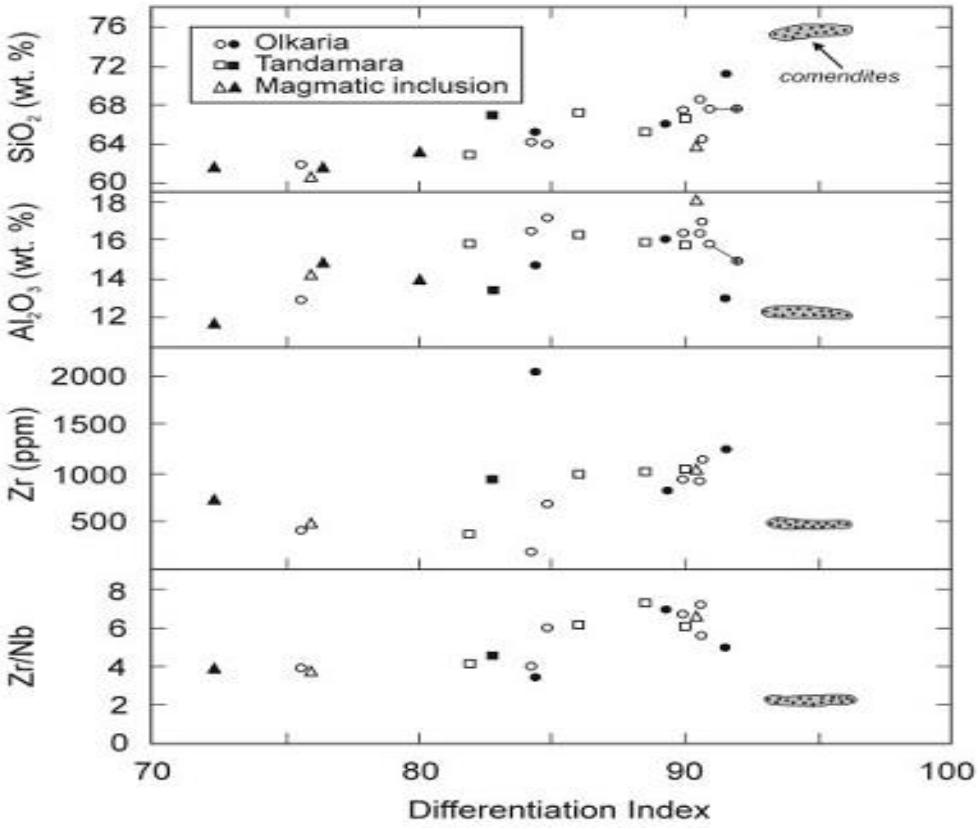

Figure 9: SiO_2, Al_2O_3, Zr abundance and Zr/Nb ratio in Olkaria trachytes as a function of Thornton-Tuttle Differentiation Index. Open symbols represent ac-normative while the dark shaded symbols represent an-normative v arieties. Shaded field represents the least evolved GOVC comendites (from Macdonald et al., 2008).

The system is said to be quite dynamic where crystals with a variety of growth and resorption histories have been juxtaposed shortly before being erupted. Repeated occurrence of different magma eruptions over short periods indicates a plumbing system with several small and independent reservoirs and conduits.

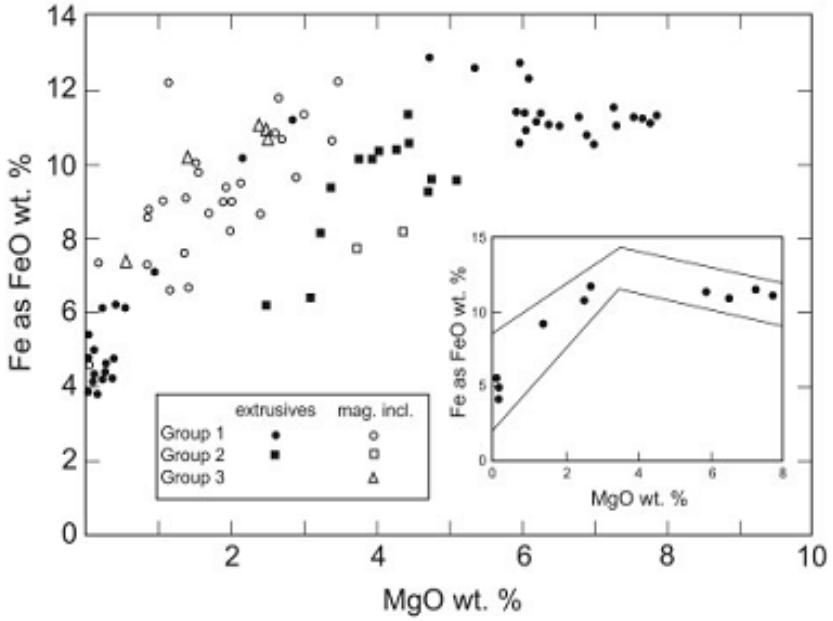

Figure 10: MgO plots against FeO for Group 1, 2, 3 extrusives (high-level plugs, dykes and bombs and blocks) and magmatic inclusions. The plot in the inset incorporates Group 1 rocks in the main plot (from Macdonald et al., 2008).

2.2.3 Sub-surface geology of the GOVC

The sub-surface geology of GOVC has been documented mainly from studies of drill cuttings obtained from geothermal wells. The sub-surface geology is divided into six litho-stratigraphic units (Figure 11). The uppermost one is the Upper Olkaria Volcanics. They are mainly comenditic lavas and their pyroclastic equivalent. Minor trachyte and basalt are also intercalated. Ash from Suswa and Longonot also form part of this unit (Omenda, 1997; Clarke et al., 1990). They are the youngest eruptives and occur from the surface down to 500 m depth. The Ololbutot comendite is the youngest lava of the Upper Volcanics, having been dated 180±50 years BP (Clarke et al., 1990).

The second unit is the Olkaria Basalt which mainly occurs between 500 m to 1000 m depth. The rock units in this stratigraphic interval include basalt flows, minor pyroclastics and trachyte. It forms the Olkaria geothermal system cap rock (Ambusso and Ouma, 1991).

The third unit is the Plateau Trachytes. These occur between 1000 m to 2600 m depth and form the reservoir rock of the Olkaria East field where they are the thickest. The unit is mainly composed of the trachyte with minor basalt and tuff intercalations.

The Mau Tuffs form the fourth unit. The tuffs are mainly consolidated and have ignimbritic texture. They form the reservoir rocks of the Olkaria West field (Omenda, 1998). They are the oldest exposed rocks in the Olkaria area.

The other two stratigraphic units are neither exposed in Olkaria area nor encountered in geothermal drill holes within Olkaria. However, they are exposed on the southern flanks of the rift. The Pre-Mau Volcanics, which form the fifth unit, are composed of trachytes,

basalts and ignimbrites. The Proterozoic Formation is the sixth unit. It forms the basement rock. It comprises amphibolite grade gneisses and schist with associated marble and quartzite of the Mozambican Group (Shackleton, 1986). Figure 12 shows the rock units and the stratigraphic correlation of drilled wells between the Olkaria East (OW-8, OW-9, OW-19 and OW-22) and the Domes field (OW-901, OW-902, and OW-903).

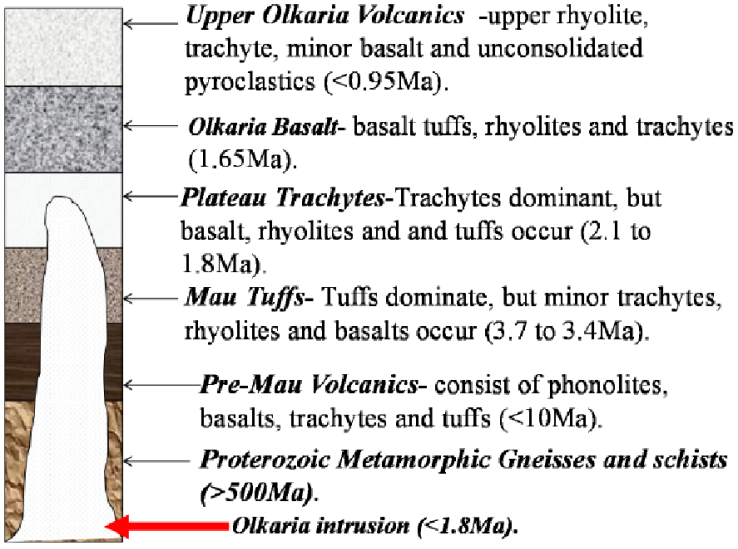

Figure 11: Stratigraphic column and age span of the Greater Olkaria Volcanic Complex (Omenda, 2000; modified by Musonye, 2012).

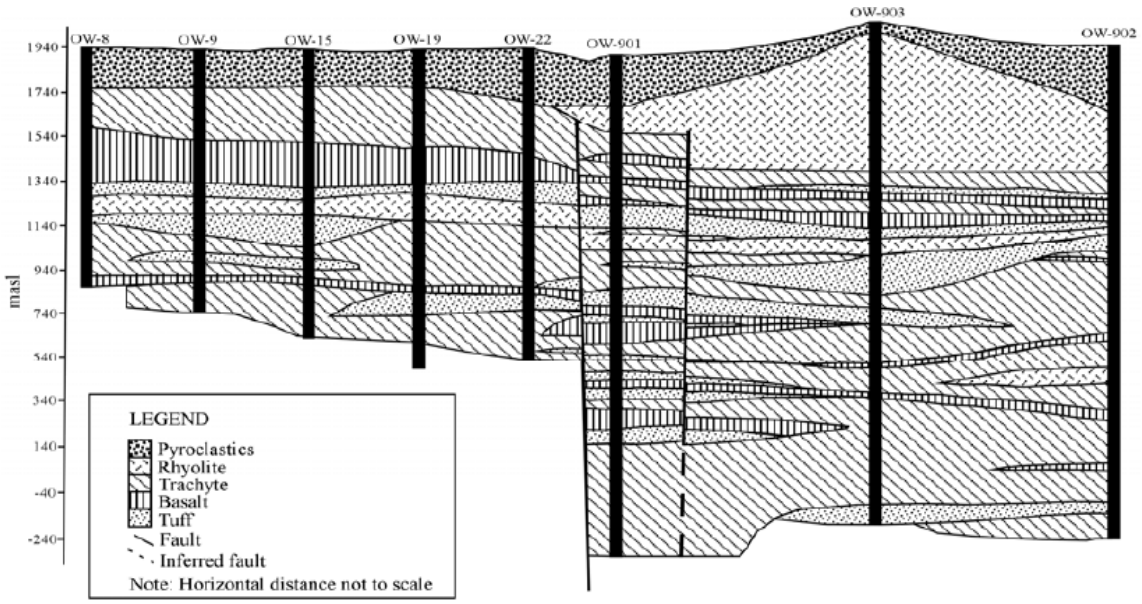

Figure 12: Rock units and stratigraphic correlation of drilled wells in Olkaria geothermal area (from Lagat, 2004).

2.3 Structures of the GOVC

The GOVC is located on the floor of the rift valley in the south central part of the Kenyan Rift. The complex is located at a point where the rift valley forms a bend from a NWW-SSE orientation to the north of this complex to a N-S orientation to the south of this complex (Figure 13 a). The main tectonic structures in GOVC include faults, fractures, the Ol Njorowa gorge, the ring structure and dyke swarms. The structures are the main controls of geothermal fluid movements. The faults are observed on the surface in the West, East and Northeast fields. They are absent in the Domes area due to the thick pyroclastic cover. However, buried faults have also been encountered in Domes as well as the Olkaria area in geothermal wells (Mungania, 1991). This is deduced from total loss of circulation returns, cave-ins, stratigraphic correlations and occasional collapse of wells during drilling. Lagat (2004) identified buried normal faults between the Olkaria East and the Domes area by correlating wells in these two fields (Figure 13 b). He also identified faults within the Domes area between wells OW-901 and OW-902. These faults have resulted in a down throw of about 300 m.

The main faults in GOVC are the ENE-WSW Olkaria fault, and NNE-SSW, N-S, NW-SE and WNW-ESE trending faults (Figure 13). The N-S and NNE-SSW faults and fractures are the youngest. The Ololbutot fissure is the most prominent of these structures, which are characterized by intense fumarolic activities. This indicates vertical permeability along the fault (Omenda, 1998).

The NW-SE and WNW-ESE striking faults are thought to be old and associated with rift development. The most prominent of them is the Gorge Farm fault, which bounds the geothermal field in the north-eastern part and runs all the way to the Domes field (Muchemi, 2000). The Suswa fault which trends NW-SE, crosses the SW corner of the geothermal area.

The Olkaria fault is interpreted as an old rejuvenated fault (Omenda, 1998). This fault intersects the northern slopes of Olkaria Hill. It is oriented in the NNE direction and is characterized on the surface by a zone of intense geothermal manifestations covering a width of 50-100 m on the northern slopes of Olkaria Hill. The Ol Njorowa gorge forms a boundary between the Domes field and the Olkaria East field. The gorge is believed to have been initiated by faulting along its trend. The gorge was deepened by a catastrophic outflow of Lake Naivasha during one of its high stands (Clarke et al., 1990). Dyke swarms with a NNE orientation are mainly observed along the Ol Njorowa gorge. Volcanic plugs have also been observed along the gorge (Otieno et. al, 2014).

The arcuate alignment of domes in the southern and eastern parts of Olkaria is another main structure. This structure is proposed to indicate a buried caldera, with the rhyolitic domes being the products of a subsequent resurgence (Clarke et al., 1990; Mungania, 1999). Omenda (1998) observed that the ring might have been produced as a result of magmatic stresses in the Olkaria magma chamber. In this hypothesis, the line of weakness, which defines the ring, was the centre of rhyolitic volcanism.

a. b.

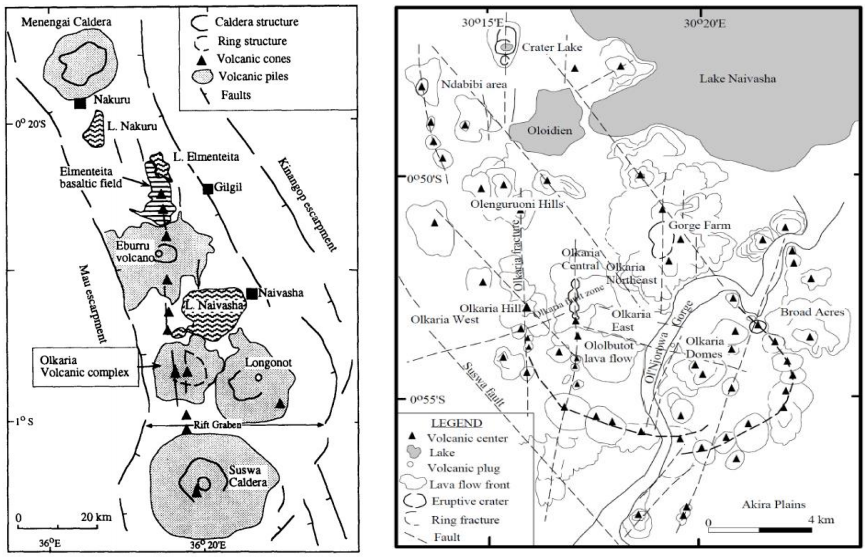

Figure 13: (a and b): A structural map of GOVC and its location within the Kenyan Rift (Omenda, 1998; Clarke et al., 1990 respectively).

2.4 Hydrogeology

The pre-Holocene faults are the main features controlling hydrologic flow in the Olkaria complex. Permeability has been enhanced in this area by recent tectonic events that caused movement along pre-existing fractures (Omenda, 1998). Studies indicate two probable sources of recharge for the Olkaria complex. The two sources are the Mau and Kinangop escarpments to the west and east of GOVC, respectively (Naylor, 1972; Ogoso-Odongo, 1986; Clarke et al., 1990 and Omenda, 1994). The water is mainly of meteoric origin. The source are the young rejuvenated N-S faults, which provide shallow recharge and control the axial groundwater flow within the geothermal system. This shallow recharge has caused temperature profile reversals, as observed in wells drilled close to the N-S trending faults.

The pre-Holocene faults provide deep recharge. The NNW-SSE and NW-SE faults are the main recharge paths. These faults are exposed on the Mau escarpment. The Olkaria fault, which trends ENE-WSW, forms one of the most important recharge channels in the Olkaria geothermal field. It transects between the Northeast and West Olkaria geothermal fields. Wells drilled to the north of this fault are liquid-dominated while those drilled to the south are liquid-dominated two-phase with an overlying steam cap (Ambusso and Ouma, 1991). The fault is pre-Holocene in age but was rejuvenated by recent tectonic events. The recharge channels for the Olkaria East and the Domes field are believed to be rift-floor faults that have not been rejuvenated (Omenda, 1998). They are not exposed in these fields due to pyroclastic cover.

Fluid flow within faulted zones is controlled by fracture permeability, while fluid flow outside fault zones is mainly horizontal and is enhanced by lithological boundaries.

Cooling joints within thick lavas provide primary permeability as well. Vesicles and vugs within the formations also enhance fluid flow within the Olkaria geothermal field. However, high susceptibility to hydrothermal alteration seals primary permeability. For example, some wells drilled in the Northwest field, where the reservoir host rock is tuff that is highly susceptible to hydrothermal alteration, have low productivity as a result of low permeability.

2.5 Geophysical exploration

The geophysical survey of the Olkaria geothermal area has been well described by Mariita (2011). Geophysical exploration has been done in the Olkaria geothermal field since the 1980s. Various geophysical techniques have been employed in the exploration, which include resistivity, seismology and gravity. The most extensively used method has been resistivity, with over 220 magnetotellurics (MT) and 160 transient electromagnetic (TEM) soundings having been done since the year 2000 (Mariita, 2009). From these soundings, low resistivity (less than 15Ωm) anomalies recorded at 1500 m a.s.l have been found to align along linear structures, mainly the NE-SW, NW-SE lineaments and the ring structure. There is also a generally low-resistivity anomaly at this depth in the Olkaria geothermal area (Figure 14). This low resistivity is attributed to low-temperature, conductive minerals, for example smectite clay. There is relatively low resistivity recorded in Olkaria West field as compared to the Northeast and East fields. The low-pH high, conductive fluids, coupled with extensively altered tuff deposits near the surface that characterize the Olkaria West field, are thought to be the cause of these relatively low-resistivity anomalies (Omenda, 2000 and Muchemi, 1999). On the other hand, the relatively high-resistivity anomalies in the Northeast and East field are attributed to high-pH fluids, coupled with less altered flood trachytes. The flood trachytes are less susceptible to alteration. Deep low resistivity in the proximity of Olkaria Hill is interpreted as a heat source for the Olkaria West geothermal field (Mariita, 2011).

MT soundings along with data from drilled wells indicate low-resistivity anomaly at 1000 m a.s.l. in the whole of the Olkaria geothermal field. This is interpreted to define the geothermal system with temperatures above 240 °C. For the East and West fields, high resistivity coincides with cold recharge areas associated with the N-S trending Ololbutot fissure and the ENE-WSW trending Olkaria fault. High resistivity is also noted in the Domes area at 500 m a.s.l, except along the ring structure. This is a result of the abundance of high-temperature, high-resistivity alteration minerals, such as chlorite and actinolite. This depth also marks the start of the reservoir zone.

Seismic monitoring of the Olkaria geothermal field started in 1985. The main purpose of the initial monitoring was to determine the seismic background of this field before full geothermal exploitation (Simiyu and Keller, 2000). The location of seismic events in geothermal areas can provide data that can be used to locate active fault zones that function as conduits for geothermal fluids. The focal depth can also be used to predict the depth of geothermal fluid circulation.

Six seismic monitoring stations were operated in the Olkaria East production field between 1996 and 1998. Simiyu and Keller (2000) interpreted these data in large part by correlation

with geological structures identified in geological studies. Seven linear alignments were noted (Figure 15). The N-S trending alignment (marked I in Figure 15) coincides with the Ololbutot fracture zone. The seismic activity along this zone may be attributed to geothermal fluid movement within the Ololbutot fissure or tectonic movements along this fissure. This fissure has been modelled as a recharge zone on the basis of downhole-temperature measurements, resistivity and geochemical signatures (Mariita, 2011). Another epicentre location (II, Figure 15) extends from SSE of the area to the centre. No mapped geological feature coincides with this trend but a buried fault is suspected to exist along this trend.

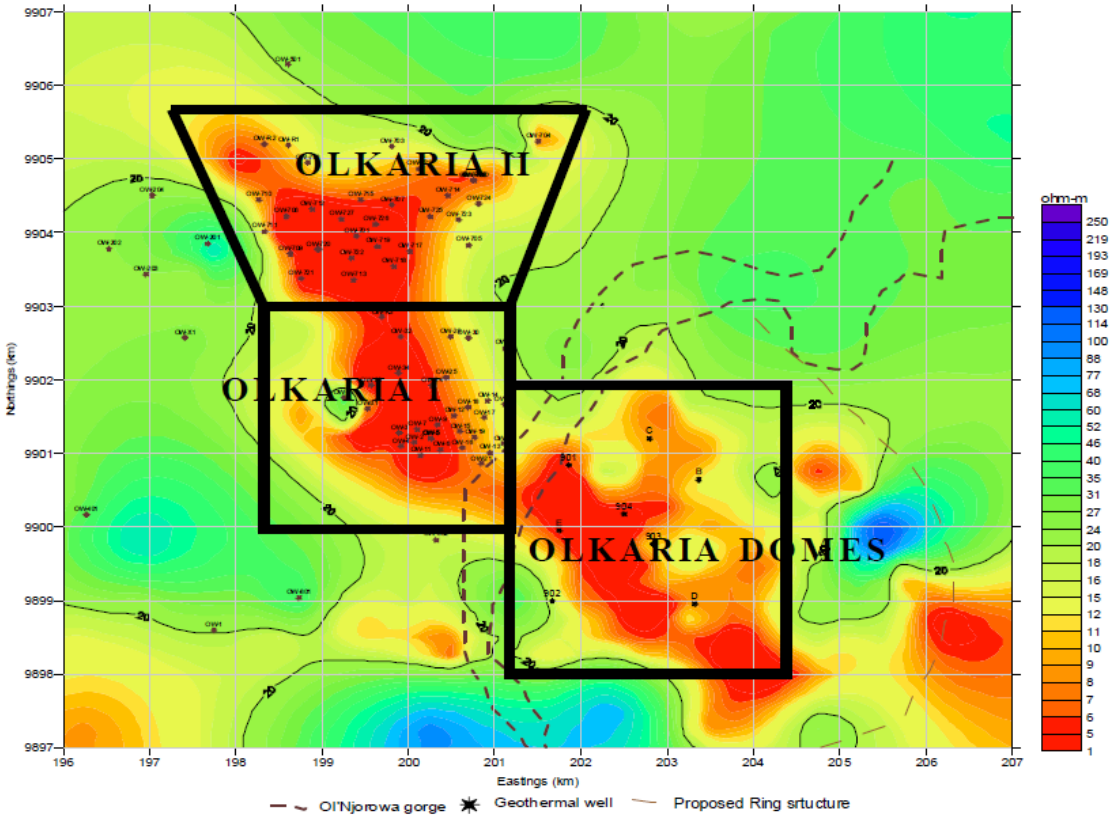

Figure 14: Resistivity distribution at 1500 m.a.s.l from TEM soundings from the Greater Olkaria Geothermal area showing Olkaria East (Olkaria I), Olkaria Northwest (Olkaria II) and the Domes field (from Ouma, 2009).

Two alignments (III and IV, Figure 15) located to the north and south of the Ololbutot lava field correlate with the two faults identified through geological mapping and gravity survey (Mungania 1995). Two other alignments trends, named V and VI (Figure 15), trend E-W to the north of Ololbutot lava field. Alignment VII is composed of events that form the NNE trend, which starts from north of the Olkaria East field. This line correlates with a NNE-SSW trending fault identified by Omenda (1998).

Shallow high-frequency seismic events and deep low-frequency events have been recorded in Olkaria West field (Mariita, 2011). The shallow high-frequency events were recorded at the intersection point between the Suswa and Olkaria faults. This is associated with an upflow zone in the Olkaria West field. There are also shallow high-frequency events and deep low-frequency events in the Olkaria East and Northeast fields and along a NW-SE

linear trend. The shallowest of these high-frequency events are associated with fluid movement and volcano-tectonic structure. The occurrence correlates with the intersection of the Ololbutot fissure and Olkaria fault. Deeper to medium-depth events along Ololbutot fissure zone have been interpreted to show fluid movement (Mariita, 2011).

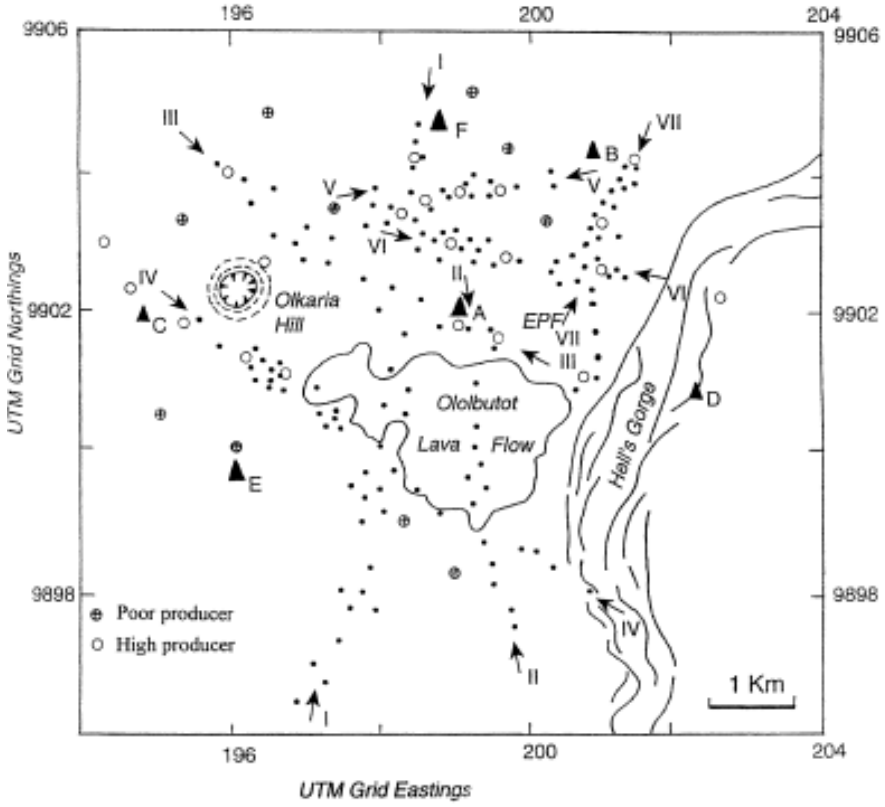

Figure 15: The six recording stations (represented by triangles), the linear alignment of the 123 epicentres (indicted by the arrows and the roman numerals) and location of geothermal wells (open circles represent high producing wells while crossed circles represent poor producing wells) (Simiyu and Keller, 2000).

3 Sampling and analytical techniques

In borehole geology and alteration mineral studies, various analytical techniques are applied. The main techniques include binocular microscope analysis, petrographic analysis, fluid inclusion analysis and X-ray diffractometry. In this study, three wells were chosen for study, OW-905A, OW-910 and OW-917. The elevation, location, casing depth and the total drilled depths are shown in Table 1. The wells were drilled between the years 1999-2014. Sampling was done at the rig during drilling, with samples collected at 2 m interval and the depth recorded continuously in a rig notebook. Depths at which losses were encountered were also recorded in the notebook.

The analytical techniques used in this study were binocular microscope analysis, petrographic microscope analysis and X-ray diffractometer (XRD) for the borehole and alteration mineralogy studies. For the study of petrochemistry, inductively coupled plasma-optical emission spectrometry (ICP-OES) analysis was applied.

3.1 Binocular microscope analysis

Binocular microscope analysis was the first analysis carried out on the drill cuttings from the wells in question. The analysis was done using a Wild Heerbrugg binocular microscope at the Iceland GeoSurvey (ÍSOR) laboratory. The technique is a visual method where samples are observed under a binocular microscope. The samples were each scooped from the sampling bags into petri dishes. To remove dust, enhance visibility and reveal obscured features such as finely disseminated sulphides (e.g. pyrite), each sample was first washed in water. The sample was then mounted on the microscope stage. The main properties studied under the binocular microscope include the primary rock forming minerals, alteration minerals, colour of the rock cuttings, rock fabrics, vein fillings, porosity, texture and grain size, intensity of alteration and the rock type. The mineral paragenetic sequence is also determined with the use of the microscope in cases where the vesicles or veinlets have not been destroyed by the drill bit. Drill cutting analysis is challenging compared to core sample analysis. The composition of drill cutting samples, especially from greater depths, may not be representative of the rocks penetrated at that particular depth. The considerable length of time it takes for samples from greater depths to reach the surface means that the recorded depth is deeper than the actual sample depth. Mixing of cuttings from different depths by the circulation fluid, especially when there are soft formations at shallower depths, also complicate identification of different lithological units. Furthermore, the crushing of the rocks by the drill bit leads to loss of detailed geological features. These complications have to be accounted for during binocular analysis. After the binocular analysis, representative samples from the encountered lithological units were selected for analysis by the use of the other techniques. A summary of the results of this analysis is presented with aid of LogPlot software (Rock Ware Inc. 2007). Detailed description of this analysis is presented in Appendices A, B and C.

3.2 Petrographic microscope analysis

The petrographic microscope analysis was done with the use of a Leitz Wetzler petrographic microscope at the ÍSOR petrography laboratory. In this analysis, minerals were identified based on their properties in plane-polarized as well as cross-polarized light. Properties identified include birefringence, cleavage, colour, pleochroism, twinning and the interference properties. 180 samples were chosen from the three wells for this study. To prepare the cuttings for this analysis, they were first dried. The dried samples were then cemented in epoxy, and then mounted on a glass slide. They were then ground to the customary thickness of 30 microns. The resulting glass slides containing the mineral grains were placed on the stage of a petrographic microscope for observation. This analysis was carried out in order to confirm rock type(s), the intensity of alteration and secondary minerals as identified in the binocular analysis, as well as to identify additional features not seen during the binocular analysis. Mineralogical evolution is also determined by noting paragenetic sequences and the association of primary and alteration minerals. In petrographic analysis, samples were chosen at intervals ranging between 30-50 m. The interval may vary outside this range, depending on the rate at which the rock units are changing or other changes observed under binocular analysis. A summary of the results together with the binocular studies were presented with the aid of the LogPlot software. Petrographic findings were also incorporated under the rock type description subtitle.

3.3 X-ray diffractometer analysis

The diffractometry analysis is based on principles of Bragg's law. It states that Bragg diffraction occurs when an electromagnetic radiation or subatomic particle waves with wavelength comparable to atomic spacing are incident upon a crystalline sample, and undergo a constructive interference (Yoshio et al., 2011). XRD analysis is mainly used to identify clays and zeolites. It can also be used to identify other minerals, for example amphiboles. However, in this study, the XRD analyses were done for the sole purpose of identifying clay minerals. In clay analysis, X-rays are diffracted by a powdered sample with preferentially oriented grains. X-ray spectra that are characteristic for different clay minerals are produced by slowly changing the diffraction angle (Yoshio et al., 2011).

Ninety samples were selected from the three wells based on the intensity of alteration. The samples were first dried. Then a teaspoon of each of the dried samples was placed in a test tube. Water enough to submerge the samples was added. The tube was mounted on a shaker and subjected to vibration for four hours. The shaking washes the clays from the drill cuttings. Drops of water from the test tubes were emplaced on a glass slide that had been washed with acetone to enhance cohesion and adhesion. These drops contain the washed clay suspension. The slides were left for twelve hours undisturbed to enable the water to evaporate and let the clay grains settle down. The slides with clay samples were run in the XRD instrument and a spectrum recorded. The slides with the samples were then placed in a container with glycol fumes for 24 hours and run in the XRD instrument and the spectra recorded. The final X-ray analysis involved heating the same samples to 550°C before running them in the XRD instrument. Peak positions, shapes, intensities and changes caused by different treatments are diagnostic for the identification of different clay

minerals. Clay mineral analysis helps in deducing the clay mineral alteration zones. From these zones, alteration temperatures of various rock units can also be inferred. A summary of the analytical results for well OW-905A were presented in Appendix D.

3.4 Inductively coupled plasma-optical emission spectrometry (ICP-OES) analysis

The ICP-OES analytical technique is a type of emission spectroscopy that uses inductively coupled plasma to produce excited atoms and ions, which emit electromagnetic radiation at certain wavelengths characteristic of a particular element (Holloway and Vaidyanathan, 2010). The intensity of the characteristic radiation is a measure of the concentration of an element in the sample. ICP is a stream of argon atoms that are inductively heated by a radio-frequency coil and ignited by a high-frequency Tesla spark to produce 6000-10,000K hot plasma (Holloway and Vaidyanathan, 2010). During analysis, the sample, which is in a solution, is passed as aerosol from a nebulizer into the argon plasma. Samples are heated (excited) to different (atomic and/or ionic) states that produce characteristic optical emissions. These emissions are separated based on their wavelength (Holloway and Vaidyanathan, 2010). Their intensities (spectrometry), which are proportional to the concentration of the element in the sample, are measured.

Under the ICP-OES study, 126 samples were selected from the top to the bottom of the three wells. Sample selection was mainly based on the binocular microscope analysis. The aim was to capture the different rock units and the various textures exhibited by the same rock unit. Both trace and major elements were determined. The major elements include Si, Ti, Fe, Al, Mn, Mg, Ca, Na, K and P. All these were recalculated to oxides. The trace elements include Sr, Ba, Zr, Y, Zn, Ni, Cu, Cr, Co, V, Sc, Rb and La. These were presented as ppm concentrations. It is important to note that mixing of samples from different depths can mask the pristine chemical composition of different rock formations. Hydrothermal alteration results in secondary mineral deposition, leaching and element mobility, and may affect the bulk chemical composition of the analysed samples. All this was taken into consideration during sample selection by the selection of homogeneous and relatively fresh samples. These factors were also taken into account during chemical data interpretation. The detailed procedure for sample preparation and analysis for this technique is presented in Appendix E.

4 Results

4.1 Introduction

The Olkaria Volcanic Complex is a high-temperature geothermal field. The fluid-rock interaction in this field has resulted in the formation of alteration minerals that reveal certain alteration sequences with depth. The sequences are comparatively uniform throughout the field with a few exceptions. To understand the fluid-rock interaction dynamics and petrogenesis of the Domes field in the southeastern part of Olkaria Volcanic Complex, wells OW-905A, OW-910 and OW-917 have been analysed. The rock cuttings from these wells provide the data needed to delineate the stratigraphy, alteration mineralogy, aquifers and the sub-surface petrochemistry in the Domes field. These observations, together with the reservoir data, enable an in-depth analysis of the variation in formation temperature and permeability across the Domes field (NW-SE traverse). The observations are explained below. Table 1 shows the geographic location (reference system is UTM), elevation, total drilled depth, production casing depth and the year each well was drilled for OW-905A, OW-910 and OW-917. The production casing size for all the three wells was 7″ slotted liners.

Table 1: Data for wells OW-905A, OW-910 and OW-917 from the Domes field.

Well number	**East (m)**	**North (m)**	**Elevation in m.a.s.l**	**Total depth (m)**	**Production casing depth (m)**	**Year of drilling**
OW-905A	202778	9901246	1947	2794	1200	Nov 2007-Jan 2008
OW-910	203732	9899738	1995	2990	950	Dec 2009-Feb 2010
OW-917	206249	9898918	2108	2990	1250	Oct 2012-Dec 2012

4.2 Description of the rock types

Judging from the binocular, petrographic and ICP-OES analyses, the study wells penetrate seven rock types. Five of these rock types were identified in all of the binocular, petrographic and ICP-OES analyses. The remaining two units were only identifiable in the ICP-OES analysis (Figure 16).

The rock types observed include pyroclastics, rhyolite, tuff, basalt, trachyte, basaltic trachy-andesite, trachy-andesite and trachy-basalt (Figure 16). The pyroclastics and rhyolites,

which form the Upper Olkaria Volcanics, mainly occupy the uppermost 500 m. They are intercalated by minor trachyte and tuff. The rhyolites occur with two different textures; spherulitic and granular. Basalt was noted to occur between 500 m to 1000 m depth. Minor trachyte, tuffs and rhyolite intercalate this unit. This unit forms the Olkaria basalt. Tuffs are mainly found intercalating the trachyte, rhyolite and basalt lava flows between 100 m to 1000 m. These tuffs are believed to have erupted between the various episodes of lava flows that formed the GOVC. The trachytes are found from 1000 m to 3000 m depth. They are the most dominant rock unit as observed in the three wells. They are intercalated by minor tuffs, rhyolite and basalt. This unit forms the plateau trachytes in the GOVC stratigraphic classification. The trachyandesites and basaltic trachyandesites were observed intercalated in rhyolites, basalts and trachyte. They occur between 350 m to 1600 m. The minor units noted are tephrite basanite and phonotephrite. Micro-granite intrusives, syenitic intrusives and basaltic dykes were also noted.

Wells OW-905A and OW-910 contain all the seven units while well OW-917 only has five units. The rocks in wells OW-905A and OW-910 show a continuous trend from basalts through basaltic trachyandesite, trachyandesite, trachyte to rhyolite in the TAS plot (Figure 27). Approximately 75% of these rocks plot in the trachyte and rhyolite fields in TAS classification scheme. One sample from well OW-905A plots as tephrite basanite, while two samples, from wells OW-905A and OW-910, plot in phonotephrite. These samples were basalt and basaltic trachyandesite in the case of OW-910 and OW-905A, respectively, with abundant altered plagioclase feldspar phenocrysts, which results in high Na_2O values as a result of albitization. Hence, their plotting in the tephrite basanite and phonotephrite fields. One trachytic tuff, three trachytic dykes and one trachytic lava plotted in the dacite field. Two of the trachytic dyke samples and one of the tuff samples were from OW-905A while two of the trachyte dyke samples were from OW-910. These rocks were highly altered with most of the sanidine having been replaced with clays. This resulted in depletion of Na_2O. Hence, the reason why they plot in the dacite field. Approximately 95% of OW-917 samples plot in the rhyolite and trachyte fields in the TAS classification scheme. Only two of the samples from well OW-917 plot in the dacite and trachy-andesite fields. The sample that plotted in dacite field was a highly altered trachyte dyke rock. Below is a brief description of the rock units and intrusions observed, while detailed descriptions are in Appendices A, B and C.

Pyroclastics

The pyroclastics in Olkaria are believed to comprise of Olkaria, Longonot and Suswa pyroclasts (Clarke et al., 1990). The Longonot and Suswa volcanoes are believed to have erupted in the same period as the Olkaria complex. Pyroclastics are found from the surface to 100 m depth. They are unconsolidated mixture of volcanic glass, scoria, pumice, tuff and rhyolite fragments. They range in colour from brown, yellow to grey. Volcanic glass is noted altering to palagonite. In thin sections, volcanic glass shows oxidation (limonite) as a result of the percolation of surface water. They occur from 0-84 m in well OW-917, 0-16 m and 292-312 m in well OW-910. No pyroclastics were observed in well OW-905A due to the loss of circulation returns encountered from 0-320 m during drilling.

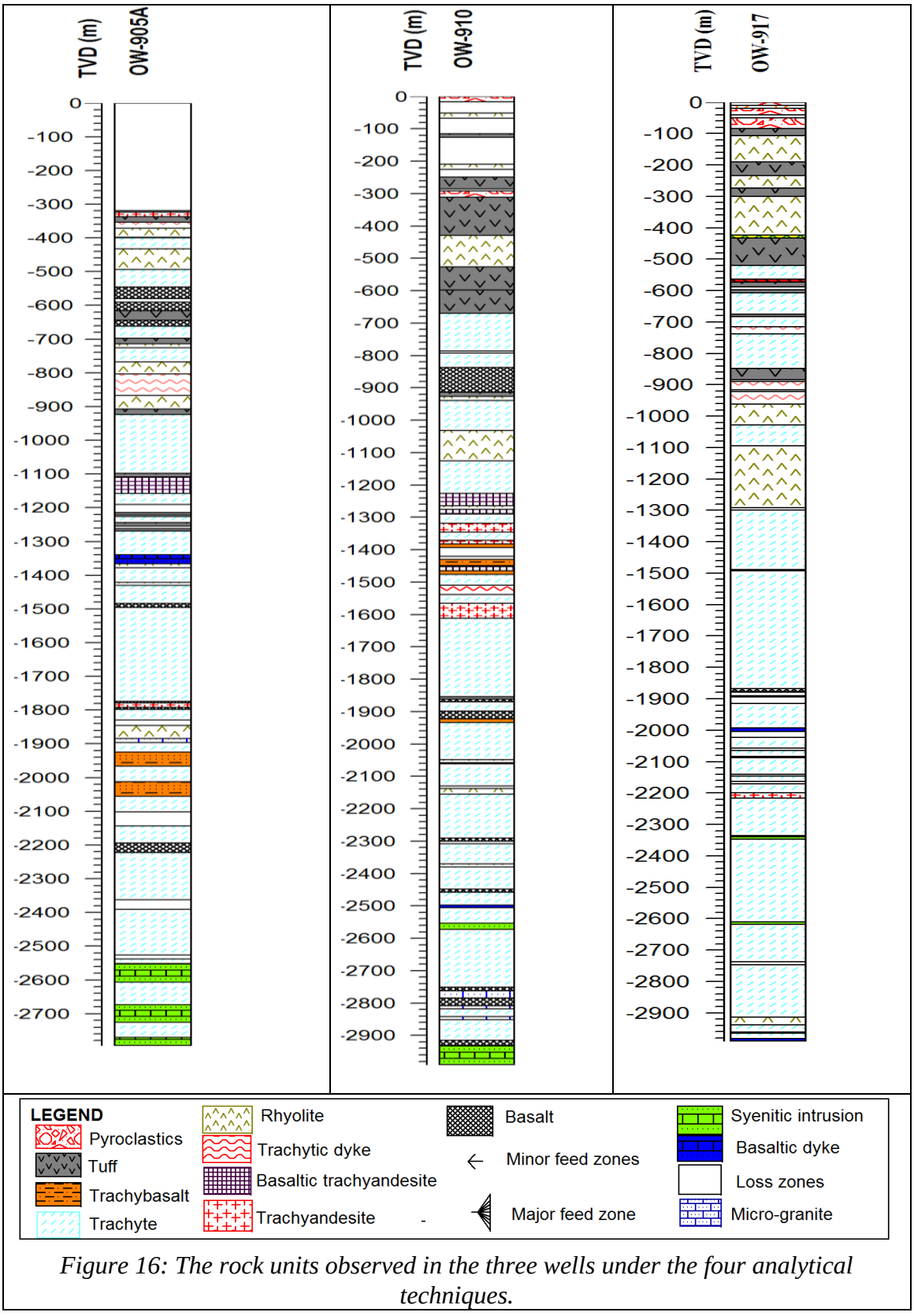

Figure 16: The rock units observed in the three wells under the four analytical techniques.

Tuff

Tuff occurs as thin layers ranging from 4 m to 30 m in thickness. Two types of tuff were identified; vitric (glassy) and lithic tuff. Lithic tuff is brown, grey to green in colour. The groundmass is lithic with subhedral to euhedral crystal fragments of quartz, aegirine/augite, amphiboles and sanidine. Fragments of trachyte, rhyolite and basalt are also observed embedded in the lithic groundmass. The fragments are rounded in some of the samples. The tuff is slightly vesicular with vesicles being filled with alteration minerals. This is the common tuff found in the three wells. Glassy tuff is white, non-crystalline and vesicular with quartz phenocrysts. The groundmass is glassy in thin sections, with subhedral to euhedral quartz and minor sanidine fragments discerned. Tuff occurs intercalating with other rocks between 0-600 m in well OW-917, 0-1900 m in OW-910 and 0-1300 m in OW-905A.

Spherulitic rhyolite

This type of rhyolite is glassy to light grey, fine grained, moderately to highly porphyritic with quartz and sanidine phenocrysts dominating the groundmass. In thin sections, the groundmass is dominated by fine-grained quartz and sanidine. Riebeckite, aegirine and augite micro-phenocrysts are also observed. The spherulites are made of bands of sanidine, quartz and pyroxene (aegirine-augite), which radiate from a central point. In well OW-905A, it is found at 868-908 m and 1366-1378 m and 1846-1844; OW-910 at 446-510 m, 926-940 and 2240-2248 m depth; and in OW-917 at 136-152, 300-424, 444-450 and 1094-1124 m depth.

Granular rhyolite

This type of rhyolite is mainly pink to brownish in colour. It ranges from aphyric to moderately porphyritic with quartz and sanidine phenocrysts. It has fine-grained sanidine and quartz forming the groundmass in which minute pyroxenes (aegirine and augite), riebeckite and magnetite are discerned. This rhyolite is highly siliceous with silica values as high as 80 wt% being recorded. This type of rhyolite is dominant in the upper 0-1500 m of the wells. It is observed at 370-398 m, 432-544 m, 714-726 m, 768-804 m, 1350-1366 m and 1422-1430 m in OW-905A; in OW-917 at 108-136 m, 234-274, 962-1028 m, 1124-1292 m and 1488-1492; and in OW-910 at 218-226 m, 430-446, 510-526, 1032-1126 m, 2048-2058 m, 2296-2308 m and 2370-2430 m.

Basalt

The basalt ranges in colour from grey, dark grey to green grey. It is fine- to medium-grained with porphyries of clinopyroxene and plagioclase feldspar. The groundmass ranges from holocrystalline to hypocrystalline with the subhedral to euhedral clinopyroxene and plagioclase crystals. The mineral grains are inter-locked in a randomized manner. Plagioclase is slightly more abundant than clinopyroxene. Olivine is seen to be replaced by clays and calcite as indicated by the shapes of these two minerals, which reflect the original olivine shape. In well OW-917, basalt is observed at 1872-1880 m and 1992-2004 m; in well OW-905A at 544-580 m, 590-616 m, 644-662 m, 1142-1158 m and 1484-1496 m; and in well OW-910 at 838-914 m, 1862-1870 m, 1898-1922 m, 2058-2062 m, 2290-2296

m, 2448-2458 m, 2498-2405 m, 2784-2808 m and 2916-2932 m. Basalt thins out towards OW-917. Basalt was used as a marker horizon to correlate the stratigraphy in the three wells. This marker horizon is at 544-616 m in OW-905A, and 839-914 m in OW-910. In OW-917, the basalt at 1872-1880 m was correlated with basalt at 2448-2458 m in well OW-910.

Light grey trachyte

This type of trachyte is whitish to light grey in colour. It is aphyric or slightly to moderately porphyritic in texture. The groundmass has abundant alkali feldspar (sanidine, minor albite and microcline), which gives the rock the whitish or light grey appearance. Phenocrysts of sanidine and pyroxenes (aegirine and augite) are embedded in the groundmass. It occurs intercalated with other rock units from 398 m in OW-905A, 520 m in OW-917 and 698 m in OW-910 to the bottom of the wells.

Flow-textured trachyte

This type is light grey to grey, fine-grained aphyric to moderately porphyritic. The groundmass is characterised by finely grained sanidine, pyroxenes and rare microcline and albite. Phenocrysts of sanidine and aegirine-augite dominate the lavas. This type of trachyte displays a flow texture (also called trachytic texture) with tabular sanidine and pyroxene crystals aligned in one direction. This orientation indicates the flow prior to cooling. This occurs intercalating with the light grey trachyte and other rock units from 398 m in OW-905A, 520 m in OW-917 and 698 m in OW-910 to the bottom of the wells.

Trachybasalt

This rock unit was noted in well OW-905A at 1924-1966 m, 2012-2056 m. In OW-910, it was found at 1382-1394 m, 1430-1450 m and 1466-1476 m. It is grey in colour, fine grained and aphyric. The groundmass is characterised by sanidine and plagioclase feldspars in which are discerned minute pyroxenes (augite), glass and opaque oxides. This rock unit was only confirmed by its chemical composition.

Basaltic trachyandesite

It was identified through its chemical composition in well OW-905A (1108-1158 m and 1774-1778 m.) and OW-910 (1226-1264 m and 1452-1466 m). It is pale green to light grey, fine to medium grained phyric rock. The groundmass is dominated by fine to medium grained sanidine and minor plagioclase feldspars in which amphiboles, clinopyroxenes and magnetite are observed. The phenocrysts are mainly sanidine, minor plagioclase and pyroxenes.

Trachyandesite

The rock appears grey to light grey in colour, fine to medium grained and moderately porphyritic in texture. The phenocrysts are sanidine and aegirine-augite pyroxenes. For the light grey fragments, the groundmass is rich in sanidine in which pyroxene mineral grains

and a few amphibole mineral grains are sparsely dispersed. The grey fragments have the groundmass made of finely grained sanidine in which minute pyroxenes (aegirine-augite) are intensely dispersed. Amphibole mineral grains mainly riebeckite is noted in thin section. This rock unit is scarce and is only identified through its chemical composition. It is identified at 1318-1346 m, 1372-1382 m and 1566-1542 m in OW-910. In OW-905, it is observed at 432-338 m and 1778-1792 m. In OW-917, it is observed at 2200-2216 m.

Basaltic dykes

They are grey to dark grey fine grained aphyric rocks. The groundmass is rich in plagioclase in which is dispersed minute clinopyroxenes. Traces of olivine in the last stages of alteration was observed in some of the dykes (OW-917 at 2982-2990 m) under the thin section analysis. The basaltic dykes are noted at 1992-2004 m, 2962-2966 m and 2982-2990 m in OW-917. In OW-905A, they are observed at 1244-1254 m and 1350-1366 m. In OW-910, they are observed at 1520-1538 m and 2498-2506 m.

Syenite intrusives

Syenite occurs as white relatively fresh medium to coarse grained rock. The groundmass is dominantly alkali feldspar in which quartz is sparsely dispersed. Minute augite-aegirine, amphiboles and magnetite are noted in the groundmass. Some of the syenite (OW-905A) shows oxidation as a result of interaction with water from the surrounding rocks. Syenite occurs in the three wells with thickness ranging from 4-58 m. In well OW-917 it occurs at 2340-2344 m, 2610-2618 m and 2914-2938 m; in OW-905A at 1884-1896 m, 2552-2606 m, 2674-2726 m and 2770-2794 m; and in OW-910 at 2554-2572 m and 2932-2990.

Micro-granite intrusives

This is white, medium-grained holocrystalline rock. The matrix is characterised by equigranular interlocking mineral grains of quartz and sanidine. The matrix has fine-grained with arfvedsonite and clinopyroxene peppering its white background colour. Minute pyroxenes are noted in the groundmass. It was observed at 2762-2784 m, 2808-2818 m, and 2842-2846 m in OW-910 and 1884-1896 m in OW-905A.

4.3 Hydrothermal alteration

A study of hydrothermal alteration provides information about the fluid-rock interaction dynamics in a geothermal field. Hydrothermal alteration is the interaction of the rock with fluids called “hydrothermal fluids” (Simmons and Browne, 2000). Hydrothermal fluids are found several hundreds of meters to kilometres beneath the surface of the earth and can either be water or gases (for example carbon dioxide). The fluids, which exhibit temperature range between 32° C to 400° C (Browne, 1978), are believed to have percolated from the surface over a long period of time. The fluids also have escaped from magma during cooling and trapped within fractures and voids in the rock. The fluids are heated either through interaction with a magma heat source or with hot crustal rocks. As the fluids heat up, they dissolve minerals from the nearby igneous source or the country

rock. The hot fluids rise due to buoyancy. As they rise, they either deposit dissolved mineral ions in vugs and voids or dissolve ions from the primary rock resulting in the formation of secondary minerals which are either stable or metastable in that depositional environment (Simmons and Browne, 2000).

The main factors affecting the rate and intensity of hydrothermal alteration in a geothermal environment include temperature, permeability, pressure, fluid composition, duration of hydrothermal activity and the mineral composition of the primary rock (Browne, 1978). Pressure does not have a direct effect on alteration but has a bearing on fluid composition as a result of boiling. In boiling conditions, CO_2 is lost and this may result in the deposition of minerals, for example bladed calcite. Hydrothermal alteration causes conspicuous changes in the rock appearance (colour and texture) and composition. However, some of the primary minerals retain a shade of their original texture. This make it easy to identify the order of replacement of the primary minerals (Table 2). In studies conducted in various geothermal fields, it has been possible to correlate alteration temperatures with alteration minerals (Kristmannsdottir, 1979). This has been achieved in systems which have remained in a steady state of thermal equilibrium over a period of time. From these studies, it has been concluded that alteration minerals are deposited at specific temperature conditions. For example, in a high-temperature geothermal field, quartz deposits at minimum temperature of 180 °C, while epidote deposits at 240 °C or higher temperature (Browne, 1978). In a system that has been at steady state thermal conditions over time, these temperatures have shown to correlate well with the formation temperatures. It therefore implies that in such systems, alteration mineral temperatures can be used to estimate the formation temperature of the system.

Table 2: Primary minerals, their alteration products and order of replacement as observed in the study wells (modified from Browne, 1984).

	Primary minerals	**Alteration products**
Most susceptible ↓	Volcanic glass	Zeolites, clays, quartz, calcite, palagonite
	Olivine	Chlorite, clay
	Pyroxenes, amphiboles	Chlorite, illite, quartz, pyrite, calcite
	Plagioclase	Calcite, albite, quartz, epidote, sphene
Least susceptible	Sanidine, microcline	Adularia, chlorite, illite, calcite
	Fe-Ti oxides	Sphene, haematite

4.3.1 Hydrothermal alteration minerals in the study wells

Olkaria geothermal field is a high-temperature geothermal field. Alteration minerals occur as deposition or replacement minerals. As deposition, they fill voids, vugs and fractures, either as layers or as vein fillings. As replacement minerals, they replace the primary rock forming minerals. In this field, the intensity of alteration and abundance of alteration minerals varies as seen in the binocular and thin section analyses. Variations were noted from sample to sample and from well to well. This can be attributed to the location of the wells in areas with different reservoir characteristics. The alteration minerals observed in the wells include hematite, sphene, albite, calcite, chalcedony, pyrite, chalcopyrite, mesolite, scolecite, phillipsite, laumontite, smectite, illite, chlorite, sphene, quartz,

wairakite, prehnite, epidote, actinolite and garnet. A summary of the minerals is shown in Figures 17, 18 and 19, while the description is as below.

Scolecite and mesolite

Scolecite and mesolite occur in wells OW-910 and OW-917 at 250-312 m and 84-590 m respectively. In well OW-905A, only mesolite occurs at 354-432 m. These minerals are observed filling in vesicles. Scolecite appears colourless, flattened in some instances and four sided in other instances. It occurs in clusters, radiating from a single point and grows thicker away from the base of growth. The grains also separate as they grow further away from the base, and display longitudinal cleavage in thin section. Mesolite occurs as thin needle-like crystals, red to white in colour. The grains separate as they radiate away from the base forming spiky ends. These are low-temperature deposition minerals associated with deposition temperatures of between 60 °C to 100 °C.

Phillipsite

This mineral was only noted in OW-917. It occurs from 84-564 m. It occurs as colourless thick tetragonal columnar crystal clusters. This is a low-temperature zeolite associated with deposition temperatures of 50 °C to 90 °C. It displays twinning and uneven cleavage in thin section. It was observed growing in vesicles.

Laumontite

Laumontite was observed in OW-910 at 1226-1990 m. It was mainly observed in basalts. It is white in colour, elongated with square ends. Laumontite is a zeolite that deposits at temperatures as high as 230 °C.

Chalcedony

This appears whitish to pale blue in colour. The crystals occur in vesicles where they appear in a spherulite-like form. In other instances, the mineral appears amorphous. It was observed at 300-412 m in OW-917 and at 398-662 m in OW-905A. This mineral was not observed in OW-910. Its deposition temperatures range from 100 °C to 180 °C.

Hematite

Hematite is a low-temperature Fe-oxide associated with the percolation of cold water into the formation in a geothermal field. It is reddish brown to greyish shiny in colour. It is formed by oxidation of magnetite. In thin section, the crystals are opaque and have a hexagonal shape. It was observed at 0-286 m in OW-917, 0-260 m in OW-910 and 320-494 m in OW-905A.

Albite

Albite was identified in thin section analysis. It appears cloudy white in colour. The crystals are anhedral to euhedral. It has uneven fracture. It is an alteration product of

plagioclase and sanidine feldspars. In the case of plagioclase, the original plagioclase twinning is obscured by the cloudy nature of albite. Albite is formed at temperatures of about 180 °C. It first occurs at 854 m in OW-910, 1278 m in OW-905A and 1364 in OW-917. It is observed down to the bottom of the wells.

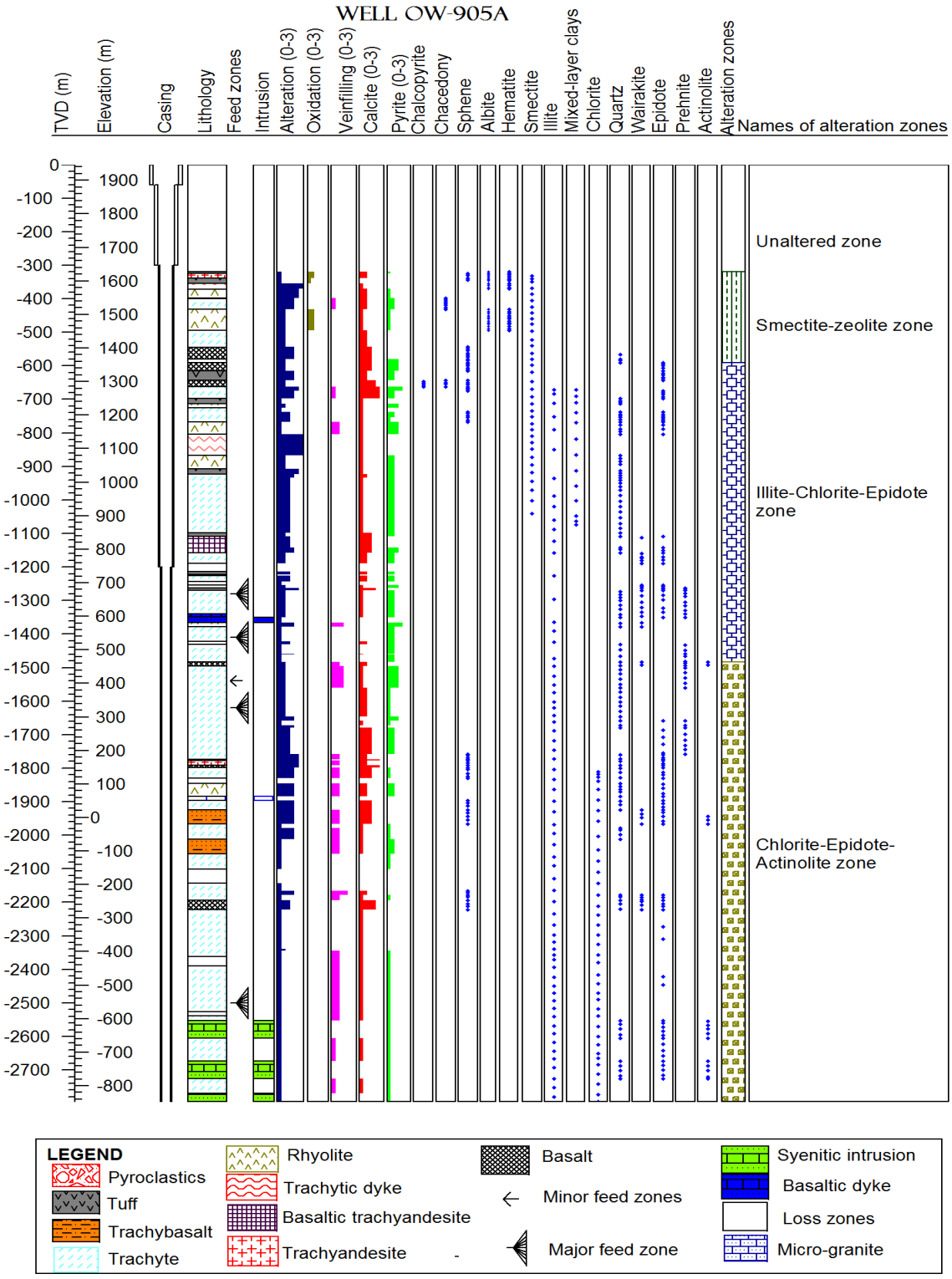

Figure 17: Lithology, alteration minerals and alteration zones of OW-905A.

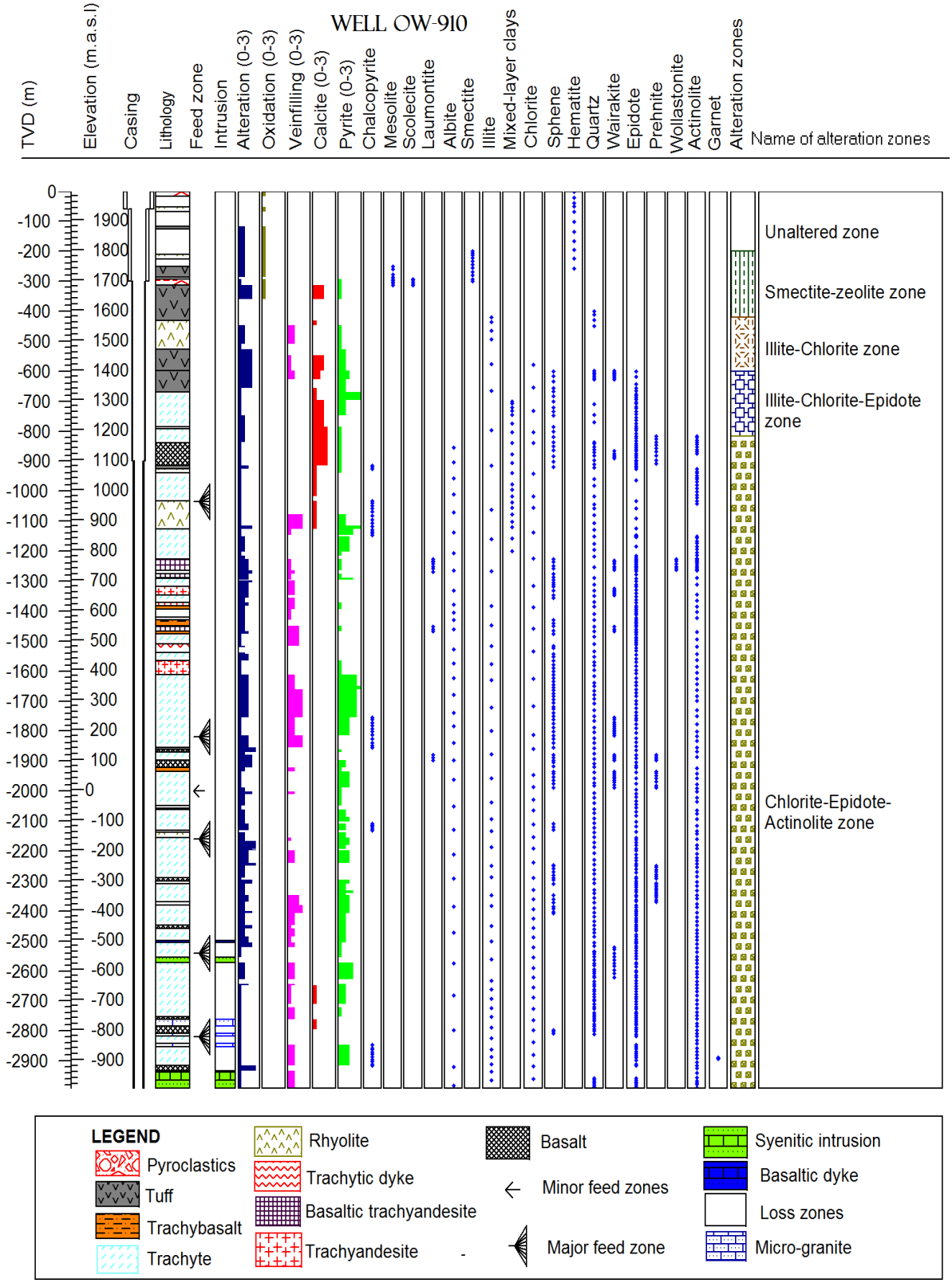

Figure 18: Lithology, alteration minerals and alteration zones of OW-910.

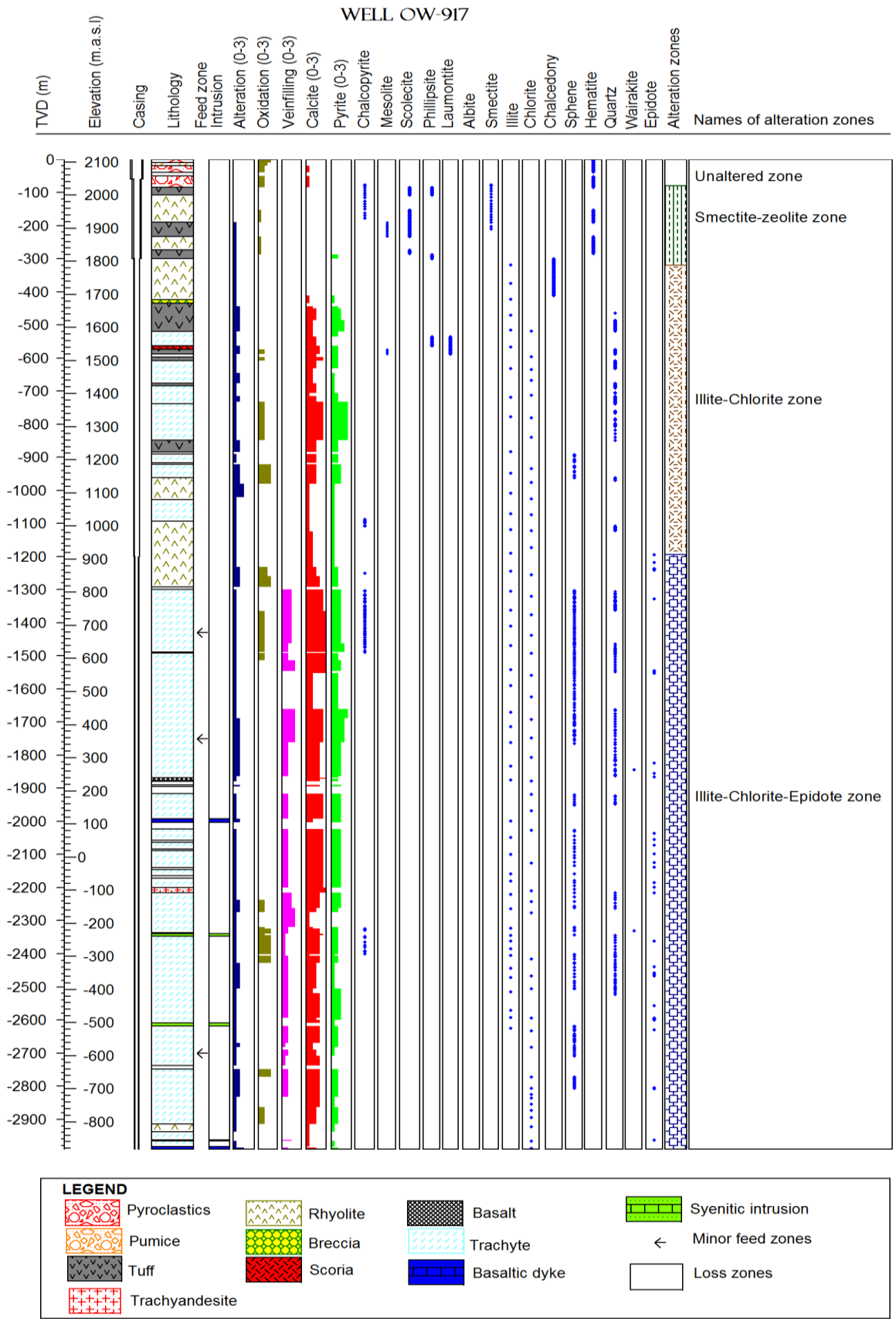

Figure 19: Lithology, alteration minerals and alteration zones of OW-917.

Chalcopyrite

Chalcopyrite appears brass yellow in colour under binocular microscope. The crystals are euhedral and are observed embedded in the rock matrix. It was observed from 1088 m in OW-917, 914 m in OW-910 and 646 in OW-905A down to the bottom of the wells, albeit intermittently.

Sphene

Sphene is observed disseminated in the rock matrix. It appears colourless to reddish brown. Under thin section analysis, it appears with acute rhombic cross section with first order birefringence colours. It was first observed at 560 m in OW-917, 656 m in OW-910 and 324 m in OW-905A.

Pyrite

Pyrite occurs as brass yellow euhedral crystals embedded in the rock matrix. In other instances it occurs as minute disseminations in the rock matrix. It varies from low abundance in OW-905A, moderate to high abundance in wells OW-910 and OW-917. In OW-917, it first appeared at 260 m, 300 m in OW-910 and 320 m in OW-905A (Figure 20, 21 and 22). It occurs in association with calcite and clays. In thin section, it was distinguished from other opaque minerals by its cubic crystal form. Pyrite is a hydrothermal mineral that indicates high permeability.

Wairakite

Wairakite is observed as depositional mineral filling vesicles and fractures. It is colourless, transparent with many faces. It occurs in clusters in most instances. It occurs in association with quartz, epidote and chlorite clay. Wairakite is a scarce mineral in the three wells. In thin sections, it appears transparent with low relief and a distinct cleavage. It was observed from 1844 m in OW-917, 598 m in OW-910 and 1112 m in OW-905A down to the bottom of the wells, albeit intermittently. Wairakite is deposited at minimum temperature of 200 °C.

Quartz

Quartz occurs as a depositional mineral filling veins, fracture planes and vesicles. It forms hexagonal transparent crystals. The mineral grains grow either as individual grains or as clusters. It was observed to be more abundant in wells OW-910 and OW-905A as compared to OW-917. Quartz also occurs in association with chlorite, wairakite and epidote. In thin sections, it has a characteristic undulating extinction and lacks cleavage. It also exhibits higher relief than the resin. Quartz deposits at 180 °C and above. It was observed from 464 m in OW-917, 400 in OW-910 and 566 m in OW-905A down to the bottom of the wells.

Prehnite

Prehnite occurs as white spherical clustered crystals. It occurs in vesicles and fractures. It has characteristic high interference colours. It appears like a bow-tie structure in thin sections. Prehnite was observed at 816 m in OW-910 and at 1262 m in OW-905A. It is scarce and occurs intermittently in the wells. Prehnite is a high-temperature mineral and occurs in association with other high-temperature minerals, including epidote and actinolite. It is deposited at a minimum temperature of about 240 °C.

Epidote

Epidote appears non-crystalline and yellow-green in colour. It occurs as a depositional mineral as well as a replacement mineral. As a depositional mineral, it fills vesicles and fractures. It occurs in euhedral to anhedral crystal form and occurs in clusters as well as individual crystals. The clustered crystals occur in a radiating manner. As a replacement mineral, it replaces feldspars and pyroxene. Epidote has high interference colours with a parallel extinction in thin section analysis. Epidote was first observed at 1218 m in OW-917, at 600 m in OW-910 and at 590 m in OW-905A. Epidote was observed in abundance in well OW-910, and lesser amount in OW-905A. These two wells had epidote as both depositional and replacement mineral. In OW-917, epidote is scarce and is only seen as a replacement mineral. It partially replaces feldspars. Epidote is a high-temperature mineral formed at minimum temperatures of 240 °C. Epidote occurs in association with actinolite, prehnite, wairakite and chlorite. In Olkaria geothermal drilling, the first appearance of epidote is used as a marker for casing depth. The variability in the abundance of epidote in the three wells can be attributed to the different reservoir characteristics (mainly temperature and permeability) in the location of the three wells. This is explained in the coming sub-chapter.

Wollastonite

Wollastonite was only observed in well OW-910 from 1226 m to 1262 m. It occurs as an aggregate of white needle-like elongated crystals. It occurs as a mineral deposited in vesicles. It appears colourless and fibrous in thin section analysis. It has high interference colours with a parallel extinction. Wollastonite occurs in association with epidote. It is a high-temperature mineral with a minimum deposition temperature of about 270 °C.

Actinolite

Actinolite occurs as feathery to fibrous white to greenish crystals growing in vesicles as a deposition mineral as well as replacing pyroxene. The tendency to replace pyroxene occurs with increasing depth with complete replacement being noted at about 1800 m in wells OW-905A and OW-910. In the fibrous form, they grow radiating from one point. It has a high relief, simple twin, 3rd order interference colours and displays pleochroism. It was first observed at 816 m in OW-910 and 1484 in well OW-905A. It occurs down to the bottom of the wells. The minimum depositional temperature of actinolite is about 290 °C.

Garnet

Garnet was observed in OW-910 at 2880-2892 m. It occurs as reddish brown regularly faced crystals which are densely packed. Garnet is a high-temperature alteration mineral deposited on the margins of intrusions. Garnet deposits at a minimum temperature of about 300 °C.

Calcite

Calcite is white in colour and is deposited in vesicles and fractures. It also occurs as a replacement mineral for feldspar, volcanic glass and pyroxene. In thin sections, calcite is transparent, has rhomboid cleavage, high birefringence and changing relief with rotation. Calcite abundance varies in the three wells. OW-917 has moderate to high abundance throughout the well. The calcite in this well was deposited in the rock matrix and vein fillings. Blades of calcite extracted from the vein filling were noted in the rock cuttings. This may be as a result of the drill bit having broken the calcite veins open. OW-910 has low levels of calcite, with most of it being observed down to 900 m only. Calcite in this well occurs filling vesicles and in other instances filling veins. It is occurring in association with clays and pyrite. Well OW-905A has low to moderate abundance, which occurs almost along the entire depth of the well. It occurs as filling vesicles and veins, as well as deposited in the groundmass. Calcite was rated at a range of 0-3 with 0 indicating total lack of calcite and 3 indicating high abundance (Figures 25, 26 and 27).

Clays

Clay minerals are deposited over a large temperature range in geothermal fields. The clay depositional temperature range is useful in delineating alteration minerals zones along the drilled depth. The type of clays deposited varies with increasing temperature. Illite and chlorite are deposited at comparatively higher temperatures (above 180 °C) than smectite (below 180 °C). Clays occur as depositional as well as replacement minerals. They replace volcanic glass, olivine, feldspar and pyroxene (table 2). In the vesicles and fractures, they occur in association with other minerals including quartz, epidote and actinolite. In the vesicles and fractures, they display a paragenetic sequence which reveals the paleo-thermal evolution of the system. Clay identification was done with the use of XRD analysis. The clays analysed in the three wells were smectite, mixed layer clays, illite and chlorite. Clay analysis for well OW-905A was carried out during this study. Clay data for wells OW-910 and OW-917 was from an earlier unpublished report (KenGen, 2012). A summary of the clay analysis data for OW-905A is shown in Appendix F. The data for the other two wells can be obtained from KenGen (2012).

Smectite

Smectite is a low-temperature alteration mineral formed at temperatures below 180 °C. It is fine-grained and brown to green in colour. In these wells, smectite occurs as an alteration product of volcanic glass, pyroxene, and Ca-rich feldspar. Smectite swells with the addition of water. The root cause is the negative charge characterising the structural layers of

smectite, causing the mineral to attract water or other polar molecules into the interlayered structure, which results in expansion (Rule, 2007). Smectite has first order interference colours and shows radiating extinction under petrographic analysis. Smectite has peaks for air dried, glycolated and heated treatment at 12 Å, 17 Å, and 10 Å respectively. Smectite was observed in wells OW-905A, OW-917 and OW-910 at depths between 332 m to 1092 m, 76 m to 210 m and 200 m to 320 m, respectively.

Mixed layer clays

Mixed layer clays in the wells represent the intermediate stage in the transformation of swelling clays to non-swelling clays. They are brown to green and fine- to coarse-grained under binocular observation. In thin sections, they are green to yellowish in colour and display strong pleochroism compared to chlorite. The chlorite diffraction peaks are at 7.16-7.36 Å for air dried and glycolated samples but clay collapses when heated. The smectite peaks range between 12.91-16.26 Å, 17.79-18.86 Å and 10.09-10.53 Å for air dried, glycolated and heated samples, respectively. In OW-905A, the mixed layer clay analysed was smectite-chlorite (Figure 20), occurring from 672 m to 1072 m. In well OW-910, the mixed layer clay was first observed between 700 m to 1200 m, in this case also smectite-chlorite. Mixed layer clays are absent in OW-917.

Illite

Illite is stable at temperatures of about 200 °C or higher. It appears colourless to yellow brown in thin section. It has a characteristic low refractive index. Illite occurs in close association with chlorite. Illite XRD peaks remain stable throughout the three treatments, the diagnostic peak occurring at between 10.29-10.63 Å. In well OW-905A, it was first observed at 672 m. It was observed to form by alteration of K-feldspars, as well as filling in vesicles and veins. It starts replacing sanidine from 1200 m depth. It occurs mainly as traces between 672 m-1500 m, whereas from 1500 m down to the bottom of the well, its abundance increases. This indicates its stability at high temperatures. Illite in OW-917 was first observed at 318 m and occurs sporadically down to the bottom of the well. In well OW-910, illite occurs from 420 m down to the bottom of the well. The abundance of illite increases with depth in all the wells.

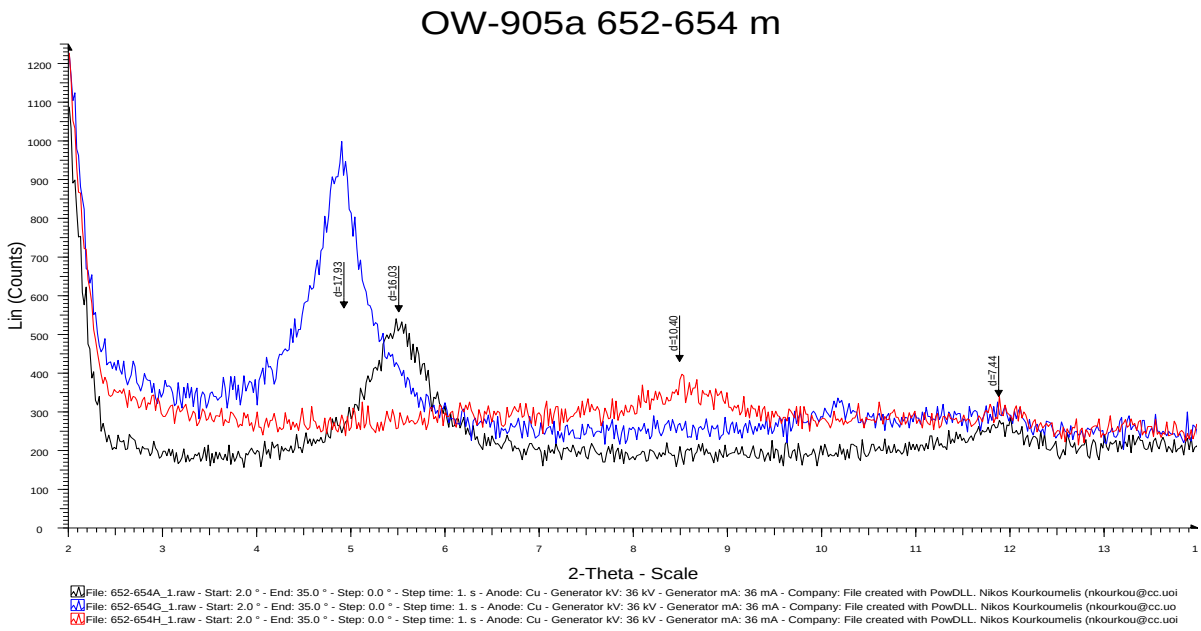

Figure 20: Mixed layer clay peaks in OW-905A showing the smectite-chlorite mixed layer.

Chlorite

Chlorite is a medium to high-temperature alteration mineral stable at over 200 °C temperature. It appears green to pale green, fine to coarse-grained filling vesicles, vugs and veins. Under thin section analysis, it is weakly pleochroic but shows a range of colours (blue-brown -purple). It also has a moderate relief. Chlorite occurs in association with illite. In OW-905A, chlorite occurs from 772 m down to the bottom of the well (Figure 21). It was noted as a deposition mineral as well as an alteration product of sanidine and pyroxene. It occurs in association with epidote, quartz, actinolite and wairakite. The chlorite in this well had peaks of between 7.16-7.36 Å for both air dried and glycolated treatment. These peaks collapse on heating. Another chlorite peak was at 14.59-14.96 Å for all the three types of treatment (air dried, glycolated and heated). In well 917, the chlorite occurs from 518 m to the bottom of the well. Chlorite is abundant compared to illite. The chlorite has more pronounced peaks at 7 Å while the 14 Å peak is highly obscured. Chlorite was first observed at 578 m in well OW-910. It occurs down to the bottom of the well. This chlorite, like in the other two wells, shows pronounced 7 Å peak with a more obscure 14 Å peak.

The chlorite peak at 7.16-7.36 Å being larger compared to the peak at 14.59-14.96 Å, as observed for samples from all three wells, is characteristic of Fe-rich chlorite (Moore et al., 1997). In this type of chlorite, the peak at 14 Å may be obscured leaving the peak at 7 Å as the only noticeable peak, as seen in most samples in the wells. Low concentration of chlorite in the samples may also result in pronounced peaks at 7 Å and obscured peak at 14 Å (Moore et al., 1997). More studies are recommended for the chlorite clays in Olkaria geothermal system in order to learn more about their chemical composition.

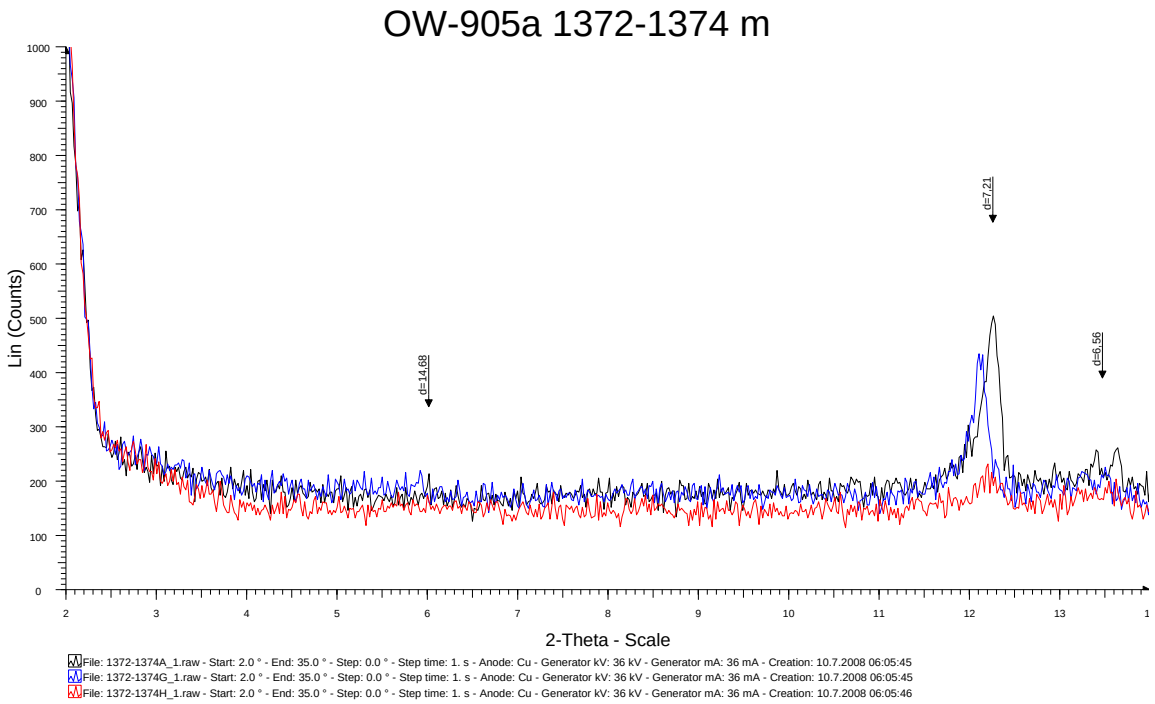

Figure 21: *Diffractogram for chlorite in OW-905A with a pronounced peak at 7 Å and a less pronounced peak at 14 Å.*

4.3.2 Alteration mineral zonation

Alteration mineral zonation is based on the distribution of alteration minerals with depth. Different alteration minerals deposit at different temperatures. These zonations can be used to vertically divide wells into sections with different alteration mineral temperatures. These temperatures can be used to approximate the formation temperatures in these zones in a system where steady-state thermal conditions have been maintained over time. However, this is not strictly the case since hydrothermal alteration is a function of many other factors (e.g. rock composition, fluid chemistry and the primary rock composition) apart from formation temperatures. From alteration mineral zones determined in Olkaria Domes (Lagat 2004, Musonye 2012, Mwangi 2012), the formation temperature is observed to increase with depth. This may be attributed to the closeness to the heat source with increasing depth. The mineral zones identified in the three wells include: Unaltered zone, smectite-zeolite zone, illite-chlorite zone, chlorite-epidote zone, chlorite-epidote-actinolite zone (Figures 17, 18 and 19).

Unaltered zone: This zone is mainly characterised by pyroclastics. In the unaltered zone, most of the primary rock forming minerals (especially volcanic glass) can still be recognized in petrographic analysis. This zone is mainly characterised by oxidation. The alteration temperature in the zone is below 50 °C. The main secondary minerals observed in this zone are iron oxides. Calcite was observed in this zone in OW-917. The unaltered zone is about 100 m thick from the surface in OW-917 and 200 m thick in OW-910. In OW-905A, there was loss of circulation returns from the surface to 320 m. This made it impossible to know where this zone exactly ends within this depth range.

Smectite-zeolite zone: Most of the minerals found in this zone are stable at temperatures below 100 °C. Smectite replaces olivine, sanidine and volcanic glass from low temperatures to a maximum of 180 °C. The main minerals found include scolecite, mesolite, phillipsite, smectite and hematite. Other minerals include chalcedony, calcite, pyrite and sphene. In OW-905A, this zone is at least 352 m thick (between 320-672 m depth). In well OW-917, this zone is 200 m thick occurring between 100 m to 300 m depth. In OW-910, the zone is 220 m thick (from 200 m to 420 m depth).

Illite-chlorite zone: This zone is characterised mainly by illite and chlorite. Other minerals present in this zone include quartz, laumontite, pyrite, calcite, chalcopyrite, and chalcedony. This zone was observed in well OW-917 from 300 m to 1226 m depth. In OW-910, it occurs from 420 m to 600 m depth. The zone was absent in OW-905A since epidote occurred at a shallower depth as compared to illite and chlorite. The temperature in this zone is above about 200 °C.

Illite-chlorite-epidote zone: This zone's upper boundary is marked by the first appearance of epidote. The main minerals observed in the zone include chlorite, epidote, illite, quartz, wairakite, calcite, pyrite and prehnite. The temperature in this zone is about 230 °C and higher. In OW-905A, it is observed from 590 m to 1484 m. In OW-917, it is observed from 1218 m down to the bottom of the well. In OW-910, it is observed from 600 m to 816 m. There is a large abundance of depositional epidote in OW-910 in this zone compared to the other two wells.

Chlorite-epidote-actinolite zone: The distinguishing feature of this zone is the first appearance of actinolite. The main minerals found in this zone include epidote, chlorite, wairakite, quartz, wollastonite, prehnite, illite and actinolite. Other minerals include pyrite, calcite, chalcopyrite, garnet and sphene. This zone has high temperatures ranging from 290 °C and higher. This is deduced from the alteration minerals observed in this zone in wells OW-905A and OW-910. In OW-905A, it occurs from 1030 m down to the bottom of the well. In well OW-910, it is observed from 816 m to the bottom of the well. OW-910 showed abundance of depositional epidote and actinolite as compared to OW-905A in this zone. Garnet was only observed in OW-910 at 2880 m. This indicates temperatures of about 300 °C.

Zeolites, quartz, epidote, actinolite and garnet index minerals were also chosen for alteration temperature correlation across the field along AB intersection which is in a NW-SE orientation (Figure 22). OW-914, which was analysed earlier (Okoo, 2011), was also included in this comparison (Figure 22). The upper boundary for the zones was marked by the first appearance of the respective index mineral in each well. For instance, the first appearance of quartz marked the top boundary of the quartz zone, the first appearance of epidote marked the top boundary of the quartz-epidote zone, actinolite appearance marked top boundary for actinolite zone and the first appearance of garnet marked the top boundary of the garnet zone.

As seen in Figure 22, the thickness of the smectite-zeolite zone is slightly greater towards OW-905A and OW-917 and decreases at OW-910 and OW-914. This indicates lower temperature at greater depth in OW-917 and OW-905A compared to OW-910 and OW-914. The quartz zone is thicker in OW-917 and thins out towards OW-905A. This zone is found at shallow depths in wells OW-910 and OW-914 and at greater depths in wells OW-

917 and OW-905A. The quartz-epidote zone occurs at shallow depth in OW-905A followed by OW-910 and OW-914. In OW-917, the top of the quartz-epidote zone occurs at greater depth. This indicates that high alteration temperatures (about 240 °C) are only encountered at greater depth in OW-917 as opposed to the other three wells, and the quartz-epidote zone is the highest alteration temperature zone found in OW-917. The actinolite zone is observed in OW-905A, OW-914 and OW-910. This zone occurs at shallow depth in well OW-910 (816 m) and at greater depth in well OW-905A (1484 m). This is the highest temperature zone observed in OW-905A. The garnet zone is observed below 1794 m depth in OW-914 and at the bottom of OW-910 (2884 m). This indicates higher temperatures (above 300 °C) at a relatively shallow depth in OW-914 compared to OW-910.

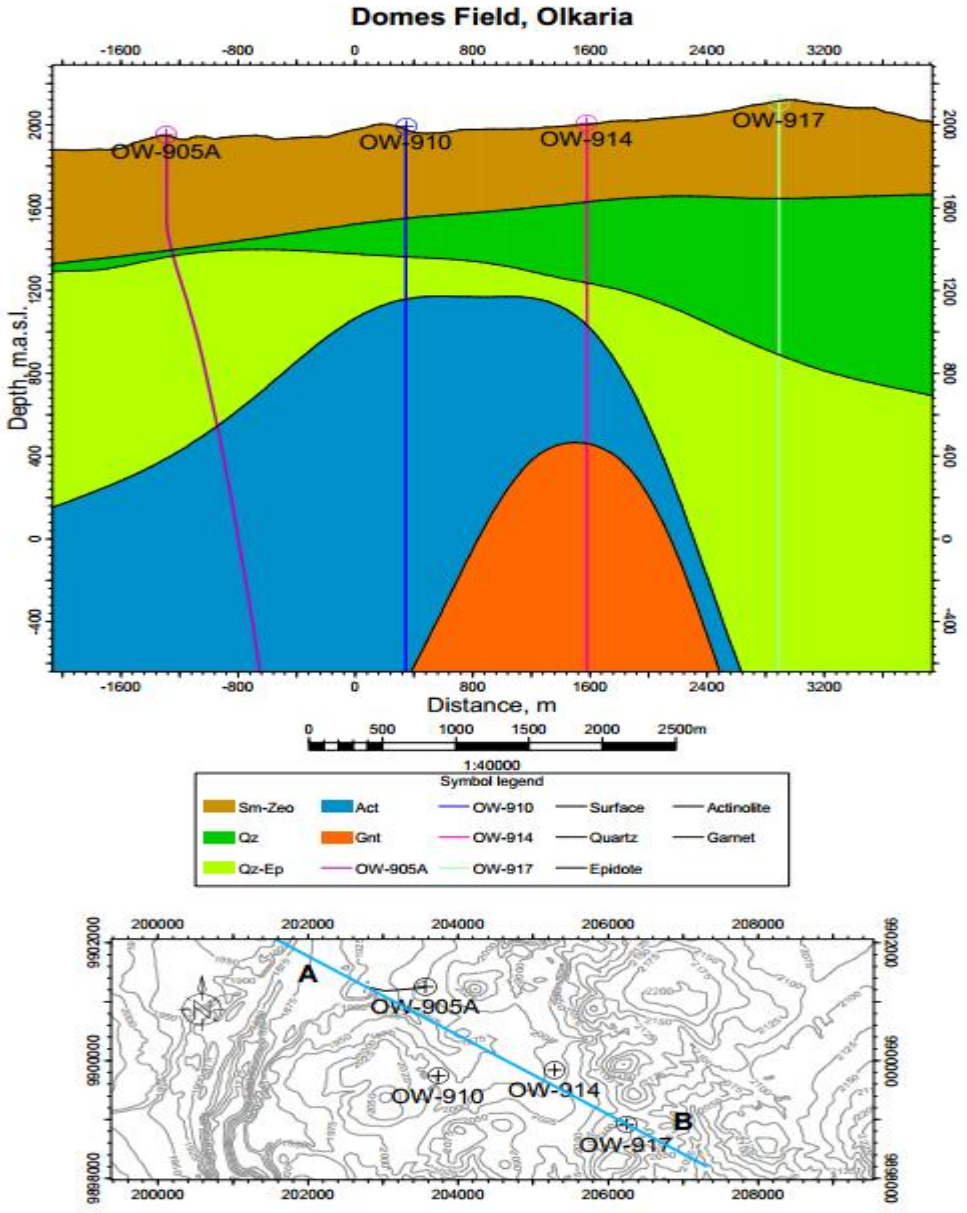

Figure 22: Alteration mineral correlation between the 4 wells along the traverse AB.

4.4 Temperature distribution across the field

Alteration temperatures are temperatures that existed at the time of the alteration minerals´ deposition. From alteration minerals observed in drilled wells, hydrothermal isograds cutting across different wells can be drawn. The index minerals chosen for this comparison include quartz, epidote, actinolite and garnet. Data from previously studied well OW-914 (Okoo, 2011) was also included in this comparison (Figure 23). This was plotted alongside the measured formation temperatures in the wells. The alteration mineral temperature isograds are not exactly parallel to the formation temperature trends. This is because hydrothermal alteration is not only a function of the formation temperature, but also the primary mineral composition and permeability. Moreover, the temperatures in some of the wells (for example OW-914) were taken before the wells had been given enough time to heat up.

From Figure 23, it can be seen that OW-905A and OW-917 have a relatively large section of their upper section (615 m and 700 m, respectively) with temperatures below 150 °C. Wells OW-910 and OW-914 have only 470 m and 500 m depth interval, respectively, from the surface with temperatures below 150 °C. In general, well OW-905A has lower temperatures with most of it in the temperature range of between 225 °C to 250 °C. The highest temperature recorded in this well is between 275 °C to 300 °C, which was measured in the deepest part of the well below 2600 m depth. OW-910 and OW-914 have higher temperatures at shallow depth with a maximum of 250 °C being recorded at 1200 m a.s.l (at about 800 m depth). From 800 m down to the bottom, the wells have temperatures ranging between 250 °C to 350 °C (Figure 23). Relatively low temperatures are recorded in OW-917 with the maximum temperature range of 225 °C to 250 °C. In most of the well (700 m to 1900 m), the recorded temperature is below 225 °C.

Some of the mineral isograds indicate high temperatures at shallow depth contrary to the formation temperature. For instance, epidote isograd plots at depth which has recorded formation temperatures of between 150 °C to 180 °C in OW-905A. Epidote isograd in wells OW-910, OW-914 and OW-917 plot at depths which have formation temperatures of between 180 °C to 220 °C. The actinolite isograd in well OW-905A plots in formation temperatures of between 180 °C to 220 °C while plotting in formation temperatures of between 220 °C to 250 °C in OW-914 and OW-910. This isograd is likely to be found at greater depth in well OW-917 region since it does not cut across the drilled depth in this well. Garnet was only observed in wells OW-910 and OW-914. Garnet isograd plots in formation temperature of over 275 °C in OW-914 and 325 °C in OW-910, but is shallower in OW-914 at 1794 m depth as compared to OW-910 where it is at 2884 m depth.

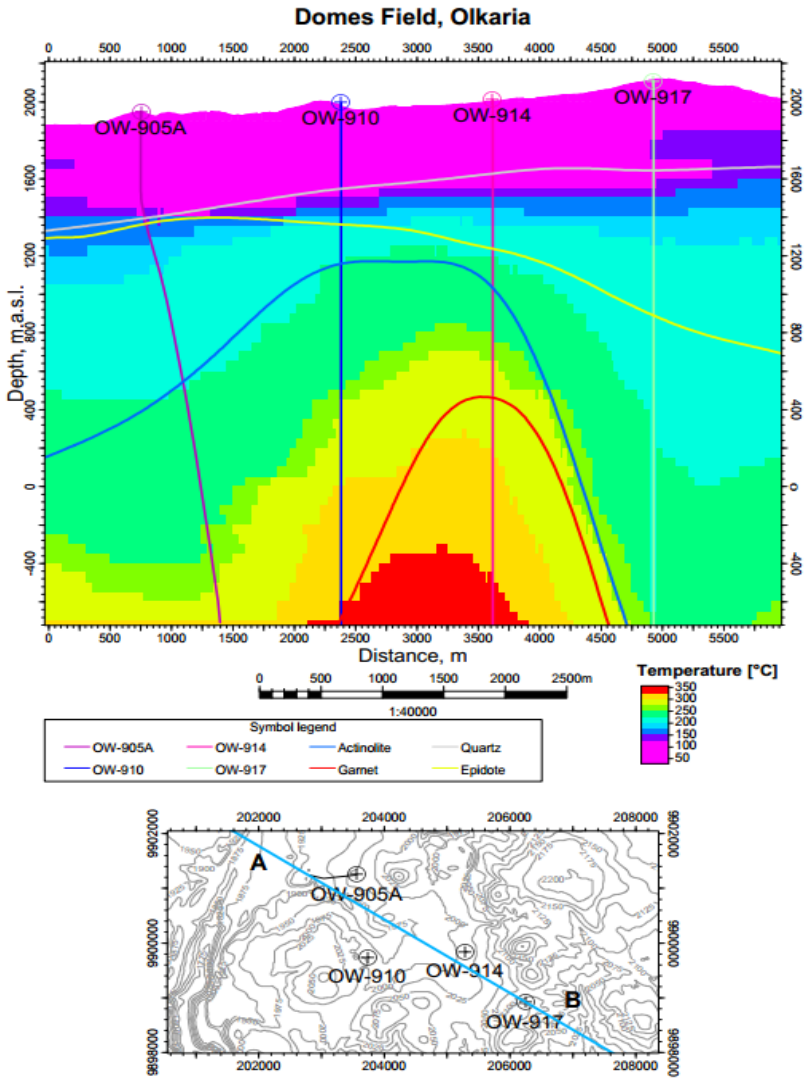

Figure 23: *Formation temperatures and alteration mineral isograds cross section across AB.*

4.5 Feed zones

According to recent stratigraphic studies (Lagat 2004, Mwangi 2012, Musonye 2012 and Okoo 2011), permeability in Domes area is enhanced by fractures, lithological contacts, joints, faulted and fractured breccia. In this study, feed zones were located on the basis of temperature recovery profiles, intensity of alteration, and the abundance of calcite and pyrite. Most of the feed zones identified from kinks in temperature recovery logs coincide with certain geological features. High alteration, abundant calcite/pyrite and/or fracturing were some of the features observed in these zones. Calcite, pyrite, vein fillings and alteration intensity are rated in the range of 0-3, where 0 depicts absence of the feature while 3 depicts high abundance. There were no major circulation losses upon which the location of feed zones could be based. However, some circulation losses occurred at shallow depth. This was as a result of the blocky rhyolitic formation. These losses were due to fractured formation and were cased off. Most of the feed zones in the three wells were located within fractured lavas and lithological boundaries.

In OW-905A, temperature recovery measurements were taken at 23, 67 and 134 days (Figure 24). The injectivity index was 240 lpm/bar. Step pumping was done at 1000 lpm, then stepped up to 1300lpm, 1600 lpm and eventually 1900 lpm. High alteration intensity was noted between 360-400 m; a zone coinciding with the water table. This intensity occurred in a trachyandesite underlying a tuff. In OW-905A, there were five feed zones noted. Four major feed zones were located at 1280 m, 1410 m, 1620 m, and 2500 m (Figure 24). One minor feed zone was located at 1540 m. The minor feed zone and the feed zone at 2500 m were located in a fractured trachyte zone as observed from the vein fillings. Medium intensity of alteration, medium to high abundance of pyrite and low abundance of calcite were observed at the feed zones. All these feed zones were located in the trachyte formation. In general, OW-905A (Figure 24) has medium to high intensity of alteration observed from 320 m down to the bottom of the well. This is coupled with moderate to high abundance of calcite and pyrite. Vein fillings are mainly observed between 1500 m to 2100 m and then from 2400 m to the bottom of the well, albeit in small amounts.

In OW-910, temperature recovery measurements were taken before, during injection and after 9 hours heating, 8 days heating, 17 days, 23 days and 29 days heating (Figure 25). The injectivity index was 187.97 lpm/bar. Step pumping was done at 1000 lpm, 1300 lpm, 1600 lpm and 1900 lpm. Six feed zones were identified in this well. A minor feed zone was identified at 2000 m in a trachyte formation. Major feed zones were identified at 1034 m (at a trachyte-rhyolite contact), 1820 m (in a trachyte formation), 2160 m (at a rhyolite-trachyte contact), 2540 m (in a trachyte formation) and at 2820 m (at a micro-granite intrusion-trachyte contact). The feed zone at 1034 m is associated with medium alteration and low abundance of calcite. The rest of the feed zones are associated with medium to high abundance of pyrite, fracturing and moderate to high intensity of alteration. Generally, moderate to high abundance of pyrite is observed from about 500 m down to the bottom of the well. Calcite is observed from 300 m to about 1200 m only. Alteration intensity is moderate to high throughout the well. Vein fillings occur in moderate to high abundance between 1100 m to 1800 m.

For OW-917, temperature recovery measurements were taken after 67, 97 and 160 days (Figure 26). Step pumping was done at 1000 lpm, 1300 lpm, 1600 lpm and 1900 lpm. The well got filled up with water at 1900 lpm forcing the step-pumping to be abandoned. Therefore, there was no injectivity index measured in this well. There were no major feed zones identified. Three minor feed zones were identified at 1430 m, 1750 m and 2700 m. These feed zones were located in trachyte formation (Figure 26). High calcite and pyrite abundance was observed at the location of these feed zones as well as the entire depth of the well. The feed zone at 2700 m was located in a zone that was moderately fractured although the veinlets were filled with calcite. The intensity of alteration is generally low in this well. Pyrite was observed in high abundance from about 400 m down to the bottom of the well. Vein fillings are observed in moderate abundance from 1200 m down to the bottom of the well. However, these vein fillings have been filled by calcite. The temperature curve deflection observed between 1000 m depth to 1200 m depth is as a result of the casing shoe effect since this well was cased at 1200 m. There were not any geological observations that coincided with these deflections to support location of a feed zone.

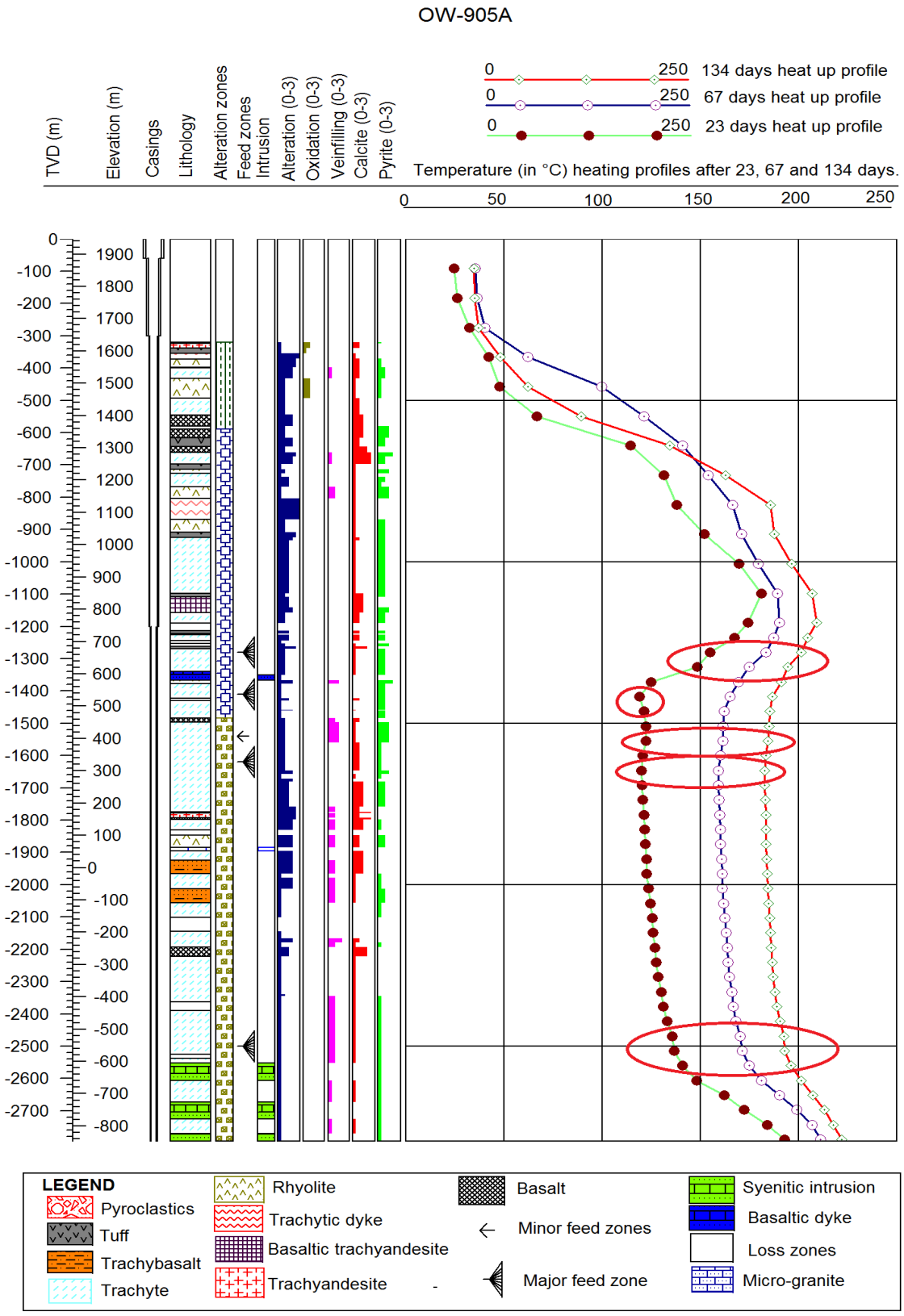

Figure 24: Aquifers in OW-905A as depicted from temperature profiles, alteration intensity and alteration mineral abundance.

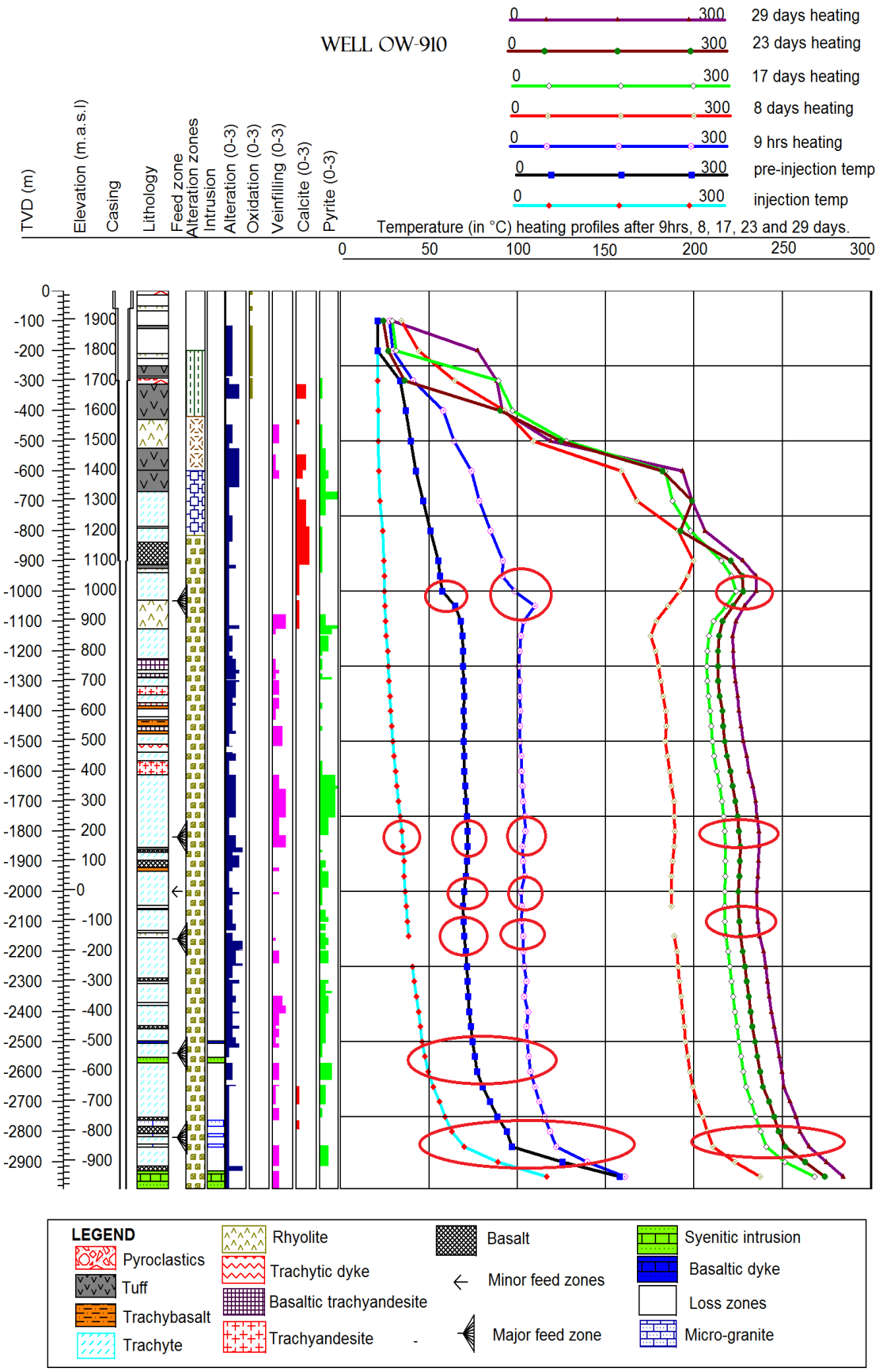

Figure 25: Aquifers in OW-910 as depicted from temperature profiles, alteration intensity and alteration mineral abundance.

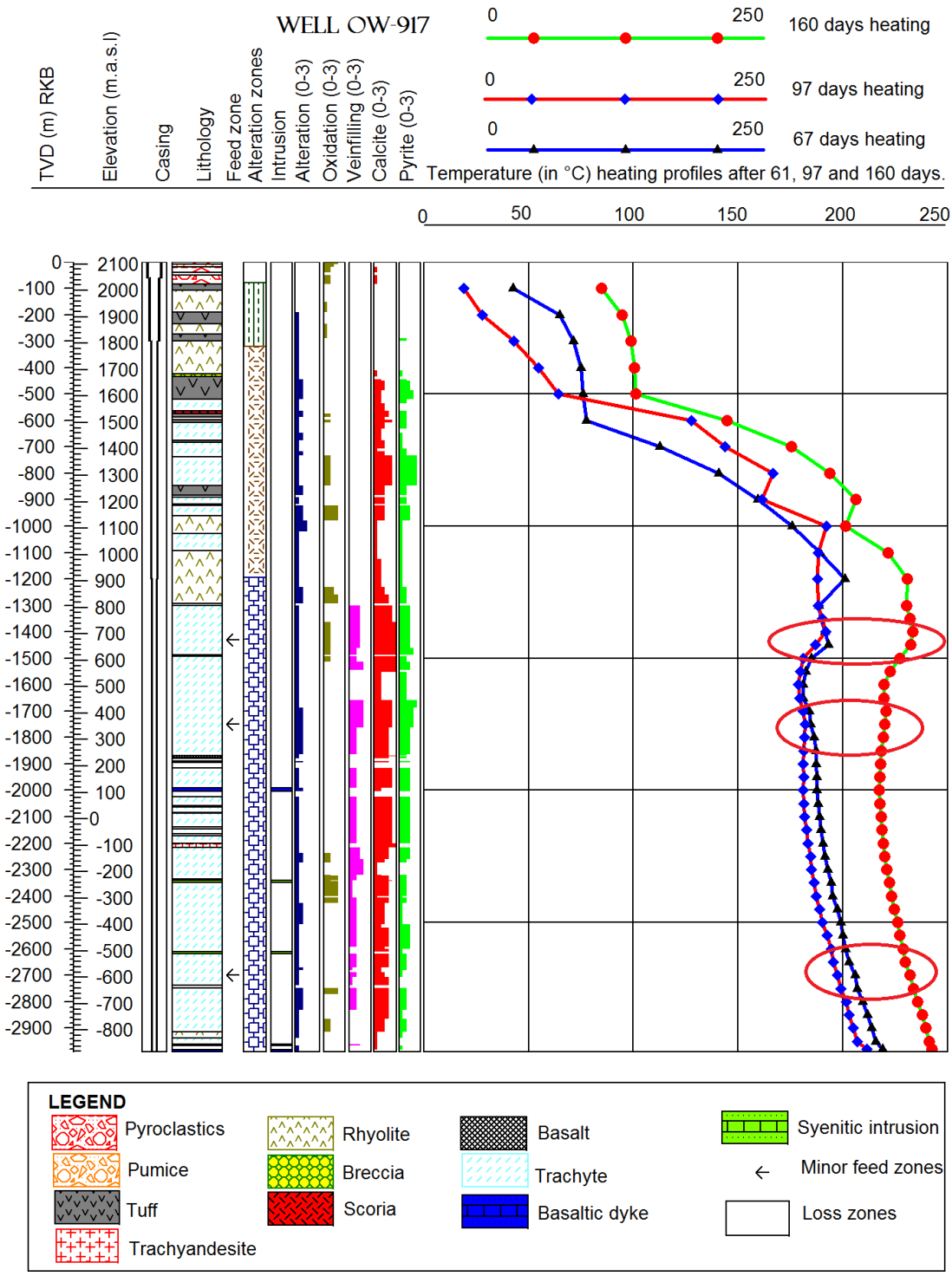

Figure 26: Aquifers in OW-917 as depicted from temperature profiles, alteration intensity and alteration mineral abundance.

4.6 Whole rock chemistry

Various techniques have been developed for the chemical analysis of igneous rocks. Among the most common used techniques are X-ray fluorescence analysis (XRF), atomic absorption spectrometry (AAS), electron probe microscope analysis and inductively coupled optical emission spectrometry (ICP-OES). These techniques are used for the analysis of major and trace elements in rocks. Moreover, petrologists have developed various methods of presenting geochemical data in order to classify the rocks. However, no single method is conclusive in classification of igneous rocks. One of the most common used methods is the total alkali (Na_2O+K_2O) verses silica (TAS) classification after Le Maitre et al. (2002). This method is widely used to separate alkaline and sub-alkaline volcanic rocks as well as subdividing volcanic rocks according to their chemical composition and grouping them in accordance with nomenclature.

4.7 Classification of rock types

The results for major and trace element analyses for the rocks from the study wells are shown in Tables 3, 4 and 5 below. The rocks were classified using TAS classification scheme (Figure 27).

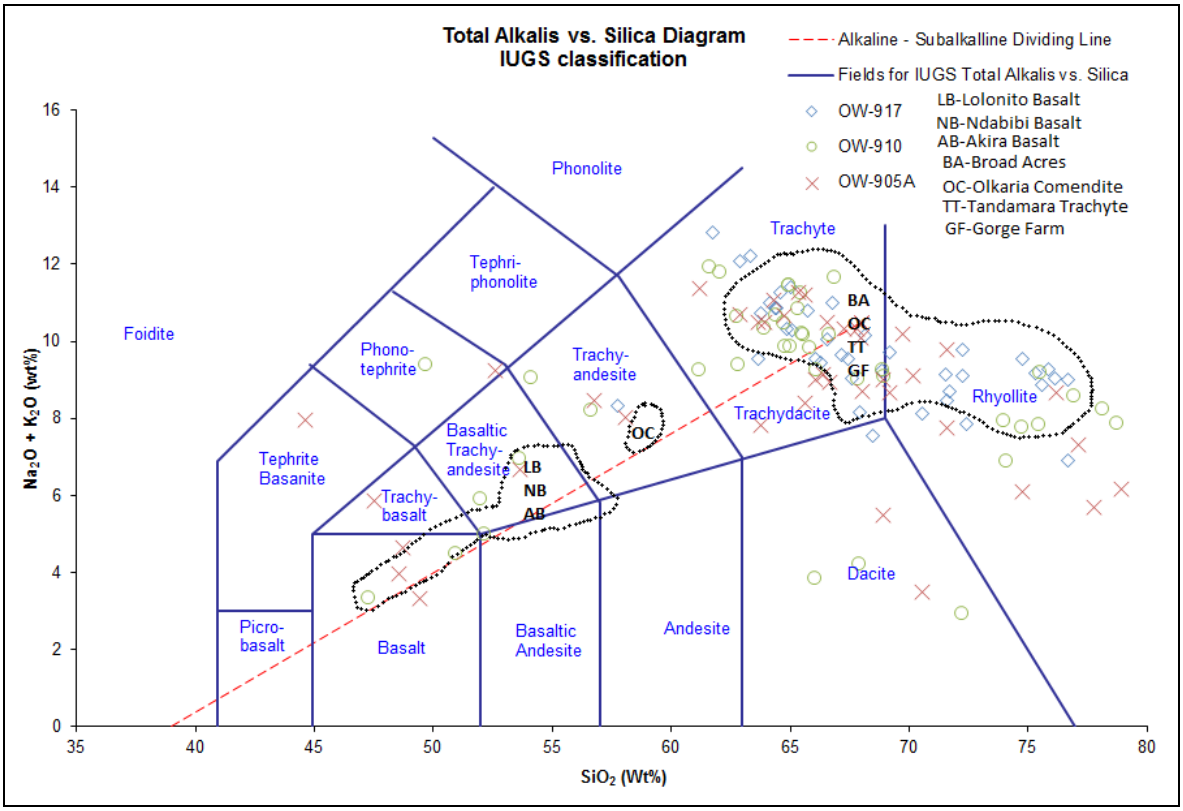

Figure 27: TAS classification scheme plot showing the compositional range for the Olkaria sub-surface rocks with the superimposed surface samples data (fields delineated with dotted lines).

From the TAS plot, the Olkaria sub-surface samples range in composition from basalt through trachyte to rhyolite. However, there is a noticeable gap between trachyandesite and trachyte. This gap may be attributed to two types of magma sources or different magma generation processes. This is explained in the subsequent section. OW-917 samples plot in the trachyte and rhyolite fields, except two samples that plot as trachyandesite and dacite. The sample that plotted in dacite was highly altered with most of the sanidine having been replaced with clays. Alteration of sanidine may result in the depletion of Na, which is a mobile element. Well OW-917 is mainly composed of highly evolved rocks, that is, rhyolites and trachytes while samples from well OW-905A and OW-910 plot in the basalt to rhyolite range. However, the bulk of these samples plot in the trachyte and rhyolite fields, an observation that is in harmony with the Olkaria stratigraphy whose major stratigraphic units are trachyte and rhyolite. One sample from OW-905A plotted in the tephrite basanite field. This sample contained abundant plagioclase phenocrysts. The two samples from OW-905A and OW-910, which plotted in the phonotephrite field, contained abundant plagioclase phenocrysts as well. These observations were made from the binocular and petrographic analyses.

The analysed surface rocks (data from Macdonald et al., 2008 and Marshall et al., 2009) exhibit similar compositional range as the sub-surface rocks. The Lolonito, Akira and Ndabibi basalts, which are found to the south and north of the proposed collapsed caldera, plot in the same field as the Olkaria sub-surface basalts. The Olkaria Comendites (OC), Tandamara Trachyte (TT), Gorge Farm (GF) rhyolites and Broad Acres (BA) rhyolites, which lie to the east but adjacent to the proposed collapsed caldera rim, plot with the sub-surface trachytes, rhyolites and trachyandesites. A few of the sub-surface samples plot in the dacite field most likely due to Na loss caused by hydrothermal alteration as observed under binocular analysis.

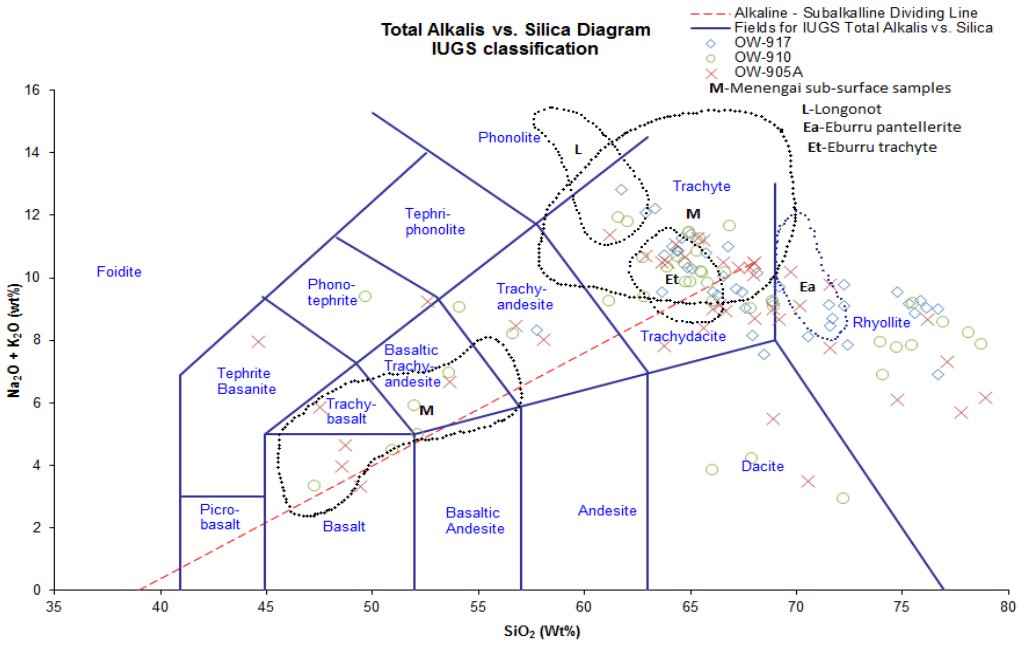

Figure 28: TAS classification plot showing Olkaria sub-surface rock samples in comparison with the samples from neighbouring volcanic centers and Menengai (fields delineated with dotted lines).

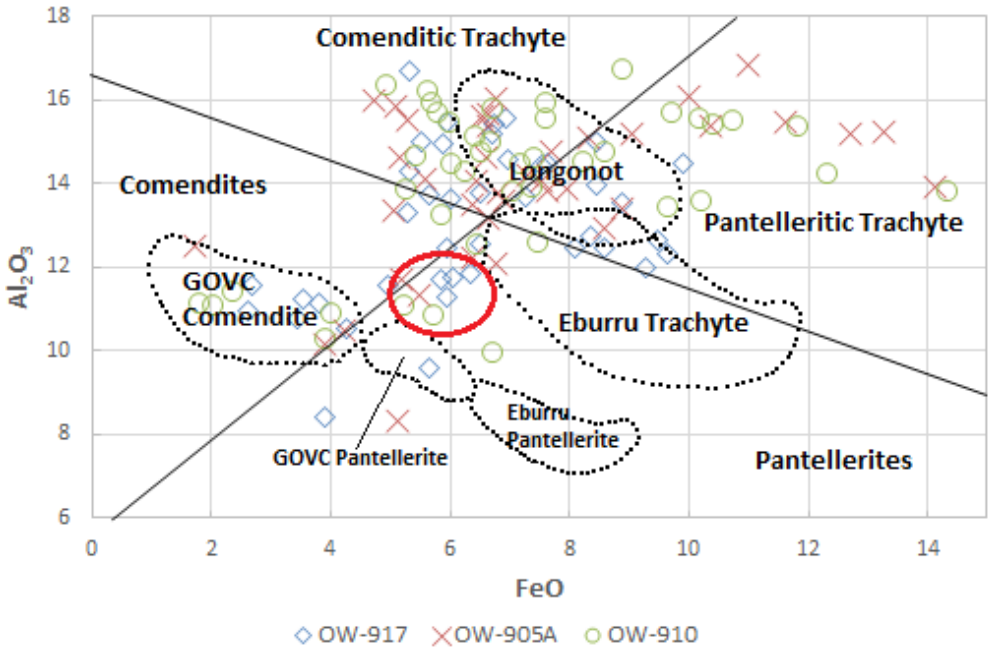

Figure 29: Al_2O_3 versus FeO classification of Olkaria sub-surface rocks and surface rocks from the neighbouring volcanic centres. (Modified from Macdonald, 1974.)

Figure 28 shows the TAS classification scheme while Figure 29 shows the Al_2O_3 versus FeO classification for Olkaria sub-surface samples in comparison to surface samples from the neighbouring volcanic centres and Menengai volcano. The Menengai data are for sub-surface samples from geothermal wells and was obtained from Mbia (2014). The Eburru and Longonot data were obtained from Clarke et al. (1990). From the TAS plot in Figure 28, it can be noticed that the Menengai sub-surface samples exhibit similar range in composition as the Olkaria sub-surface samples with a noticeable absence of rocks with trachyandesitic composition. This indicates similar processes of magma generation and differentiation occurred at these volcanic complexes. Mbia (2014), proposed that fractional crystallisation, partial melting and assimilation were the main processes involved in magma differentiation in Menengai volcanic complex. However, unlike the Olkaria samples, some of the Menengai trachytes show comparatively higher alkalinity than the Olkaria trachytes. Some of the Olkaria sub-surface trachytes plot within the same field as the Longonot trachyte. Eburru, which is a rhyolitic volcanic complex like Olkaria, has its trachyte and pantellerite plotting in the same field as the Olkaria sub-surface trachyte and rhyolite.

The trachytes and rhyolites from the three wells are peralkaline and thus the Al_2O_3 versus FeO plot from Macdonald (1974) is used for further classification (Figure 29). The fields of comendite, comenditic trachyte, pantelleritic trachyte and pantellerite on the Al_2O_3 versus FeO are from Macdonald (1974). From Figure 29, it can be seen that the Olkaria sub-surface samples show variability in general differentiation trends. The Al2O3 versus FeO plot also shows the general differentiation trends of the neighbouring volcanic centers. Some of the Olkaria sub-surface samples plot within the same field as the Longonot trachyte. Like the samples from Longonot, the borehole samples from Olkaria traverse the division between comenditic trachyte and pantelleritic trachyte, but the samples from Olkaria have considerably larger range of FeO content.

Table 3:Whole rock chemical analysis data for well OW-905A.

WELL OW-905A																				
Depth(m)	**330**	**384**	**410**	**492**	**514**	**554**	**630**	**656**	**704**	**718**	**762**	**784**	**836**	**950**	**1028**	**1116**	**1250**	**1305**	**1404**	**1466**
Major elements (wt %)																				
SiO_2	58.10	71.59	70.18	67.27	67.83	48.73	74.78	49.44	77.75	78.93	64.34	77.10	68.90	67.97	69.71	53.65	70.55	66.40	69.18	66.66
Al_2O_3	16.05	11.35	12.10	14.06	13.50	16.85	11.69	15.48	10.47	8.31	15.61	10.14	14.05	14.13	13.34	15.40	13.83	14.19	13.19	13.87
FeO	6.77	5.48	6.77	6.45	6.37	11.00	5.20	11.61	4.24	5.13	6.53	3.89	7.53	5.59	5.06	10.38	7.63	7.31	6.63	7.95
MnO	0.15	0.16	0.20	0.23	0.22	0.23	0.18	0.23	0.13	0.12	0.20	0.12	0.20	0.21	0.18	0.24	0.22	0.27	0.27	0.27
MgO	3.10	0.09	0.04	0.17	0.14	4.14	0.33	6.78	0.33	0.24	0.38	0.11	0.95	0.19	0.09	3.81	1.16	0.36	0.25	0.29
CaO	6.26	0.80	0.94	0.74	0.86	11.53	1.02	11.04	0.73	0.47	0.93	0.70	1.95	1.03	0.75	7.39	1.73	1.14	0.91	0.91
Na_2O	4.25	4.98	4.48	5.11	5.23	3.21	2.14	2.48	1.06	1.98	5.39	1.93	1.62	4.52	4.72	3.94	0.93	3.95	3.62	3.87
K_2O	3.79	4.81	4.61	5.21	5.10	1.45	3.95	0.83	4.65	4.18	5.67	5.39	3.88	5.56	5.47	2.74	2.58	5.18	5.04	5.07
TiO_2	1.09	0.51	0.48	0.55	0.53	2.33	0.41	1.74	0.29	0.26	0.60	0.33	0.58	0.59	0.51	1.98	0.98	0.90	0.63	0.80
P_2O_5	0.21	0.04	0.01	0.02	0.02	0.34	0.03	0.19	0.04	0.01	0.06	0.02	0.07	0.05	0.04	0.28	0.17	0.11	0.03	0.05
Trace elements (ppm)																				
Ba	1133.90	40.03	13.95	49.07	39.72	423.42	58.33	314.45	38.39	27.81	36.94	31.46	142.94	145.88	71.11	461.47	201.93	31.66	18.69	20.65
Co	26.07	3.23	2.92	4.20	4.94	51.50	2.75	55.04	2.53	0.88	5.35	2.68	7.21	4.46	3.31	39.18	13.16	6.49	4.03	6.58
Cr	60.72	5.17	9.70	2.62	4.44	43.54	7.13	52.24	14.20	8.00	5.32	15.31	4.63	6.85	6.35	14.56	18.07	3.39	10.37	4.09
Cu	37.46	20.01	18.67	38.50	101.43	83.93	21.05	62.48	26.47	20.93	37.38	30.21	132.95	16.69	14.70	35.73	34.16	17.78	34.76	61.15
La	60.16	180.90	199.67	180.09	170.46	46.00	287.70	25.84	304.74	271.05	314.08	215.50	211.27	147.89	118.47	77.24	171.37	166.05	233.63	288.50
Ni	34.22	17.96	15.06	50.73	187.14	92.30	9.04	64.35	27.24	8.17	32.66	31.56	222.99	10.07	3.99	26.70	32.62	6.29	26.47	96.68
Rb	26.71	159.98	91.20	190.98	148.80	0.00	171.05	3.60	223.75	333.20	105.30	267.08	139.76	160.58	227.82	37.59	187.60	310.51	176.76	136.67
Sc	20.11	1.03	0.83	2.19	1.94	30.12	1.27	38.66	1.62	0.82	2.41	0.53	2.47	5.58	3.87	21.10	8.09	4.95	2.96	4.33
Sr	241.71	12.38	4.90	7.39	7.28	477.80	40.62	355.73	30.33	19.59	22.35	14.20	113.57	15.40	13.25	399.17	60.17	15.08	13.83	11.89
V	108.55	10.26	8.23	6.70	7.17	305.74	19.52	321.41	29.27	25.62	17.71	15.15	16.01	7.99	6.04	232.29	69.15	8.15	12.20	11.20
Y	39.78	138.54	141.43	109.87	116.41	34.78	199.10	27.74	287.77	333.00	199.73	189.13	169.57	103.19	91.93	55.57	123.26	114.64	158.84	167.61
Zn	91.19	179.70	227.39	178.34	186.01	110.98	219.91	116.30	244.68	281.21	155.96	130.79	244.98	152.86	115.93	153.75	205.87	180.60	227.30	257.50
Zr	424.47	1046.15	1097.60	999.64	1085.49	225.23	1709.20	142.31	2014.24	2349.54	1770.50	1669.92	1360.95	859.26	745.81	411.98	1117.42	1108.64	1598.41	1671.63
Depth(m)	**1494**	**1528**	**1620**	**1648**	**1718**	**1758**	**1778**	**1794**	**1852**	**1888**	**1946**	**1970**	**2062**	**2084**	**2210**	**2282**	**2342**	**2398**	**2602**	**2794**
Major elements (wt %)																				
SiO_2	48.54	68.05	63.92	66.53	66.09	63.76	56.76	52.58	71.60	76.18	47.51	65.63	68.88	65.62	44.59	65.36	63.64	64.77	62.90	61.19
Al_2O_3	15.20	13.59	15.65	13.79	12.95	14.61	15.21	16.08	12.24	12.49	15.26	13.38	14.64	15.85	13.94	15.50	16.01	15.40	14.79	15.12
FeO	12.69	6.89	6.65	6.82	8.60	6.59	9.03	10.00	6.37	1.72	13.27	8.89	5.17	5.11	14.11	5.29	4.72	6.64	7.70	8.31
MnO	0.20	0.26	0.24	0.30	0.33	0.21	0.26	0.25	0.16	0.04	0.20	0.35	0.23	0.26	0.25	0.25	0.19	0.32	0.29	0.32
MgO	6.39	0.26	0.36	0.20	0.31	1.24	1.27	1.60	0.19	0.08	4.72	0.46	0.29	0.37	3.40	0.40	0.91	0.35	0.46	0.48
CaO	9.51	1.16	1.38	1.15	1.49	4.36	5.99	6.56	0.72	0.56	7.17	1.57	0.77	0.50	9.22	0.92	2.29	0.73	1.98	1.99
Na_2O	2.87	5.07	5.30	5.49	4.41	3.51	5.77	7.01	2.67	3.66	3.90	4.49	4.21	5.97	4.90	5.74	6.57	6.29	5.70	5.66
K_2O	1.10	3.64	5.21	5.00	4.60	4.31	2.68	2.24	5.09	5.02	1.96	3.89	4.81	5.24	3.07	5.54	3.94	4.38	5.01	5.72
TiO_2	2.79	0.77	1.00	0.52	0.76	1.00	2.10	2.59	0.60	0.12	4.52	0.86	0.77	0.80	4.62	0.77	1.16	0.84	0.85	0.91
P_2O_5	0.53	0.05	0.13	0.03	0.05	0.20	0.73	0.93	0.06	0.00	1.24	0.07	0.12	0.11	1.59	0.11	0.37	0.09	0.14	0.15
Trace elements (ppm)																				
Ba	363.56	18.41	217.64	67.29	26.10	420.69	370.45	389.87	84.72	21.66	850.28	56.88	105.90	114.92	1364.67	49.99	951.92	21.51	384.91	494.88
Co	64.34	5.54	8.66	3.52	5.36	12.70	35.07	45.17	4.63	0.00	68.42	7.30	5.47	5.11	70.37	5.53	11.18	6.28	8.48	7.41
Cr	44.60	2.91	9.11	6.28	4.35	16.25	37.04	47.75	3.18	4.76	5.89	3.51	4.98	3.68	31.73	4.15	4.24	5.25	4.80	3.83
Cu	80.57	17.64	21.42	21.95	19.09	26.57	41.93	55.68	27.24	19.39	34.30	21.13	19.07	16.26	95.17	17.29	16.44	21.74	86.13	32.01
La	28.60	264.49	181.67	153.66	442.49	154.45	92.39	61.17	324.47	74.08	58.52	418.94	104.76	113.71	52.31	146.06	92.75	170.39	114.31	103.89
Ni	102.26	6.82	11.76	39.42	12.29	15.31	39.02	65.59	31.92	7.43	22.10	4.26	8.17	5.32	59.69	10.19	5.38	12.47	148.45	18.42
Rb	0.00	121.19	122.64	172.81	119.17	77.39	59.32	31.46	150.36	573.94	0.00	135.10	201.70	769.50	0.00	134.32	82.25	132.40	113.61	74.24
Sc	33.26	3.95	5.95	2.17	2.89	7.86	19.75	25.46	3.09	0.51	23.47	3.34	6.04	6.33	27.22	5.80	7.08	7.17	16.22	18.51
Sr	449.38	13.82	22.29	14.10	15.13	102.56	276.84	321.26	27.93	18.90	780.41	29.65	24.34	13.31	686.19	16.67	185.08	11.51	34.12	43.78
V	331.34	13.84	6.95	6.62	21.61	30.85	125.38	156.25	22.31	5.57	251.05	24.54	5.70	4.53	313.40	8.06	29.64	7.02	13.09	11.52
Y	32.75	160.25	99.85	100.49	268.94	100.81	64.36	44.81	190.21	102.45	39.45	259.10	57.51	58.23	35.75	72.03	42.74	98.26	90.04	71.49
Zn	117.10	252.47	167.58	195.14	327.94	152.87	138.80	146.53	176.31	90.11	140.66	321.60	134.31	135.43	129.72	165.02	112.25	238.12	162.87	157.34
Zr	153.47	1706.63	978.78	919.21	2894.66	957.62	561.21	314.47	2125.77	398.19	283.36	2811.58	508.30	558.91	137.75	731.33	550.45	998.73	707.96	512.54

Table 4: Whole rock chemical analysis data for well OW-910.

WELL OW-910																					
Depth (m)	**66**	**418**	**436**	**476**	**590**	**722**	**772**	**844**	**894**	**988**	**1008**	**1082**	**1106**	**1248**	**1376**	**1388**	**1426**	**1440**	**1458**	**1470**	**1490**
Major elements in wt %																					
SiO_2	75.46	78.70	78.08	76.91	67.84	64.91	64.90	50.92	47.26	62.02	61.59	73.96	74.70	51.93	61.13	56.62	62.79	63.90	53.61	52.09	64.74
Al_2O_3	10.31	11.13	11.08	11.44	13.60	16.21	15.93	15.52	15.40	15.57	15.94	10.85	11.09	15.45	14.78	15.73	14.55	15.48	14.25	15.58	14.65
FeO	3.90	1.78	2.01	2.34	10.20	5.61	5.69	10.72	11.80	7.58	7.60	5.71	5.23	10.40	8.60	9.72	8.21	5.98	12.30	10.17	7.40
MnO	0.06	0.03	0.04	0.05	0.30	0.21	0.18	0.20	0.21	0.27	0.28	0.18	0.13	0.17	0.27	0.17	0.43	0.20	0.32	0.19	0.27
MgO	0.00	0.01	0.00	0.00	0.90	0.23	0.22	5.59	7.38	0.42	0.40	0.05	0.07	4.66	1.15	1.71	0.60	0.53	2.35	5.56	0.45
CaO	0.38	0.21	0.28	0.31	1.32	0.68	0.91	10.03	11.76	1.40	1.34	0.63	0.46	9.26	3.35	4.24	2.65	2.12	7.18	9.33	1.43
Na_2O	5.06	3.66	3.83	3.99	0.18	5.96	6.31	3.19	2.67	6.24	6.81	3.46	3.13	3.26	5.06	5.21	5.06	5.83	4.49	3.15	5.46
K_2O	4.16	4.23	4.42	4.62	4.06	5.53	5.18	1.33	0.70	5.58	5.13	4.49	4.65	2.68	4.21	3.03	4.35	4.52	2.50	1.87	4.42
TiO_2	0.15	0.09	0.10	0.14	1.17	0.52	0.51	2.00	2.43	0.60	0.59	0.46	0.38	1.74	1.15	2.28	1.06	0.96	2.40	1.67	0.89
P_2O_5	0.00	0.00	0.00	0.00	0.15	0.04	0.04	0.33	0.23	0.05	0.05	0.01	0.01	0.25	0.13	1.03	0.15	0.24	0.39	0.27	0.12
Trace elements (ppm)																					
Ba	5.37	4.94	3.72	4.24	153.98	39.61	37.81	302.62	246.57	23.78	21.94	8.07	11.31	1322.29	216.43	1445.01	151.19	1432.03	656.55	491.81	140.34
Co	0.00	0.00	0.00	0.00	16.50	2.55	2.63	47.03	64.22	5.11	4.62	2.63	1.50	42.58	13.25	25.86	14.17	8.71	53.42	45.20	7.51
Cr	2.66	5.12	2.46	4.01	3.35	3.34	3.12	115.94	61.30	5.49	7.33	28.82	6.48	19.60	22.34	12.96	17.48	16.96	24.31	19.63	10.36
Cu	22.91	16.07	16.72	16.84	19.16	12.51	20.73	68.67	94.58	26.89	25.21	16.05	21.30	22.42	26.92	25.11	29.85	34.61	33.67	24.58	15.80
La	187.88	79.56	77.99	82.45	228.91	99.65	112.51	45.71	23.98	300.41	284.87	197.73	161.23	23.19	130.68	79.11	126.07	70.14	88.90	21.75	158.24
Ni	7.52	8.60	2.86	4.55	6.36	1.31	8.59	75.04	87.15	7.10	6.59	13.08	13.80	20.96	18.96	20.21	25.20	42.14	13.27	20.89	9.55
Rb	1690.16	239.22	237.02	225.06	366.31	85.84	176.35	14.36	0.00	91.57	144.33	203.96	136.53	16.71	143.79	70.47	126.05	161.16	88.52	22.04	192.07
Sc	0.10	0.00	0.00	0.00	7.97	1.60	1.88	34.03	37.04	2.33	2.18	0.30	0.24	19.38	10.68	17.79	7.43	11.27	23.79	17.58	5.60
Sr	7.88	3.39	1.88	3.33	31.65	9.24	10.96	368.42	450.03	16.41	12.06	6.13	4.76	224.30	91.99	266.49	44.05	59.61	317.97	156.36	26.42
V	20.76	8.79	9.04	9.66	70.30	4.50	5.15	258.57	309.60	17.32	15.04	9.05	7.62	142.53	51.85	63.14	18.11	14.02	208.44	120.35	12.53
Y	416.15	130.16	131.79	159.50	178.15	67.01	74.60	41.66	21.96	185.47	208.37	145.87	114.70	18.41	90.32	78.11	107.89	59.06	63.43	17.60	109.64
Zn	326.25	139.31	139.15	164.29	265.90	136.61	168.23	130.85	119.21	215.66	233.01	212.64	195.48	74.88	171.29	157.18	167.10	109.67	148.03	88.94	178.74
Zr	2533.54	969.88	977.97	1206.05	1381.12	555.58	634.11	267.54	101.10	1778.28	1814.98	1205.76	941.57	124.81	700.76	424.98	735.04	460.90	438.84	115.53	997.46
Depth (m)	**1524**	**1530**	**1600**	**1630**	**1710**	**1790**	**1976**	**2078**	**2244**	**2262**	**2294**	**2332**	**2544**	**2554**	**2660**	**2732**	**2766**	**2832**	**2898**	**2950**	**2968**
Major elements in wt %																					
SiO_2	72.21	66.03	54.09	67.83	66.06	64.38	68.86	65.47	74.07	64.68	49.65	68.91	64.96	62.74	65.80	65.50	75.40	66.61	65.29	66.83	65.38
Al_2O_3	13.82	16.75	13.48	12.58	13.90	15.15	13.28	14.30	9.98	15.02	13.82	12.55	14.50	15.81	14.76	15.73	10.92	14.69	16.36	13.86	14.50
FeO	7.04	8.89	9.65	7.48	7.36	6.40	5.85	6.24	6.70	6.68	14.33	6.44	7.17	6.70	6.52	5.78	4.01	5.43	4.92	5.26	6.01
MnO	0.14	0.06	0.29	0.26	0.27	0.26	0.23	0.24	0.22	0.27	0.34	0.25	0.39	0.28	0.30	0.26	0.10	0.25	0.25	0.23	0.25
MgO	0.96	1.49	2.98	0.33	0.42	0.43	0.38	0.55	0.28	0.36	3.00	0.40	0.58	0.55	0.47	0.44	0.15	0.48	0.36	0.39	0.43
CaO	1.20	1.30	8.17	1.43	1.57	1.39	1.16	1.89	1.03	1.46	4.50	1.51	1.45	1.91	1.25	1.10	1.04	1.39	1.02	0.87	1.09
Na_2O	0.53	0.29	6.11	4.28	4.85	5.43	3.95	5.02	3.08	6.24	2.58	4.79	4.59	5.69	4.45	4.98	4.01	5.31	5.22	6.62	6.10
K_2O	2.44	3.59	2.97	4.76	4.44	5.28	5.33	5.22	3.83	4.25	6.84	4.30	5.30	4.96	5.39	5.22	3.86	4.89	5.63	5.08	5.17
TiO_2	1.25	1.33	1.82	0.77	0.84	0.99	0.62	0.76	0.56	0.82	3.43	0.57	0.81	1.03	0.77	0.75	0.25	0.70	0.70	0.63	0.81
P_2O_5	0.18	0.16	0.33	0.06	0.06	0.12	0.03	0.08	0.07	0.06	1.29	0.04	0.08	0.12	0.09	0.09	0.02	0.09	0.09	0.08	0.11
Trace elements (ppm)																					
Ba	344.73	219.36	240.90	31.63	40.34	211.08	75.33	154.98	122.85	63.98	458.79	50.99	89.16	199.34	69.28	48.84	22.66	76.23	64.96	40.63	51.61
Co	18.10	20.84	34.58	6.12	6.33	8.23	5.05	8.52	4.24	5.93	56.07	4.21	7.23	9.22	5.25	5.57	2.15	5.02	5.17	4.19	7.66
Cr	34.30	12.29	11.17	20.53	12.10	16.94	9.33	44.70	4.62	14.93	18.62	16.35	3.30	16.34	15.35	20.35	34.62	15.02	15.49	15.20	9.80
Cu	26.37	16.80	23.79	18.00	22.47	27.93	18.40	24.24	12.80	18.31	27.19	16.37	22.04	34.09	22.42	30.86	71.16	26.84	24.18	15.26	15.58
La	150.74	76.86	64.24	232.88	220.07	155.07	256.42	187.20	165.64	174.06	120.02	227.49	179.84	167.93	186.31	147.85	104.97	133.72	142.61	129.72	123.48
Ni	24.58	11.67	12.36	8.91	16.77	25.20	7.95	14.67	3.46	18.96	31.14	4.18	18.85	19.77	10.26	27.16	93.66	26.79	19.90	4.27	6.77
Rb	234.40	33.14	37.56	128.83	179.99	72.70	538.64	167.58	119.48	156.11	54.96	176.11	44.08	75.82	163.81	183.54	234.31	94.63	179.24	214.95	183.60
Sc	10.42	7.04	12.58	4.21	4.65	5.84	3.97	6.16	2.52	5.83	30.23	3.27	2.22	4.85	5.33	5.44	0.85	5.19	5.13	4.22	5.14
Sr	58.76	25.12	149.28	13.15	21.57	24.53	29.07	51.04	20.66	26.13	128.96	28.39	20.89	49.35	26.04	23.19	15.17	36.41	19.21	16.90	10.41
V	102.99	55.70	113.06	13.35	21.58	11.11	25.79	27.39	16.68	9.15	212.09	16.01	13.33	17.19	11.78	8.25	13.21	11.51	9.73	8.44	7.87
Y	123.68	44.23	48.19	150.51	149.31	99.13	153.15	124.12	99.29	100.77	100. 77	120.80	96.60	110.44	113.96	87.37	165.43	90.44	81.33	89.96	92.33
Zn	160.72	154.91	137.91	226.57	189.66	167.71	227.67	198.04	192.90	208.23	251.97	263.05	227.28	184.98	218.22	181.61	223.38	162.77	182.39	116.94	168.53
Zr	914.08	427.46	407.64	1471.50	1503.51	957.13	1578.57	1266.34	1177.86	866.20	596.93	1498.63	1094.34	1105.65	1166.47	779.19	1422.36	862.84	881.65	829.12	834.88

Table 5:Whole rock cheminal analysis data for well OW-917.

WELL OW-917																					
Major elements (wt%)																					
Depth(m)	**90**	**120**	**144**	**160**	**262**	**286**	**350**	**430**	**520**	**548**	**594**	**624**	**636**	**662**	**704**	**716**	**788**	**830**	**868**	**890**	**968**
SiO_2	76.66	75.30	74.78	75.85	76.12	66.80	75.56	72.24	65.71	62.89	61.74	64.45	64.85	65.02	64.16	66.56	64.61	64.37	66.31	68.48	80.40
Al_2O_3	10.96	11.23	11.13	10.75	11.58	13.65	10.55	11.56	15.47	15.57	13.95	12.33	12.66	11.98	13.52	12.75	14.43	14.48	13.70	12.47	8.43
FeO	2.62	3.55	3.79	3.44	2.68	6.01	4.28	4.97	5.96	6.92	8.45	9.64	9.49	9.28	8.89	8.36	7.52	7.63	7.27	8.08	3.91
MnO	0.05	0.06	0.06	0.05	0.03	0.21	0.06	0.12	0.21	0.24	0.29	0.37	0.28	0.30	0.30	0.29	0.26	0.27	0.24	0.24	0.08
MgO	0.00	0.00	0.00	0.00	0.00	0.10	0.00	0.12	0.21	0.30	0.33	0.30	0.31	0.15	0.10	0.13	0.11	0.25	0.31	0.56	0.06
CaO	0.27	0.22	0.20	0.18	0.21	1.60	0.19	0.58	0.84	1.18	1.40	1.13	1.18	1.00	1.19	1.00	1.03	1.32	1.90	1.61	0.26
Na_2O	4.41	4.77	4.95	4.89	4.53	6.10	4.63	5.26	5.26	6.91	8.04	6.37	6.17	7.21	6.32	4.94	6.35	5.93	5.08	4.02	1.95
K_2O	4.59	4.40	4.60	4.41	4.51	4.90	4.25	4.51	5.53	5.18	4.79	4.50	4.16	4.19	4.69	5.12	4.93	4.96	4.35	3.54	4.42
TiO_2	0.15	0.18	0.18	0.17	0.16	0.44	0.17	0.29	0.56	0.59	0.68	0.60	0.60	0.59	0.61	0.60	0.61	0.62	0.57	0.62	0.20
P_2O_5	0.00	0.00	0.00	0.00	0.00	0.03	0.00	0.02	0.07	0.05	0.14	0.05	0.05	0.04	0.04	0.06	0.03	0.04	0.11	0.13	0.02
Trace elements (ppm)																					
Ba	19.52	6.56	4.32	6.99	3.88	29.02	10.19	39.50	53.14	36.86	162.90	39.20	39.87	28.15	41.42	47.27	53.52	41.00	201.83	139.48	15.91
Co	0.00	0.00	0.00	0.00	0.00	1.99	0.00	0.51	3.51	3.71	4.87	3.67	4.66	3.32	3.20	4.49	3.43	3.42	4.38	7.32	0.00
Cr	3.94	3.17	2.05	1.98	2.72	2.89	18.87	3.15	2.96	2.17	2.57	2.49	2.47	2.14	21.63	2.32	2.41	2.74	5.65	24.60	1.90
Cu	18.05	21.23	21.99	21.79	20.91	17.73	20.91	19.38	17.55	16.81	20.04	19.98	17.22	18.64	18.13	15.15	15.53	18.08	16.20	22.38	14.47
La	95.44	111.62	139.57	113.07	93.08	112.35	116.10	176.95	158.68	156.31	182.38	212.56	270.92	230.48	156.93	204.32	122.40	121.95	128.76	182.72	261.55
Ni	4.38	4.66	5.35	5.53	22.51	3.13	7.02	2.52	4.39	2.25	3.25	11.13	2.55	8.15	7.69	3.72	2.59	8.04	5.79	14.20	1.66
Rb	425.49	352.38	271.59	183.36	232.17	134.14	369.54	205.72	333.70	112.71	125.98	173.11	128.58	296.99	194.45	118.45	149.64	220.23	132.33	230.32	268.50
Sc	0.00	0.00	0.00	0.00	0.00	1.31	0.00	0.84	2.57	2.85	3.21	0.80	0.94	0.68	0.97	1.64	1.14	1.08	2.48	4.06	0.10
Sr	5.67	3.42	3.37	3.22	2.52	7.15	3.33	12.07	21.56	10.52	30.31	17.52	15.37	14.44	14.61	17.97	9.24	11.77	41.97	61.71	12.00
V	15.41	14.68	16.31	14.59	9.69	7.64	14.38	18.99	7.41	5.68	11.00	8.84	9.79	8.50	6.00	7.53	4.10	3.51	13.55	39.91	14.02
Y	194.76	246.80	264.49	221.79	158.54	137.51	264.74	288.48	104.98	103.14	127.26	177.11	174.52	167.71	126.87	136.26	80.97	90.74	97.17	143.26	190.03
Zn	198.97	337.34	305.46	282.82	177.37	194.30	300.03	306.35	142.68	176.56	232.53	294.73	292.72	275.06	224.12	217.83	163.61	170.96	141.61	247.25	167.87
Zr	1821.91	1732.89	2008.28	1825.65	1085.81	994.11	1986.15	2193.12	928.56	985.99	1070.50	1472.16	1439.87	1389.89	971.82	1011.31	670.08	729.66	732.88	1189.36	1725.73
Major elements (wt%)																					
Depth(m)	**1010**	**1098**	**1176**	**1250**	**1386**	**1406**	**1488**	**1524**	**1666**	**1714**	**2074**	**2152**	**2208**	**2312**	**2364**	**2398**	**2554**	**2620**	**2680**	**2734**	
SiO_2	76.66	72.26	71.54	71.70	69.19	68.13	71.59	68.84	67.60	67.45	63.68	63.32	57.74	67.92	72.44	70.54	66.09	65.08	67.18	63.74	
Al_2O_3	9.60	11.28	11.76	11.86	13.33	14.31	12.46	13.71	14.97	13.78	15.01	16.72	14.49	12.46	11.71	12.56	14.57	15.21	15.01	15.44	
FeO	5.65	5.94	6.05	6.34	5.28	5.31	5.94	5.64	5.89	6.50	8.46	5.31	9.90	8.59	5.84	6.49	6.96	6.72	5.52	6.75	
MnO	0.11	0.16	0.16	0.11	0.13	0.14	0.15	0.14	0.18	0.19	0.28	0.28	0.24	0.29	0.22	0.22	0.24	0.24	0.18	0.24	
MgO	0.06	0.10	0.11	0.08	0.22	0.23	0.12	0.34	0.35	0.36	0.46	0.46	2.06	0.25	0.15	0.15	0.29	0.31	0.32	0.39	
CaO	0.23	0.48	0.58	0.53	1.24	1.02	0.60	1.29	1.17	1.29	1.31	0.53	4.27	1.27	0.81	0.91	1.23	0.97	0.89	1.31	
Na_2O	2.28	4.72	4.50	3.25	4.37	4.88	3.83	3.68	4.00	4.46	4.25	7.66	4.11	3.81	3.90	4.53	4.80	5.26	4.67	5.45	
K_2O	4.63	4.38	4.66	5.45	5.33	5.27	4.62	5.56	5.04	5.08	5.28	4.58	4.21	4.36	3.97	3.61	4.77	5.03	4.97	5.27	
TiO_2	0.24	0.35	0.36	0.40	0.51	0.46	0.42	0.51	0.52	0.60	0.92	0.90	2.02	0.70	0.67	0.65	0.76	0.88	0.92	1.10	
P_2O_5	0.00	0.01	0.01	0.02	0.05	0.03	0.02	0.06	0.05	0.07	0.14	0.13	0.70	0.05	0.07	0.04	0.07	0.10	0.16	0.14	
Trace elements (ppm)																					
Ba	15.23	30.26	33.46	49.08	67.36	59.45	39.18	75.61	53.24	78.25	122.54	111.65	1150.77	51.90	37.30	25.70	53.63	152.29	342.24	351.78	
Co	0.00	1.34	2.04	2.17	4.40	2.89	2.22	4.52	4.17	6.98	8.66	5.37	28.17	5.97	4.09	15.94	4.98	7.08	29.77	11.94	
Cr	2.23	2.90	5.16	12.61	12.04	9.24	6.76	7.58	14.85	44.35	16.42	2.68	7.74	114.29	8.50	11.48	12.77	20.52	19.77	36.91	
Cu	26.75	16.97	17.42	16.23	35.42	22.95	18.70	21.39	20.24	27.40	27.67	13.89	23.60	18.15	15.89	15.49	17.92	19.16	16.38	23.74	
La	329.24	256.58	229.43	263.99	192.01	168.76	197.45	199.38	178.98	195.13	148.28	98.19	88.48	296.60	205.34	215.22	179.74	172.03	140.35	108.70	
Ni	11.32	8.75	3.69	3.76	4.05	7.86	4.61	6.90	3.54	5.18	17.57	4.12	5.57	6.45	22.60	3.09	4.61	9.45	5.18	14.21	
Rb	2798.73	803.61	276.75	234.20	1558.49	238.44	267.81	189.66	186.80	147.12	117.51	181.12	117.35	156.82	297.86	1087.37	196.54	147.15	165.33	165.02	
Sc	0.10	0.49	0.50	0.92	2.90	1.88	1.11	2.71	2.49	2.99	4.52	6.52	18.13	3.05	3.12	3.02	4.55	5.14	4.85	5.05	
Sr	12.67	12.00	13.16	17.94	38.18	37.94	16.75	44.87	24.50	30.73	23.51	19.35	252.23	18.31	14.64	12.43	16.87	18.22	33.54	44.08	
V	14.96	13.58	14.83	18.03	27.63	23.60	18.62	32.34	24.58	30.50	13.34	5.09	109.03	60.37	11.48	11.95	11.36	8.36	12.36	14.44	
Y	234.68	194.01	196.87	188.20	144.58	143.36	189.08	149.73	148.81	144.11	138.16	63.88	79.44	183.34	136.74	137.85	128.28	105.24	92.56	79.22	
Zn	189.24	249.10	248.67	186.99	160.98	182.98	207.13	180.36	194.75	189.54	222.80	170.22	142.29	269.63	178.06	186.58	186.82	173.73	125.35	141.74	
Zr	1849.79	1682.33	1715.85	1682.39	1292.95	1273.15	1670.52	1327.24	1395.25	1268.73	1174.34	593.19	578.90	1742.63	1285.69	1327.53	1263.92	1021.34	891.66	735.62	

The Olkaria sub-surface trachyte samples show a continuous evolution from the pantelleritic trachyte to comenditic trachyte. A few of the samples plot within the Eburru trachyte field, but generally Eburru trachytes have lower Al_2O_3 contents at comparable FeO contents. Most of the rhyolitic samples from the Olkaria sub-surface samples plot within the comendite field. The samples circled red show a different composition from that previously observed in the Olkaria surface pantellerites. These samples are rhyolites and occur at 1082 m and 1106 m in well OW-910, at 384 m and 410 m in OW-905A and at 1078 m, 1176 m and 1250 m in OW-917. The rhyolitic units are separated by trachytic units in the three wells.

4.8 Effects of hydrothermal alteration on the rock chemistry

Hydrothermal alteration involves the change in chemical composition of the rock as a result of fluid-rock interaction. In the geothermal field, alteration mainly entails filling of primary porosity or replacement of the primary minerals by secondary minerals. In the case of pore filling, lower concentrations of immobile elements will be recorded in whole rock analyses as a result of mass dilution (Franzson et al., 2008). In this paper, surface sample data from Macdonald et al. (2008) and Marshall et al. (2009) were used to represent the least altered rock data. Rock units found at depth are prone to the kinematics that affects the intensity of hydrothermal alteration as compared to the surface rocks. That is the reason why the surface samples were chosen to represent the least altered samples.

Major elements were plotted against SiO_2 in order to assess the effects of alteration on whole rock composition. Rb, Ba, Sr, Ni, La and Y were also plotted against Zr. The boundaries delineated by the broken line represent the least altered surface samples. The Rb, Sr, Cr, La and Y versus Zr plots indicate that hydrothermal process has had insignificant effect on trace element concentration except for Ba and Rb (Figure 30). Ba is a constituent element of feldspars. It is mobile and is easily leached from the rock through hydrothermal processes. Rb being an alkali metal is easily leached from the plagioclase by hydrothermal processes. This explains why there is scattering in Rb and Ba versus Zr plots. Cr, La, Sr, and Y are immobile and least affected by hydrothermal processes. From these plots, it can be concluded that the hydrothermal process has had so little effect on the rock chemistry that the analyses can be used to infer about the geochemical evolution of these sub-surface rocks from GOVC.

From the major element versus SiO_2 plots (Figure 31), it can be clearly seen that the hydrothermal process has no significant effect on the chemical composition of the subsurface rocks, except for Na_2O, which shows high scattering as compared to the surface rocks. Alkali feldspars are the dominant rock forming minerals for the trachytes and rhyolites, which are the most dominant rock types in the studied wells. Na is a constituent element of alkali feldspars. It is mobile and easily leached from the rock by hydrothermal processes. This accounts for the scattering observed in the sub-surface rocks as compared to the surface rocks on the Na_2O versus SiO_2 plot. The minor scatter seen in the other plots may relate to background ‘noise’ as a result of analyses of porphyritic samples.

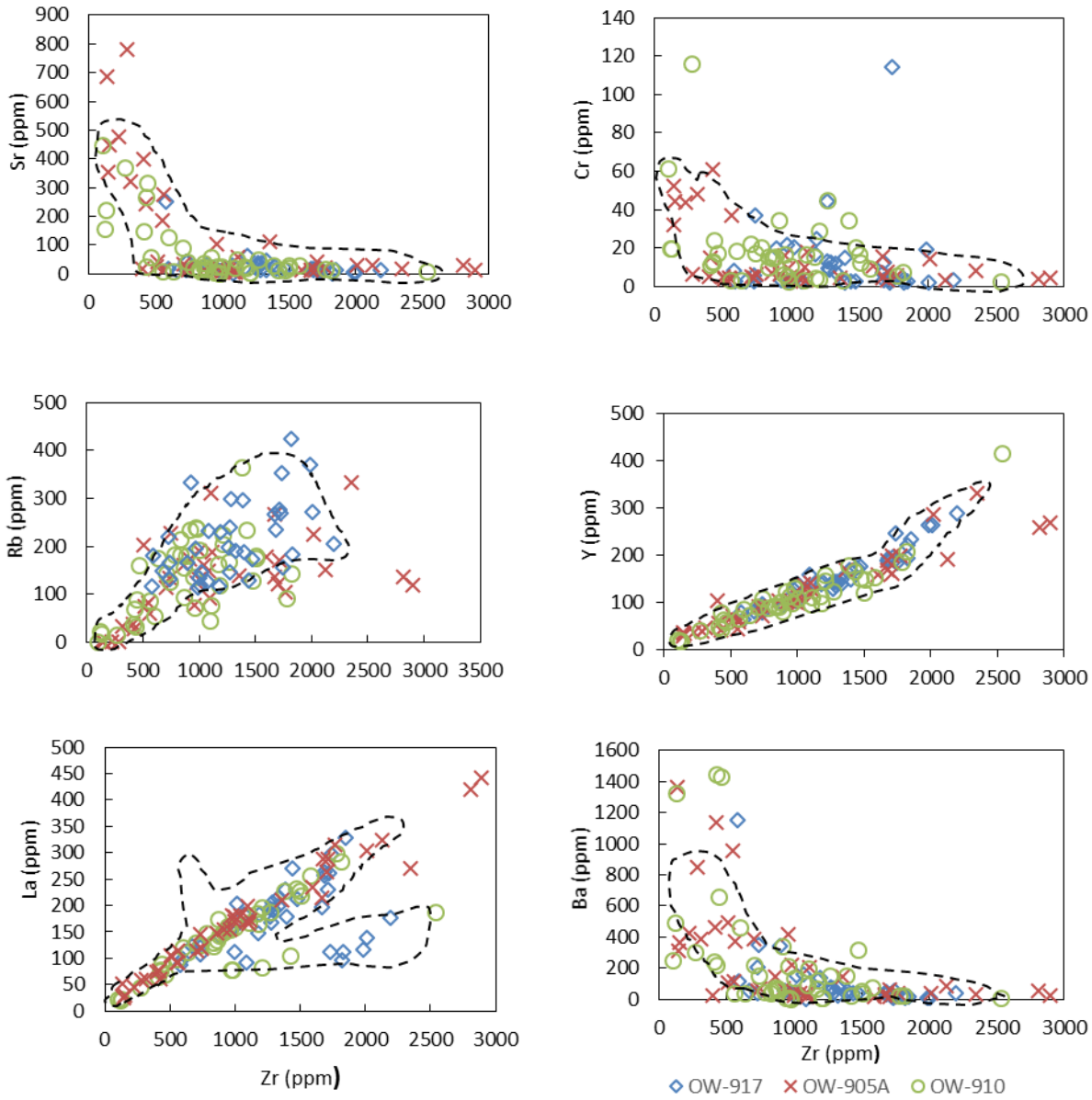

Figure 30: Whole-rock trace element abundances as a function of Zr for the surface and sub-surface samples (The broken lines outline the fields for the surface samples).

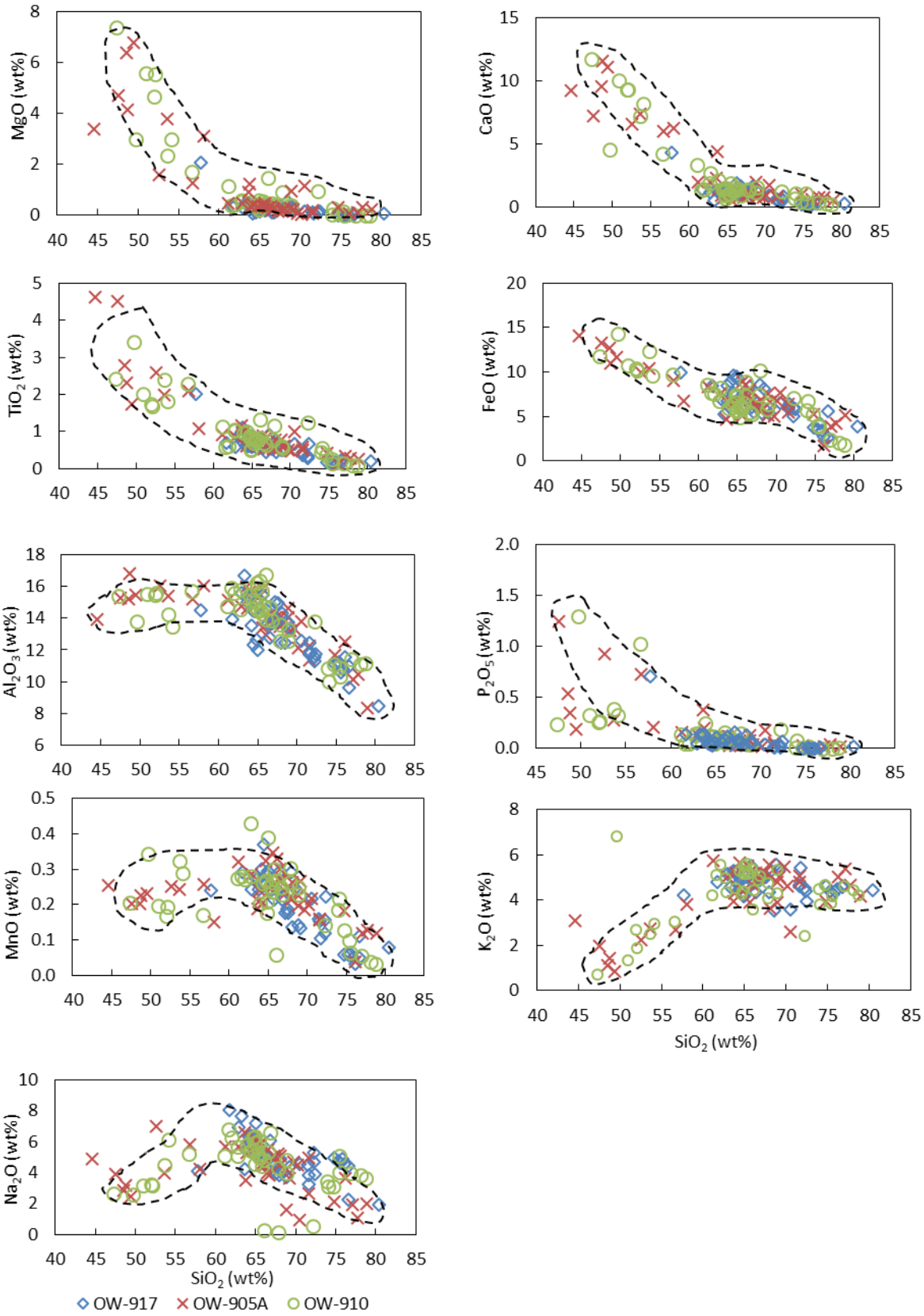

Figure 31: *Whole-rock major element abundances as a function of SiO_2 for the surface and sub-surface samples (The broken lines outline the fields for the surface samples).*

4.9 Geochemical evolution of the Greater Olkaria Volcanic Complex

Geochemical evolution of the Olkaria volcanic complex has been discussed by Macdonald et al. (2008) and Marshall et al. (2009) by the use of surface sample compositions. In their studies, they analysed silicic rocks from within the collapsed caldera and the complex in general and mafic rock samples from the periphery of the caldera. In the present analysis, we are looking at silicic and mafic sub-surface rock samples. These samples are drill cuttings sampled from the surface down to a depth of 2900 m. This gives us an opportunity to identify the similarities between magmas buried beneath the collapsed caldera and the silicic surface rocks of the GOVC and the mafic emplacements on its periphery. It also enables us to decipher the range of magmatic composition beneath the complex.120 samples from three wells; OW-905A, OW-910 and OW-917, located in the Domes area of Olkaria geothermal area, were used in this study.

To determine the change in the concentration of major elements during magmatic differentiation, SiO_2 was used as an index of differentiation. All major, as well as trace elements, were plotted against SiO_2 on Harker diagrams. The trends on Harker diagrams represent liquid lines of descent. Liquid lines of descent are simply coherent trends on Harker diagrams that are generally considered to represent the course of chemical evolution of magmas as consequence of processes such as fractional crystallisation (Wilson, 1989).

SiO_2 values in the samples show a remarkably wide range of variation from 44% to 80.4%, making SiO_2 content suitable as an index of differentiation. Even though there is a wide range of SiO_2 values, most of the samples have their SiO_2 values in the range of 64% and 80%. Overall, with increasing SiO_2, there is a decrease in Al_2O_3, CaO, TiO_2, MnO, MgO, P_2O_5 and FeO contents (Figure 32). Mg, Al and Fe have a high tendency to go into olivine, clinopyroxene and plagioclase crystal phases in the early stages of fractional crystallisation. Ca goes into plagioclase while Mn goes into olivine and orthopyroxene. Fe and Ti is also reduced from the melt through fractionation of FeTi-oxides, for example ilmenite and magnetite. P goes into apatite and tends to reduce with increased fractionation. On the other hand, Na_2O and K_2O generally increase up to approximately 62% SiO_2 and then start to decrease. Na and K behave incompatibly until advanced stages of fractionation (Wilson, 1989). Na and K goes into plagioclase and alkali feldspars at advanced stage of fractionation even though more of K fractionates in the alkali feldspars compared to plagioclase. It can be clearly seen from the plots that there is a change in mineral phases that crystallises from the magma at 62% SiO_2. The major elements versus SiO_2 trends are coherent with crystal fractionation process. It can generally be seen that all the OW-917 samples are highly evolved. They have high SiO_2 content and only plot between 62% and 81% SiO_2 in all the plots. OW-905A and OW-910 have a wide range of evolution with some of the samples being comparatively less evolved, while others are highly evolved and plot in the same range as OW-917.

For the trace elements, Zr was used as an index of differentiation on the Harker diagrams to depict the evolution trends in the three wells. Zr is a highly incompatible element that is resistant to mobilisation (Franzson et al., 2008). It shows a wide range of concentration, from 100-2600 ppm in the study samples. La and Y are incompatible elements and will remain in the melt during fractionation. There is a positive correlation between Y and La

versus Zr plot with a kink being noticed at 1700 ppm Zr (Figure 33). This indicates that other source components may have been involved in the petrogenesis of these rocks, for example anatexis of syenite as indicated by Marshall et al. (2009). The positive correlation of the trend for the majority of the samples in the La versus Zr plot is consistent with the explanation that fractional crystallisation is governing the compositional evolution of the sub-surface rocks.

Ba, Sr, Co, Ni, V and Cr generally decrease with increasing Zr. These elements are compatible and reduce in concentration as they are removed from the melt with increased crystal fractionation. Sr goes into the alkali feldspars as well as plagioclase. Co goes into magnetite as FeTi-oxides fractionates from the melt. Small amount of Ba goes into plagioclase while a high percentage is incorporated in alkali feldspars. Its concentration therefore starts decreasing significantly as it is incorporated in sanidine. V goes into orthopyroxene and magnetite while Ni and Cr goes into olivine, orthopyroxene and clinopyroxene in the initial stages of fractionation. There is an increase in Rb with increasing SiO_2 until a certain point when it assumes an almost horizontal trend. Rb, like Na and K, remains incompatible during the initial stages of fractional crystallisation. It is later incorporated into the alkali feldspars.

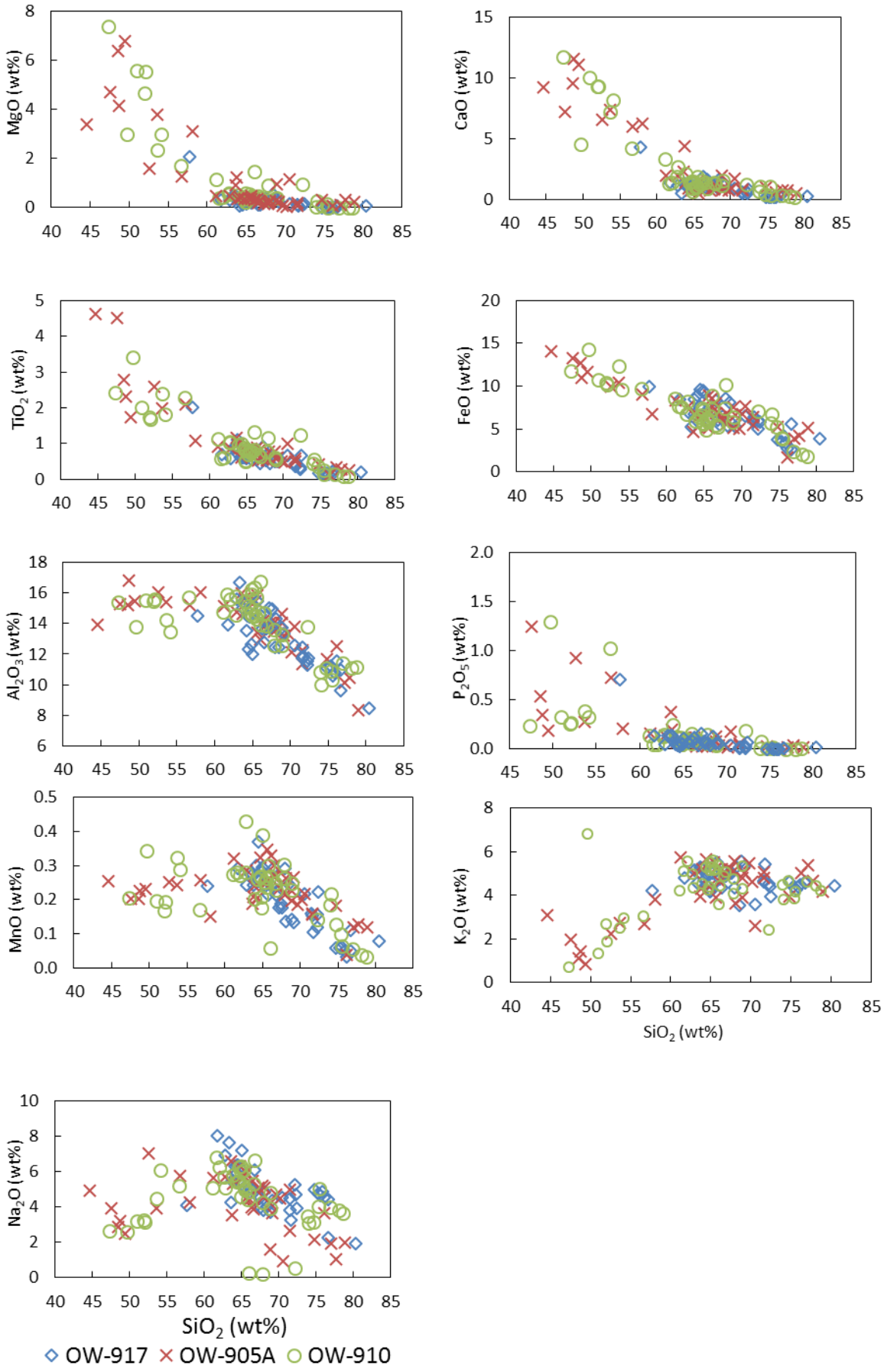

Figure 32: Whole-rock major element abundances as a function of SiO_2.

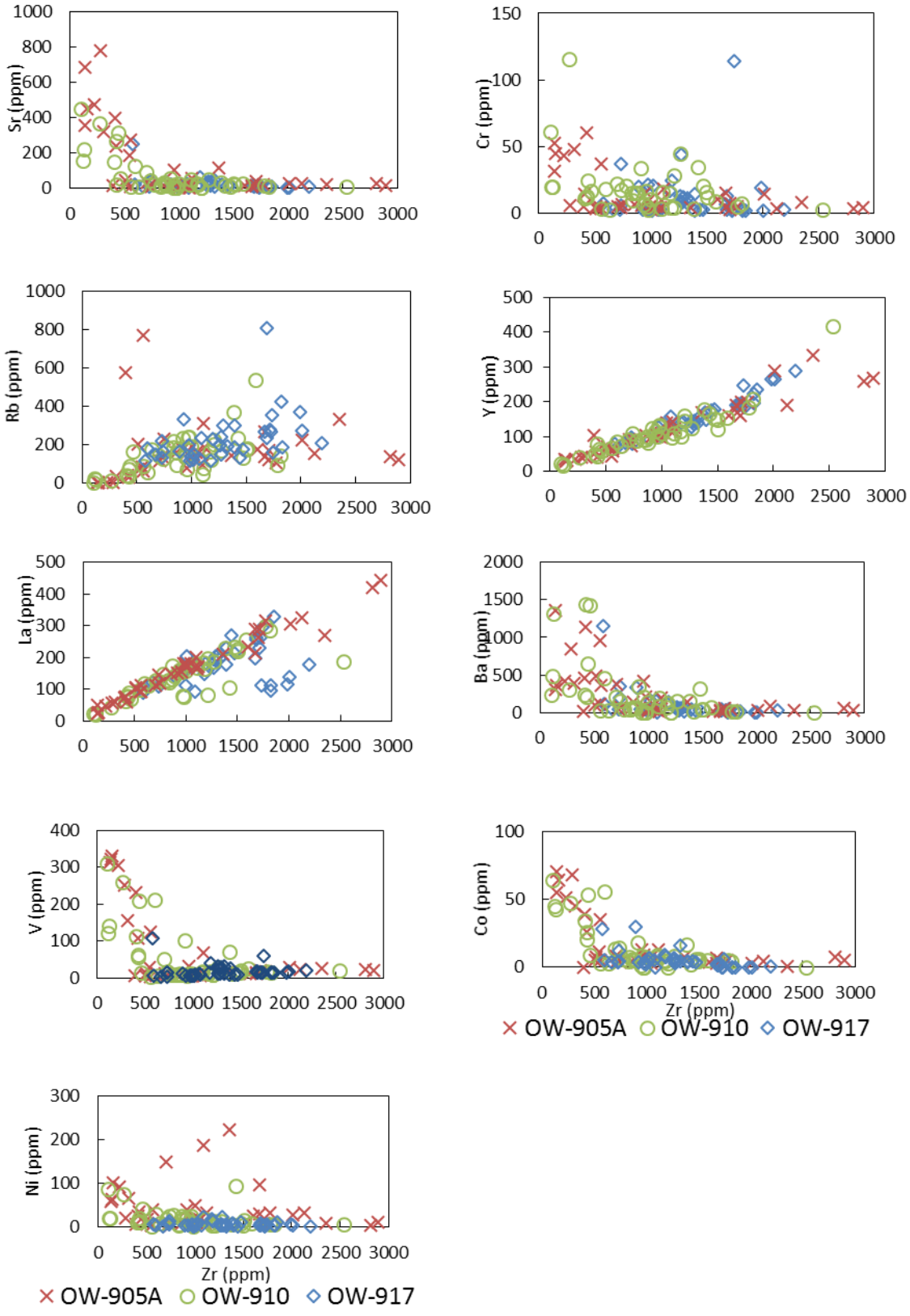

Figure 33: Whole-rock trace element abundances as a function of Zr.

4.10 Magma differentiation processes

The major element versus SiO_2 (Figure 32) and trace elements versus Zr plots (Figure 33) show that fractional crystallisation was the main differentiation process involved in the generation of the sub-surface rocks. During fractional crystallisation, Zr, Y and La concentration will increase with advancing fractionation. Only a fractional crystallisation process is likely to preserve the constant concentration ratio of two incompatible elements (Wilson, 1989). The major element versus SiO_2 and trace elements versus Zr plots are consistent with fractionation of olivine-clinopyroxene-plagioclase mineral phases in the basaltic magmas, clinopyroxene-plagioclase-Fe-Ti oxides-apatite ± olivine in the intermediate magmas and sanidine-clinopyroxene-Fe-Ti oxides-apatite in the silicic magmas.

The La versus Zr, Y versus Zr and La/Zr versus Zr plots show that other magma modification processes might have played a role in the generation of the rhyolitic rocks. There is a clear change in the trend at 1778 ppm Zr on the Y versus Zr plot (Figure 34). The samples that plot along this new trend are rhyolites mostly coming from well OW-917. These rhyolites are from 90-400 m depth. These samples are also noted to plot outside the trend on the La versus Zr (Figure 34) and the La/Zr against Zr plots (Figure 35). According to Macdonald et al. (2008), rhyolites were mainly formed by fractional crystallisation of trachytes and partial melting of syenites. This might explain the variation in the trend along which the 90-400 m depth rhyolites plot, namely, the composition of these rhyolites might have been modified through partial melting of syenites. On the La/Zr versus Zr plot (figure 35) two trends can be discerned within the basalt-trachyte suite that have a La/Zr ratio of 0.15 to 0.20. This small shift may be attributed to different magma mixing that was involved in generation of basalt-trachyte suite.

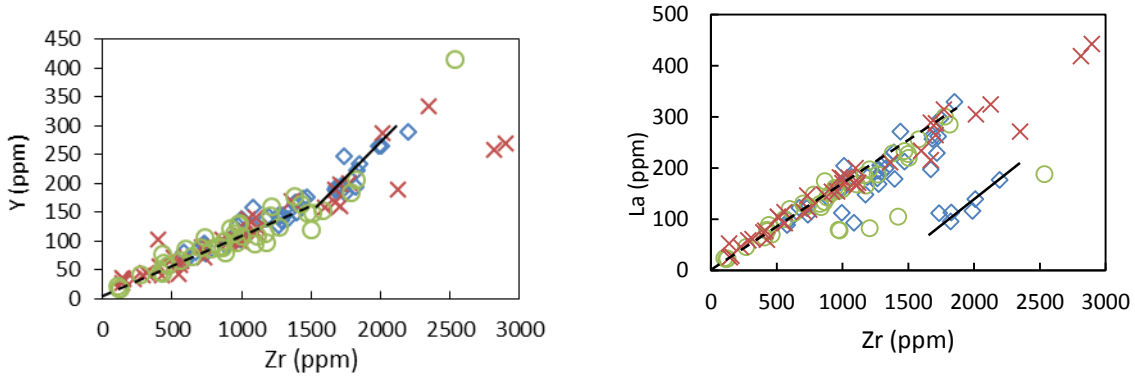

Figure 34: Y versus Zr and La versus Zr plot showing fractional crystallisation (broken line) and other magma modification processes (continuous line), probably crustal anatexis or magma mixing.

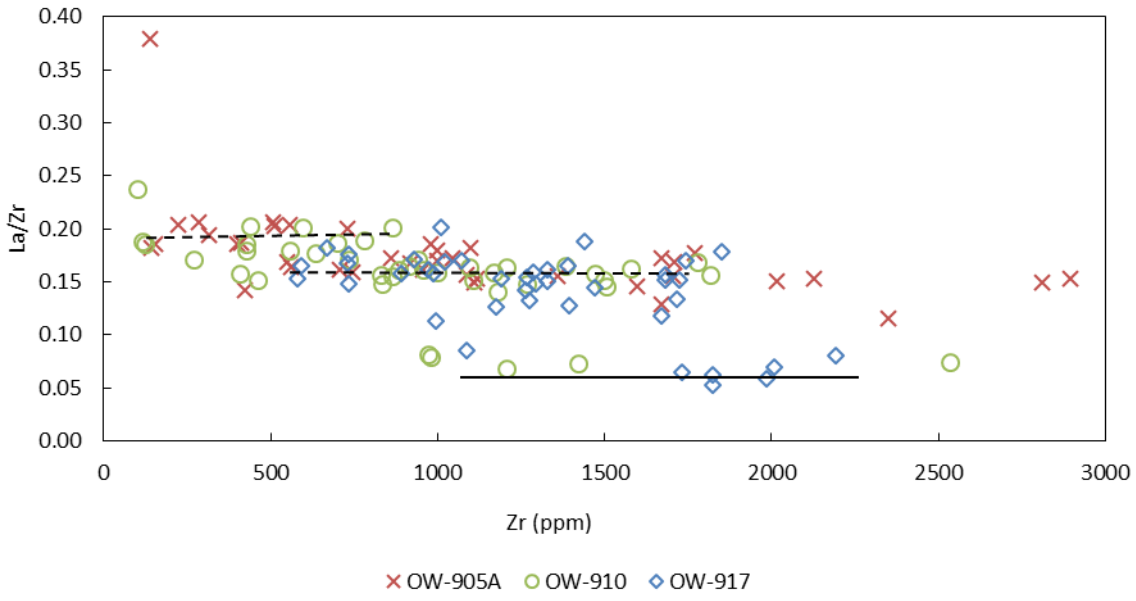

Figure 35: Ratio of La/Zr as a function of Zr showing the basalt-rhyolite trends (broken line) and the trend of the rhyolite samples (continous line) that plot off the general trends.

4.11 Eruption episodes

Lavas that are cogenetic will have more or less similar concentrations of incompatible trace elements (Wilson, 1989). During fractional crystallisation, the concentration of Y, La and Zr will be low in the early stages of fractionation. With increased fractionation, these concentrations increases, reaching their maximum values in the most fractionated rock. In a basalt-rhyolite suite, the La, Y and Zr will have a low concentration in the basalts but higher in the trachytes and rhyolites. Their concentration in different trachytes and rhyolites will depend on the degree of evolution of these rocks. Plots of Y, La and Zr against depth may show recurring shifts of concentration of these elements from low to high if a volcano has had episodic eruptions.

A comparison was made for trace element variation with depth for the three wells. Y, La and Zr values were plotted against depth (Figures 36, 37 and 39). La/Zr and Y/Zr were also plotted against depth (Figures 38). From the trace element plots, the eruption episodes can be subdivided into various units and correlated according to the concentration pattern of these elements with depth.

From the Zr, Y and La plot, these elements are seen to decrease in concentration from the surface to a low at 1800 m a.s.l and 1600 m a.s.l in wells OW-917 and OW-910, respectively. The rocks found in this depth range are rhyolite and tuff. Low concentrations of Zr, Y and La are also recorded in basalt at 1800 m a.s.l and 1200 m a.s.l in OW-905A and OW-910, respectively. The concentration in Zr, Y and La observed in the rhyolite at 1200 m a.s.l in OW-905A, 900 m a.s.l in OW-910 and 1300 m a.s.l in OW-917 show similar range and drop towards the trachyte found beneath. Different types of intermediate magma compositions start being observed at 1900 m a.s.l in OW-905A and 1750 m a.s.l in OW-910. This indicates that there were temporal compositional variations in the eruption events that led to the build-up of the GOVC. The concentrations of these two elements are

consistent at the mentioned depth in the three wells. The top 500 m show low ratios of La/Zr as compared to 500-2990 m in well OW-910 and OW-917. In contrast, the Y/Zr values are higher in this zone. This shift observed in the upper 500 m of the two wells is probably due to assimilation or partial melting magma modification processes.

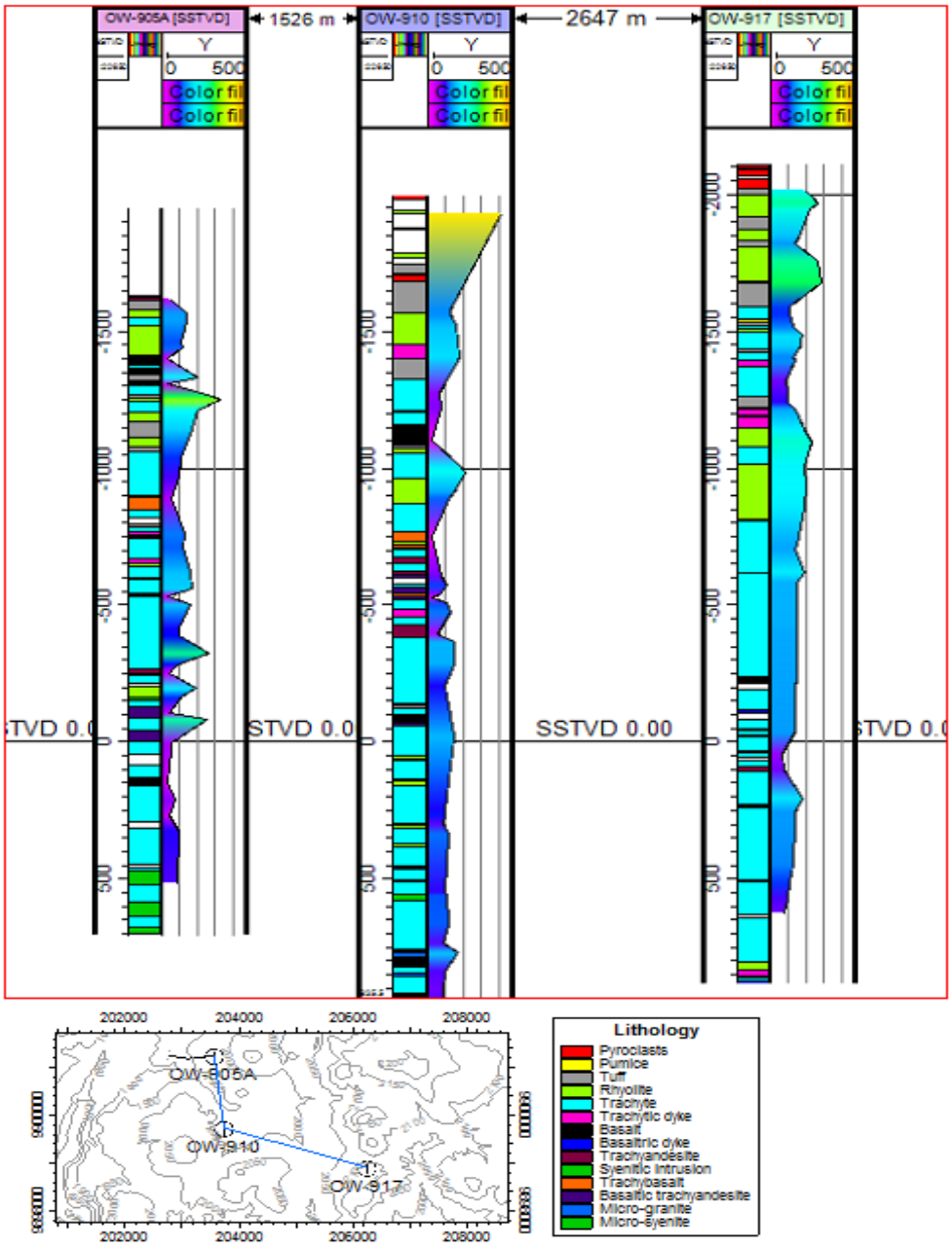

Figure 36: A plot of Y concentration as a function of depth in the study wells. The colours indicate concentration in ppm at each depth.

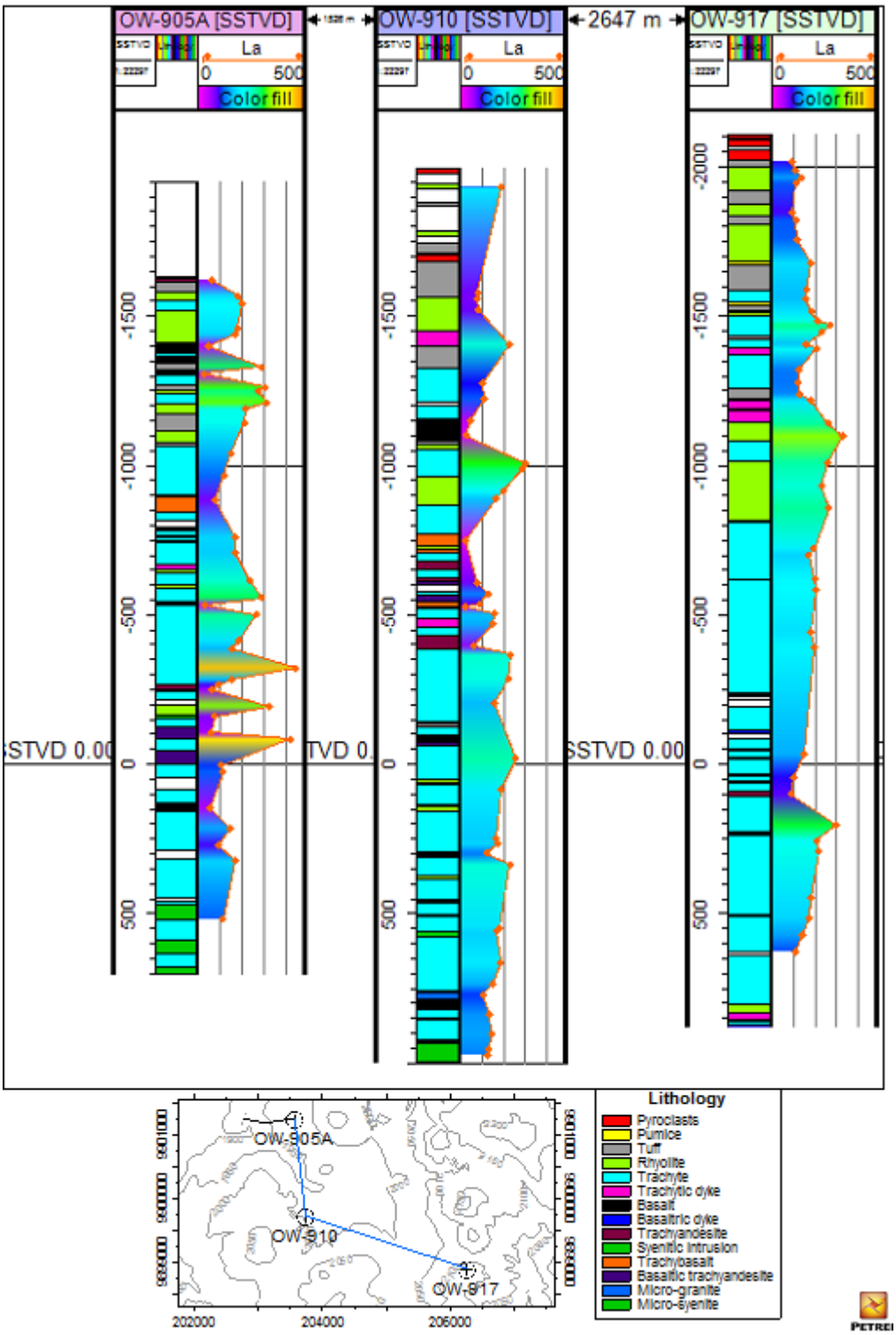

Figure 37: A plot of La concentration as a function of depth in the study wells. The colours indicate concentration in ppm at each depth.

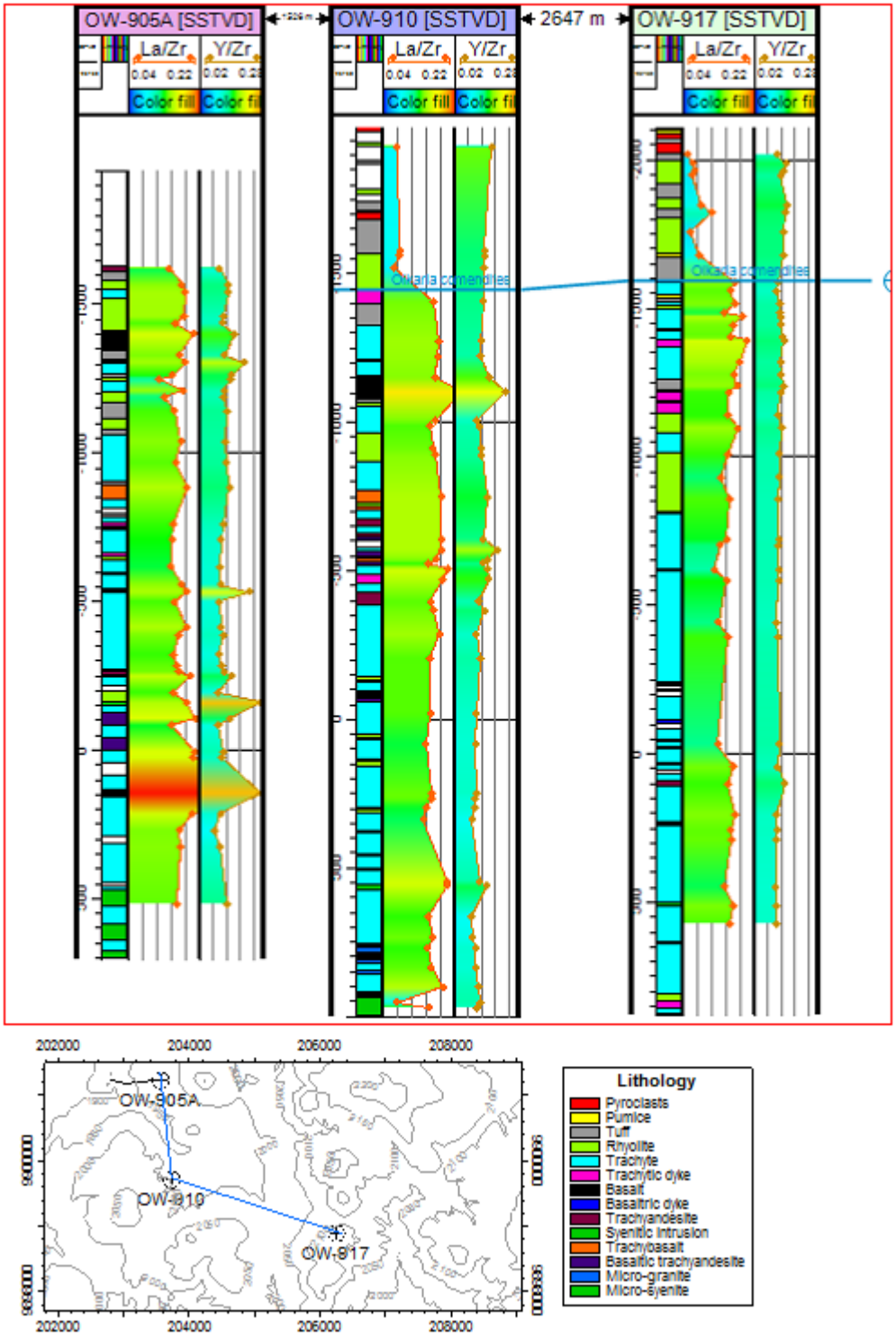

Figure 38: A plot of La/Zr and Y/Zr ratios as a function of depth in the study wells. The colours indicate concentration at each depth. Olkaria comendites line demarcates the change in the La/Zr and Y/Zr ratios.

4.12 Stratigraphic correlation

The Olkaria geothermal field has been subjected to a series of tectonic events that were associated with the formation of the EARS. These events, which included faulting, intrusion and extrusion of magmatic material, resulted into unconformities. Some of the unconformities are buried, which makes them only identifiable through geological well correlation. Lagat (2004) made a geological correlation of wells OW-901, OW-902, OW-903 drilled in the Domes area with wells OW-08, OW-15, OW-19 and OW-22 drilled in the Olkaria East field. He found a similarity between the Olkaria East field and the Domes field. Lagat (2004) also inferred buried faults between the Olkaria East and the Domes fields, as well as within the Domes field. These are normal faults with a downthrow of 300 m.

In this study, rock unit correlation was based on the binocular, petrographic and trace element analysis. As explained earlier under rock type description, two types of rhyolite and trachyte were observed in the study wells. Moreover, different rock units have different trace element concentration. Zr was used in this case since it is immobile and incompatible and its concentration is reflecting the extent of fractional crystallisation and may thus outline magma evolution cycles within the subsurface volcanic pile of GOVC. The top 100 m of the wells is composed of pyroclastics (Figure 39). The pyroclastics layer accounts for the losses in well OW-905A. Observations from other studied wells indicate that pyroclastics cover between 0 m to about 150 m in the Domes area (Musonye, 2012; Mwangi 2012 and Lagat 2004). Comenditic rhyolite is found between 100 m to 400 m. This rhyolite has a characteristic pinkish colour (also referred to as the granular rhyolite in rock type description). This zone has trachyte and tuff rocks intercalating the rhyolite. The trace element concentrations are consistent in this unit as described under the eruption episodes subtitle. The Olkaria basalt occurs between 400 m to 700 m. Wells OW-905A and OW-910 cut the basalt rock unit between 544-662 m and 839-914 m depth respectively. The basalt unit thins out towards OW-917. The basalt is intercalated by tuffs and trachyte in OW-905A. The spherulitic rhyolite, referred to as rhyolite in Figure 39, occurs between 800-1300 m in the three wells. This rhyolite is thicker in OW-905A as compared to OW-910 and OW-917 even though it is intercalated by tuffs in OW-905A. Intermediate rocks start appearing at 1100 m and 1210 m in OW-905A and OW-910, respectively. This marks a new regime and there is a clear downthrow displacement seen in OW-910. The appearance of intermediate rocks probably marks the boundary between the Olkaria series associated with the formation of GOVC ~22 ka years ago and the older stratigraphy associated with the earlier magmatism.

The trachyte series forms most part of the stratigraphy. It is found between 1000 m to the bottom of the wells. The trachyte has different textures and shows variation in trace element concentrations. The trachyte series is intercalated by basalts, trachy-andesite, basaltic trachy-andesite and trachybasalt. Most of these mafic rock units are found in OW-910 and OW-905A.Thin rhyolite units also intercalate the trachyte. At some depths, the trachytes are massive with thickness up to 100 m. There is an increased number of intrusion occurring from 1800 m to 3000 m. The intrusions observed include basaltic dykes, syenitic intrusions and micro-granite. These numerous intrusions are as a result of enhanced magmatic activity at these depths which are at a closer vicinity to the magmatic source.

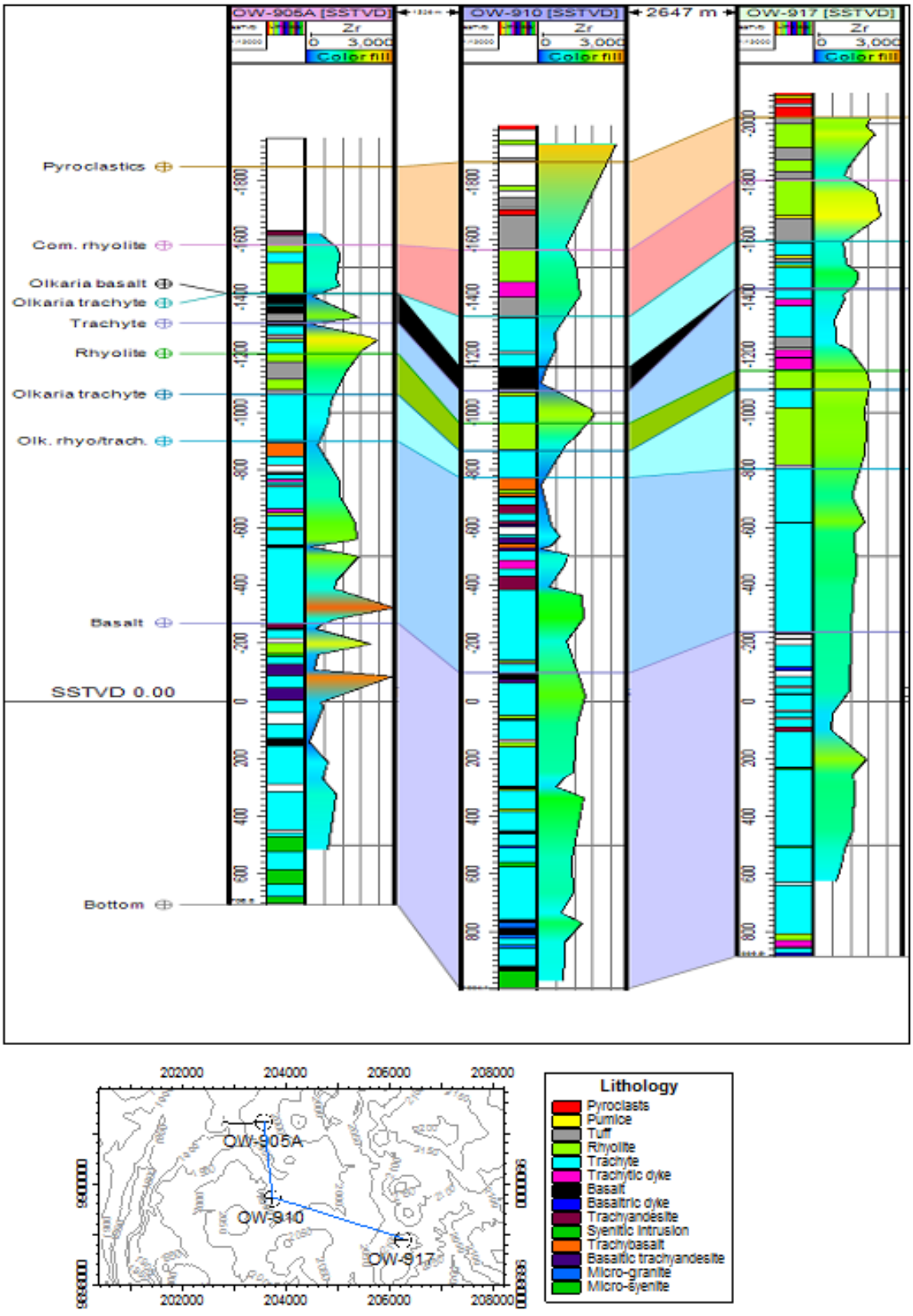

Figure 39: Stratigraphy and stratigraphic correlation of the wells based on binocular, petrographic and petrochemistry data. The colours indicate the concentration in ppm at each depth.

From the stratigraphic correlation, there is a probable fault between wells OW-905A and OW-910, which has resulted in a downthrow of about 295 m. Between OW-910 and OW-917, a probable fault has resulted in a downthrow of about 300 m. This observation relate well with the structural mapping which indicate faults have been inferred between wells OW-905A and OW-910, with the main inferred fault trending in ENE-SWS direction. The downthrow between OW-910 and OW-917 may relate with the ring structure whose formation is associated with caldera collapse.

4.13 Comparison of the sub-surface rocks with the surface rock data

Rhyolitic and basaltic compositional samples were taken for the comparison of sub-surface and surface rock compositions. The rhyolite surface data was obtained from Marshall et al. (2009), while the basaltic data was obtained from Macdonald et al (2008). The surface basaltic composition is mainly from the periphery of the complex, which is Akira, Lolonito and Ndabibi. Y versus Zr as well as La versus Zr plots were used. The broken lines demarcate the fractionation trends for the surface samples.

The surface samples on the Y versus Zr rhyolite plots (Figure 40) show two trends (a and b), similar to the ones observed from the sub-surface samples. The Arcuate Domes, Gorge Farm and Ololbutot rhyolites plot in both the two trends. Well OW-917 mainly plot in b and OW-910 mainly plot in a while OW-905A in both a and b. For the La versus Zr plot, three fractionation trends a, b, and c can be seen (Figure 41). The various fractionation trends indicate different eruption episodes associated with the pre-caldera and post-caldera formations of the GOVC. Most of the Gorge Farm rhyolite plot in trend c, while most of the Arcuate Domes samples plot in trend b. Trend a has two Ololbutot samples plotting in it. Even though well OW-917 is drilled next to the ring structure where the Arcuate Domes are located, it does not plot in trend b, in which the Arcuate Domes surface samples plot. Well OW-917 is drilled next to a rhyolitic dome whose formation belong to the Middle Comendite Member (O^3) of the post-caldera Olkaria formation (Figure 42). The Gorge Farm rhyolite deposit also belongs to this formation. Hence, the Gorge Farm and well OW-917 rhyolites might be cogenetic. This explains why most of the OW-917 samples plot in trend c. Other samples from OW-917 plot in the Ololbutot trend a. This might indicate that Ololbutot lava and some of the OW-917 samples share a cogenetic source. Well OW-905A which is located close to the Ololbutot lava flow has two samples plotting in trend a. This might indicate the rhyolites in well OW-905A have a similar source with the Ololbutot surface samples.

The basaltic liquid line of descent on the two plots (Figure 43) indicate that the Akira, Lolonito and Ndabibi basalts had a similar parental magma with the sub-surface samples but evolved on different trends. The dotted line shows the liquid line descent along which majority of the surface samples plot. The surface samples took time before being erupted onto the surface. During this period, they might have been subjected to other magmatic processes, hence showing the variation in the evolution trends. Alternatively, they may have come from or mixed with other basaltic magmas from the neighbouring volcanoes.

Further studies on the isotope composition is recommended in order to outline magmatic relationship between the basalts on the periphery and within the subsurface of the GOVC.

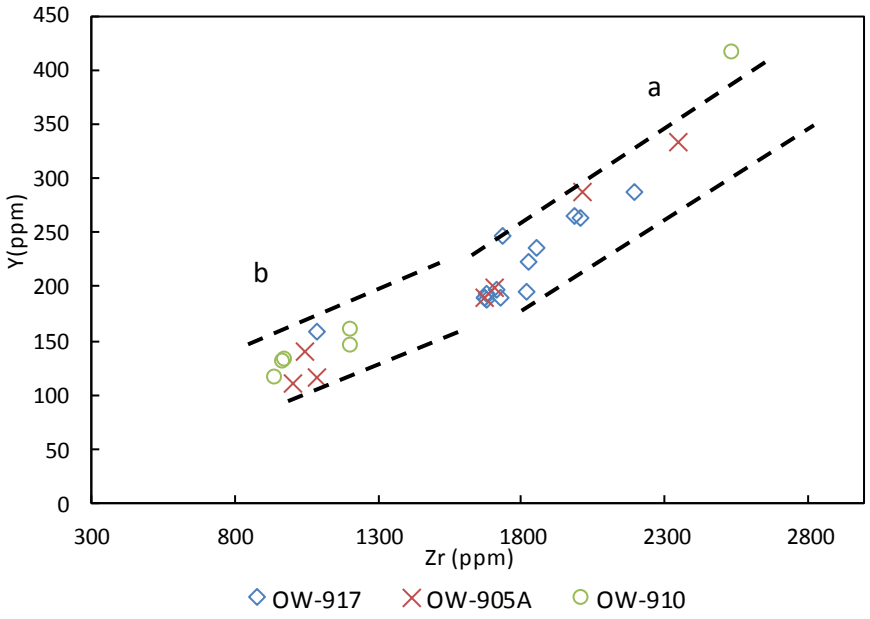

Figure 40: *Y versus Zr plot showing the boundaries (broken line) within which the surface samples plot and data points for the sub-surface rhyolites*

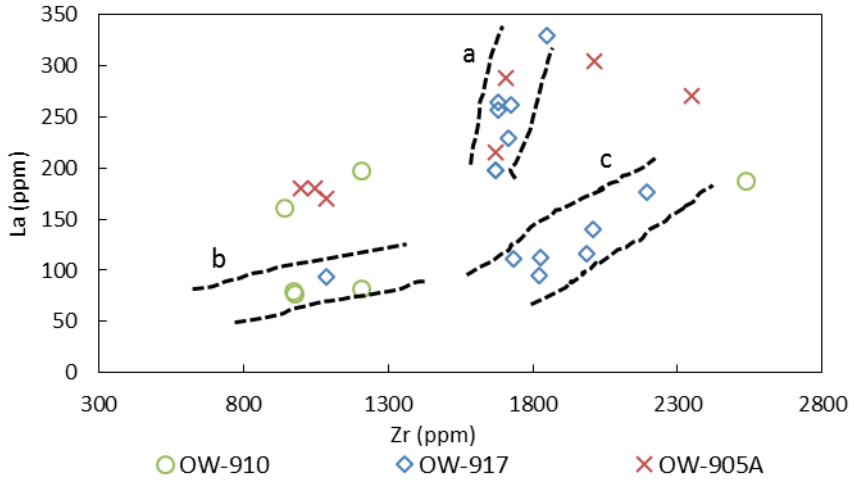

Figure 41: La versus Zr plot showing the boundaries (broken line) within which the surface samples plot and data points for the sub-surface rhyolites.

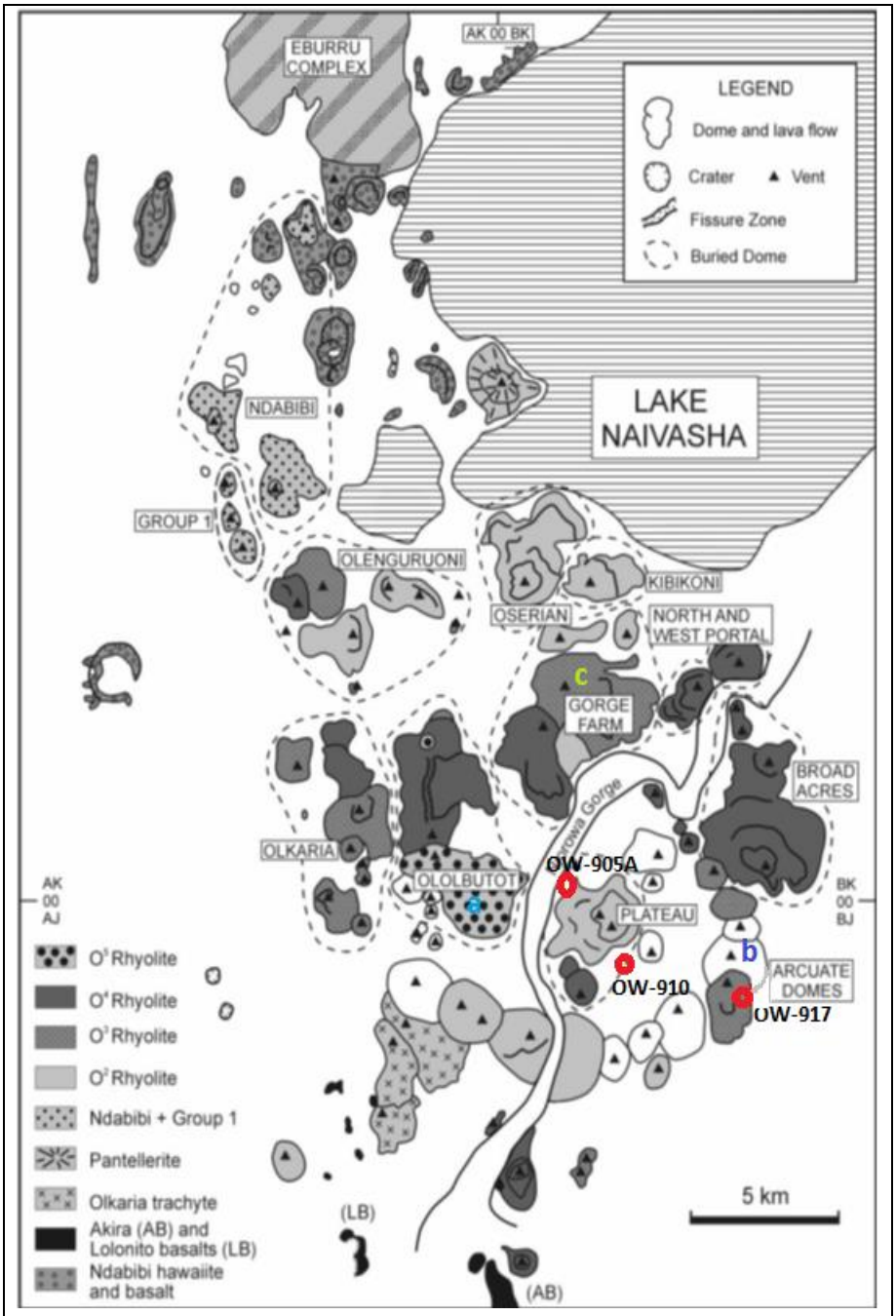

Figure 42: The surface geology of GOVC with the location of the study wells in the Domes field (Modified from Marshall et al., 2009). The letters a, b and c represent lavas which plot in the trend shown in figure 41.

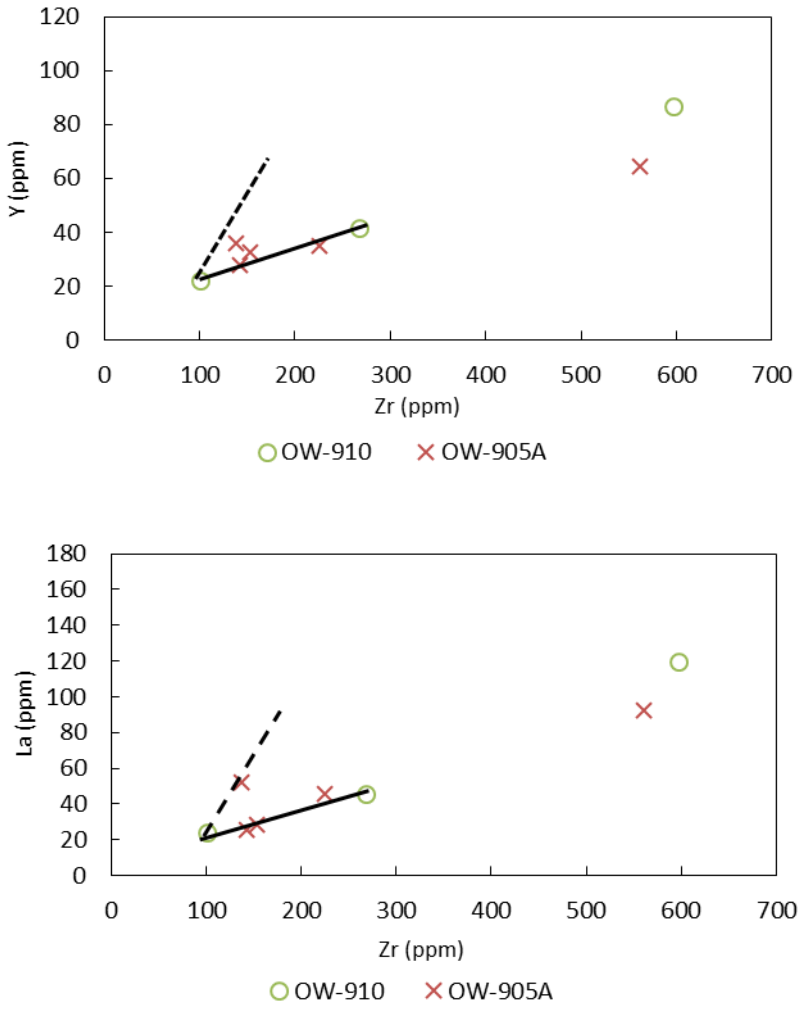

Figure 43: Y verus Zr and La versus Zr plot with lines of descent for the sub-surface basalts (broken line) and surface basalts (continous line) found on the periphery of GOVC.

5 Discussion

The surface geology of Olkaria geothermal area is dominated by comenditic rhyolite and pyroclasts. These surface rocks are Pliocene to Holocene in age (Clarke et al., 1990). The ICP-OES major and trace element analyses of drill cuttings from the Domes area reveal that the sub-surface strata are composed of basalts, trachy-basalt, basaltic trachyandesite, trachyandesite, trachyte, rhyolite and tuffs. Intrusives include syenitic intrusions, trachytic dykes, basaltic dykes and micro-granite. Wells OW-905A and OW-910 cut through all these types of rocks, while OW-917 only cuts through trachyte and rhyolite rock units. The variation of the rocks in the basalt-rhyolite range in wells OW-910 and OW-905A shows that the development of GOVC was characterised by episodic magmatic events. The GOVC has been subjected to numerous tectonic events, some of which were regional and associated with the rift formation while others were local. These events led to the development of fractures and faults, some of which are buried beneath the pyroclastic cover. Stratigraphic correlations indicate a downthrow displacement of the rock units in well OW-910 as compared to OW-905A and OW-917. The occurrence of basaltic-intermediate magmas in wells OW-905A and OW-910, contrary to OW-917, indicates the probability of a buried major structural divide between OW-910 and OW-917. The proposed caldera (Clarke et al., 1990) might have inhibited the flow of mafic lavas, especially in the upper 1000 m, outside the caldera. The intermediate magmas start appearing at 1100 m and 1200 m depth in OW-905A and OW-910, respectively. This indicates a displacement in the downthrow at OW-910. The appearance of intermediate rocks probably marks the boundary between the Olkaria series which is associated with the formation of GOVC beginning approximately 22 ka years ago and the older stratigraphy associated with the earlier magmatism. The upper 500 m of the stratigraphy is dominated by pyroclastic rocks, tuff and rhyolite lava. The basalt occurs between 500 m to 1000 m. From 1000 m to 3000 m the dominant rock type is trachyte. Omenda (2000) linked the occurrence of pyroclastic rocks and rhyolite near the surface and trachytes at depth to the extensive differentiation that occurred in a magma chamber beneath the Olkaria Volcanic complex. The intrusives are generally found between 1800 m to 3000 m. Intrusives are formed as a result of fresh magma pulses being injected into the overlying formations. The volumes associated with these pulses are too small to push the magmas all the way up to the surface. Hence the magmas cool and solidify between the rock strata at depth. Geophysical studies have indicated the magma chamber to be at 7-10 km depth (Omenda, 2000; Simiyu and Keller, 1997).

Hydrothermal alteration is a function of primary rock composition, permeability, temperature, duration of the hydrothermal activity, fluid composition and pressure (Brown 1978). Studies of hydrothermal alteration have been able to link different minerals to particular temperatures. Temperatures affect the crystal lattice of minerals, hence determining the stability of certain minerals at certain temperatures. Certain minerals are associated with good permeability in geothermal systems. Pyrite for example, is a hydrothermal alteration mineral that denotes good permeability in geothermal systems. Calcite indicates good permeability even though its deposition can lead to the sealing of the

permeability pathways. Calcite and pyrite are deposited over a wide range of temperatures with temperatures as low as 50 °C to temperatures as high as 280 °C (Lagat, 2004). This makes it difficult to use them as temperature indicators. However, coupled with other alteration minerals present in a well, they can be used to indicate earlier permeability and temperature conditions. Minerals observed in the study wells reveal the prograde variation, as seen in other high-temperature geothermal fields. High-temperature minerals, for example epidote, actinolite and garnet, are found at greater depth, while low-temperature minerals, for example smectite and zeolites, are found at shallow depth.

In Domes area, there is a variation in the occurrence of alteration minerals along a NW-SE traverse. The high abundance of calcite in well OW-917 as compared to the other wells affects its permeability, hence the scarcity in abundance of high-temperature alteration minerals. Fractures that enhance permeability were seen to be filled by calcite, as revealed by the presence of calcite veins. The abundance of calcite and pyrite in OW-917, as well as the scarcity of high-temperature alteration minerals indicates that calcite and pyrite were deposited at low temperatures. According to Simmons and Christenson (1993), calcite may deposit from hydrolysis (that is replacement of calcium alumina silicates), boiling of geothermal fluids (that is from fluids having high dissolved carbon dioxide concentration and in the absence of a mineral buffer) and heating of cooler peripheral geothermal fluids. The calcite deposited in OW-917 is associated with the heating of cooler peripheral geothermal fluids. This is confirmed by the scarcity of high temperature alteration minerals and the low intensity of alteration observed from the surface down to the bottom of the well. Well OW-917 stratigraphy mainly comprise of trachytes and rhyolites which are mainly K feldspar rich rocks. This rules out the possibility of hydrolysis as the main process involved in calcite deposition in this well. This well is located adjacent to the postulated ring structure. A model of single phase up-flow by Lagat (2004) shows down-flow to the northeast and east of the Domes area outside the ring structure, with up-flow on the inside of the ring structure. This might have resulted in convective mixing in the OW-917 region, hence deposition of calcite. The abundance of moderate to high intensity of alteration, high-temperature alteration minerals, for example garnet, actinolite, epidote, prehnite, wairakite and quartz, alongside pyrite, in well OW-910 indicates good permeability, as well as high temperatures in this region. Calcite was scarce in this well and only observed down to 1000 m depth. The moderate abundance of high-temperature minerals in OW-905A indicates lower temperatures in this region compared to the region at well OW-910. However, the high abundance of pyrite, moderate to high alteration intensity and low to moderate abundance of calcite indicate that permeability is good in this region.

The temperature variation along the NW-SE traverse reveals that there is high temperature at shallow depth near the OW-910, followed by OW-905A, while the OW-917 area has low temperatures (below 230 °C) from the surface to 3000 m depth. The formation temperature measurements relate well with the alteration mineral zonation. The high formation temperature measured at shallow depth in OW-910, coupled with the high power production of wells drilled in this area, indicates that the heat source for the Domes geothermal area is located in this region (Figure 44). The greater depth at which high-temperature alteration minerals occur in OW-905A, as well as where high formation temperature are measured, relate to the distance of this well from the centre of upflow (Figure 44). Moreover, this well is located in an area believed to be a recharge zone for the

Domes area. The Ol Njorowa gorge, which divides the Olkaria East and Domes fields, is located close to the OW-905A area. This gorge is also believed to be a conduit that feeds cold water in this part of the Domes area. Well OW-905A was not able to discharge during the discharge test. OW-917 is located outside the postulated caldera rim but adjacent to the ring structure. The down-flow in this zone, coupled with the distance of this well from the heat source, as well as other structural barriers (the ring structure), has greatly lowered the formation temperatures in this zone. Low temperatures measured at great depth are in tandem with these observations. The upper limit of the epidote zone, which is the highest temperature mineral zone in this well, is found at greater depth as compared to wells OW-905A and OW-910. This well was not able to discharge during the discharge test. The relation between the alteration mineral isograds and the formation temperatures indicates the existence of two thermal episodes in the Olkaria geothermal field. High-temperature mineral isograds occur at shallow depth at lower formation temperature than the temperature of deposition. Epidote and actinolite isograds in wells OW-905A and OW-917 are present where formation temperatures are lower. This indicates that higher temperature existed at shallower depth in the past as compared to today. The garnet isograd in OW-914 and OW-910 occurs at a depth with formation temperatures of above 300 °C. This indicates heating up in this zone. Tectonic activities and magmatic intrusions associated with the recent eruption could be the source of this heat.

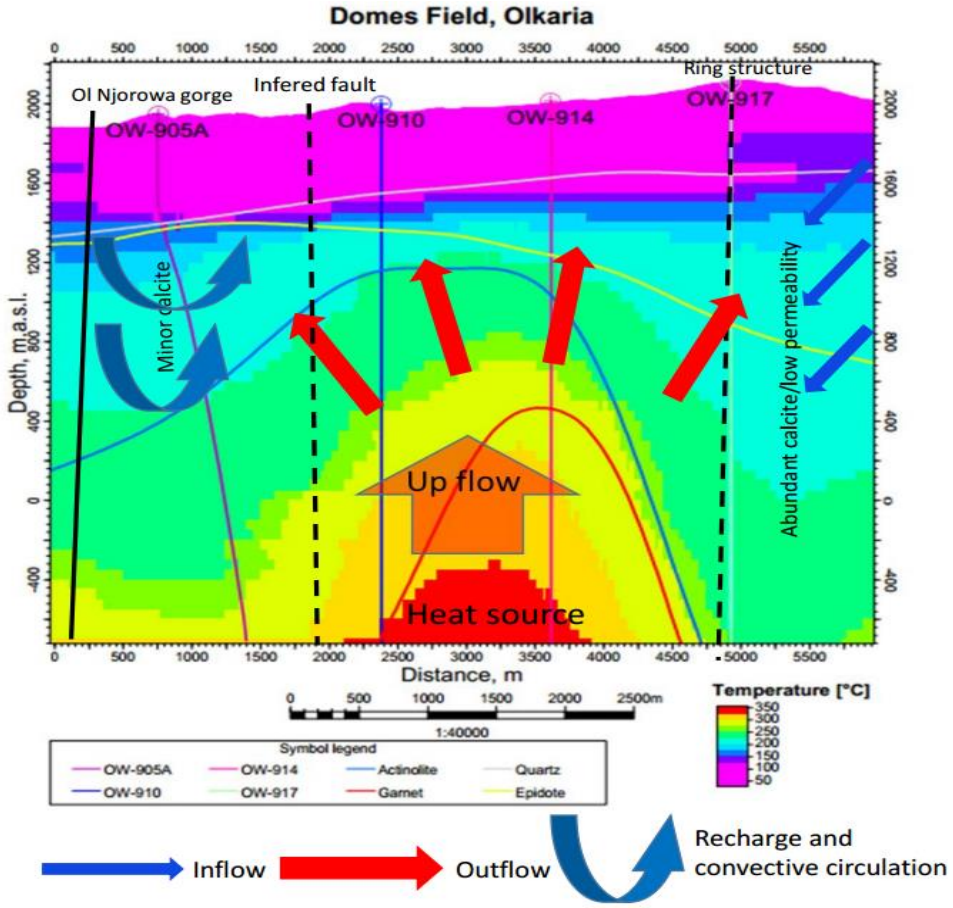

Figure 44:Conceptual model based on the reseacrh findings of this study.

Feed zones in the study wells were mainly associated with fractured rocks and lithological boundaries. Well OW-917 has only minor feed zones. This is attributed to the low permeability that characterises the stratigraphy in this well. The rocks show moderate fracturing but the high calcite abundance associated with the formation in OW-917 has sealed the primary and secondary permeability pathways. The well was filled up with water during test pumping. The feed zones in OW-910 were associated with fractured rocks, as well as lithological boundaries. One of the feed zones was located at a trachyte-micro-granitic intrusion contact. The formations in this well show moderate fracturing. The well had high intensity of alteration, moderate to high abundance of pyrite but no calcite below 1000 m. This indicates good permeability and explains the numerous feed zones observed in this well. Feed zones in OW-905A are associated with fractured rocks. Low to moderate abundance of calcite and high alteration intensity are observed in this well. The fracturing and the low to moderate abundance of calcite have enhanced permeability, hence the feed zones observed in this well. The feed zone at 1280 m depth in OW-905A is associated with a major drop in measured formation temperature. This feed zone is probably cold and affects the feed zones that are below 1280 m depth. In general, all the feed zones in the three wells are located below 1200 m depth. This may indicate that the formation becomes more fractured below this depth.

Major and trace element analyses of the rocks from the study wells show that the rocks have a continuous distribution on the TAS classification with a compositional range from basalts through trachybasalt, basaltic trachyandesite, trachyandesite to trachytes and rhyolites. In their initial surface studies, Macdonald et al. (2008) and Marshall et al. (2009) pointed out the possibility that the full range of magmatic compositions is present beneath the complex. This study has proven this, as seen from the fields in which the rocks plot in the TAS classification scheme. Fractional crystallisation is the main magma differentiation process that generated the wide range of magmas with different compositions. Magma modification processes such as crustal anatexis, are revealed by the compositional variation of rocks. The change in the gradient of the trends observed on the two plots indicates a different process coming in which alters the course of the fractionation process. Four rhyolite samples obtained from the top 400 m of well OW-917 plot off the trend in these plots. These rocks might be from a different magma source compared to the rest of the rocks. Macdonald et al. (2008) indicated that partial melting of syenite might have played a part in the generation of comendites. This process may have been controlling the formation of the rocks that plot off the trend. Further study of isotope composition is recommended to ascertain this.

All the rocks in OW-917, except one trachyandesite sample, have SiO_2 concentration of over 64% SiO_2, indicating that they are highly evolved and only have the alkali feldspar as a fractionating phase. The samples from the other two wells represent the two intervals of fractionation observed in this study. Well OW-917 lies on the outer margin of the ring structure. This area is associated with rhyolitic domes, which were built up during the post-caldera magmatism. This explains why the rocks in this well are rich in silica and only include trachyte and rhyolite. The samples from wells OW-905A and OW-910 have SiO_2 ranging from 44% to 80%. This compositional range is attributed to the fact that these wells are located within the caldera where magmas from both the pre-caldera and post-caldera magmatic events where extruded. The basaltic magmas erupted within the caldera were not voluminous enough to flow all the way outside the caldera. Mobile elements like

Na_2O, Ba and Rb show scattering as a result of being leached from the original rock through hydrothermal process. However, this leaching was in the same confines like least altered surface samples.

The trace element plots containing the sub-surface and surface rhyolite data show different liquid lines of descent. The Y versus Zr and La versus Zr plots show two trends for both surface and sub-surface rocks. This indicates the probability of two component mixing of magmas ranging from mugearites to benmoreites at deep levels, or crustal anatexis of syenites as stated by Macdonald et al. (2008). The basalts from the drilled wells and those from the periphery plot on different liquid lines of descent on Y versus Zr and La versus Zr plots. They show similar parental source but different fractionation path. The basaltic magmas found on the periphery of the complex might have come from within the complex and flowed along dykes and emplaced on the periphery of the complex.

Figure 45 illustrates the magmatic processes involved in the formation of GOVC. The basaltic magma source drives the system. Macdonald et al. (2008) stated that the basaltic magmas are intruded as dykes. Mixing of basalt-basalt and basalt-intermediate magmas occurs as the basaltic magma fractionate and ascend to the surface. Basaltic magma is driven along dykes and erupted on the periphery of the volcano. The low density trachytic trap inhibits the basaltic magma from rising in large volumes through it. However, small pulses of basaltic and intermediate magmas manage to pass through this trap and are erupted as thin layers underneath the volcano. The basaltic magma ascending through dykes and the trap undergoes different modification processes, probably hybridization, crustal assimilation or further mixing. This is revealed by the different liquid lines of descend shown by the two basalt samples on the Y versus Zr and La versus Zr plots. The intermediate magma fractionate through trachytes to rhyolites. The compositional and textural range in the trachytes can only be explained by the presence of several discrete magma chambers in which varied levels of differentiation take place. During trachytic fractionation, small magma pulses escape and are deposited as syenitic dykes. The trachytes are believed to have formed at the basement-rift fill interface at approximately 5-6 km (Marshall et al., 2009). Some of the trachytes are erupted onto the surface while others undergo further fractionation to comenditic rhyolites. The rhyolite chamber undergoes further fractionation producing rocks with a different degree of evolution. Some of the syenites deposited through fractionation of the trachyte mush are melted and fractionated to produce rhyolites. Volatiles lower the melting point of the syenites.

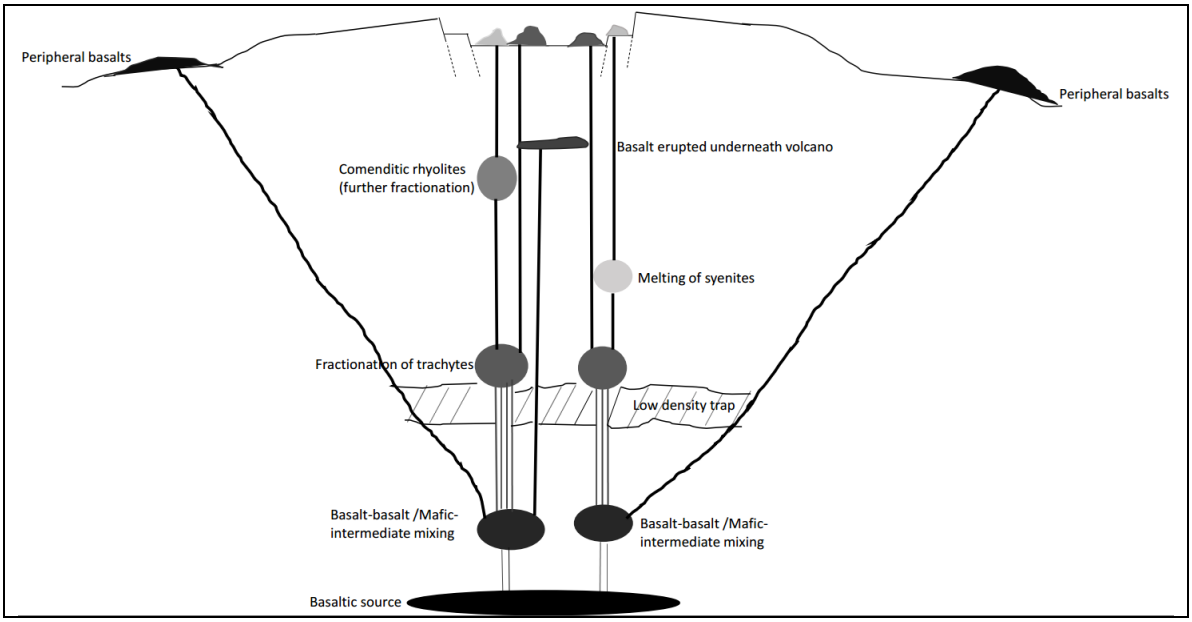

Figure 45:The magmatic processes and the plumbing system involved in the formation of GOVC (Not drawn to scale). Fractionation of trachyte is at ~5-6 km (Marshall et al., 2009).

6 Conclusion and recommendation

6.1 Conclusion

The subsurface rock composition of the GOVC ranges from basalt through intermediate lavas to rhyolite. The main differentiation process was fractional crystallisation. Other magma modification processes, for example magma mixing, crustal anatexis and assimilation, might have modified the magmas. The evolution trends show that anatexis of syenite might also have been involved in generating the rhyolite rocks.

The subsurface and surface rhyolites were generated by similar magmatic differentiation processes. The peripheral basalts seem to have been erupted from within the complex.

The textural and compositional variation seen in the subsurface rocks is a result of magma modification that took place in discrete magma chambers associated with the GOVC plumbing system.

The hydrothermal processes have little effect on the chemical rock composition.

From the stratigraphic correlation, there is a probability of existence of a mega structure between wells OW-905A, OW-910 and OW-917. For OW-905A and OW-910, this might be a buried fault while for OW-910 and OW-917 it might be the rim of the collapsed caldera.

Hydrothermal alteration mineral deposition greatly varies across the field. It affects permeability, which in turn affects the well output. The OW-917 area has high calcite content which has greatly affected permeability in this region.

Formation temperature varies across the field with higher temperatures being recorded at shallow depth in the OW-910 area. The OW-905A is a recharge zone and only records higher temperatures at greater depth compared to OW-910. OW-917 is located on the periphery of the geothermal system and close to a down-flow. This area has low temperatures at greater depth. There is a heat source located beneath the OW-910 area.

Two thermal regimes have existed in Olkaria geothermal system, as indicated by alteration minerals and formation temperatures. The earlier regime had high temperatures at shallow depth and existed during deposition of the alteration minerals while the current regime has high temperatures at greater depth compared to the early regime.

6.2 Recommendations

For geothermal development, the area east of the ring structure in the Domes field should be approached cautiously. More geophysical work should be done in this area in order to target faults and fractures before more drilling is conducted.

Radiogenic isotope study of the subsurface rocks is recommended to ascertain the similarity in the magmatic source of the subsurface and surface rocks.

Petrochemical analysis of wells drilled further away from the ring structure for example well OW-922 is recommended to strengthen the geochemical stratigraphic correlation between the inside and the outside caldera rim.

References

Ambusso, W.J., and Ouma, P.A., 1991: Thermodynamic and permeability structure of Olkaria Northeast field: Olkaria fault. Geothermal Resource Council Transactions, 15, 237-242.

Baker, B.H., and Wohlenberg, J., 1971: Structural evolution of the Kenya Rift Valley. Nature, 229,538-542.

Baker, B.H, Mohr, P.A, and Williams, L.A.J., 1972: Geology of the Eastern Rift System of Africa. Geological Society of America, Special Paper 136, 1-67.

Baker, B.H., Goles, G.G., Leeman, W.P. and Lindstrom, M.M., 1977: Geochemistry and petrogenesis of basalt-benmoreite-trachyte suite from southern part of the Gregory rift, Kenya. Contrib. Min. Petrol. Vol. 64, p. 303-332.

Baker, B.H., Mitchel, J.G., and Williams, L.A.J., 1988: Stratigraphy, geochronology and volcano-tectonic evolution of the Kedong-Naivasha-Kinangop region, Gregory Rift Valley, Kenya. Geological Society of London, 145,107-116.

Bechtel, T.D., Forsyth, D.W., and Swain, S.W., 1987: Mechanism of isostatic compensation in the vicinity of the East Africa Rift, Kenya. Geophysics, 90, 445-465.

Black, S., Macdonald, R. and Kelly, M.R., 1997: Crustal origin of the peralkaline rhyolites from Kenya; evidence from U-series disequilibrium and Th-isotopes. Journ. Petro. Vol. 38, p. 277-297.

Browne, P.R.L., 1978: Hydrothermal alteration in active geothermal fields. *Annual Review Earth and Planetary Sciences, 6,* 229–250.

Browne, P.R.L., 1984: Subsurface stratigraphy and hydrothermal alteration of the eastern section of the Olkaria geothermal field, Kenya. *Proceedings of the 6th New Zealand Geothermal Workshop, Geothermal Institute, Auckland,* 33-41.

Corti, G., 2011: Evolution and characteristics of continental rifting: Analog modelling-inspired view and comparison with examples from the East Africa Rift System, *Tectonophysics,* doi:10.1016/j.tecto.2011.06.010

Clarke, M. C. G., Woodhall, D. G., Allen, D., Darling, G., 1990: Geological, Volcanological and hydrogeological controls of the occurrence of geothermal activity in the area surrounding Lake Naivasha. *Min. of Energy, Nairobi, report* 150, 138 pp.

Class, C., Altherr, R., Volker, F., Eberz, G. and McCulloch, M.T., 1994: Geochemistry of Quaternary alkali basalts from the Huri Hills, northern Kenya. Chemical Geology, vol. 113, p. 1-22.

Davies, G.R., Macdonald, R., 1987: Crustal influences in the petrogenesis of the Naivasha basalt-comendite complex, combined trace elements and SR-Pb isotope constraints. *Journal of petrology 28, 1009-1031.*

Dunkley, P.N., Smith, M., Allen, D.J., and Darling, W.G., 1993: The geothermal activity and geology of Northern sector of Kenya Rift Valley. *British geological survey research report, 93, 1.*

Ferrara, G. and Treuil, M., 1974: Petrological implications of trace elements and isotopic distributions in basalt-pantellerite suites. Bull. Volcano. vol. 38, p. 548-574.

Franzson, H., Zierenberg, R. and Schiffman, P., 2008: Chemical transport in geothermal systems in Iceland, Evidence from hydrothermal alteration. Journal of Volcanology and Geothermal Research.

Goles, G.G., 1976: Some constraints on the origin of phonolites from the Gregory rift, Kenya and inferences concerning basaltic magmas in the rift system. Lithos vol. 9, p. 1-8.

Hay, D.E. and Wendlandt, R.F., 1995: The origin of Kenya plateau type phonolites; results of high pressure/high temperature experiments in the systems, phonolites-H_2O and phonolites-H_2O-CO_2. *Journal of Geophysics. Res. Vol. 100, pp 401-410.*

Hay, D.E., Wendlandt, R.F. and Wendlandt, E.D. 1995a: The origin of Kenya rift plateau type flood phonolites; evidence from geochemical studies of fusion of lower crust modified by alkali basalt Magmatism. Journ. Geophy. Res., vol. 100, p. 411-422.

Henry, W.J., Mechie, J., Maguire, P.K.H., Khan, M.A., Prodehl, C., Keller, G.R., and Patel, J., 1990: A seismic investigation of the Kenya rift valley. Geophysics J. Int., 100-1,107-130.

Heumann, A., Davies, G.R., 2002: U-Th disequilibrium and Rb-Sr age constraints on the magmatic evolution of peralkaline rhyolites from Kenya. *Journal of Petrology 43, 557-577.*

Holloway,.H.p and Vidyanathan, P., 2010: Characterization of Metals and Alloys. 2nd ed. New York: Momentum press LLC. 261.

Jestin, F., Huchon, P., & Gaulier, J. M. (1994). The Somalia plate and the East African Rift System: present-day kinematics. *Geophysical Journal International, 116*(3), 637-654.

Keller, G.r., Prodehl, C., Mechie, J., Fuchs, K., Khan, M.A., Maguire, P.K.H., Mooney, W.D.,Achauer, U., Davis, P.M., Meyer, R.P., Braile, L.W., Nyambok, I.O. and Thompson, G.A., 1994: The East Africa rift system in the light of KRISP 90. In: Prodehl, C., Keller, G.R. and Khan, M.A. (eds.): Crustal and upper mantle structure of the Kenya rift. Tectonophysics vol. 236, p. 465-483.

Kristmannsdóttir, H., 1979: "Alteration of Basaltic Rocks by Hydrothermal-Activity at 100-300° C." *Developments in sedimentology* 27 (1979): 359-367.

KenGen 2012: Stratigraphy and hydrothermal alteration mineralogy of well OW-910 and OW-917. KenGen internal report (unpublished).

Lagat, J.K., 2004: Geology, hydrothermal alteration and fluid inclusion studies of the Olkaria Domes geothermal field, Kenya. University of Iceland, MSc thesis, UNU-GTP, Iceland, report 2, 71 pp.

Latin, D., Norry, M.J and Tarzey, R. J.E., 1993: Magmatism in the Gregory rift, East Africa; evidence for melting generation by a plume. Journ. Petrol. Vol. 34, p. 1007-10027.

Le Maitre, Roger Walter, Albert Streckeisen, B. Zanettin, M. J. Le Bas, B. Bonin, and P. Bateman, eds, 2002:. Igneous rocks: a classification and glossary of terms: recommendations of the International Union of Geological Sciences Subcommission on the Systematics of Igneous Rocks. *Cambridge University Press*.

Macdonald, R. (1974): Nomenclature and petrochemistry of the peralkaline oversaturated extrusive rocks. *Bulletin volcanologique*, *38*(2), 498-516.

MacDonald, R., Davies, G.R., Bliss, C.M., Leat, P.T., Bailey, D.K., and Smith, R.L., 1987: Geochemistry of high silica peralkaline rhyolites, Naivasha, Kenya rift valley. J. Petrology, 28,979-1008.

Macdonald, Raymond, N. W. Rogers, J. G. Fitton, S. Black, and M. Smith 2001: "Plume–lithosphere interactions in the generation of the basalts of the Kenya Rift, East Africa." *Journal of Petrology* 42, no. 5, 877-900.

Macdonald, R., Black, H.E., Fitton, J.G., Marshall, A.S., Nejbert, K., Rodgers, N.W., and Tindle, A.G., 2008: The roles of fractional crystallization, magma mixing, crystal mush remobilization and volatile-melt interactions in the genesis of a young basalt-peralkaline rhyolite suite, the Greater Olkaria volcanic complex, Kenya Rift Valley. J. Volcanology, 49-8, 1515-1547.

Mariita, N.O., 2009: Exploration history of Olkaria geothermal field by use of geophysics. Paper presented at “Short Course IV on Exploration for Geothermal Resources”, organized by UNU-GTP, KenGen and GDC, Lake Naivasha, Kenya, 13 pp.

Mariita, N.O., 2011: Exploration history of Olkaria geothermal field by use of geophysics. Paper presented at “Short Course IV on Exploration for Geothermal Resources”, organized by UNU-GTP, KenGen and GDC, Lake Naivasha, Kenya, 13 pp.

Marshall, A.S., MacDonald, R., Rogers, N.W., Fitton, J.G., Tindle, A.G., Nejbert, K., and Hinton, R.W., 2009: Fractionation of peralkaline silicic magmas: the Greater Olkaria volcanic complex, Kenya Rift Valley. J. Petrology, 50,323-359.

Mechie, J., Keller, R.R., Prodehl, C., Khan, M.A. and Gaciri, S.J., 1997: A model for structure, composition and evolution of the Kenya rift; in structure and dynamic processes in the lithosphere of the Afro-Arabian rift system. Fuchs, K., Artherr, R., Mulller, B., and Prodehl, C. (eds.). Tectonophysics, vol. 278, p. 95-119.

Moore, M. D. and Reynolds, Jr., 1997: X-ray diffraction and the identification and analysis of clay minerals. 18th ed. 378 p. New York: Oxford University Press.

Muchemi, G.G., 1999: Conceptual model of the Olkaria geothermal field. KenGen, internal report, 19 pp.

Muchemi, G.G., 2000: Conceptual model of Olkaria geothermal field. KenGen internal report, 13 pp (unpublished).

Mungania, J., 1995: Tephra deposits in Olkaria and the surrounding areas. Kenya Power, Unpublished Report, 7 pp.
Mungania, J., 1999: Geological report of well OW-714. Kenya Power Company internal report.

Musonye, X.S., 2012: Borehole geology and alteration mineralogy of well OW-914A, Domes area, Olkaria geothermal field, Central Kenya Rift. Report 23, 501-540.

Mbia, P.K., 2014: Sub-surface geology, petrology and hydrothermal alteration of Menengai geothermal field, Kenya. Report 1, 87 pp.

Mwangi, D.W., 2012: Borehole geology and hydrothermal mineralisation of well OW–916, Olkaria Domes geothermal field, Naivasha, Kenya. Report 24, 541-571.

Naylor, W.I., 1972: Geology of the Eburru and Olkaria prospects. UN Geothermal Exploration Project, report.

Nash, W.P., Carmichael, I.S.E. and Johnson, R.W., 1969: The mineralogy and petrology of Mt. Suswa, Kenya. Journ. Petrol. Vol. 10, p. 409-439.

Ofwona, C., Omenda, P., Mariita, N., Wambugu, J., Mwawongo, G., and Kubo, B., 2006: Surface geothermal exploration of Korosi and Chepchuk prospects. KenGen internal report, 44 pp.

Ogoso-Odongo, M.E., 1986: Geology of Olkaria geothermal field. Geothermics, 15, 741-748.

Okoo, J. A., 2011: Hydrothermal alteration mineralogy of well OW-914, olkaria domes field, kenya. Proceedings, Kenya Geothermal Conference 2011, Kenyatta International Conference
Center, Nairobi, November 21-22, 2011.

Onacha, S.A., 1993: Resistivity studies of the Olkaria-Domes geothermal project. KenGen, internal report.

Omenda, P.A., 1993: Geological investigation of Suswa geothermal prospect, Kenya. KPC Internal report, 35pp.

Omenda, P.A., 1994: The geological structure of the Olkaria west geothermal field, Kenya. Proceedings of the 19th Stanford Geothermal Reservoir Engineering Workshop, Stanford University, Stanford, Ca, 125-130.

Omenda, P. A., 1997: The Geochemical Evolution of Quaternary Volcanism in the South-Central Portion of the Kenya Rift.

Omenda, P.A., 1998: The geology of well OW-901. KenGen, internal report. Ambusso, W.J., and Ouma, P.A., 1991: Thermodynamic and permeability structure of Olkaria Northeast field: Olkaria fault. Geothermal Resource Council Transactions, 15, 237-242.

Omenda, P.A., 2000: Anatectic origin of comendite in Olkaria geothermal field, Kenya Rift; Geothermal evidence of syenitic protholith. African J. Science & Technology, Science & Engineering Series, 1, 39-47.

Otieno, V., Munyiri, S., Wanjohi, D., Okoo, J. and Wanjohi A., 2014: Structural mapping of Olkaria Southwest, Olkaria geothermal field, 5th May-20th July 2014, 46pp, KenGen internal report (unpublished).

Ouma, p., 2009: Geothermal Exploration and Development of the Olkaria Geothermal Field. *Short Course IV on Exploration for Geothermal Resources*, Lake Naivasha, Kenya, November 1-22, 2009.

Ouma, p., 2011: Geothermal Exploration and Development of the Olkaria Geothermal Field. *Short Course IV on Exploration for Geothermal Resources*, Lake Naivasha, Kenya, October 27-November 18, 2011.

Riaroh, D. and Okoth, W., 1994: The geothermal fields of the Kenya rift. Tectophysics 236, 117-130.

Rockware INC., 2007: *Log Plot program*. Rockware Inc., USA.

Rule A. C, 2007: Smectite Clay Products Teaching Materials. Journal of Geoscience Education, 2007.

Scaillet, B., Macdonald, R., 2001: Phase relations of peralkaline silicic magmas and petrogenetic implications. *Journal of Petrology 42, 825-845.*

Shackleton, R.M., 1986: Precambrian collision tectonics in Africa. In: Coward, M.P., and Ries, A.C. (eds.), Collision tectonics. Geol. Soc. Spec. Publ., 19,329-349.

Simiyu, S.M., Omenda, P.A., Keller, G.R and Antony, E.Y., 1995: Geophysical and geological evidence of the occurrence of shallow intrusion in the Naivasha sub-basin of the Kenya rift. AGU Fall 1995 meeting, Abst. F657, V21A-12.

Simiyu, S.M., and Keller, G.R., 1997: An integrated analysis of lithospheric structure across the East African plateau based on gravity anomalies and recent seismic studies. In: Fuchs, K.

Simiyu, S.M., and Keller, G.R., 2000: Seismic monitoring of the Olkaria Geothermal area, Kenya Rift valley. Journal of Volcanology and Geothermal Research, 95 (2000), 197-208.

Simiyu, S.M., Oduong, E.O., and Mboya, T.K., 1998: Shear wave attenuation beneath the Olkaria volcanic field. KenGen, internal report.

Simiyu, M. S., 2010: Status of Geothermal Exploration IN Kenya and Future Plans for its Development. *Proceedings World Geothermal Congress,* 25-29 April 2010.

Simmons, S. F., & Browne, P. R. (2000): Hydrothermal minerals and precious metals in the Broadlands-Ohaaki geothermal system: Implications for understanding low-sulfidation epithermal environments. *Economic Geology*,*95*(5), 971-999.

Simmons, S.F. and Christens, B.W., 1993: Towards a united Theory on Calcite Formation in Boiling Geothermal Systems. 15th Proc. Newzealand Geothermal Workshop. Pp: 145-148.

Smith, M., and Mosley, P., 1993: Crustal heterogeneity and basement influence on the development of the Kenya rift, East Africa. Tectonics, 12, 591-606.

Weaver, S.D., Scael, J.S.C. and Gibson, I.L., 1972: Trace element data relevant to the origin of trachyte and pantelleritic lavas of the east Africa Rift system. Contrib. Min. Petrol. Vol. 36, p. 181-194.

Williams, L.A.J., 1972: The Kenya rift volcanics: a note on volumes and chemical composition. Tectonophysics, 15, 83-96.

Wilson, B. Marjorie, 1989: *Igneous petrogenesis a global tectonic approach*. Springer Science & Business Media, 1989.

Yoshio, W., Eiichiro, M. and Kozo, S., 2011: X-ray Diffraction Crystallography. New York: Springer Heidelberg Dordrecht. P 67-80.

Appendix

AA: Detailed description of stratigraphy for well OW-905A as observed under binocular and petrographic microscope analysis.

0-320 m No sample (Loss of circulation returns)

320-324 m Tuff. Green to brown fine grained formation. It is moderately porphyritic with sanidine phenocrysts. The rock is highly vesicular with the vesicles being filled with green and brown clays. A few trachytic fragments noted in this sample. Alteration minerals: pyrite, hematite, clays, chlorite, calcite and platy calcite.

324-338 m Trachyandesite. Grey fine grained slight porphyritic rocks with phenocrysts of pyroxene and feldspars. It is moderately vesicular with the vesicles filling with brown and pale green clays. Mesolite also noted in the vesicles. The rock is slightly oxidised to brown iron oxides. Chlorite vein observed at 330-332 m. Sphene is noted as an alteration product of iron oxides. Alteration minerals: calcite, hematite, chlorite, illite, amorphous and platy calcite and sphene.

338-344 m Tuff. Pale green to grey fine grained rock sample. It is moderately porphyritic with feldspar phenocrysts. It is moderately vesicular with the vesicles filled with illite, smectite and chlorite clays. It is slightly altered to pale green clays. A few trachyte and basalt rock fragments noted mixed in this sample. Alteration minerals: clays, chlorite, sphene and oxides.

344-354 m Trachytic tuff. Dark grey fine grained rock sample. Phenocrysts of pyroxene and feldspars are noted. The rock is slightly vesicular with vesicles filled with brown clays. The feldspar rich groundmass is noted altering to green clays. Alteration minerals: clays and oxides.

354-370 m Tuff. Pale green fine grained rock. The groundmass is quite lithic with quartz and feldspar crystal fragments embedded in the lithic groundmass. It is highly altered to kaolinite clays which swells on adding water. Alteration minerals: clays (kaolinite and smectite), oxides, calcite and zeolites (mesolite).

370-398 m Rhyolite. Brown to white fine grained highly porphyritic rock with phenocrysts of sanidine, pyroxene and quartz. The sanidine phenocrysts are in abundance, followed by quartz with a few pyroxenes. The pyroxenes and the feldspar rich groundmass alters to brown and green clays. The formation is slightly vesicular with the vesicles being filled

with zeolites. It is moderately to highly altered to brown and green clays. Alteration minerals: chlorite, clays, zeolites (mesolite), pyrite and calcite.

398-432 m Trachyte. Green to slightly brown fine grained rock. It is moderately to highly porphyritic with phenocrysts of pyroxene and sanidine. The formation is slightly fractured with the fractures filling with chalcedony. It is moderately to highly altered to green clays with the groundmass being the most altered. Alteration minerals: chlorite, clays (illite, smectite), chalcedony, pyrite, zeolites (mesolite) and calcite.

432-494 m Rhyolite. Brown to white fine grained rock. The rock is highly porphyritic with sanidine, pyroxene and quartz phenocrysts. Pyroxene is noted to alter to brown and green clays. The rock is slightly vesicular. It is slightly altered to brown and green clays. Alteration minerals: clays, calcite, pyrite and oxides.

494-544 m Trachyte. Pink to pale green crystalline rock. It is slightly porphyritic with sanidine, pyroxene and quartz phenocrysts. The rock is slightly altered to brown and green clays. The pyroxenes are seen altering to brown and green clays. Alteration minerals: calcite and clays.

544-580 m Basalt. Brown to dark grey medium grained rock. The rock is rich in feldspar and pyroxenes with the groundmass being enriched in plagioclase. The rock is highly porphyritic with plagioclase and pyroxene phenocrysts. The rock is moderately altered to brown clays. Epidote colouration noted at 548-550 m while first appearance of epidote noted at 554-556 m. Alteration minerals: clays, calcite, chlorite, epidote, sphene, platy calcite at 564-566 m and quartz at 566-568 m.

580-590 m Trachyte. Grey fine grained slightly porphyritic rock with phenocrysts of sanidine being noted. It is slightly altered to brown and green clays. Pyrite is discerned in the groundmass. Alteration minerals: pyrite, calcite, clays, sphene, quartz.

590-616 m Basalt. Brown to dark grey medium grained rock. The rock is rich in plagioclase and pyroxenes with the groundmass being enriched in plagioclase. The rock is highly porphyritic with plagioclase and pyroxene phenocrysts. The rock is moderately altered to brown clays. Alteration minerals: clays, epidote, chlorite and sphene.

616-644 m Tuff. Pale green fine grained rock. Feldspars alters to epidote. The rock is highly chloritised. At 616-620 m there is high alteration to green clays and epidote, an indication of fluid flow. Alteration minerals: epidote, chlorite, clays, calcite and pyrite.

644-662 m Basalt. Dark grey fine to medium grained rock. Some of the fragments are glassy. It is moderately porphyritic with phenocrysts of plagioclase and pyroxene characterising the plagioclase rich groundmass. The formation is slightly vesicular with the vesicles filled with brown and green clays. Alteration minerals: clays, chlorite, chalcedony, sphene chalcopyrite and epidote.

662-674 m Trachyte. Pale green to white fine grained rock. It is slightly porphyritic with pyroxene phenocrysts discerned in the feldspar rich groundmass. The rock is highly bleached. Euhedral pyrite cubes are discerned in the groundmass. Trachytic texture noted

in a few of the bleached samples. Alteration minerals: calcite, pyrite, clays, sphene and chlorite.

674-698 m Trachyte. Brown to grey fine grained slightly porphyritic rock with phenocrysts of pyroxene. Pyrite is noted discerned in the groundmass. The rock is highly fractured with fracture planes filling with brown and green clays. The rock is highly altered to brown clays indicating a probable feed zone. Alteration minerals: chlorite, clays, pyrite, epidote and calcite.

698-714 m Vitric tuff. White cryptocrystalline slightly vesicular rock. Phenocrysts of quartz and pyroxene are noted in the groundmass. The vesicles are filled with quartz. There is oxidation noted between 706-714 m with formation of brown oxides. The formation is slightly altered to green clays. Alteration minerals: calcite, clays, quartz and chlorite.

714-726 m Rhyolite. Pink grey fine grained slightly porphyritic rock. Euhedral quartz and pyroxene mineral grains are discerned in the groundmass. The formation is slightly altered to brown and green clays. Alteration minerals: pyrite, chlorite, calcite and clays.

726-738 m Trachyte. Grey fine grained moderately porphyritic rock with pyroxene and feldspar phenocrysts. The rock is slightly altered to green clays. Alteration minerals: calcite, clays and chlorite.

738-754 m Trachyte. White, brown to pale green fine grained rock. The sample has a mixture of trachytic textures. Minute pyroxene grains are discerned in the groundmass. Pyrite cubes have been noted in some of the fragments. Pyroxenes are seen altering to green clays. The rock is bleached to green clays. Alteration minerals: chlorite, pyrite, sphene, epidote, calcite and quartz.

754-768 m Trachyte. Light grey fine grained moderately porphyritic rock with pyroxene and feldspar phenocrysts. The groundmass is enriched with sanidine and pyroxene mineral grains. The formation is slightly altered to chlorite clays. Sanidine is noted altering to epidote. Alteration minerals: epidote, calcite, quartz, pyrite, chlorite and sphene.

768-804 m Rhyolite. Pink fine grained moderately to highly porphyritic with quartz phenocrysts dominating the feldspar rich groundmass. A few pyroxenes are also noted in the groundmass. The rock is highly fractured and slightly vesicular. Spherulitic texture is noted with pyroxenes and feldspars radiating from a central point. Fracture planes and vesicles are filled with euhedral secondary quartz in clusters and as individual crystals too. The formation is slightly altered to chlorite. Pyrite noted in the groundmass. Alteration minerals: chlorite, quartz, pyrite, calcite and minor epidote.

804-868 m Tuff. Green to grey finely grained rock. The groundmass is lithic with crystal fragments of feldspars, pyroxenes and rare quartz embedded in the groundmass. Rounded lithic fragments of rhyolite, trachyte and basalt are noted in the groundmass too. The formation is highly altered to green clays which swell on adding water. Alteration minerals: kaolinite clays and calcite.

868-908 m Trachyte. Brown to pink fine grained moderately porphyritic rock with quartz porphyries characterising the groundmass. Minute pyroxene is discerned in the finely

grained quartz and feldspar rich groundmass. The formation is slightly altered to brown clays. Pyrite are noted in the groundmass. Alteration minerals: pyrite, clays, chlorite and quartz.

908-924 m Lithic tuff. Brown fine grained rock. The formation has a lithic groundmass composed of rounded trachyte, basalt and rhyolite lithic fragments. A few pale green trachyte fragments also noted mixed in this sample. The rock is highly altered to brown clays. Alteration minerals: pyrite, kaolinite clays, chlorite and calcite.

924-934 m Trachyte. White to pale green fine grained slightly porphyritic rock with sanidine phenocrysts. Minute pyroxenes noted in the groundmass. The rock is slightly vesicular with vesicles being filled with quartz grains. The formation is highly chloritised to pale green clays. Alteration minerals: calcite, quartz, chlorite and clays.

934-1098 m Trachyte Grey to light grey fine grained moderately porphyritic rock with pyroxene and sanidine phenocrysts. Pyroxenes shows moderate alteration to green clays. The rock is slightly fractured between 956-970 m with the micro veins being filled with quartz and pyrite veins. The rock is highly bleached between 956-970 m making it white in colour. Alteration minerals: clays, chlorite, quartz, pyrite and calcite.

1098-1108 m Tuff. Brown to pale green fine grained. The sample contains a mixture of trachyte and rhyolite fragments. The formation is highly altered to brown clays. Alteration minerals: pyrite, calcite, chlorite and clays.

1108-1142 m Basaltic trachyandesite. Green grey to dark grey fine grained to medium grained rock slightly porphyritic rock with plagioclase and pyroxene phenocrysts. The rock is rich is plagioclase which inter-grows with pyroxenes in the groundmass. The rock is slightly altered with green and brown clays. Crystalline epidote observed at 1108-1110 m. Wairakite noted at 1112-1114 m. Paragenetic sequence noted at 1120-1122 m. Alteration minerals: epidote, chlorite, clays, quartz, wairakite and calcite.

1142-1158 m Basaltic trachyandesite. Pale green to brown mixed sample. The sample has trachyte, rhyolite and basalt fragments with basalt fragments forming the bulk of the sample. The rock contains a few phenocrysts of plagioclase and pyroxene. The basaltic fragments are highly chloritised forming green clays. Alteration minerals: pyrite, calcite, chlorite, clays, epidote and quartz.

1158-1190 m Trachyte. Light grey to grey fine grained slightly porphyritic rock with phenocrysts of sanidine and pyroxene noted. Minimal disseminations of pyroxene in the feldspar rich groundmass noted. The formation is slightly altered with the pyroxenes noted altering to green clays. Alteration minerals: pyrite, calcite, chlorite, wairakite and minor epidote.

1190-1214 m No sample (Loss of circulation returns).

1214-1222 m. Tuff. Green to brown fine grained rock. The groundmass is lithic with pumice, glass and lava fragments discerned in the groundmass. The formation is moderately altered to brown clays. Alteration minerals: pyrite, calcite, clays and chlorite.

1222-1226 m No sample (Loss of circulation returns)

1226-1250 m Trachyte. Pale green to white fine grained highly chloritised rock. Partial losses noted at 1232-1238 m. The rock is highly altered to green clays. Alteration minerals: chlorite, clays and pyrite.

1250-1254 m Basaltic dyke. Grey to dark grey fine grained to cryptocrystalline rock. The rock is relatively fresh. The dark grey fragments are as a result of heat from the intrusion. Alteration minerals: clays, magnetite.

1254-1262 m Trachyte. Light to grey fine grained rock with sanidine phenocrysts embedded in the feldspar rich groundmass. Minute pyroxene mineral are also disseminated in groundmass. Feldspar is noted altering to epidote. The rock is relatively altered to green clays. Alteration minerals: epidote, calcite, wairakite and pyrite.

1262-1270 m Tuff. Grey to pale brown fine grained highly vesicular rock. The vesicles are filled with coarse grained green clays and epidote. Lithic fragments of shards of glass, trachyte and rhyolite are noted. The formation is moderately to highly altered to green and brown clays. Alteration minerals: epidote, calcite, wairakite, prehnite, chlorite and clays.

1270-1350 m Trachyte. Light grey fine grained aphyric rock. The groundmass is feldspar rich and minute pyroxene is discerned in the groundmass. The pyroxenes are noted altering to green clays. The rock is massive and moderately altered to green clays. At 1292-1320 m, the rock is vesicular with the vesicles being filled with coarse grained pale green clays, quartz, prehnite and epidote. Alteration minerals: pyrite, calcite, chlorite, quartz, prehnite, wairakite and epidote.

1350-1366 m Basaltic dyke. Dark grey fine grained to cryptocrystalline aphyric rock. The rock is relatively fresh. Some fragments, which are rich in feldspar, are noted to be highly altered to pale green clays. These fragments are likely to be from the margins of the intrusion. Alteration minerals: clays.

1366-1378 Rhyolite. Pink to brown fine grained slightly porphyritic rock with phenocrysts of quartz and sanidine. The formation is slightly vesicular with vesicles being filled with green clays, quartz and wollastonite. Cubes of pyrite is noted in the groundmass. Veins filled with quartz are noted. The rock is slightly altered to green clays with high alteration noted at 1372-1378 m. Alteration minerals: wairakite, quartz, chlorite, pyrite and clays.

1378-1422 m Trachyte Green grey to light grey fine grained slightly porphyritic rock with feldspars phenocrysts. A few pyroxene are discerned in the groundmass. The rock is slightly vesicular with the vesicles filled with green clays. The rock is slightly altered to green clays. Pyrite is noted in the groundmass. Alteration minerals: clays, chlorite and pyrite.

1422-1430 m Rhyolite. Pink to brown fine grained rock. The rock is moderately porphyritic with quartz phenocrysts. The rock is slightly to moderately altered to brown and green clays. Pyrite is disseminated in the groundmass. Alteration minerals: chlorite, calcite, pyrite and clays.

1430-1484 m Trachyte. Grey, green grey to brown fine grained rock slightly porphyritic rock with sanidine phenocrysts. Minute pyroxenes are discerned in the feldspar rich groundmass. Pyroxenes are observed altering to green clays. The rock is highly vesicular with some of the vesicles noted to be filled with euhedral quartz crystals, which is seen growing in association with prehnite in some instances. There is high alteration and vesicularity noted at 1458-1462 m. Minimal calcite noted. Alteration minerals: calcite, pyrite, chlorite, quartz and prehnite.

148401496 m Basalt. Dark grey to green grey fine grained rock. The formation is rich in plagioclase and pyroxene. It is slightly porphyritic with plagioclase and pyroxene phenocrysts. The rock is vesicular with the vesicles being filled with chlorite clays, quartz, and epidote. Crystalline epidote noted at 1486-1488 m. Epidote is noted growing in association with actinolite and prehnite. Veinlets filled with epidote noted. Calcite is noted filling in vugs. The rock is weakly altered to green clays. Alteration minerals: epidote, actinolite, quartz, prehnite, wairakite, chlorite, calcite and clays.

1496-1560 m Trachyte Green grey, grey to brown grey fine grained slightly to moderately porphyritic rock. Sanidine phenocrysts noted. The formation is slightly to moderately vesicular with the vesicles being filled with coarse grained green clays. Veinlets, vugs and vesicles are filled with quartz and pale green chlorite clays. Calcite fills in vugs and veinlets at 1534-1542 m. The rock is highly oxidised (it is white in colour) between 1538-1546 m with increased vesicles. Cubes of pyrite noted and prehnite grows on top of quartz in a paragenetic sequence at 1558-1560 m. Alteration minerals: chlorite, quartz, clays, pyrite, calcite and prehnite.

1560-1646 m Trachyte. Grey fine grained moderately porphyritic rock with sanidine phenocrysts. The feldspars show alteration to albite. The formation is slightly vesicular with the vesicles mainly filled with chlorite clays and quartz. Calcite is present in moderate abundance with minute pyroxenes noted in the groundmass. The rock is slightly altered to brown clays. Alteration minerals: calcite, quartz, chlorite, clays and pyrite.

1646-1650 m Trachyte. Green grey, highly glassy and slightly porphyritic rock with sanidine phenocrysts. Pyroxenes are discerned in the groundmass. Alteration minerals: pyrite, chlorite, albite and illite.

1650-1658 m Trachyte. Brown grey, fine grained slightly porphyritic rock with sanidine phenocrysts. The sanidines have altered to green clays. The rock is slightly vesicular with the vesicles being filled with pyrite. Alteration minerals: pyrite, chlorite, albite and illite

1658-1672 m Trachyte. Grey fine grained moderately porphyritic rock with sanidine phenocrysts. The feldspars shows alteration to albite. The formation is slightly vesicular with the vesicles mainly filled with chlorite clays and quartz. Calcite is present in moderate abundance with minute pyroxenes noted in the groundmass. The rock is slightly altered to brown clays. Vesicles are filled with epidote and actinolite fills vesicles at 1658-1668 m. Prehnite also noted. Alteration minerals: epidote, pyrite, prehnite, quartz and actinolite.

1672-1680 m Trachyte. Pale green fine grained aphyric rock. The formation is slightly vesicular with vesicles filled with quartz and prehnite. The rock is highly chloritised to pale green clays. Alteration minerals: prehnite, quartz and chlorite.

1680-1758 m Trachyte. Brownish grey to greenish grey fine grained slightly porphyritic rock with sanidine phenocrysts. The sanidine grains are altering to green clays. The rock is slightly vesicular with the vesicles being filled with pyrite. It is moderately altered at 1698-1722 m with the formation of brown clays. Epidote observed at 1698-1700 m and 1708-1710 m. Veins filled with quartz, calcite and pale green chlorite clays noted. Calcite is noted filling in vugs. Alteration minerals: epidote, calcite, prehnite, pyrite, chlorite and clays.

1758-1774 m Trachyte. Pale green to light grey grained rock. The rock is highly altered with numerous sphene patches observed in the groundmass. It is highly bleached and altered to green clays. Feldspars alters to epidote. Vugs are filled with green clays and epidote. Quartz and epidote veins noted. Alteration minerals: epidote, sphene, calcite, chlorite and quartz.

1774-1778 m Basalt. Green grey fine grained highly mafic rock. The rock is highly altered to green clays. Calcite is abundant and epidote is seen replacing feldspars. Alteration minerals: sphene, epidote, chlorite and clays.

1778-1792 m Trachyandesite. Pale green to light grey grained rock. The rock is highly altered with numerous sphene patches observed in the groundmass. Trachytic texture is observed in the groundmass. It is highly bleached and altered to green clays. Feldspars alters to epidote. Vugs are filled with green clays and epidote. Quartz and epidote veins noted. Alteration minerals: epidote, sphene, calcite, quartz and chlorite.

1792-1798 m Basalt. Greenish grey, fine grained highly mafic rock. The rock is highly altered to green clays. Calcite is abundant and epidote is seen replacing feldspars. Alteration minerals: sphene, epidote, chlorite and clays.

1798-1830 m Trachyte. Light grey to brown fine grained highly porphyritic rock with feldspar phenocrysts. Fault breccia and scoria fragments noted at 1814-1816 m. The rock is slightly vesicular. The vesicles and vugs are filled with course grained green clays and epidote. The rock is moderately to highly altered to green clays. The groundmass is altered to brown clays. Alteration minerals: epidote, calcite, quartz, sphene, chlorite and clays.

1830-1846 m No sample (Loss of circulation returns).

1846-1884 m Rhyolite. Pale green to brown fine grained slightly porphyritic, slightly vesicular. Quartz and sanidine phenocrysts are observed. Vesicles filled with coarse grained green clays and quartz. Rock is highly altered to pale green clays. Minute pyroxenes are discerned in the groundmass with some of them noted altering to green clays. Quartz and chlorite veinlets noted at 1874-1876 m indicating fracturing at this depth. Alteration minerals: chlorite, calcite, pyrite, illite clays, quartz and epidote.

1884-1896 m Micro-granite intrusion. White fine grained rock. Quartz mineral grains are noted inter-grown with feldspars with quartz forming about 30% of the grains. Minute

pyroxenes are note discerned in the groundmass and they are noted altering to green clays. The rock is relatively fresh. Alteration minerals: chlorite.

1896-1924 m Trachyte. Pale green fine grained slightly porphyritic rock. The rock is fractured with veins filled with epidote and chlorite. The rock is highly altered at 1912-1920 m with formation of green clays. Numerous sphene in the groundmass at 1910-1912 m. Epidote is noted as an alteration product of feldspar. Alteration minerals: Epidote, quartz, chlorite and sphene.

1924-1966 m Trachybasalt. Green grey fine grained aphyric rock. The formation is slightly vesicular with vesicles and vugs filled with green chlorite clays, epidote and actinolite in that paragenetic sequence (1944-1948m). Epidote is noted as replacement of feldspars and depositional mineral. Veinlets of albite and chlorite noted. There is abundance of epidote and actinolite at 1934-1936 m and 1944-1946 m. Alteration minerals: epidote, chlorite, sphene, actinolite, calcite, albite and wairakite.

1966-1978 m Trachyte. Grey fine grained slightly porphyritic rock. The formation is characterised by minute pyroxene and feldspar in the groundmass. The rock is slightly altered to green clays. Pyrite is sparsely discerned in the groundmass. Alteration minerals: chlorite, pyrite and calcite.

1978-2012 m Trachyte. Light grey, pale green to brown fine grained rock. Rock is aphyric. Fault breccia fragments are noted in the sample at 1982-1984 m and 1988-1990 m. Pyrite cubes are disseminated in the groundmass. The rock is fractured as indicated by presence of mineral veinlets mainly filled with dark green clays. The rock is moderately to highly altered to green and brown clays. Alteration minerals: chlorite, calcite, clays, pyrite and quartz.

2012-2056 m Trachybasalt. Green grey fine grained aphyric rock. The formation is slightly vesicular with vesicles and vugs filled by green chlorite clays, epidote and actinolite. Epidote is noted as replacement of feldspars and depositional mineral. Veinlets of albite and chlorite noted. Alteration minerals: chlorite, pyrite and calcite.

2056-2070 m Trachyte. Light grey fine grained rock. Rock is aphyric with minute pyroxenes discerned in the felsic rich groundmass. The groundmass is noted altering to pale green clays. Alteration minerals: chlorite, calcite and pyrite.

2070-2102 m Trachyte. Light grey to grey fine grained rock. It is slightly porphyritic with feldspar phenocrysts. Rock is slightly altered to green clays. Few pyrite cubes noted in some of the fragments. Alteration minerals: pyrite, chlorite and clays.

2102-2144 m No sample (Loss of circulation returns).

2144-2166 m Trachyte. Light grey to grey fine grained rock. It is slightly porphyritic with feldspar phenocrysts. Rock is slightly altered to green clays. Few pyrite cubes noted in some of the fragments. Alteration minerals: chlorite and clays.

2166-2178 m Trachyte. White to light green fine grained slightly porphyritic rock with feldspar phenocrysts. The rock is fractured with veinlets of green clays, calcite and quartz

noted. Epidote is seen as an alteration product of feldspars. Alteration minerals: chlorite, calcite, clays and sphene.

2178-2194 m Trachyte Light grey fine grained feldspar rich rock. It is slightly porphyritic with feldspar phenocrysts. Rock is fractured with veins filled with green clays and quartz. Quartz is noted growing in association with green chlorite clays. Rock is slightly altered to green clays. Alteration minerals: epidote, quartz, calcite, pyrite, sphene, chlorite, clays and wairakite.

2194-2222 m Basalt. Dark grey to green grey fine grained to crystalline rock. The rock is rich in plagioclase. Epidote is noted growing in association with wairakite, quartz and calcite. The formation is slightly altered to green clays. Sphene is abundance. Alteration minerals: epidote, calcite, chlorite, quartz, wairakite and sphene.

2222-2340 m Trachyte. Light grey fine grained rock. The rock is slightly to moderately porphyritic with feldspar phenocrysts. The rock is dense and relatively fresh with the groundmass showing minimal alteration to green clays. Epidote noted in small quantities. Alteration minerals: epidote, calcite and clays.

2340-2344 m Trachyte. White to grey fine grain grained rock. The rock has Rhyolite and trachyte fragments. The formation is slightly altered to green clays. Alteration minerals: chlorite and clays.

2344-2362 m Trachyte. Light grey to grey fine grained rock. The rock is aphyric to slightly porphyritic. The groundmass is seen to slightly alter to green clays. Minor epidote noted. Alteration minerals: chlorite, calcite, pyrite and epidote.

2362-2390 m No sample (Loss of circulation returns).

2390-2526 m Trachyte. Light grey to grey fine grained rock. The rock is aphyric to slightly porphyritic. The groundmass is seen to slightly alter to green clays. Minor epidote noted. Alteration minerals: chlorite, calcite, pyrite and epidote at 2422-2426 m and 2446-2448 m.

2526-2538 m No sample (Loss of circulation returns).

2538-2552 m Trachyte. Light grey to grey fine grained rock. The rock is aphyric to slightly porphyritic. The groundmass is seen to slightly alter to green clays. Minor epidote noted. Minor losses noted at 2542-2548 m. Alteration minerals: chlorite, calcite, pyrite and epidote.

2552-2606 m Syenitic intrusion. White equigranular feldspar rich rock. The rock has quartz mineral grains inter-grown sparsely with feldspar dominating mineral grains. The rock is slightly vesicular with thin films of green clays and actinolite. The groundmass has spots of pyroxene, which shows slight alteration to green clays. Alteration minerals: epidote, actinolite, chlorite, clays, pyrite and quartz.

2606-2674 m Trachyte. Light grey to grey fine grained aphyric rock. The groundmass is feldspar rich with pyroxene disseminated in it. Veinlets filled with black minerals noted. The rock is slightly altered to green clays. Alteration minerals: calcite, chlorite, pyrite and minor epidote.

2674-2726 m Syenitic intrusion. White to pale green medium grained, equigranular rock. The groundmass is characterised by feldspar mineral grains with minor medium grained quartz inter-growing with them. Spots of disseminated pyroxene are noted in the groundmass. The pyroxenes are altered to green clays giving the rock the pale green colour. Alteration minerals: actinolite, epidote, chlorite, clays, pyrite and quartz.

2726-2770 m Trachyte. Light grey fine grained aphyric formation. The rock has feldspar rich groundmass in which minute pyroxenes are discerned. Veinlets filled with green clays and black minerals noted. The rock is slightly altered to green clays. Alteration minerals: clays, chlorite and pyrite.

2770-2794 m Syenitic intrusion. White to pale green medium grained rock. The groundmass is equigranular with feldspar and quartz and feldspar forming the groundmass. The quartz forms about 4% of the groundmass. Pyroxenes are sparsely discerned in the groundmass and are seen to alter to green clays. Alteration minerals: chlorite, illite and pyrite.

AB: Detailed description of stratigraphy for well OW-910 as observed under binocular and petrographic microscope analysis.

0-16 m Pyroclastics. Light grey to slightly brown unconsolidated glass dominated pyroclastics. Fragments of consolidated ash also found. Pumice fragments are observed in abundance. The rock fragments are highly vesicular and some of the volcanic glass reveals flow texture marked by the striations. Minimal alteration observed in the glass with formation of yellow palagonite and brown oxides. Alteration minerals: oxides and palagonite.

16-52 m No sample (Loss of circulation returns)

52-68 m Rhyolite. Grey fine grained glassy sample with euhedral quartz and feldspar crystals dominating in the groundmass. The rock is vesicular with numerous pyroxene grains with some showing alteration to iron oxides. Alteration minerals: oxides.

68-116 m *No sample (Loss of circulation returns)*

116-118 m Tuff. Light grey, fine grained slightly porphyritic sample. It has feldspar phenocrysts. It is slightly vesicular and has pyroxene grains, which shows oxidation to iron oxides/alteration to brown clays. Alteration minerals: oxides and clays.

118-218 m *No sample (Loss of circulation returns)*

218-226 m Rhyolite. White to brown moderately porphyritic mix of rhyolite and glassy tuff. Phenocrysts of sanidine dominate the groundmass. The pyroxenes in the groundmass have

been coated with brown oxides giving the sample the brownish appearance. The pyroxene shows alteration to green clays in other instances. Alteration minerals: oxides and clays.

226-250 m *No sample (Loss of circulation returns)*

250-286 m Lithic tuff. Pale green to white heterogeneous lithic tuff, which contains glassy tuff, rhyolite and lithic tuff fragments, which are abundant. The groundmass is lithic and moderately vesicular. Porphyries of quartz and feldspar embedded in the groundmass. Some of the vesicles have analcime zeolite crystals (From 256 m depth downwards). The whitish rock fragments are glassier. The rock shows minimal alteration with the formation of dark green clays (altering from pyroxenes). Minimal oxidation noted with formation of iron oxides (Mainly observed in the glassy fragments). Alteration minerals: zeolites (analcime), oxides, clays (illite and mixed layer clays)

286-292 m No sample (Loss of circulation returns)

292-312 m Pyroclastics. Pale green to brown fine grained unconsolidated mix of rhyolite, tuff, trachyte and volcanic glass sample. Some of the fragments are highly vesicular and glassy. Vesicles filled with green clays. Paragenetic sequence noted with white clays depositing first followed by dark green clays. Vesicles are filled with mesolite. Veins filled with chalcedony noted. Low hydrothermal alteration noted. Alteration minerals: clays, pyrite, Zeolites (scolecite, mesolite), chalcedony and oxides.

312-360 m Tuff. Red brown slightly porphyritic rock sample. A few feldspar phenocrysts found in the groundmass. The sample is highly oxidized. It shows high alteration to brown clays. Calcite is abundant. Probable feed zone. Alteration minerals: calcite, clays and pyrite.

360-430 m Glassy tuff. White fine grained rock. Pyrite is sparsely dispersed in the groundmass. The rock shows minimal hydrothermal alteration with formation of clays. The groundmass is finely grained with quartz phenocrysts. Alteration minerals: pyrite and clays.

430-446 m Rhyolite. White fine grained rock. The rock has a tinge of pinkish colour in the groundmass. The rock is massive and slightly porphyritic with pyroxenes and quartz phenocrysts. Slightly altered to brown clays with the pyroxenes being the ones observed altering. Alteration minerals: oxides and clays.

446-510 m Rhyolite. Light grey to pale green fine grained slightly porphyritic rhyolite. Quartz phenocrysts are embedded in the groundmass. The groundmass is characterised by finely grained quartz and sanidine into which pyroxene grains are observed. The rock is fractured as seen by micro veins filled with pale green clays. The rock is slightly altered to green clays. Alteration minerals: chlorite and clays. Alteration minerals: chlorite and pyrite.

510-526 m Rhyolite. White to pink fine grained rock sample. The groundmass is embedded with quartz and sanidine phenocrysts. Clusters of pyroxene are also observed in the groundmass. The clusters are oxidized on the surface and some of them show alteration to pale green clays. Slightly altered to green clays. Alteration minerals: chlorite, pyrite and oxides.

526-546 m Tuff. Brown fine grained rock. The groundmass is lithic and characterised by sanidine and quartz crystal fragments. Slightly vesicular with vesicles filled with pale green clay and pyrite. The rock shows slight alterated to green clays. A few rhyolitic fragments are noted. Alteration minerals: chlorite, clays and pyrite.

546-598 m Tuff. Green fine grained tuff. The groundmass is lithic with a few vesicles being noted. The vesicles are filled with pale green clays. The groundmass is characterised by pyrite disseminations. Calcite noted in moderate abundance. Micro veins filled with pyrite noted. Paragenetic sequence with pale green clays being deposited first followed by calcite noted in the vesicles. Alteration minerals: pyrite, calcite, clays.

598-626 m Lithic tuff. White to pale green with some brown grey rock sample. The groundmass is disseminated with euhedral pyrite crystals. A few pale green rhyolite fragments also noted. Some of the rock fragments have vesicles, which are filled with quartz and wairakite. The rock is fractured as indicated by the presence of quartz veins and fractured planes which shows deposition of pyrite. Alteration minerals: pyrite, calcite, quartz, wairakite and clays.

626-656 m Lithic tuff. Red brown fine grained phyric rock sample. The groundmass is lithic. Pyrite cubes noted in the groundmass. Epidote noted replacing sanidine at 648 m. The tuff is highly altered to green clays. Alteration minerals: pyrite, chlorite and clays.

656-670 m Lithic tuff. Pale green fine grained lithic tuff. The groundmass is lithic and is characterised by sphene in the rock matrix. Pyrite is embedded in the rock matrix. Slightly altered to green clays (Pyroxene are seen to alter). Alteration minerals: chlorite, pyrite, calcite, epidote and sphene.

670-696 m Lithic tuff. Pale green to white, fine grained lithic tuff. It is slightly porphyritic with phenocrysts of pyroxene being observed in some fragments. The pyroxene phenocrysts are partially altered to green clays. Euhedral crystals of pyrite is embedded in the groundmass. Paragenetic sequence observed with crystals of pyrite depositing first followed by green clays. Epidote if noted altering from feldspars. Alteration minerals: chlorite, pyrite, epidote, sphene and calcite.

696-786 m Trachyte. Grey to light grey fine grained slightly to moderately porphyritic rock. Phenocrysts are feldspars. The groundmass is mainly pyroxene and feldspar mineral grains. The rock is slightly altered to brown clays. Pyrite and calcite noted in moderate abundance. Partial losses noted at 732-734m and 736-738m. A few basaltic and tuff fragments noted between 748-750 m. Alteration minerals: clays, calcite and epidote.

786-792 m Losses

792-838 m Trachyte. Light grey more felsic fine grained rock. It is more aphyric and it's mainly characterised by finely grained pyroxene and feldspar mineral grains. High vesicularity noted between 816-838 m with the vesicles being filled with green chlorite clays onto which grows epidote. Actinolite grows on top of epidote, which is deposited on top of quartz grains in vesicles in a paragenetic sequence. Basaltic intrusion fragments noted at 808-816 m. However, they form a small fraction of the rock fragments. Partial

losses noted at 810-814 m and 822-824 m. Alteration minerals: epidote, chlorite, illite, actinolite, calcite and sphene.

838-870 m Basalt. Light grey to dark grey medium grained crystalline rock sample. The groundmass is highly crystalline. It is aphyric, though a few fragments contain scarce pyroxene and feldspars phenocrysts. The rock is highly vesicular with vesicles being filled with alteration minerals in a paragenetic sequence (green clays-quartz-epidote-actinolite). Alteration minerals are in abundance. The rock is slightly altered to brown and green clays. Alteration minerals: calcite, quartz, epidote, sphene, actinolite, chlorite and prehnite (816 m).

870-914 m Basalt. Dark grey to green fine grained basaltic rock. The groundmass is characterised by abundant plagioclase and pyroxenes. Well-developed euhedral and elongated epidote crystals noted growing in vesicles. Some of the vesicles are noted filled with fine grained pale green clays and prehnite. Platy calcite noted. Brown clays noted between 904-908 m. Alteration minerals: epidote, calcite, sphene, prehnite, chlorite, clays, pyrite, quartz and wairakite.

914-926 m Tuff. Light green to brown fine grained rock sample. The groundmass is lithic in some fragments and glassy in others. Phenocrysts of pyroxene are noted in the groundmass. The groundmass is altering to green clays and epidote. A few pyrite cubes are noted in the fragments. The rock is chloritised making it appear green in colour. The rock is moderately altered to green chlorite clays. Sphene is noted in abundance. Alteration minerals: epidote, chlorite, calcite, pyrite, sphene and chalcopyrite.

926-940 m Rhyolite. White to light grey fine grained rock. The groundmass in some of the fragments has phenocrysts of quartz. Minute pyroxenes are discerned in the more felsic groundmass. The pyroxenes are altering to actinolite. The sample is slightly altered to green fine grained clays. Alteration minerals: chlorite and actinolite.

940-1016 m Trachyte Light grey fine grained rock sample. The groundmass is defined by minute pyroxene sparsely discerned in the felsic groundmass. The rock is slightly porphyritic with pyroxene phenocrysts. The rock has sphene, which is disseminated in the groundmass. The pyroxenes shows alteration to actinolite. The rock is slightly altered to green clays. Alteration minerals: chlorite, actinolite, illite and calcite.

1016-1024 m Trachyte. Browne fine grained highly altered rock. The rock is slightly porphyritic with pyroxene phenocrysts. The rock is fractured as indicated by veins, which are filled with black minerals. A few tuff fragments noted in this sample. Alteration minerals: clays and pyrite.

1024-1032 m Trachyte. White fine grained rock sample. The groundmass has minute pyroxenes discerned in it. The sample is slightly porphyritic with quartz phenocrysts being noted in the groundmass. The rock is slightly altered to green clays with the pyroxenes being the ones altering to green clays. Alteration minerals: pyrite and chlorite.

1032-1126 m Rhyolite. Pink to brown, fine grained and slightly to moderately porphyritic rock. The rock has pyroxene mineral grains discerned in the groundmass. The groundmass

is mainly characterised by feldspars. The rock has abundant pyrite and some chalcopyrite is also noted. It becomes more porphyritic and highly fractured at 1078 m (veins filled with mafic minerals noted at this depth downwards). Feldspar phenocrysts are noted to alter to light green fine grained clays. High alteration noted between 1114-1126 m with minute pyrite noted at this depth. Alteration minerals: pyrite, chlorite, traces of epidote, calcite and chalcopyrite.

1130-1146 m Trachyte. Light grey to grey fine grained phyric rock. The rock has pyroxene and sanidine mineral grain forming the groundmass. The mineral grains reveal a flow texture with this texture being highly pronounced between 1130-1136 m. The sample is slightly altered except at 1144-1146 m where high alteration is noted. There is abundant chalcopyrite at 1146 m. Minute pyrite is disseminated in the groundmass. The rock is slightly altered to brown clays and veins filled with green clays are noted. Alteration minerals: pyrite, chalcopyrite, traces of epidote and traces of chlorite.

1146-1150 m Trachyte. Light grey, fine grained relatively fresh trachyte. The rock has pyroxene mineral grains intergrown with feldspars. The rock is relatively fresh. Epidote observed altering from feldspars. Alteration minerals: epidote.

1150-1202 m Trachyte. Light grey to slightly brown fine grained slightly porphyritic trachyte. The rock is moderately to highly fractured at 1150-1154 m. At this depth, euhedral quartz and actinolite crystals are noted growing in fractures. The groundmass is mainly characterised by sanidine, while dissemination of pyroxene is in the groundmass. The rock is slightly altered to pale green chlorite clays. Epidote is noted to alter from sanidine. Alteration minerals: actinolite, quartz, pyrite, chlorite, clays and traces of epidote.

1202-1216 m Trachyte. Grey, fine grained rock sample. Slightly porphyritic with pyroxene phenocrysts. The groundmass is characterised by sanidine and pyroxene. Trachytic texture noted. The rock is slightly altered to clays. Alteration minerals: clays and pyrite.

1216-1226 m Trachyte. Brown, fine grained rock. The groundmass is mainly made of fine grained brown material in which feldspars can be seen altering to green clays and epidote. The rock shows moderate to high alteration to clays and epidote. The rock is fractured as observed by the presence of fracture planes. Fracture planes are characterised by euhedral secondary quartz crystals. Alteration minerals: epidote, chlorite, clays and quartz.

1226-1264 m Basaltic trachyandesite. Dark grey to pale green fine grained porphyritic rock. Phenocrysts of sanidine fill the groundmass. Oxidation has turned the sample pale green between 1226-1240 m. The rock has abundant crystalline epidote. The epidote is seen to grow in association with actinolite in most cases and in other instances it grows in association with euhedral quartz and wollastonite. Where found growing in association with wollastonite and actinolite, epidote is deposited first followed by wollastonite and then actinolite. Paragenetic sequence of dark green clays followed by pale green clays

noted. Abundant crystalline epidote noted. Alteration minerals: epidote, actinolite, wollastonite, quartz, chlorite, pyrite, sphene and wairakite (1236 m).

1264-1276 m Rhyolitic. Brown, fine grained moderately porphyritic rock. Phenocrysts are mainly quartz, feldspars and pyroxenes. The groundmass is highly altered to brown clays. Veins filled with epidote and chlorite observed. Quartz growing along fractured planes observed. A few rhyolite rock fragments noted. Alteration minerals: epidote, clays, quartz and chlorite.

1276-1288 m Basaltic trachyandesite. Dark grey to pale green fine grained porphyritic rock. Phenocrysts of sanidine fill the groundmass. The rock has abundant crystalline epidote. The epidote is seen to grow in association with actinolite in most cases and in other instances it grows in association with euhedral quartz and wollastonite. Alteration minerals: epidote, actinolite, quartz, chlorite and sphene.

1288-1290 m No sample (Loss of circulation returns)

1290-1296 m Trachyte. Light grey fine grained rock sample. It is slightly vesicular and slightly fractured with the vesicles /fracture planes being filled with pale green clays, epidote, actinolite and quartz minerals. Paragenetic sequence is noted with green clays being deposited, followed by epidote and actinolite. Abundant pyrite noted. The rock is slightly altered to white and green clays. Veins filled with pyrite noted. Epidote is noted being formed from alteration of feldspars and equally as a deposition mineral in the vesicles (crystalline epidote). Alteration minerals: quartz, epidote, actinolite, chlorite, and clays.

1296-1298 m No sample (Loss of circulation returns)

1298-1318 m Trachyte. Light grey to brown fine grained rock. Slightly porphyritic with pyroxene phenocrysts. The groundmass is mainly composed of fine grained feldspars and pyroxene mineral grains. The rock is moderately vesicular and fractured. Vesicles filled with chlorite-quartz-epidote-actinolite in that paragenetic sequence are noted. High alteration is noted at 1298-1304m with the groundmass forming brown clays. Veins filled with epidote are noted. Alteration minerals: quartz, epidote, actinolite, chlorite, clays and sphene.

1318-1346 m Trachyandesite. Heterogeneous mix of fine grained grey to dark grey trachyte and basalt rock fragments. The rock is slightly fractured. Fractures filled with chlorite, epidote, quartz, actinolite are noted. Actinolite is observed in abundance. Epidote is observed altering from feldspars as well as depositing in vesicles in crystalline form. Epidote veins also noted. High alteration noted at 1342-1346 m with formation of brown clays. Alteration minerals: quartz, chlorite, epidote, actinolite, wairakite (1332 m), clays and sphene.

1346-1356 m Trachytic tuff. Brown to green fine grained rock. The groundmass is mainly glassy. The rock is moderately to highly altered to green and brown clays. Fractures filled with crystalline epidote.

1356-1372 m Trachyte. Brown/light grey slightly porphyritic fine grained rock. Trachytic texture noted. Phenocrysts are mainly pyroxenes. Groundmass mainly composed of feldspars and or pyroxenes. The rock is slightly altered to brown/green clays. Few tuff and basalt fragments noted. Alteration minerals: epidote, quartz, chlorite, clays and sphene.

1372-1382 m Trachyandesite. Light grey to brown moderately grained highly crystalline and highly porphyritic rock. Phenocrysts of pyroxene are discerned in the groundmass in abundance. The groundmass is mainly composed of feldspars. Pyroxenes alter to actinolite. Actinolite also deposits in vesicles and fractures. The rock shows moderate alteration to brown and green clays. Crystalline epidote noted growing in fractures. Epidote grows in association with actinolite in a paragenetic sequence. Epidote also alters from feldspars. Alteration minerals: quartz, epidote, actinolite, chlorite and clays.

1382-1394 m Trachybasalt. Grey fine grained slightly porphyritic rock. Porphyries of feldspars are noted. The groundmass is dominated by fine grained pyroxene/feldspars with relatively higher abundance of pyroxene giving it the grey colour. Epidote alters from feldspars. The rock is slightly fractured. Crystalline epidote deposits in the fractures. Actinolite grows in association with epidote. The rock is slightly altered to pale green chlorite clays and brown clays. Alteration minerals: epidote, actinolite, quartz, chlorite and clays.

1294-1420 m No sample (Loss of circulation returns)

1420-1430 m Trachyte. Light grey, fine grained highly porphyritic rock. Phenocrysts are mainly pyroxene. Groundmass is feldspar rich giving the rock a more felsic colour. Crystalline epidote deposits in fractures. Feldspars alters to epidote. Pyroxene alters to actinolite. Actinolite is also noted depositing in fractures and vesicles. The rock is slightly altered to green clays. Veins filled with chlorite noted. Alteration minerals: epidote, actinolite, quartz, chlorite and clays.

1430-1450 m Trachybasalt. Grey, fine grained slightly porphyritic rock. Porphyries are mainly feldspars with a few pyroxenes. Groundmass mainly dominated by finely grained feldspar and pyroxene with relatively abundant pyroxenes giving it the grey colouration. Plenty of sphene observed in the groundmass. The rock is slightly altered to green clays. Alteration minerals: epidote, sphene, chlorite and quartz.

1450-1452 m. No sample (Loss of circulation returns)

1452-1466 m Basaltic trachyandesite. Pale green to dark grey fine grained porphyritic rock. The rock has been highly chloritised. Phenocrysts of pyroxene are observed in the groundmass. The rock is moderately altered to brown clays. The pyroxenes show alteration to green clays. Veins filled with epidote observed. Wairakite, quartz fill vesicles. Alteration minerals: epidote, quartz, wairakite, chlorite, clays and sphene.

1466-1476 m Trachybasalt. Grey, fine grained slightly porphyritic rock. Phenocrysts are mainly sanidine with a few pyroxenes. Groundmass mainly dominated by finely grained feldspar and pyroxene with relatively abundant pyroxenes giving it the grey colouration. Plenty of sphene observed in the groundmass. The rock is slightly altered to green clays. Alteration minerals: epidote, quartz, actinolite, sphene, chlorite and clays.

1476-1516 m Trachyte. Light grey, fine grained slightly porphyritic rock. Phenocrysts are mainly pyroxenes, which are abundantly distributed in the groundmass. The rock is massive and shows slight alteration. Minimal mineral deposits deposited. Crystalline epidote observed. Veins filled with chlorite noted. Groundmass alters to green clays. Alteration minerals: epidote, quartz, chlorite and clays.

1516-1520 m Trachyte. White to pale green, fine grained trachyte. It is aphyric. Minute pyroxenes are observed in the groundmass. Rock is slightly altered to green clays and moderately bleached. Alteration minerals: chlorite, epidote, clays and sphene.

1520-1538 m Trachytic dyke. Dark grey, fine grained rock. The basalt is relatively fresh with sphene distributed in the groundmass. Alteration minerals: *Sphene.*

1538-1542 m Trachyte. White to pale green fine grained rock sample. It is aphyric. Minute pyroxenes are observed in the groundmass. The rock is slightly vesicular with the vesicles filled with quartz crystals. Rock is slightly altered to green clays and moderately bleached. Alteration minerals: chlorite, epidote, quartz, clays and sphene.

1542-1566 m Trachyte. Light grey to brownish fine grained rock. It is aphyric. The rock is moderately altered to brown clays. Pyroxene is observed gradually altering to actinolite. Alteration minerals are less abundant. The rock is slightly bleached at 1154-1564 m giving it white colouration. Alteration minerals: epidote, actinolite, quartz and sphene.

1566-1612 m Trachyandesite. Light grey fine grained rock sample. It is moderately porphyritic with feldspar and pyroxene porphyries. Feldspar porphyries are noted altering to epidote. Euhedral crystalline epidote also noted depositing in fractures and vesicles. Pyroxene alters to actinolite. Actinolite also deposits in vesicles and fractures. Rock is slightly altered to brown clays. Some pyroxene shows gradual alteration through chlorite-actinolite. A paragenetic sequence noted with chlorite-epidote-actinolite (1590-1592 m). Alteration minerals: epidote, actinolite, chlorite, clays, pyrite and sphene.

1612-1754 m Trachyte. Light grey to brown fine grained sample. It is aphyric with minute pyroxene in feldspar rich groundmass. Pyroxene noted to alter to actinolite in some instances and depositing in fractures in other instances. The rock is highly fractured with euhedral quartz crystals precipitating along fracture planes. Abundant pyrite noted. Paragenetic sequence noted at 1620-1622 m and 1720-1722 m with actinolite growing on top of quartz. Feldspars alters to epidote. The rock is slightly to moderately altered to green and brown clays. High alteration noted at 1690-1692 m. Epidote veins noted at 1620-1622 m. Alteration minerals: pyrite, chlorite, quartz, epidote, actinolite, clays and sphene.

1754-1814 m Trachyte. Light grey fine grained highly porphyritic formation. Phenocrysts of feldspars and pyroxene noted. The rock is slightly vesicular with the vesicles being filled with euhedral quartz crystals. The rock is fractured with fracture planes filling with pyrite and green clays. The rock is slightly altered to green clays and epidote, but the sanidine are replaced partly by these minerals. Alteration minerals: epidote, chlorite, quartz, sphene, clays, chalcopyrite, actinolite and wairakite.

1814-1854 m Trachyte. Light grey to brown fine grained trachyte. It is slightly porphyritic with feldspar phenocrysts. It is highly fractured with abundant micro vein fillings with brown clays and green clays. Actinolite is relatively abundant and is noted to form from alteration of pyroxene as well as depositing in fractures. At 1838-1840 a paragenetic sequence is noted with actinolite growing on top of euhedral quartz crystals. Alteration minerals: epidote, chlorite, clays, quartz, actinolite, chalcopyrite, pyrite and sphene.

1854-1862 m Lithic tuff. Brown, fine grained lithic rock sample. Lithic fragments comprising of quartz, feldspars and pyroxene are embedded in the lithic groundmass. Alteration minerals: clays.

1862-1870 m Basalt. Pale green to dark grey fine grained sample. Rock is highly bleached giving it pale green colour. Groundmass is rich in pyroxene. Abundant actinolite and epidote, which are found growing in association with one another. It is highly altered to green clays. Sphene is in abundance. Alteration minerals: epidote, actinolite, chlorite, clays and quartz.

1870-1880 m Trachyte. Light grey, fine grained trachyte. It is aphyric with minute pyroxenes discerned in the feldspar dominated groundmass. Pyroxene alters to actinolite. The rock is slightly altered to brown clays. Alteration minerals: epidote, chlorite, actinolite, clays and quartz.

1880-1898 m Trachyte. Light grey, fine grained slightly porphyritic rock sample. Porphyries of feldspar and pyroxene noted. Pyroxenes show gradual alteration to actinolite. Paragenetic sequence noted with white clays depositing first followed by chlorite-epidote in a vesicle. The groundmass is moderately to highly altered to green and brown clays. Alteration minerals: epidote, chlorite, actinolite, clays, sphene, prehnite, wairakite and quartz.

1898-1922 m Basalt. Dark grey to greenish, fine grained and slightly porphyritic basalt with pyroxene phenocrysts. Abundant sphene noted. It is moderately to highly altered to green and brown clays. The rock is relatively bleached as from 1910-1922 m. Epidote is in abundance. Alteration minerals: epidote, chlorite, clays, sphene and quartz.

1922-1934 m Trachybasalt. Grey fine grained slightly porphyritic rock with phenocrysts of sanidine. Groundmass is dominated by finely grained pyroxene, sanidine and a few plagioclase. Pyroxene dominates the groundmass giving the rock texture that lies between basalt and trachyte. It is slightly altered to green clays. Alteration minerals: epidote, actinolite, quartz, chlorite and clays.

1934-1988 m Trachyte. Light grey, fine grained moderately porphyritic rock with phenocrysts of large feldspars and small pyroxenes. Groundmass is feldspar rich. Rock is slightly altered to green chlorite clays. The rock is vesicular with green clays, quartz and actinolite filling in the vesicles. Pyroxene alters to actinolite. Alteration minerals: pyrite, epidote, prehnite, actinolite, sphene, chlorite, clays, quartz and wairakite.

1988-2048 m Trachyte. Light grey fine grained slightly porphyritic rock. The groundmass is rich in feldspars in which finely grained pyroxenes are discerned. Porphyries are mainly feldspars. Actinolite occurs as an alteration product of pyroxene as well as a depositional mineral. Rock shows fracturing with epidote veins noted at 2002-2004m. Euhedral quartz noted in fractures. Rock is slightly altered to green and brown clays. Alteration minerals: epidote, quartz, actinolite, chlorite, pyrite and clays.

2048-2058 m Rhyolite. Pink, fine grained slightly porphyritic trachyte with feldspars and pyroxene. A few rhyolite fragments noted with quartz phenocrysts. The rock is slightly altered to brown clays. Alteration minerals: clays, epidote and chlorite.

2058-2062 m Basalt. Dark grey to greenish, fine grained slightly porphyritic rock with feldspar and pyroxene phenocrysts. Groundmass is rich in pyroxenes. Rock slightly altered to brown and green clays. Alteration minerals: chlorite, epidote and quartz.

2062-2086 m Trachyte. Light grey, fine grained slightly porphyritic rock. Phenocrysts are pyroxene, which are discerned in sanidine rich groundmass. The feldspar groundmass and porphyries are altering to epidote. Pyroxene alters to chlorite and actinolite. Vesicles filled with euhedral quartz noted.

2086-2102 m Trachyte. Light grey to brown, fine grained and slightly to moderately porphyritic rock with phenocrysts of feldspar. Groundmass is mainly feldspars with minute pyroxenes discerned in it. Pyroxenes are observed altering to actinolite and green chlorite clays. A few tuff fragments noted. Actinolite moderately abundant. Alteration minerals: actinolite, epidote, chlorite, quartz, clays.

2102-2108 m Trachyte. Light grey, fine grained aphyric trachyte. The groundmass is characterised by sanidine in which minute pyroxenes are discerned. The rock shows slight alteration to green chlorite and brown clays. Alteration minerals: chlorite, epidote and clays.

2108-2130 m Trachyte. Light grey to brownish grey, fine grained and slightly porphyritic trachyte. Groundmass is mainly feldspar rich with minute pyroxenes discerned in it. Pyroxene alters to actinolite and green chlorite clays. Paragenetic sequence noted at 2120-2122 m with actinolite growing on top of chlorite. Alteration minerals: actinolite, epidote, sphene, chlorite, quartz, clays and chalcopyrite.

2130-2138 m. No sample (Loss of circulation returns)

2138-2156 m Rhyolite. Light grey to grey, feldspar rich, fine grained and slightly porphyritic rhyolite. Pyroxene and quartz phenocrysts dominate. The grey fragments are few but more rich in pyroxenes. Pyroxenes are highly altered to green clays and actinolite. Actinolite deposits in fractures and veins. Actinolite is relatively abundant. Alteration minerals: actinolite, epidote and chlorite.

2156-2166 m Trachyte. Light grey, fine grained and slightly porphyritic trachyte with phenocrysts of feldspar and pyroxene dominating. Groundmass is characterised by feldspars within which minute pyroxenes are discerned. Pyroxene phenocrysts show gradual alteration to actinolite. Rock is slightly altered to green and brown clays. Alteration minerals: actinolite, epidote, chlorite, clays and quartz.

2166-2180 m Trachyte. Brown, fine grained moderately porphyritic rock. The rock is highly altered to brown clays. Phenocrysts are mainly feldspars. Alteration minerals: clays, epidote and quartz.

2180-2194 m Trachyte. Brownish to light grey, fine grained slightly to moderately porphyritic trachyte. Phenocrysts are mainly feldspars and pyroxene. Pyroxenes alter to actinolite and green clays. Rock is highly altered to brown and green clays. Alteration minerals: quartz, clays, epidote and actinolite.

2194-2196 m Trachyte. Pale green fine grained trachyte. The rock is highly chloritised. Remnants of trachytic texture noted in the chloritised fragments. Alteration minerals: chlorite, clays and quartz.

2196-2198 m Trachyte. Brown, fine grained heterogeneous sample. Sample has a mix of trachyte, tuff and rhyolite fragments. Trachytic fragments are in abundance. They reveal trachytic texture with pyroxene and sanidine mineral grains showing a flow orientation. Phenocrysts of quartz, pyroxene and feldspars noted. The groundmass is highly altered to brown clays. Alteration minerals: clays, actinolite and chlorite.

2198-2240 m Trachyte. Light grey, fine grained highly porphyritic trachyte with phenocrysts of feldspars. It is slightly vesicular with vesicles filled with quartz. It is moderately altered to green clays with pyroxenes altering to actinolite and green clays. Alteration minerals: actinolite, chlorite, epidote, quartz, clays and pyrite.

2240-2246 m Trachyte. Grey, fine grained aphyric trachyte. The groundmass has numerous minute pyroxenes in relative abundance. The rock is slightly altered. The rock is slightly altered to green clays. Alteration minerals: clays.

2246-2248 m Trachyte. Brown, fine grained slightly porphyritic rock with phenocrysts of sanidine. The groundmass is rich in feldspars in which minute pyroxenes are discerned in. The rock is highly altered to brown clays. Alteration minerals: clays, chlorite, actinolite and sphene.

2248-2290 m Trachyte. Light grey, fine grained rock with phenocrysts of feldspars and pyroxenes. Rock is slightly altered to brown clays. Alteration minerals: pyrite, epidote, sphene and prehnite.

2290-2296 m Basalt. Dark grey to green, fine grained slightly porphyritic basalt with abundance of pyroxene phenocrysts. Rock is slightly altered to green clays and epidote. Epidote observed in abundance as a deposition mineral. Alteration minerals: epidote, chlorite and quartz.

2296-2308 m Rhyolite. Pink to light grey, fine grained and highly porphyritic rhyolite with phenocrysts of quartz and pyroxenes. It is slightly to moderately porphyritic. Groundmass is rich in pink coloured feldspars. Rock is moderately altered to brown clays. Alteration minerals: pyrite, epidote, sphene and chlorite.

2308-2348 m Trachyte. Light grey, fine grained and moderately porphyritic trachyte with phenocrysts being mainly feldspars and pyroxene. Groundmass is mainly feldspathic. Pyroxene alters to actinolite, while feldspars alters to epidote. Relatively abundant pyrite and actinolite noted at 2332 m. Rock is relatively altered to brown clays. Quartz noted in vesicles. Paragenetic sequence noted (quartz-prehnite-actinolite). Alteration minerals: epidote, clays, actinolite, quartz, pyrite and prehnite.

2348-2370 m Trachyte. Grey fine grained aphyric trachyte with. Flow texture noted in the groundmass. Rock is vesicular in which occurs euhedral quartz crystals and prehnite. Veins filled with chlorite noted. It is moderately altered to chlorite. A few pyroxenes noted to alter to actinolite. Sphene is noted in the groundmass. Alteration minerals: sphene, epidote, actinolite, prehnite, chlorite, quartz and pyrite.

2370-2380 m Rhyolite. Pink, fine grained and slightly porphyritic rhyolite with phenocrysts of pyroxene and quartz. It is fractured with veins filled with chlorite. The rock is slightly altered to green clays with some pyroxenes noted to alter to green clays and actinolite. Alteration minerals: epidote, actinolite, pyrite and chlorite.

2380-2408 m Trachyte. Light grey, fine grained trachyte. Flow texture noted with pyroxene and sanidine mineral grains. The rock is moderately porphyritic with sanidine phenocrysts. The rock is fractured with micro veins filled with white clays, chlorite and mafic minerals. The rock is slightly altered to brownish clays. Alteration minerals: epidote, sphene, chlorite, pyrite, clays and actinolite.

2408-2430 m Trachyte. Pink, fine grained highly porphyritic trachyte with phenocrysts being mainly feldspars and pyroxene. Groundmass is mainly sanidine. Pyroxene alters to actinolite while feldspars alters to epidote. Rock is slightly altered to chlorite and brown clays. Quartz noted in vesicles. Paragenetic sequence noted (quartz-prehnite-actinolite). It is slightly fractured with micro veins filled with white clays and mafic minerals. Alteration minerals: epidote, chlorite and clays.

2430-2448 m Trachyte. Light grey, fine grained rock. Flow texture noted with pyroxene and sanidine mineral grains being oriented in one direction in a flow-like manner. The rock is moderately porphyritic with sanidine phenocrysts. The rock is fractured with micro veins

filled with chlorite clay mineral. The rock is slightly altered to chlorite and brown clays. Alteration minerals: epidote, actinolite, chlorite, quartz, clays and pyrite.

2448-2458 m Basalt. Pale green to greenish and dark grey, fine grained basalt. A few rhyolite and trachyte fragments noted. Fragments of a basaltic dyke are noted, which may have intruded in vicinity. The rock is highly chloritised to green clays. Alteration minerals: epidote, quartz, chlorite, pyrite and actinolite.

2458-2498 m Trachyte. Light grey, fine grained and moderately porphyritic trachyte with pyroxene and sanidine phenocrysts. Minute pyroxene discerned in the feldspar rich groundmass. Actinolite deposits in vugs and veins. Rock is slightly altered to brown clays. Alteration minerals: epidote, pyrite, actinolite, chlorite and quartz.

2498-2506 m Basaltic dyke. Dark grey to green, fine grained basalt. Moderately porphyritic with phenocrysts of pyroxene and feldspars. Abundant epidote (alteration mineral mainly from feldspars) noted. Rock is moderately altered to chlorite clays. Alteration minerals: epidote, chlorite, quartz and pyrite.

2506-2520 m Trachyte. Pale green to grey, fine grained and moderately to slightly porphyritic rock. The phenocrysts are mainly pyroxenes and feldspars. The rock is chloritised. It is moderately to highly altered to green clays. Alteration minerals: epidote, chlorite, pyrite, quartz and actinolite.

2520-2554 m Trachyte. Light grey, fine grained and slightly porphyritic trachyte. Phenocrysts are mainly feldspars and pyroxenes. The rock is slightly altered to green clays. Wairakite is noted. Alteration minerals: epidote, wairakite, chlorite and quartz.

2554-2572 m Syenitic intrusion. Whitish, fine grained and moderately porphyritic rock. Phenocrysts of pyroxene, feldspars and a few quartz are noted. Rock is slightly altered to green clays. Vesicles noted filled with euhedral quartz, wairakite and chlorite. Alteration minerals: epidote, wairakite and chlorite.

2572-2628 m Trachyte. Light grey to grey, fine grained moderately porphyritic with sanidine and pyroxene phenocrysts noted. Groundmass is mainly feldspar rich with minute pyroxenes discerned in it. Epidote noted as an alteration product of feldspar as well as deposited in vesicles and vugs in crystalline form. Quartz noted growing in fractures. Epidote veins noted. Rock is slightly altered to green clays. Alteration minerals: epidote, actinolite, wairakite, chlorite, pyrite and quartz.

2628-2648 m Trachyte. Light grey to pale green trachyte. Rock is moderately porphyritic with phenocrysts of pyroxene and feldspars. Rock is fractured with pyrite veins being noted. Epidote noted as alteration product of feldspars. Alteration minerals: epidote, actinolite, chlorite and pyrite.

2648-2710 m Trachyte. Ash white, fine grained trachyte. The groundmass is feldspar dominated with no phenocrysts. Minute pyroxenes are discerned in moderate abundance in the groundmass. The rock shows slight alteration to pale green clays. Alteration minerals: epidote, actinolite, chlorite, calcite and pyrite.

2710-2722 m Trachyte. White to pale green, fine grained aphyric trachyte. Specs of pyroxene noted in some of the fragments. Some of the fragments shows high bleaching and is highly altered to green clays. Alteration minerals: epidote and chlorite.

2722-2752 m Trachyte. White to light grey, fine grained aphyric trachyte with pyroxene phenocrysts. Groundmass is dominantly feldspar rich with minute pyroxenes, which tend to show flow texture in some of the fragments. The rock is slightly altered to green clays. Feldspars seen altering to epidote. Veins filled with chlorite noted. Alteration minerals: chlorite, pyrite, epidote and actinolite.

2752-2762 m Basalt. Dark grey to green, fine grained basalt. Groundmass is dominated by pyroxenes with plagioclase feldspars. The feldspars and pyroxenes are altered to chlorite. Rock is fractured with clays depositing on the planar fractured surface. Alteration minerals: epidote, chlorite and clays.

2762-2784 m Micro-granite. White, medium grained intrusion. It is porphyritic with phenocrysts of quartz and feldspars intergrown. The groundmass has moderate pyroxene mineral grains discerned in it. The groundmass is feldspar rich. The rock is relatively fresh. A few of the pyroxenes are noted to alter to green clays. Alteration minerals: chlorite, actinolite and epidote.

2784-2808 m Basalt. Dark grey to greenish, fine to medium grained basalt. The rock is aphyric. The groundmass is characterised by pyroxene and feldspars. It is slightly altered to sphene and chlorite. Alteration minerals: chlorite, sphene and epidote.

2808-2818 m Micro-granite. White, medium grained intrusion. It is porphyritic with phenocrysts of quartz and feldspars intergrown. The groundmass has moderate amounts of pyroxene mineral grains disseminated in it. The groundmass is feldspar rich. The rock is relatively fresh. A few of the pyroxenes are noted to alter to green clays. Alteration minerals: chlorite, actinolite and epidote.

2818-2842 m Trachyte. White to light grey, fine grained slightly porphyritic rock with phenocrysts of pyroxenes. Groundmass is characterised by sanidine mineral grains, which shows orientation flow texture. It is slightly altered to green clays. Pyroxene is noted altering to actinolite. Alteration minerals: chlorite and actinolite.

2842-2846 m Micro-granite. White, medium grained intrusion. It is porphyritic with phenocrysts of quartz and feldspars intergrown. The groundmass has moderate pyroxene mineral grains discerned in it. The groundmass is feldspar rich. The rock is relatively fresh. A few of the pyroxenes are noted to alter to green clays. Alteration minerals: chlorite and actinolite.

2846-2916 m Trachyte. Light grey to brownish grey, fine grained trachyte. It is highly porphyritic with sanidine and pyroxene phenocrysts dominating the groundmass. There is high level of pyrite deposition. The groundmass is feldspar rich. A few of the pyroxene alters to chlorite and actinolite. Alteration minerals: actinolite, chlorite, epidote, chalcopyrite, pyrite and garnets (2888-2890 m).

2916-2932 m Basalt. Pale green highly bleached basaltic rock. The groundmass has grains of feldspar and pyroxene, which have been bleached to pale green. Rock is slightly porphyritic and highly altered to pale green clays. Alteration minerals: chlorite and actinolite.

2932-2958 m Syenitic intrusion. White, medium grained highly porphyritic syenite. Phenocrysts are mainly sanidine and quartz with some pyroxenes. Rock is slightly altered to green clays. Alteration minerals: chlorite and actinolite.

2958-2990 m Micro-syenitic intrusion. White to light grey, medium grained and highly porphyritic syenite. Groundmass is rich in sanidine and a few quartz phenocrysts. The groundmass has fresh pyroxene mineral grains discerned in the feldspar rich groundmass. The rock is fresh with a few actinolite crystals noted as deposition mineral. Alteration minerals: actinolite.

AC: Detailed description of stratigraphy for well OW-917 as observed under binocular and petrographic microscope analysis.

0-10 m. Pyroclastics. Unconsolidated light grey to brown, fine grained heterogeneous mix of volcanic glass, obsidian, pumice and tuff fragments. It is oxidised to brown oxides. No hydrothermal alteration noted. Alteration minerals: oxides.

10-20 m. Pumice. Light grey, glassy textured and highly vesicular pumice. Some of the vesicles have brown oxides linings. Most of the vesicles are empty. Rock is moderately oxidised to brown oxides. No hydrothermal alteration noted. Alteration minerals: oxides.

20-40 m. Pyroclastics. Unconsolidated, light grey heterogeneous mixture of pumice, volcanic glass, rhyolite and obsidian fragments. The glassy groundmass in pumice is undergoing palagonisation forming palagonite. Rock is oxidised to brown oxides. No hydrothermal alteration noted. Alteration minerals: calcite, oxides and palagonite.

40-50 m. No sample (Loss of circulation returns).

50-84 m. Pyroclastics Unconsolidated light brown to yellow mixture of pumice, scoria, tuff, rhyolite and obsidian rock sample. Quartz mineral fragments are also noted. The rock is palagonised forming the yellow palagonite clays. Rock is slightly oxidised to brown clays. No hydrothermal alteration noted. Alteration minerals: calcite, oxides and palagonite.

84-108 m. Glassy tuff. White, highly glassy tuff. It is vesicular with some of vesicles being filled with phillipsite and scolecite zeolites. Quartz and feldspar grains are noted in the groundmass. Alteration minerals: zeolites (scolecite and phillipsite).

108-136 m. Rhyolite. White to pinkish, fine grained porphyritic rhyolite with quartz phenocrysts. It is relatively fresh and compact. Alteration minerals: No alteration mineral noted.

136-152 m. Rhyolite. Light grey, fine grained and highly porphyritic rhyolite with quartz phenocrysts dominating. Groundmass is feldspar rich with minute pyroxenes discerned in it. Banding (bands of feldspar and pyroxenes is noted in some grains. The rock is relatively fresh. Alteration minerals: No alteration minerals noted.

152-190 m. Rhyolite. Light brown, fine grained and highly porphyritic rhyolite with phenocrysts of quartz and sanidine. Slight oxidation to brown clays noted. Amphiboles are noted with some of them being coated with brown oxides. The rock is relatively fresh. Alteration minerals: zeolites (scolecite) and oxides.

190-234 m. Lithic? Tuff. Light brown to light grey, fine grained tuff. The groundmass is lithic with quartz and feldspar phenocrysts lithic fragments embedded in the lithic groundmass. The sample is moderately vesicular with vesicles being filled with scolecite and mesolite. The rock is slightly altered to green clays. Alteration minerals: Zeolites (scolecite, mesolite) and clays.

234-274 m. Rhyolite. Light brown to white, fine grained highly porphyritic rock with quartz and sanidine porphyries. Rock is relatively fresh and compact. It is slightly altered and oxidised to brown clays and brown oxides respectively. Alteration minerals: clays and oxides.

274-284 m. Tuff. Light brown to light grey, fine grained mixed rock composed of with rhyolite, volcanic glass and tuff fragments. The tuff fragments are in abundance. Scolecite is noted growing in vesicles, which characterise the tuff fragments. The rock is slightly altered to green and brown clays. Alteration minerals: zeolites (scolecite), clays and oxides.

284-288 m. Lithic tuff. Light brown, homogeneous fine grained lithic tuff. Groundmass is lithic with lithic fragments of quartz and pyroxenes embedded in it. Rock is slightly altered to brown clays. Alteration minerals: clays.

288-300 m. Tuff. Light grey to green, fine grained tuff. The groundmass is lithic with quartz, pyroxenes and sanidine lithic fragments noted. Rock is slightly altered to brown clays. Phillipsite noted deposited in the vesicles. Alteration minerals: zeolites (phillipsite) and clays.

300-424 m. Rhyolite. Light grey, fine grained felsic rhyolite. Rock is highly porphyritic with phenocrysts of quartz, sanidine and pyroxenes. The rhyolite has spherulitic texture with this texture being highly pronounced between 320-370 m. The spherulites are mainly made of pyroxene and sanidine mineral grains, which radiate from a central location. Pyrite noted between 410-424 m. The rock is relatively compact. Alteration minerals: clays, chalcedony and pyrite.

424-434 m Breccia. Grey to light grey, fine grained breccia. Slightly vesicular with clay infillings. Some grains exhibit ignimbritic texture with lenses of welded glass. The rock is slightly altered to brown clays. Alteration minerals: clays and pyrite.

434-444 m Tuff. Brown, fine grained highly vesicular tuff. Groundmass is lithic with minute feldspar lithic fragments noted. The glass crystal fragments are noted to alter to green clays. Alteration minerals: clays.

444-450 m Rhyolitic tuff. Light grey to pale green, fine grained rhyolitic tuff. Groundmass is lithic. Rock is slightly altered to green and brown clays. Alteration minerals: pyrite, calcite and clays.

480-486 m Tuff. Brown, fine grained tuff. Rock has a lithic-rich groundmass in which cubes of pyrite are embedded. Vesicles filled with quartz and green clays. Alteration minerals: quartz, clays, pyrite and calcite.

486-520 m Trachytic tuff. Light grey to pale green, fine grained tuff. Rock has lithic groundmass with sanidine lithic fragments noted. Cubes of pyrite are noted embedded in the groundmass. Rock is slightly altered to green clays. Alteration minerals: pyrite, clays, quartz and calcite.

520-536 m Trachyte. Light grey fine grained aphyric trachyte. Groundmass is mainly feldspar rich with minute pyroxene fragments discerned. It is slightly altered to green clays. Alteration minerals: pyrite, calcite (dogs tooth calcite at 526-528 m), clays and zeolites (laumontite).

536-564 m Trachyte. Grey, fine grained rock. It has pyroxene mineral grains forming approximately 30% of the groundmass. The rock is dense and massive. Rock is slightly altered to green clays. Fragments with euhedral vesicles and pyroxenes noted at 562-564 m. The fragments at this depth are highly felsic with elongated pyroxene crystalline crystals. Alteration minerals: calcite, clays, zeolites (laumontite, phillipsite).

564-574 m Scoria. Grey, fine grained highly vesicular rock fragments. The vesicles are filled by phillipsite zeolites. Platy calcite noted. Cubes of pyrite noted embedded in the matrix. Rock is slightly to moderately altered to brown clays. Alteration minerals: pyrite, calcite, clays and zeolites (phillipsite).

574-588 m Tuff. Grey fine grained highly vesicular tuff. Vesicles are filled with calcite, numerous quartz, clays and zeolites. Lithic ash cement fragments of trachyte and rhyolite. Rock is moderately altered to brown clays. Alteration minerals: quartz, pyrite, calcite, clays oxide and zeolites (mesolite and phillipsite).

588-598 m Trachyte. Light grey to green, fine grained trachyte. The rock is feldspar rich and has numerous pyroxenes discerned in the groundmass. Trachytic texture noted. Rock is slightly altered to green clays. Alteration minerals: calcite, clays and pyrite.

598-608 m Tuff. Light grey to brown fine grained tuff. The light grey fragments have rounded feldspar fragments cemented with the lithic fragments. The brown fragments are all lithic. The rock is slightly altered to brown clays. A few trachytic fragments are noted. Alteration minerals: oxides, pyrite, clays and calcite.

608-632 m Trachyte. Light grey to dark grey, fine grained trachyte. Rock is highly felsic with groundmass being dominantly feldspar in which a few pyroxene mineral grains are embedded. The pyroxene ranges from minute size to medium grained. Rock is vesicular between 608-614 m. The vesicles are filled with quartz and clays. Slight oxidation noted at 608-624 m. The rock is generally slightly altered to green clays. Alteration minerals: pyrite, quartz, calcite and clays.

632-646 m Trachyte. Dark grey, fine grained trachyte. The rock has feldspar rich groundmass into which are embedded medium grained pyroxenes. Rock is slightly altered to green clays. Alteration minerals: calcite and clays.

646-676 m Trachyte. Light grey to greenish, fine grained and slightly to moderately porphyritic trachyte. Groundmass is feldspar rich with pyroxene and minor sanidine phenocrysts sparsely discerned in the groundmass. The rock is slightly altered to green clays. Rock is moderately chloritised giving it the green colour. It is slightly altered to green fine grained clays. Mineral banding is observed. Alteration minerals: clays, calcite and pyrite.

676-684 m Tuff. Brown, fine grained tuff. The rock is lithic and the rock is moderately vesicular. The vesicles are filled with numerous small euhedral quartz mineral grains. Rock is slightly altered to brown clays. A few blue cryptocrystalline tuff fragments also noted. Alteration minerals: pyrite, clays, calcite and quartz.

684-706 m Trachyte. Light grey, fine grained aphyric trachyte. The rock is massive. It is slightly vesicular with vesicles filled with quartz mineral grains. It is slightly altered to greenish clays and has moderately abundant calcite. Alteration minerals: pyrite, quartz, calcite and clays.

706-716 m Trachyte. Light grey, medium grained feldspar rich lava. It is moderately porphyritic with phenocrysts of sanidine. Minor pyrite is disseminated in the groundmass. Veins filled with calcite noted. Alteration minerals: calcite, pyrite and clays.

716-732 m Tuff. Grey, cryptocrystalline tuff. The rock shows flow texture indicating the dynamic changes that happened during eruption. It is fractured and veins filled with calcite, quartz and clays are noted. Vesicles filled with clays are also noted. Rock is moderately to highly altered to greenish clays. Alteration minerals: clays, pyrite and quartz.

732-848 m Trachyte. Grey, fine grained slightly to moderately porphyritic trachyte. Porphyries of sanidine noted. Pyrite is discerned in the groundmass. The groundmass is altered to calcite with some of the calcite depositing in vesicles in the few fragments that have vesicles. Rock is highly altered at 732-740 m with a few tuff fragments noted here. Rock is relatively oxidised. Quartz noted in vesicles at 732-740 m. The rock is massive. Alteration minerals: pyrite, calcite, clays and quartz.

848-884 m Crystalline tuff. Brown, fine grained tuff. The groundmass is lithic with minute lithic fragments of feldspar and pyroxene embedded. The rock is slightly vesicular and the vesicles are filled with clays and pyrite. Pyrite is noted discerned in the groundmass as well. Alteration minerals: pyrite, clays and calcite.

884-890 No sample (Loss of circulation returns)

890-916 m Trachyte. Light grey, cryptocrystalline to fine grained rock. The rock is slightly vesicular with clays filling the vesicle linings. Groundmass is lithic with minute pyroxene fragments dispersed in the groundmass. The groundmass is altered to green clays. Formation is moderately altered to green clays. Alteration minerals: chlorite, calcite, pyrite, clays, sphene and wollastonite at 898-900 m.

916-922 m No sample (Loss of circulation returns)

922-962 m Trachyte. Light grey, cryptocrystalline to fine grained rock. Groundmass is lithic with a few fragments of pyroxene. Slightly vesicular with vesicles filled with pyrite. Rock moderately altered to green clays. Calcite is moderately abundant and platy calcite is also noted. Formation is slightly oxidised at 944-962 m. Alteration minerals: pyrite, calcite, chlorite, sphene and illite.

962-974 m Rhyolite. Pink and green, fine grained rhyolite with quartz phenocrysts in the moderately porphyritic groundmass. The rock is moderately bleached to green clays. The rock is vesicular with the vesicles being filled with secondary quartz, clays and pyrite. Rock is moderately altered to green clays. Alteration minerals: quartz, chlorite, clays, calcite and pyrite.

974-1028 m Rhyolite. Brown to pink, fine grained aphyric to slightly porphyritic rock with feldspar porphyries and quartz porphyries in other instances. It is moderately altered to brown clays. Rock is slightly vesicular with vesicles being filled with pyrite, quartz and clays. Mineral banding noted with feldspars banding with pyroxene layers. Alteration minerals: calcite, chlorite and clays.

1028-1054 m Trachyte. Light brown with some green-grey colour and fine grained trachyte. It is slightly vesicular with clays linings on the vesicles. Some of the fragments

are highly oxidised while others are fresh. Alteration minerals: pyrite, calcite, clays and chlorite.

1054-1088 m Trachyte. Fine grained slightly porphyritic rock with phenocrysts of feldspar noted. Flow texture noted with elongate sanidine and pyroxene mineral grains. The feldspar shows alteration to green clays. Pyrite discerned in the groundmass. Alteration minerals: clays, chlorite, pyrite and calcite.

1088-1094 m Trachyte. Grey medium grained, heterogeneous, feldspar rich and slightly porphyritic trachyte with sanidine phenocrysts. Flow texture is distinct with elongate sanidine phenocrysts, which are beginning to alter to green clays. Formation is massive. Alteration minerals: pyrite, calcite, chlorite, illite and chalcopyrite.

1094-1108 m Trachyte. Light grey, fine grained trachyte. Rock is feldspar rich with medium grained pyroxenes disseminated in the groundmass. Rock is relatively fresh. Alteration minerals: calcite, pyrite and chalcopyrite.

1108-1124 m Rhyolite. Brown grey fine grained slightly porphyritic trachyte with sanidine and quartz phenocrysts. Some of the fragments are aphyric. Rock is slightly vesicular with calcite linings and quartz crystals. Minute pyroxenes discerned in abundance in the groundmass. Rock is slightly altered to green and brown clays. Rock is compact. Alteration minerals: pyrite, calcite (platy), clays and quartz.

1124-1232 m Rhyolite. Pink and brown, fine grained, highly porphyritic rock. Phenocrysts of feldspar, quartz and pyroxene are noted. Slight alteration to green clays noted. Rock is rich in feldspars. Alteration minerals: pyrite, calcite, clays, chlorite and epidote colouration noted at 1194-1196 m and 1218-1220 m.

1232-1292 m Rhyolite. Grey brown, fine grained and slightly porphyritic rhyolite with porphyries of sanidine in the groundmass. Minor medium sized quartz phenocrysts also noted. Vesicles linings characterised by calcite and green clays. Groundmass alters to calcite. Rock is moderately oxidised giving it the brown colour appearance. The rock is slightly altered to green clays. Pyrite is sparsely discerned in the groundmass. Platy calcite noted. Alteration minerals: pyrite, calcite, chlorite, epidote colouration at 1236-1240 m, clays, chalcopyrite and chalcedony.

1292-1300 m No sample (Loss of circulation returns)

1300-1364 m Trachyte. Light grey, fine grained heterogeneous mixture of trachyte, rhyolite and tuff fragments. Trachyte rock fragments are in abundance. The fragments are vesicular with vesicles being filled with euhedral quartz. The rock is highly fractured with abundant pyrite filling fracture planes. Calcite fills vesicles and micro veins and is in abundance. High chloritisation noted at 1358-1360 m. Epidote noted at 1328-1330 m. Alteration minerals: epidote, chlorite, calcite, pyrite, chalcopyrite, sphene, clays and quartz.

1364-1462 m Trachyte. Pink to light grey, fine grained slightly porphyritic rock. The rock is slightly porphyritic and highly porous with vesicles and vugs filling with fine grained

pale green clays. Vesicles are also filled with euhedral secondary quartz. Veins filled with dark green clays noted. Platy calcite noted at 14410-1412m and 1438-1440m. The rock is slightly altered to brown and green clays. Alteration minerals: pyrite, calcite, sphene, chlorite, chalcopyrite and clays.

1462-1488 m Trachyte. Light grey, fine to medium grained, slightly porphyritic trachyte. It is porous with the vesicles and vugs filling with green clays and calcite. The rock is slightly oxidised. The rock is moderately altered to brown and green clays. Abundant calcite noted. High alteration noted at 1486-1488m. Alteration minerals: pyrite, calcite, clays, sphene, chalcopyrite and quartz.

1488-1492 m Trachyte (intrusion). Light grey, cryptocrystalline aphyric rock. Chilled margins of an intrusion are observed. Distinct flow textures and striations are noted indicating lava flow. Green clays are noted replacing feldspars. The rock is slightly altered to fine grained green clays. Alteration minerals: clays.

1492-1514 m Trachyte. Light grey, fine grained slightly porphyritic rock with sanidine phenocrysts embedded in the groundmass. The rock is highly fractured and moderately to highly oxidised. Rock is vesicular with vesicles being filled with coarse grained and fine grained green clays and calcite. Groundmass also alters to calcite. The rock is moderately altered to green and brown clays. Alteration minerals: pyrite, quartz, calcite, sphene, chlorite and clays.

1514-1552 m Trachyte. Light grey to greenish, fine grained and slightly porphyritic rock sample. The rock is highly fractured with the micro veins being filled with quartz, calcite and chlorite. Vesicles are filled with coarse grained green clays and calcite. Formation is moderately altered to green clays. Epidote colouration noted at 1544-1546 m. Alteration minerals: quartz, sphene, calcite, pyrite, chlorite, clays and epidote.

1552-1660 m Trachyte. Brown, light grey to pale green trachyte. The formation exhibit a variety of trachyte textures. It is slightly vesicular with the vesicles being filled with calcite and green clays. Some of the fragments are highly felsic with minute pyroxene sparsely discerned in the groundmass while others have pyroxene embedded in the feldspar rich groundmass. The formation is slightly to moderately altered to green clays. Alteration minerals: chlorite, calcite, pyrite, clays and sphene.

1660-1688 m Trachyte. White to pale green, fine grained and poorly porphyritic rock. The rock is highly fractured with the micro veins being filled with quartz, pyrite, calcite and green clays. Pyrite cubes are also noted embedded in the groundmass in abundance. Calcite fills vugs in abundance. Alteration minerals: pyrite, quartz, calcite, chlorite and sphene.

1688-1762 m Trachyte. Grey to brown, fine grained weakly porphyritic trachyte. Some of the fragments show flow banding while others are brown, slightly porous with coarse and fine grained green clays and calcite infillings. Formation is slightly fractured with pyrite, chalcopyrite and green clays filling in the vesicles. The rock is moderately chloritised to green clays and slightly altered to brown clays. Alteration minerals: pyrite, quartz, chlorite and sphene.

1762-1864 m Trachyte. Heterogeneous mixture of trachyte with various texture and ranging from grey, dark grey, light grey to pale green in colour. The dark grey fragments are mainly basaltic and are mainly found between 1800-1824 m forming approximately 20% of the sample. This indicates there is a thin basaltic unit in between the trachytes. The trachyte is highly vesicular with the vesicles being filled with quartz, coarse grained and fine grained chlorite clays. The rock is slightly fractured with micro veins being filled with pyrite and chlorite clays. The rock is moderately to highly altered to green and brown clays. Alteration minerals: clays, chlorite, pyrite, calcite (platy at 1792-1794 m), sphene and quartz.

1864-1868 m *Trachyte.* Light grey to pale green, fine grained and weakly porphyritic trachyte. Groundmass is feldspathic with specs of pyroxene, which occur in a flow textured pattern. The rock is slightly vesicular with the vesicles being filled with calcite. Calcite is observed to deposit in association with wairakite at 1686-1688m. The rock is slightly altered to green chlorite clays. Alteration minerals: calcite, pyrite, chlorite and wairakite.

1868-1872 m Basalt. Light grey to dark grey and green grey basalt. The rock is slightly to moderately altered to green clays. Alteration minerals: Epidote, calcite, sphene and quartz

1872-1880 m Trachyte. Light grey to pale green, fine grained and weakly porphyritic trachyte. Groundmass is feldspathic with specs of pyroxene, which have a trachytic flow texture. The rock is slightly vesicular with the vesicles being filled with calcite. The rock is slightly altered to green chlorite clays. Alteration minerals: sphene, calcite and chlorite.

1880-1890 m No sample (Loss of circulation returns)

1890-1894 m Trachyte. Pale green, fine grained aphyric rock formation. It is vesicular with vesicles being filled with calcite. Rock is highly chloritised to green chlorite clays. Alteration minerals: traces of epidote at 1890-1892 m, calcite, pyrite and chlorite.

1894-1916 m No sample (Loss of circulation returns).

1916-1992 m Trachyte. Light grey to pale green, fine grained and weakly porphyritic trachyte. The rock is rich in feldspars with specs of pyroxene embedded in the feldspar rich groundmass. The rock is weakly vesicular with vesicles filling with calcite and green clays. The rock is slightly to moderately altered to brown and green clays. Pyrite cubes noted. Quartz noted filling in vesicles. From 1960-1992 m, the rock is highly fractured with high alteration to brown clays being noted. Alteration minerals: quartz, calcite, pyrite, clays, chlorite and sphene.

1992-2004 m Basaltic dyke. Dark grey to green, fine grained aphyric basalt. It is slightly fractured and vesicles filled with green clays and calcite. Alteration minerals: calcite and clays.

2004-2024 m No sample (Loss of circulation returns).

2024-2058 m Trachyte. Light grey to pale green, fine grained aphyric trachyte. The rock has groundmass rich in feldspar with specs of pyroxenes. Groundmass is moderately to

highly bleached with formation of green clays. The rock is slightly vesicular with the vesicles filled calcite and quartz. The rock is slightly fractured with the veins filled with chlorite clays. Epidote is noted to alter from feldspars. Alteration minerals: epidote, calcite, chlorite, sphene and pyrite.

2058-2064 m No sample (Loss of circulation returns)

2064-2084 Trachyte. Light grey to pale green, fine grained aphyric trachyte. The rock has groundmass rich in feldspar with specs of pyroxenes. Groundmass is moderately to highly bleached with formation of green clays. The rock is slightly vesicular with the vesicles filled calcite and quartz. Calcite is noted in abundance with micro veins being filled with calcite and green clays. Epidote is noted to alter from feldspars. Alteration minerals: epidote, calcite, chlorite, sphene and pyrite.

2084-2088 m. No sample (Loss of circulation returns).

2088-2140 m Trachyte. Light grey to pale green, fine grained aphyric trachyte. The rock has groundmass rich in feldspar with specs of pyroxenes. Groundmass is moderately to highly bleached with formation of pale green clays. The rock is slightly vesicular with the vesicles filled with calcite and quartz. The rock is slightly fractured with the veins filled with chlorite clays. Alteration minerals: epidote, calcite, chlorite, sphene and pyrite.

2140-2146 m No sample (Loss of circulation returns)

2146-2164 m Trachyte. Light grey to pale green, fine grained aphyric trachyte. The rock has groundmass rich in feldspar with specs of pyroxenes. Groundmass is moderately to highly bleached with formation of green clays. The rock is slightly vesicular with the vesicles filled calcite and quartz. The rock is slightly fractured with the veins filled with chlorite clays. Alteration minerals: epidote, calcite, chlorite, sphene and pyrite.

2164-2172 m No sample (Loss of circulation returns)

2172-2200 m Trachyte. Light grey to pale green fine grained aphyric trachyte. The rock has groundmass rich in feldspar with specs of pyroxenes. Groundmass is moderately to highly bleached with formation of green clays. The rock is slightly vesicular with the vesicles filled calcite and quartz. The rock is slightly fractured with the veins filled with chlorite clays. Epidote is noted to alter from feldspars. Alteration minerals: epidote, calcite, chlorite, sphene and pyrite.

2200-2216 m Trachyandesite. Green to dark grey, fine to medium grained aphyric trachyandesite. Groundmass is rich in plagioclase and pyroxene. The rock is slightly altered to green clays. Alteration minerals: calcite, epidote, sphene and chlorite.

2216-2238 m Trachyte. Light brown to pale green with occasional light grey, fine grained aphyric trachyte. The rock is vesicular with the vesicles being filled with green clays. It is moderately fractured with the fractures being filled with numerous euhedral quartz crystals. Micro veins filled with pyrite and calcite are noted. Alteration minerals: clays, chlorite, pyrite, calcite, sphene and quartz.

2238-2262 m Trachyte. Pale green to light brown aphyric trachyte. The groundmass is rich in feldspars and is highly chloritised. Specs of pyroxene are discerned in the groundmass. The rock is porous with vesicles and vugs being filled with green clays and calcite. Pyrite is also noted. Quartz is seen growing along fracture planes, in vugs and vesicles. Alteration minerals: epidote at 2246-2248 m, calcite, quartz, chlorite, pyrite and sphene.

2262-2274 m Trachyte. Light brown to light green, fine grained trachyte. The lava exhibit various trachytic textures. The rock is highly porous and fractured with the vugs and veins being filled with green clays and calcite. Quartz also noted growing along fracture planes. Alteration minerals: pyrite, clays, chlorite and calcite.

2274-2320 m Trachyte. Grey, fine grained, aphyric trachyte. The rock is relatively compact. Calcite is abundant and mainly within the groundmass. The rock is slightly altered to green clays. Alteration minerals: calcite, clays and pyrite.

2320-2324 m Trachyte. Light grey to pale green, fine grained, aphyric trachyte with occasional cryptocrystalline fragments. The rock is fractured and pyrite is noted filling in veins. The rock is moderately altered to green clays. Alteration minerals: calcite, sphene, clays and pyrite.

2324-2336 m Trachyte. Light grey to brown, fine grained aphyric trachyte. The rock has vugs and vesicles filled with green clays and calcite. The rock is moderately oxidised. Chalcopyrite also noted filling the vesicles. Alteration minerals: calcite, sphene, pyrite, clays, chlorite, chalcopyrite and wairakite at 2330-2332 m.

2336-2340 m No sample Loss of circulation returns).

2340-2344 Syenitic intrusion. White, medium grained feldspar rich syenite. The groundmass is characterised by medium grained quartz and feldspar mineral grains with quartz forming approximately 5% of the groundmass. A few trachyte fragments noted. Alteration minerals: chlorite, calcite, pyrite, sphene and clays.

2344-2402 m Trachyte. Light grey to brown, fine grained aphyric trachyte. The sample is slightly vesicular and slightly fractured. Quartz, chalcopyrite and pyrite grow along the fracture planes. Vesicles filled with brown and green clays noted. Calcite is abundant in the groundmass, in vugs and vesicles. A few pale green fragments are also noted. Slight oxidation noted at 2360-2364 m. Alteration minerals: quartz, calcite, pyrite, clays, epidote colouration at 2362-2364 m, and chalcopyrite.

2402-2406 m Trachyte. Grey, fine grained aphyric trachyte. Vugs and vesicles are filled with chlorite clays, quartz and calcite. The rock is slightly altered to green clays. Alteration minerals: calcite, chlorite, pyrite, clays and sphene.

2406-2428 m Trachyte. Light grey to brown, fine grained aphyric trachyte. The sample is slightly vesicular and slightly fractured. Quartz, chalcopyrite and pyrite grow along the fracture planes. Vesicles filled with brown and green clays noted. Calcite is abundant in the groundmass, in vugs and vesicles. Alteration minerals: quartz, calcite, sphene, pyrite and clays.

2428-2506 m Trachyte. Grey to light grey, fine grained weakly porphyritic trachyte. It is moderately to highly fractured with euhedral quartz grains filling the fracture planes. It is slightly vesicular with vesicles and vugs filled with green chlorite clays, calcite and mafic minerals. Epidote colouration is noted at 2438-2440 m, 2458-64 m. Veins filled with quartz are noted between 2500-2502 m and 2506-2508 m. The formation shows slight intensity of alteration to green clays. Partial losses noted between 2442-2446 m and 2450-2452 m. Alteration minerals: epidote, sphene, chlorite, sphene and quartz.

2506-2520 m Trachyte. Light grey, fine grained and slightly porphyritic trachyte. Groundmass is rich in feldspars with pyroxenes dispersed in a random manner in the groundmass. Phenocrysts of sanidine are noted. The formation is slightly altered to brown clays. Veins filled with quartz are noted. Alteration minerals: quartz, pyrite, calcite and clays.

2520-2594 m Trachyte. Grey, fine grained and weakly porphyritic trachyte. The rock is slightly fractured with the fractures being filled with euhedral quartz. The rock is slightly altered to brown clays. Epidote noted at 2556-2558 m. Alteration minerals: calcite, epidote, pyrite and clays.

2594-2600 m Trachyte. White to grey and occasional pale green, fine grained, aphyric trachyte. The rock exhibits trachytic texture. The rock is bleached forming pale green clays. It is moderately altered to green clays. Alteration minerals: chlorite, pyrite, clays and epidote.

2600-2610 m Trachyte. Grey, fine grained trachyte. It is slightly oxidised. The rock is slightly altered to brown clays. Alteration minerals: clays, calcite and pyrite.

2610-2618 m Syenitic intrusion. White, medium grained feldspar rich syenite. The groundmass is characterised by medium grained quartz and feldspar mineral grains with quartz forming approximately 5% of the groundmass. A few trachyte fragments noted. Alteration minerals: chlorite, calcite, pyrite, sphene and clays.

2618-2670 m Trachyte. Light grey, fine grained and weakly porphyritic trachyte. The unit is slightly fractured with the fracture planes being filled with quartz. It is slightly vesicular with green clays and calcite filling the vesicles. The rock is slightly altered to green clays. Epidote colouration noted at 2630-2632 m. Alteration minerals: platy calcite at 2662-2664 m, pyrite, chlorite, clays, sphene and sphene.

2670-2682 m Trachyte. White grey, fine grained, aphyric rock trachyte. The rock is highly felsic with minute pyroxene discerned in the groundmass. The rock is moderately vesicular with vesicles filled with coarse grained green clays, quartz and calcite. The rock is slightly to moderately altered to green clays. Alteration minerals: platy calcite at 2678-2680 m, sphene, chlorite and pyrite.

2682-2690 m Trachyte. Light grey, weakly porphyritic fine grained trachyte. Rock shows trachytic texture in some of the fragments. The formation is slightly altered to brown clays. Alteration minerals: calcite, clays and pyrite.

2690-2708 m Trachyte. Grey, fine grained aphyric trachyte. It is slightly vesicular with calcite filling in vesicles and veinlets. The formation is slightly altered to green clays. Alteration minerals: calcite, sphene, pyrite and clays.

2708-2738 m Trachyte. White to light grey, fine grained moderately porphyritic trachyte with feldspar rich groundmass in which are embedded sanidine phenocrysts. Specs of pyroxene are noted in the groundmass. The sample is relatively fresh with slight alteration to green clays. The rock is slightly fractured with micro veins, which are filled with green clays and calcite. Alteration minerals: calcite and clays.

2738-2748 m No sample (Loss of circulation returns).

2748-2773 Trachyte. Light grey, fine grained aphyric trachyte. The rock is moderately vesicular and moderately fractured. Vesicles are filled with green clays and red brown oxides. Veins filled with green clays are noted. The formation is moderately altered to brown clays. Alteration minerals: pyrite, calcite, chlorite and clays.

2772-2832 m Trachyte. Light grey, fine grained and slightly to moderately porphyritic trachyte. The rock is slightly fractured. Vesicles and vugs are filled with coarse grained green clays and calcite. Veins are filled with clays. It is slightly altered to green clays. Feldspars are noted altering to epidote at 2804-2808 m. Partial losses noted at 2828-2842 m. Alteration minerals: pyrite, epidote, calcite, chlorite, clays and sphene.

2832-2864 m Trachyte. Grey, fine grained aphyric trachyte. The formation is relatively fresh with minimal clay and calcite deposition. It is slightly fractured with veins being filled with brown and green clays. Alteration minerals: calcite, clays and pyrite.

2864-2914 m Trachyte. Light grey, fine grained slightly porphyritic trachyte. Sanidine phenocrysts are noted. The rock is feldspar rich and relatively fresh. Green clays are noted as products of feldspar alteration. Slight oxidation noted. Alteration minerals: clays, pyrite and calcite.

2914-2938 m Syenitic intrusion. White, medium grained feldspar rich syenite. Medium grained quartz grains noted sparsely disseminated in medium grained sanidine dominated matrix. The rock is relatively fresh. Specs of pyroxenes are noted sparsely discerned in the groundmass. Alteration minerals: clays, calcite and pyrite.

2938-2962 m Trachyte. Light grey, fine grained, aphyric to weakly porphyritic trachyte. The rock has specs of pyroxenes dispersed in the feldspar rich groundmass. The rock is

relatively fresh with slight alteration to green clays being noted. Alteration minerals: chlorite, clays, calcite and pyrite.

2962-2966 m Basaltic dyke. Dark grey, cryptocrystalline and slightly porphyritic rock fragments. Porphyries of pyroxenes noted. The formation is highly fractured with quartz veins being noted. The rock is relatively fresh. Alteration minerals: clays, quartz and epidote at 2962-2964 m.

2966-2982 Trachyte. Light grey, fine grained, aphyric to weakly porphyritic massive trachyte. The rock is feldspar rich with pyroxene mineral grains discerned in the feldspar rich groundmass. The formation is slightly altered to green clays. Alteration minerals: calcite, clays and pyrite.

2982-2990 m Basaltic dyke. Dark grey, cryptocrystalline and slightly porphyritic basaltic dyke. Porphyries of pyroxenes noted. The formation is highly fractured with quartz veins being noted. The rock is relatively fresh. Alteration minerals: clays

AD: XRD analysis for clay minerals from OW-905A

OW-905A CLAY ANALYSIS APPENDIX

(m)	d(001) A	d(001) G	d(001) H	d(002)	Mineral	Type	Other minerals
332-334	14.66	18.04	10.51		Smectite	Sm.	Feldspars
352-354	14.59	18.26	10.47		Smectite	Sm.	Feldspars
372-374	13.51	18.9	10.44		Smectite	Sm.	Feldspars
392-394	13.51	18.9	10.44		Smectite	Sm.	Feldspars
412-414	13.51	18.4	10.44		Smectite	Sm.	Feldspars, Amphiboles
432-434	13.51	18.4	10.44		Smectite	Sm.	Feldspars, Amphiboles
472-474	12.93	17.76	10.44		Smectite	Sm.	Feldspars, Amphiboles
492-494	12.93	17.76	10.44		Smectite	Sm.	Feldspars, Amphiboles
512-514	12.93	17.76	12.93		Smectite	Sm.	Feldspars, Amphiboles
572-574	15.35	17.45	10.44		Smectite	Sm.	Feldspars
612-614	14.68	17.45	10.5		Smectite	Sm.	Feldspars
652-654	16.03	17.93	10.4		Smectite	Sm.	
672-674	15.73, 10.40	15.73, 10.40	15.73, 10.40	7.31, HIT=0	Chlorite + Illite	Chl: ill	
692-694	No clear peaks	No clear peaks	No clear peaks	No clear peaks	No clear peaks	No clear peaks	
712-714	No clear peaks	No clear peaks	No clear peaks	No clear peaks	No clear peaks	No clear peaks	
732-734	14.85, 10.29	14.85, 10.29	14.85, 10.29	7.21, HIT=0	Chlorite + Illite	Chl: ill	
752-754	14.85, 10.29	14.85, 10.29	14.85, 10.29	7.31, HIT=0	Chlorite + Illite	Chl: ill	
772-774	14.78, 10.41	14.78, 10.41	14.78, 10.41	7.26, HIT=0	Chlorite + Illite	Chl: ill	
812-814	15.35	18.11	10.27		Smectite (traces)	Sm.	
852-854	16.26	17.65	10.33		Smectite	Sm.	
872-874	12.91	17.55	10.09	7.24, HIT=0	Chlorite +	Chl:sm	
892-894	15.46	17.79	10.28	7.28, HIT=0	Chlorite +	Chl:sm	Feldspars
912-914	13.15	18.15	10.53	7.28, HIT=0	Chlorite +	Chl:sm	
952-954	15.33	17.97	10.53	7.22, HIT=0	Chlorite +	Chl:sm	
972-974	13.31	17.79	10.37		Smectite	Sm.	
1032-1034	13.27	18.86	10.48		Smectite	Sm.	Feldspars
1052-1054	14.83	18.67	10.48	7.36, HIT=0	Chlorite +	Chl:sm	Feldspars
1072-1074	14.45	17.79	10.34	7.26, HIT=0	Chlorite +	Chl:sm	Feldspars
1092-1094	13.08	17.72	10.48		Smectite	Sm.	Feldspars, Amphiboles
1112-1114	15.15, 10.32	15.15, 10.32	15.15, 10.32	7.33, HIT=0	Chlorite + Illite	Chl: ill	Feldspars
1274-1274	-	-	-	7.29, HIT=0	Chlorite	Chl.	Feldspars
1292-1294	14.59	14.59	14.59	7.26, HIT=0	Chlorite	Chl.	Feldspars
1312-1314	-	-	-	7.26, HIT=0	Chlorite	Chl.	Feldspars

Depth (m)	d(001) A	d(001) G	d(001) H	d(002)	Mineral	Type	Other minerals
1312-1314	-	-	-	7.26, HIT=0	Chlorite	Chl.	Feldspars
1332-1334	-	-	-	7.17, HIT=0	Chlorite	Chl.	Feldspars
1352-1354	14.68	14.68	14.68	7.21, HIT=0	Chlorite	Chl.	Feldspars
1372-1374	14.68	14.68	14.68	7.21, HIT=0	Chlorite	Chl.	Feldspars
1392-1394	14.68, 10.33	14.68, 10.33	14.68, 10.33	7.21, HIT=0	Chlorite + Illite	Chl: ill	Feldspars
1412-1414	12.31	12.31	12.31	7.21, HIT=0	Chlorite	Chl.	Feldspars
1432-1434	-	-	-	7.17, HIT=0	Chlorite	Chl.	Feldspars
1452-1454	-	-	-	7.17, HIT=0	Chlorite	Chl.	Feldspars
1472-1474	12.31	12.31	12.31	7.17, HIT=0	Chlorite + Illite	Chl: ill	
1492-1494	10.51	10.51	10.51		Illite (traces)	ill	
1512-1514	10.35	10.35	10.35	7.23, HIT=0	Chlorite + Illite	Chl: ill	Feldspars
1552-1554	-	-	-	7.33, HIT=0	Chlorite	Chl.	Feldspars
1572-1574	10.35	10.35	10.35	7.21, HIT=0	Chlorite + Illite	Chl: ill	Feldspars
1592-1594	-	-	-	7.23, HIT=0	Chlorite	Chl.	Feldspars
1612-1614	-	-	-	7.23, HIT=0	Chlorite	Chl.	Feldspars
1632-1634	10.35	10.35	10.35	7.23, HIT=0	Chlorite + Illite	Chl: ill	Feldspars
1652-1654	10.35	10.35	10.35	7.23, HIT=0	Chlorite + Illite	Chl: ill	Feldspars
1692-1694	10.35	10.35	10.35	7.23, HIT=0	Chlorite + Illite	Chl: ill	Feldspars
1732-1734	10.35	10.35	10.35	7.23, HIT=0	Chlorite + Illite	Chl: ill	Feldspars
1754-1754	10.35	10.35	10.35	7.23, HIT=0	Chlorite + Illite	Chl: ill	Feldspars
1772-1774	10.35	10.35	10.35	7.32, HIT=0	Chlorite + Illite	Chl: ill	Feldspars
1792-1794	10.45	10.45	10.45	7.32, HIT=0	Chlorite + Illite	Chl: ill	Feldspars
1812-1814	10.45	10.45	10.45	7.28, HIT=0	Chlorite + Illite	Chl: ill	Feldspars
1892-1894	14.94, 10.45	14.94, 10.45	14.94, 10.45	7.28, HIT=0	Chlorite + Illite	Chl: ill	Feldspars
1912-1914	14.94, 10.45	14.94, 10.45	14.94, 10.45	7.28, HIT=0	Chlorite + Illite	Chl: ill	Feldspars
1952-1954	14.63, 10.45	14.63, 10.45	14.63, 10.45	7.18, HIT=0	Chlorite + Illite	Chl: ill	Feldspars
1972-1974	14.63, 10.40	14.63, 10.40	14.63, 10.40	7.22, HIT=0	Chlorite + Illite	Chl: ill	Feldspars
1992-1994	14.63, 10.29	14.63, 10.29	14.63, 10.29	7.18, HIT=0	Chlorite + Illite	Chl: ill	Feldspars
2012-2014	14.96, 10.54	14.96, 10.54	14.96, 10.54	7.28, HIT=0	Chlorite + Illite	Chl: ill	Feldspars
2032-2034	14.96, 10.54	14.96, 10.54	14.96, 10.54	7.28, HIT=0	Chlorite + Illite	Chl: ill	Feldspars
2052-2054	14.96, 10.54	14.96, 10.54	14.96, 10.54	7.28, HIT=0	Chlorite + Illite	Chl: ill	Feldspars
2072-2074	14.96, 10.44	14.96, 10.44	14.96, 10.44	7.22, HIT=0	Chlorite + Illite	Chl: ill	Feldspars
2152-2154	14.96, 10.44	14.96, 10.44	14.96, 10.44	7.26, HIT=0	Chlorite + Illite	Chl: ill	Feldspars
2172-2174	14.96, 10.63	14.96, 10.63	14.96, 10.63	7.31, HIT=0	Chlorite + Illite	Chl: ill	Feldspars
2192-2194	14.96, 10.53	14.96, 10.53	14.96, 10.53	7.31, HIT=0	Chlorite + Illite	Chl: ill	Feldspars
2212-2214	14.96, 10.50	14.96, 10.50	14.96, 10.50	7.31, HIT=0	Chlorite + Illite	Chl: ill	Feldspars
2252-2254	15.14, 10.26	15.14, 10.26	15.14, 10.26	7.31, HIT=0	Chlorite + Illite	Chl: ill	Feldspars
2272-2274	15.14, 10.43	15.14, 10.43	15.14, 10.43	7.31, HIT=0	Chlorite + Illite	Chl: ill	Feldspars
2352-2354	15.14, 10.43	15.14, 10.43	15.14, 10.43	7.31, HIT=0	Chlorite + Illite	Chl: ill	Feldspars
2392-2394	15.14, 10.43	15.14, 10.43	15.14, 10.43	7.31, HIT=0	Chlorite + Illite	Chl: ill	Feldspars
2412-2414	15.14, 10.43	15.14, 10.43	15.14, 10.43	7.31, HIT=0	Chlorite + Illite	Chl: ill	Feldspars
2432-2434	15.15, 10.48	15.15, 10.48	15.15, 10.48	7.32, HIT=0	Chlorite + Illite	Chl: ill	Feldspars
2452-2454	15.15, 10.48	15.15, 10.48	15.15, 10.48	7.32, HIT=0	Chlorite + Illite	Chl: ill	Feldspars
2472-2474	15.15, 10.48	15.15, 10.48	15.15, 10.48	7.32, HIT=0	Chlorite + Illite	Chl: ill	Feldspars
2492-2494	15.14, 10.24	15.14, 10.24	15.14, 10.24	7.32, HIT=0	Chlorite + Illite	Chl: ill	Feldspars
2632-2634	15.14, 10.45	15.14, 10.45	15.14, 10.45	7.32, HIT=0	Chlorite + Illite	Chl: ill	Feldspars
2650-2654	15.14, 10.34	15.14, 10.34	15.14, 10.34	7.32, HIT=0	Chlorite + Illite	Chl: ill	Feldspars
2672-2674	14.68, 10.34	14.68, 10.34	14.68, 10.34	7.32, HIT=0	Chlorite + Illite	Chl: ill	Feldspars
2692-2694	14.68, 10.43	14.68, 10.43	14.68, 10.43	7.32, HIT=0	Chlorite + Illite	Chl: ill	Feldspars, Amphiboles
2712-2714	14.68, 10.43	14.68, 10.43	14.68, 10.43	7.32, HIT=0	Chlorite + Illite	Chl: ill	Feldspars, Amphiboles
2732-2734	14.68, 10.26	14.68, 10.26	14.68, 10.26	7.32, HIT=0	Chlorite + Illite	Chl: ill	Feldspars, Amphiboles
2752-2754	14.68, 10.43	14.68, 10.43	14.68, 10.43	7.32, HIT=0	Chlorite + Illite	Chl: ill	Feldspars, Amphiboles
2772-2774	14.68, 10.43	14.68, 10.43	14.68, 10.43	7.32, HIT=0	Chlorite + Illite	Chl: ill	Feldspars, Amphiboles
2792-2794	14.68, 10.43	14.68, 10.43	14.68, 10.43	7.32, HIT=0	Chlorite + Illite	Chl: ill	Feldspars, Amphiboles

AE: Procedure for ICP-OES analysis

The rock cuttings were ground in an agate mortar to about 100 mesh powder.

100 mg ± 2 mg of the sample was weighed in an epicure graphite crucible in which it was added 200 mg ± 2 mg of lithium metaborate flux ($LiBO_2$) and mixed. Six working standards samples were prepared for instrument calibration and fluctuation monitoring. 250 mg ± 2 mg of ATHO, BALK and BTHO standard samples were mixed with 500 mg ± 2 mg of lithium metaborate flux. 100 mg ± 2 mg of K-1919, RGM-1 and BIR-1 were mixed with 200 mg ± 2 mg of lithium metaborate flux.

This were fused in an electric furnace at 1000 °C for 30 minutes. The fused bead was transferred into a bottle containing 30 ml of complexion acid mixture (5% conc HNO3, 1.33% HCL and 1.33% semi-saturated oxalic acid) after being allowed to cool for 30 minutes. The bead and the complexion acid solution were stirred in a centrifuge to complete dissolution. The sample was then ready for ICP-OES analysis.

Analytical session (Spectra CIROS ICP-spectrometer) began by running the three calibration standards (ATHO, BALK and BTHO). The spectra vision was used to calculate a two to three calibration line for each element.

Instrumental reference sample (REF) for monitoring any fluctuations that may occur during analysis was made by mixing three equal parts of the three reference samples. The REF was analysed at the beginning of the session and at 10 sample interval throughout the analytical session. The BTHO standard sample was analysed within each batch of 10 samples in order to monitor instrument reproducibility in multiple analysis.

The raw data were pasted into a correction spreadsheet. The analytical sums for the raw data varied from 98-102 weight percentage. The whole batch analysis was normalised to 100% sum. The spread sheet then calculated time dependent variation down each column (element) of the analysis by finding the difference between the first and the last reading of the reference sample. The total variation was then divided into 10 equal parts. Each line was corrected by adding the variation-increment which was then added to all subsequent lines of batch. The sums were normalized to 100%.

The insignificant time dependent variation-correction was applied to the batch. This made the values of the reference samples at the beginning and end of the sample batch equal.